COUPLED BE-FE APPROACH FOR INTERIOR-EXTERIOR STRUCTURAL ACOUSTICS OF A MULTI-DOMAIN LAMINATED COMPOSITE CAVITY

Thesis submitted by

SUBHANKAR PRAMANIK

Doctor of Philosophy (Engineering)

Department of Civil Engineering

Faculty Council of Engineering & Technology

Jadavpur University

Kolkata, India

2025

JADAVPUR UNIVERSITY
KOLKATA – 700032, INDIA

INDEX NO: 03/18/E

1. **Title of the thesis:**

   Coupled BE-FE Approach for Interior-Exterior Structural Acoustics of a Multi-Domain Laminated Composite Cavity

2. **Name, Designation & Institution of the Supervisor: Dr. Sreyashi Das**

Associate Professor
Department of Civil Engineering
Jadavpur University
Kolkata 700032
India

3. **List of Publications:**

Journal Publications

[1] Subhankar Pramanik, Sreyashi Das & Arup Guha Niyogi, **"Free Vibration and Buckling Analysis of Stiffened Sandwich Plates with Repeated Fold"**, *J. Inst. Eng. India Ser. C* **102**, 87–98 (2021). https://doi.org/10.1007/s40032-020-00627-x

[2] Debalina Basu, Subhankar Pramanik, Sreyashi Das & Arup Guha Niyogi, **" Finite Element Free Vibration Analysis of Functionally Graded Folded Plates"**, *Iran J Sci Technol Trans Mech Eng* **47**, 697–716 (2023). https://doi.org/10.1007/s40997-022-00539-4

[3] Subhankar Pramanik, Sreyashi Das & Arup Guha Niyogi, "**Vibroacoustic Analysis of Laminated Composite L-shaped Acoustic Cavity using Multi-domain Coupled BE-FE Method"**, Journal of Theoretical and Computational Acoustics. 2024. https://doi.org/10.1142/S2591728524500129

[4] Subhankar Pramanik, Sreyashi Das & Arup Guha Niyogi, **"Passive Control of Acoustic Response within Stiffened Thin Laminated Composite Cavities using FE-BE Method",** Journal of Vibration Engineering & Technologies, **13**, 533 (2025). https://doi.org/10.1007/s42417-025-02079-y

4. List of Patents – Nil

5. List of Presentations in National / International Conferences:

[1] Subhankar Pramanik, Sreyashi Das**, "Free Vibration and Buckling of Sandwich Plate with Cut-out"**, *11th Structural Engineering Convention – 2018, Jadavpur University, Kolkata, India, December 19 - 21, 2018 Paper No. 20180105.*

[2] Subhankar Pramanik, Sreyashi Das, and Arup Guha Niyogi, "**Interior Acoustic Analysis of Rectangular Shaped Rigid Cavity with Opening"**, *7th International Congress on Computational Mechanics and Simulation,* 11-13 December 2019, IIT Mandi, India. Paper ID: ICCMS19SD024996. https://doi.org/10.1007/978-981-15-8315-5_32

[3] Subhankar Pramanik, Sreyashi Das, and Arup Guha Niyogi, **"Buckling Analysis of Laminated Composite Rectangular Cavity with Cutout"**, 1st Online International Conference on Recent Advances in Computational and Experimental Mechanics, September 4-6, 2020, IIT Kharagpur, Paper ID: ICRACEM/2020/AM-20-037

[4] Subhankar Pramanik, Sreyashi Das, and Arup Guha Niyogi, (2023), "**Buckling and Free Vibration Analysis of Arch Shaped Sandwich Plates"**. In: Fonseca de Oliveira Correia, J.A., Choudhury, S., Dutta, S. (eds) Advances in Structural Mechanics and Applications. ASMA 2021. Structural Integrity, vol 26. Springer, Cham. https://doi.org/10.1007/978-3-031-05509-6_30

[5] Subhankar Pramanik, Sreyashi Das, Arup Guha Niyogi, **"Interior and Exterior Vibroacoustic Analysis of Composite Flexible Cavity",** Proceedings of XVI Vibration Engineering & Technology of Machinery (VETOMAC – 2021). 16-18 December 2021, Paper ID: 202

[6] Subhankar Pramanik, Sreyashi Das, Arup Guha Niyogi, **"Acoustic Analysis of Partially Flexible Cavity with Opening",** Proceedings of the 12th Structural Engineering Convention, SEC 2022, https://doi.org/10.38208/acp.v1.694

[7] Sourish Dandapat, Sreyashi Das, Subhankar Pramanik, **"Dynamic Analysis of Simply Supported Functionally Graded Plates"**, Proceedings of the 12th Structural Engineering Convention, SEC 2022, https://doi.org/10.38208/acp.v1.470

PROFORMA – I

"Statement of Originality"

I **Shri SUBHANKAR PRAMANIK** registered on 4th June 2018 do hereby declare that this thesis entitled "**COUPLED BE-FE APPROACH FOR INTERIOR-EXTERIOR STRUCTURAL ACOUSTICS OF A MULTI-DOMAIN LAMINATED COMPOSITE CAVITY**" contains a literature survey and original research work done by the undersigned candidate as part of Doctoral studies.

All information in this thesis been obtained and presented in accordance with existing academic rules and ethical conduct. I declare that, as required by these rules and conduct, I have fully cited and referred all materials and results that are not original to this work.

I also declare that I have checked this thesis as per the "Policy on Anti Plagiarism, Jadavpur University, 2019", and the level of similarity as checked by iThenticate software is **6** %.

Subhankar Pramanik

Signature of Candidate:

Date: 01/12/25

Certified by Supervisor:

Sreyashi Das 01/12/25

(Dr. Sreyashi Das)
Associate Professor
Department of Civil Engineering
Jadavpur University
Kolkata 700032
India

Associate Professor
Department of Civil Engineering
Jadavpur University
Kolkata-700 032

PROFORMA - 2

CERTIFICATE FROM THE SUPERVISOR

This is to certify that the thesis entitled **"COUPLED BE-FE APPROACH FOR INTERIOR-EXTERIOR STRUCTURAL ACOUSTICS OF A MULTI-DOMAIN LAMINATED COMPOSITE CAVITY"** submitted by **Shri SUBHANKAR PRAMANIK**, who got his name registered on 4th June, 2018 for the award of Ph.D. (Engg.) degree of Jadavpur University is absolutely based upon his own work under the supervision of **Dr. Sreyashi Das** and that neither his thesis nor any part of the thesis has been submitted for any degree/diploma or any other academic award anywhere before.

Sreyashi Das 01/12/25

Dr. Sreyashi Das
Associate Professor
Department of Civil Engineering
Jadavpur University
Kolkata 700032
India

Associate Professor
Department of Civil Engineering
Jadavpur University
Kolkata-700 032

ACKNOWLEDGEMENTS

I am profoundly grateful to my supervisor, Dr. Sreyashi Das, Professor in the Department of Civil Engineering at Jadavpur University, for proposing the research problem and providing unwavering encouragement, inspiration, and invaluable guidance throughout my research journey. Her consistent and insightful evaluation during this period is deeply appreciated and sincerely acknowledged.

I extend my deepest gratitude to the faculty of the Department of Civil Engineering at Jadavpur University for their unwavering support throughout the various stages of my research. Their collective guidance and cooperation have been instrumental in the successful completion of this work. I am profoundly thankful to my research advisor, Prof. Arup Guha Niyogi, whose critical insights and expert guidance have been invaluable in navigating the complexities of my research problem. His mentorship has significantly contributed to the development of efficient solutions and the overall success of this study. I also wish to express my sincere appreciation to Prof. Partha Bhattacharya for his valuable feedback and constructive discussions during my presentations. His expertise and thoughtful interactions have greatly enhanced the quality and depth of my research. I would like to express my heartfelt gratitude to my co-researcher, Biplab Adhikari, whose guidance felt like that of an elder brother, and my friend Surajit Biswas, for their unwavering support and inspiration throughout this journey. Their contributions have been invaluable and deeply appreciated.

I would like to express my profound gratitude to my parents and my esteemed uncle, Ranjit Pramanik, for their blessings and unwavering support, which have served as a constant source of encouragement and motivation. I also wish to extend my sincere appreciation to my spouse for her steadfast encouragement, invaluable inspiration, and assistance during the course of this work. Finally, I am deeply grateful to my little daughter, Shudiksha, whose innocent smiles, endless patience, and quiet strength have been my greatest comfort during the many long hours spent away from her while working on this thesis. Her loving presence has been a constant source of joy and motivation, and I dedicate this work to her with all my love.

Date: 01/12/25

Place: Kolkata

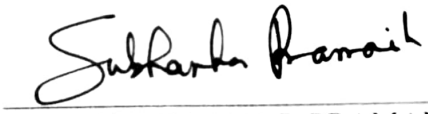

SUBHANKAR PRAMANIK

DECLARATION

This work has not previously been submitted for a degree or diploma in any University. To the best of my knowledge and belief, the thesis contains no material previously published or written by another person except where due reference is made in the thesis itself.

Date: 01/12/25

Place: Kolkata

Subhankar Pramanik

SUBHANKAR PRAMANIK

Dedicated

To

My Family and Friends

CONTENTS

LIST OF TABLES

LIST OF FIGURES

LIST OF FIGURES

LIST OF FIGURES

LIST OF FIGURES

NOTATIONS

a, b	Sides of the plate along x and y axes
A_{ij}	Extensional stiffnesses of the laminate
$[A]^e$	Area matrix in mobility relation with elements a_{ij}^e
α	Shear correction factor for first-order shear correction factor
B	Bulk modulus for the acoustic fluid
B_{ij}	Coupling stiffnesses of the laminate
$[B]$	Linear strain–displacement matrix
c	Velocity of sound
c_{ij}	Elastic coefficient along principal directions
c'_{ij}	Elastic coefficient along any user-defined axis system
C	Damping coefficient
$C(P)$	Solid angle subtended at point P divided by 4π
$diag$	Indicator of diagonal matrix
$\{d\}$	Nodal displacement array for the structure
$\{\dot{d}\}$	Nodal velocity array for the structure
$\{\ddot{d}\}$	Nodal acceleration array for the structure
D_{ij}	Bending stiffnesses of the laminate
$[D]$	Constitutive matrix for a laminate
E	Young's moduli of isotropic plate
E_1, E_2	Young's moduli along the 1 and 2 axes, respectively
e_1, e_2	Hygrothermal strains of a lamina along 1 and 2 axes, respectively.
e_x, e_y, e_{xy}	Hygrothermal strains of a lamina about x and y axes, respectively
$G_{12}, G_{23}, G_{13},$	Shear modulus in 1-2, 2-3 and 1-3 principal planes
$[\rho]$	Density matrix of plates
I	$= \int_{-h/2}^{h/2} \rho \, dz$ for plates Inertia matrix
$[J]$	Jacobian matrix

NOTATIONS

$\|J\|$	Determinant of the Jacobian
k	Wavenumber
K_x, K_y, K_{xy}	Curvature terms for a plate element
$[K_e]$	Element stiffness matrix
$[M]$	Structural mass matrix
$[M_e]$	Element mass matrix
$[T]$	The coordinate transformation matrix
M_x, M_y, M_{xy}	Resultant moments in plates per unit length
$N_i, i = 1 \dots 8$	Quadratic shape functions
p^*	Green's function for the Helmholtz equation
p_j	Nodal acoustic pressure at node j
$[Q']$	The mobility matrix
Q_x, Q_y	Transverse shear forces per unit length along x = constant and y = constant lines for a plate
r	The distance between two points P and Q
R_1	The real part of the radiation impedance of a rigid circular piston over an infinite baffle
S	Notation to indicate surface
t	Thickness of plate
U	Potential energy of deformation
u	The x-component of structural displacement
u_i	Component form of the structural displacement vector
$\{\boldsymbol{v}\}$	Nodal velocity matrix
u_0	Mid-plane displacement for a plate along the x-direction
v_0	Mid-plane displacement for a plate along the y-direction
V	Notation to indicate the domain or volume of a region of interest
w	Displacement along the Cartesian z-direction
X_1	The imaginary part of the radiation impedance of a rigid circular piston on an infinite baffle
x, y, z	Global Cartesian coordinate system

NOTATIONS

x_i	Coordinates of any point
Y	Acoustic Admittance
Z_r	The radiation impedance of a rigid circular piston on an infinite baffle
H_1	First-order Struve function
J_1	First-order first-kind Bessel
$\epsilon, \epsilon_{ij}, [\epsilon]$	Strain in general, tensorial and matrix forms
φ_x, φ_y	Average shear strains in x and y directions on a plate
$\emptyset$	Initial phase lag
$[\Phi]$	Mass-normalized mode shape ensemble
γ	Shear strain
η_1, η_2	Intrinsic coordinates defined to implement Gauss quadrature
λ	Acoustic wavelength
ν_{ij}	Poisson's ratio of transverse strain in the j direction to axial strain in i direction when stressed along i-direction only
θ	Fiber angle
$\theta_x, \theta_y, \theta_z$	Total rotations of a plate element along x, y and z-directions
ρ	Mass density per unit volume
$[\rho]$	Inertia matrix
$\sigma, \sigma_{ij}, [\sigma]$	General, tensorial and matrix forms of stress
τ_{ij}	Shear stresses
ω_i	Natural frequencies of the structure in radians
Ω	Forcing frequency imposed on the structure in radians
ξ_1, ξ_2	Intrinsic coordinates used to implement Gauss quadrature rules
ξ_i	Modal damping ratios
ψ	Solid angle
p^j	Nodal pressure at the j^{th}domain
p_i^j	Nodal pressure at the i^{th} interface and the j^{th}domain
v^j	Nodal velocity at the j^{th} domain

NOTATIONS

v_i^j	Nodal velocity at the i^{th} interface and the j^{th} domain
H^j	Pressure coefficient for j^{th}domain
H_i^j	Pressure coefficient i^{th} interface and for j^{th}domain
G^j	Velocity coefficient for j^{th}domain
G_i^j	Velocity coefficient i^{th} interface and for j^{th}domain
ne	Total number of elements in BEM
nn	Total number of nodes in BEM
ω_k	Natural frequency kth mode in radian/second
ξ_k	Damping ratio for kth mode

ABSTRACT

Acoustic analysis of vibrating cavities is of paramount importance due to immense impact of noise on the healthy existence of mankind. Excessive exposure to high sound pressure levels (SPL) causes severe health hazards like hearing damage, mental stress, physiological, endocrine, and cardiovascular damage, etc. and badly affects the quality of work and productivity. Conversely, good acoustic design can lead to contentment, pleasure, safety and sound health for people. Higher noise level poses a serious threat both for the passengers inside the automobiles and pedestrians on the road. Hence, over the past several years, customer's demand for acoustic comfort has become an important criterion for vehicle selection. There are strict legal regulations on noise emission levels too.

Because of the inflated cost of structural materials and scarcity of fossil fuel, it is important to make the vehicular cabin structures lighter and fuel-efficient. Consequently, designers prefer lightweight structural materials with high specific strength and stiffness, such as, laminated composites, over conventional materials. Unlike rigid walls, thin and flexible walls modify the noise and vibration level and thus alter the acoustic response both inside and outside of the vehicle considerably, thus necessitating coupled structural acoustic (CSA) analysis. Again, irregular geometry of the cavity and radiation of sound from fully or partially opened windows in vehicles make the analysis more challenging. As active noise cancellation escalates the overall cost, passive noise cancellation methods such as adding absorbent layer or stiffeners along with modifying the damping, can be adopted to control the sound pressure level for the comfort of passengers.

Hence, considering real-world scenarios, the present study adopts a multidomain framework that partitions the acoustic cavity into smaller subdomains interconnected by intermediate interface layers which facilitates a comprehensive analysis of the multi-domain Boundary Element Method (BEM) for coupled interior and exterior domains. An in-house software has been developed in MATLAB environment to investigate the vibroacoustic response of a three-dimensional vehicular acoustic cavity having a combination of rigid and flexible panels, with complex boundaries involving absorbent layers and opening, using coupled finite element and multi-domain boundary element analysis. Exact analysis of SPL at the exterior domain have been evaluated using continuity condition at the window surface. The program developed is versatile enough to handle cavities of any shape and multiple interacting boundary panels with arbitrary position of opening.

The program has been verified with analytical and experimental data available in the literature to ensure accuracy. The finite element analysis of the flexible panels is done using first order shear deformation theory with an eight-noded isoparametric element and folded plate transformations are applied to modify the structural stiffness and mass matrices from local to global coordinates prior to assembly. The nodal sound pressure levels at flexible boundaries are determined using mobility relationship obtained from the finite element structural analysis.

The sound pressure levels have been evaluated both at the interior and exterior cavity and it has been demonstrated that the shape of the flexible acoustic domain along with the presence of opening alters the modal characteristics of the structure causing considerable modifications in the sound pressure level (SPL) pattern. The SPL inside the vehicle cavity can also be modified by judiciously stiffening the enclosure. Examples reveal that one can restrict the acoustic output at the resonant frequencies by suitably adding absorbents.

1

Introduction

Acoustic analysis of vibrating cavities is of paramount importance due to immense impact of noise on the healthy existence of mankind. Uncontrolled sound lends to various health hazards. Excessive exposure to high sound pressure levels (SPL) causes hearing damage and even hearing impairment along with other ailments like mental stress, physiological, endocrinal and cardiovascular damage and foetal disorders. It badly affects the level of mental concentration, quality of work, learning and productivity. Apart from these, acoustic fatigue could cause structural damage or even premature failure and devaluation of property. Conversely, good acoustic design can lead to contentment, pleasure, safety and sound health for people.

Higher noise level poses a serious threat both for the passengers inside the automobiles and pedestrians on the road. Hence, over the past several years, customer's demand for acoustic comfort has become an important criterion for vehicle selection. There are strict legal regulations on noise emission levels too. Automotive manufacturers invest a lot of effort and money to improve and enhance the vibroacoustic performance of their products. Because of inflated cost of structural materials and scarcity of fossil fuel, it is important to make the vehicular cabin structures lighter and, hence, fuel-efficient. Consequentially, designers prefer lightweight structural materials with high specific strength and stiffness, such as, laminated composites, over conventional materials. Laminated composite materials comprise of thin laminae of matrix with reinforcing fibres arranged at predefined orientations according to requirements and design specification. The matrix may be plastics, carbon or metal whereas

the fibres may be natural, synthetic or metallic, depending upon the usage, wear and tear, hygro-thermal environment, stiffness and strength requirements. Laminated composite cabin walls being flexible, unlike rigid walls, modify the noise and vibration level and thus alter the acoustic response both inside and outside of the vehicle considerably. Hence, careful design measures should be undertaken to mitigate the noise to acceptable level after detail vibroacoustic analysis of structures in the working frequency range (20 to 250 Hz). Apart from vehicular cabins, interior acoustic analysis has many practical applications in the design of control rooms, aircraft interiors, ship cabins and duct systems.

There are many practical examples in which an interior acoustic space is connected to an exterior domain through one or more openings. The radiation of sound from an open duct, transmission of sound into a room through an open window, and radiation of sound from fully or partially opened window in vehicles are some examples. These types of problems are termed as exterior acoustic problem. The geometry of the structure too influences the vibroacoustic analysis significantly.

The noise level in a vehicular structure can be controlled in two ways, namely, active noise cancellation (ANC) and passive noise cancellation (PNC). ANC uses microphones and digital signal processor to generate an opposite sound to cancel out unwanted noise. PNC uses the design of the cavity to isolate the risers from ambient noise rather than cancelling out. As ANC can escalate the overall cost, PNC is a preferred choice of many consumers. This can be achieved by various techniques:

- Control of acoustic noise responses through structural design optimisation
- Reduction of acoustic noise by selectively applying absorbent layers
- Mitigation of acoustic noise via strategically placed localised added masses
- Suppression of acoustic noise through the incorporation of additional damping elements
- Isolation of acoustic noise responses using the resilient mounting system

As the composite constructions are gradually replacing the traditional usage of metals in car chassis due to their extremely high specific strength and stiffness, however, being thin and flexible, they interact with the acoustic medium and dramatically alter the sound pressure level pattern compared to that of rigid structures. Only coupled structural acoustic (CSA) research can determine this response pattern. Because the behaviour of composite structures is far more complex than that of isotropic structures, a coupled composite structure-acoustic field analysis

has many practical implications. As a result, a detailed study is required before composites can be used effectively in the mechanical, automotive and aviation sectors.

Tools for Numerical Analysis:

For simple-shaped structures, like spherical or cylindrical, the fluid structure interaction problems can be solved theoretically. However, in real-world scenarios, the structure's form being complex, numerical analysis is a must.

Any physical problem may be described as a differential equation. These differential equations, when simple in form, can be solved using the classical technique of analysis. However, for big complex structures with multiple boundary conditions, numerical techniques will be necessary to get the desired results. These sorts of equations can be solved using the finite difference technique, the finite element method, or the boundary element method. For acoustic analysis, the finite element method and boundary element method have been used generally.

1.1 Finite Element Method (FEM)

For many years, the finite element method has been utilized to solve a variety of engineering problems. It is an effective technique where the continuum structure is discretized into finite-sized elements which are connected at nodes. The equilibrium equations for the entire structure are obtained by assembling the element matrices ensuring continuity of displacement at the nodes. The nodal parameters are then solved using the variational principle. This method can yield reasonably accurate solutions for free vibration of structures under various boundary conditions.

1.2 Boundary Element Method (BEM)

The Boundary Element Method (BEM) is a powerful technique for analysing the behaviour of mechanical systems, particularly engineering structures subjected to external loading. In this context, "loading" refers broadly to any external source that produces a non-zero field function describing the system's response, such as temperature, displacement, or stress fields. This external source could be heat, surface tractions, body forces, or even non-homogeneous boundary conditions like support settlement. BEM is now widely applied across various engineering fields, including potential theory, acoustics, torsion, electric and magnetic field theory, elastostatics, elastodynamics, plate and shell analysis, transient heat transfer,

viscoelasticity, viscoplasticity, fracture mechanics, water waves, viscous fluid flow, groundwater flow, and thermoelasticity. Additionally, BEM is employed to investigate the micro-mechanical behaviour of fibre-reinforced composite materials.

In principle, the method is based on finding the unknown solutions at the boundary, considering a second set of known boundary solutions, derived from Green's solution of the governing equation, the two solutions being connected through the Gauss Divergence theorem, for a set of given boundary conditions. The boundary conditions are incorporated into the system equation before going for the solution. Any solution that is needed inside the domain can be calculated from the boundary solutions, once the boundary values are known.

1.3 Boundary Element Method (BEM) over Finite Element Method (FEM)

Comparison of BEM and FEM

i. The primary difference between BEM and FEM is that the FEM discretizes the entire domain (volume or area) while the BEM only discretizes the boundary, thus reducing the dimensionality of the problem by *one*. This makes BEM more efficient for problems with infinite or unbounded domains.
ii. BEM relies on integral equations, while FEM is based on differential equations.
iii. BEM produces fully populated element matrices whereas FEM produces sparse element matrices.

The Boundary Element Method (BEM) offers several advantages over the Finite Element Method (FEM), particularly for certain classes of problems where FEM can be less effective and more laborious. The main reasons are:

i. Discretization Requirements: FEM requires discretization over the entire domain occupied by the body, which can make generating and inspecting the finite element mesh difficult, laborious, and time-consuming, especially for complex geometries with features like holes, notches, or corners. These areas often require mesh refinement and a high element density due to large solution gradients.
ii. Model Modification: Modifying the discretized model to improve solution accuracy or to reflect design changes can be challenging, demanding significant effort and time.

iii. Infinite Domains: For problems involving infinite domains, such as half-space or the complementary domain to a finite one, FEM necessitates the creation of artificial closed boundaries. This can reduce accuracy and sometimes result in spurious or incorrect solutions.

iv. Higher-Order Differential Equations: For problems described by differential equations of fourth or higher order (such as plate or shell equations of sixth, eighth, or higher order), the conformity requirements are so stringent that using FEM can become impractical due to the tedious nature of the job.

In contrast, the Boundary Element Method (BEM) offers several significant advantages:

i. Boundary Discretisation: BEM requires discretisation only over the boundary of the body, simplifying numerical modelling and reducing the number of unknowns by an order of magnitude. This makes remodelling to reflect design changes straightforward.

ii. Infinite Domain Handling: For infinite domains, BEM formulates the problem as an exterior one, with the fundamental solution satisfying conditions at infinity. This allows computer programs developed for finite domains to be adapted with minimal modifications to solve infinite domain problems, which is not feasible with FEM.

iii. Effective Derivative Computation: BEM is particularly effective at computing derivatives of the field function, such as fluxes, strains, stresses, and moments. It easily handles concentrated forces and moments, whether inside the domain or on the boundary.

iv. Solution Evaluation: BEM allows the evaluation of the solution and its derivatives at any point within the domain and at any time. This is possible because BEM uses an integral representation of the solution as a continuous mathematical expression, which can be differentiated and used as a mathematical formula. In contrast, FEM provides solutions only at nodal points.

v. Geometric Peculiarities: BEM is well-suited for solving problems in domains with geometric peculiarities, such as cracks.

1.4 Boundary Element Method for Acoustic Analysis

Over recent decades, the Boundary Element Method (BEM) has garnered significant attention from researchers and has become a vital technique for the computational solution of numerous physical problems. Similar to the well-known Finite Element Method (FEM) and Finite Difference Method (FDM), BEM is fundamentally a method for solving partial differential equations (PDEs) and can only be utilized when the physical problem can be expressed in such terms. BEM has been applied to a variety of topics, including stress analysis, potential flow, fracture mechanics, and acoustics.

Acoustics, an important branch of physical science, deals with acoustic fields in fluid domains such as air or water, the two most important acoustic media. The linear wave equation serves as a suitable model for many fluids and is often used for air and water media. In numerous physical situations, the acoustic field is periodic, which allows the wave equation to be reduced to a sequence of Helmholtz equations through Fourier decomposition, with one Helmholtz equation for each sample frequency. Solutions to acoustic problems are thus obtained by considering these individual Helmholtz problems.

The Helmholtz equation, which governs a range of domain classes, can be solved using the Boundary Element Method. Consequently, BEM has attracted the interest of engineers working on applications such as the sound output of a loudspeaker, noise from a radiating source like an engine, and the interior acoustic modes of an enclosure such as a vehicle interior. BEM is equally applicable in underwater acoustics and can be used to model the scattering effect of an obstruction in the ocean or to determine the acoustic field surrounding a sonar transducer.

One of the key advantages of the Boundary Element Method is that only the boundary of the domain of the PDE requires discretization, effectively reducing the problem's dimensionality by one. For example, an equation governing a three-dimensional region is transformed into one over its surface. In scenarios where the domain extends beyond the boundary, such as in acoustic radiation and scattering models, the domain is infinite, making the advantages of BEM

even more pronounced. The equation governing the infinite domain is reduced to an equation over the finite boundary, highlighting BEM's efficiency and effectiveness.

1.5 Importance of Present Research

Nowadays, lightweight composite materials with high specific strength and stiffness are being preferred for manufacturing vehicular cabin structures due to high fuel efficiency. The walls of the composite cavities, being thin and flexible, modifies the acoustic response both inside and outside the cavities, thus necessitating structural acoustic coupling analysis. In South East Asia, the climate being hot and humid, the windows of the vehicles could be fully or partially open in different combinations for a particular vehicle. These windows, considering as leakage surfaces, affect the sound pressure level requiring a coupled interior-exterior acoustic analysis. Considering strict regulations in noise emission standards and comfort level of passengers inside the vehicle as well as that of pedestrians on road makes the structural acoustic interior-exterior coupling analysis a very important one.

Again, the shape of the vehicular cavity plays an important role in the distribution of sound pressure level inside and outside the cavity. A reliable numerical model is required to describe complex vibroacoustic behaviour for irregular shaped domain both for rigid and flexible structure. The single domain boundary element method can be used appropriately in simple cavity structures where the source and observation points are connected inside the domain. However, in complex boundary configurations, the generation of sound fields may be prone to errors where this direct connection is disrupted. Therefore, multi-domain boundary element analysis is essential, where an interface layer between two domains is applied ensuring that every point within each domain behaves consistently as either a source or an observation point to avoid erroneous results.

Controlling noise using passive tools without considerably increasing cabin mass is also one important consideration as use of active noise control of the systems would escalate the cost. Hence, considering real-world scenarios, the present study adopts a multi-domain framework that partitions the acoustic cavity into smaller subdomains interconnected by intermediate interface layers. This framework facilitates a comprehensive analysis of the multi-domain Boundary Element Method (BEM) for coupled interior and exterior domains, specifically applied to the vibroacoustic behaviour of a car-shaped cavity.

1.6 *Organization of the Present Thesis*

The present thesis has been organized in the following manner:

Chapter 1 provides a comprehensive introduction to the thesis, addressing the challenges associated with vibroacoustic analysis and exploring potential computational solutions using the Finite Element Method (FEM) and the Boundary Element Method (BEM). It begins with an overview of FEM and BEM, followed by a comparative analysis that highlights the advantages of BEM over FEM. The chapter further examines the application of multi-domain BEM in acoustic analysis, emphasizing its relevance to the present research. Additionally, the importance of the study is discussed, and the chapter concludes with an outline of the thesis organization, summarizing the key aspects covered in each chapter.

Chapter 2 presents an extensive literature review, covering significant studies relevant to the research. It discusses the free vibration analysis of composite plates using FEM, followed by an overview of key books on acoustic analysis. The chapter then explores the application of BEM in acoustic domain analysis, coupled structural acoustics (CSA) analysis, and interior acoustics using multi-domain approaches. Finally, it examines exterior acoustic analysis, providing a foundation for understanding existing research and identifying gaps addressed in this study. The literature review concludes with a discussion on the research gap, objectives, scope, and detailed roadmap of the present research.

Chapter 3 presents the theoretical formulation underlying the study, beginning with the formulation for laminated composite folded plate structures. It then introduces the mobility relation, followed by an in-depth required formulation for the acoustic domain, covering single-domain, multi-domain, and exterior acoustic problem. The chapter further explores the multi-domain interior-exterior coupling formulation and discusses different boundary conditions, including rigid boundaries, interaction boundaries, boundaries with absorbent layers, and boundaries with openings. Finally, post-processing techniques are addressed, along with a flowchart illustrating the algorithm used in the study.

Chapter 4 focuses on the free vibration analysis of composite folded plate structures, beginning with a validation study that is divided into four parts: stiffened laminated composite plate

structures, isotropic one-fold plate structures, sandwich plate structures, and sandwich one-fold plate structures. This is followed by a mesh convergence study to ensure accuracy in numerical modelling. The chapter then presents three case studies: the free vibration analysis of a cantilever one-fold composite plate, the free vibration study of a sandwich corrugated plate, and the analysis of a sandwich corrugated plate with a stiffener. Finally, the chapter concludes with key findings from the analyses.

Chapter 5 examines the acoustic response within thin laminated composite stiffened cavities, starting with a finite element mesh convergence study. This is followed by a validation study of the Internal Coupled Structural Acoustic (ICSA) formulation using both isotropic and orthotropic laminated composite rectangular cavities. The chapter then presents numerical case studies, beginning with the variation of sound pressure levels (SPL) in stiffened and unstiffened acoustic cavities for different stiffener widths. It further investigates SPL variations due to changes in flexible wall thickness, damping ratios, and the position and number of stiffeners. Additionally, a comparative analysis of displacement at the cavity boundary is conducted, providing insights into out-of-plane and in-plane displacements. Various figures illustrate mode shapes, SPL distributions, and displacement variations, enhancing the understanding of acoustic behaviour in stiffened cavities. The chapter concludes with a discussion of the findings, highlighting key observations and implications.

Chapter 6 focuses on the vibroacoustic analysis of laminated composite L-shaped acoustic cavities using the multi-domain method. It begins with numerical case studies analysing an L-shaped rigid cavity, a rigid L-shaped box with an absorbent layer, and a rigid partly opened L-shaped box. The analysis then extends to flexible laminated composite L-shaped cavities, starting with a validation study that includes interior coupled structural acoustic (ICSA) analysis and multi-domain acoustic analysis in flexible cavities with absorbent layers. A mesh convergence study follows to ensure numerical accuracy. The chapter further presents case studies on the vibroacoustic behaviour of an L-shaped flexible cavity and a partially opened L-shaped flexible cavity with an absorbent layer. Finally, the chapter concludes by summarizing key findings from the analyses, providing insights into the acoustic behaviour of L-shaped cavities under different conditions.

Chapter 7 presents the vibroacoustic analysis of a laminated composite car-shaped acoustic cavity using the multi-domain method. It begins with validation studies covering rigid interior-

exterior coupling, interior coupled structural acoustic analysis for flexible cavities, and multi-domain acoustic analysis in flexible cavities with absorbent layers. The chapter then explores case studies, starting with the vibroacoustic analysis of a car-shaped model with a rigid cavity, followed by an analysis of a partially flexible cavity. Further investigations focus on a second car-shaped model, examining interior-exterior multi-domain coupling in a partially flexible cavity. Key aspects analysed include the effects of flexibility at domain and boundary points, the impact of adding absorbent layers, variations in damping ratios, and the influence of different locations. The chapter presents sound pressure level plots for Boundary 4-D along with contour plots illustrating the interior and exterior domains at varying sound pressure levels at certain forcing frequencies. The chapter concludes by summarizing the findings, providing insights into the vibroacoustic behaviour of car-shaped cavities under varying conditions.

Chapter 8 provides a comprehensive conclusion to the research, summarizing the key findings and insights gained from the study. It begins with an overview of the major outcomes, followed by a detailed discussion of the results in the context of vibroacoustic analysis. The chapter also highlights potential areas for future research, suggesting possible extensions and advancements in the field. Finally, it presents a statement of contribution, outlining the novel aspects of the study and its significance in advancing computational vibroacoustic analysis.

2

Literature Reviews

The coupled dynamic response of elastic structures in contact with fluids experiencing small-amplitude vibration in relation to an equilibrium position is the focus of structural acoustics of a cavity. The coupling for lighter fluids, such as air, can be one-way, meaning that the fluid response is influenced by the structural vibration but not the other way around, or two-way, like in the violin. Determining and lowering sound pressure levels in car and airplane cabins are the problems of interest in structural acoustics involving air. Presence of opening in the cavity that allows sound to be emitted into the surrounding environment, makes the acoustic analysis more complex. Again, the problem becomes challenging from practical standpoint, if the cavity's shape is composed of several irregularly shaped domains.

Stiffening the structure with plates increases its stiffness even further, which causes the sound pressure level inside the enclosed structure to fluctuate once more. Additionally, using absorbent layer lowers the sound pressure level in a specific frequency range, which is the designers' ultimate goal.

Ideally finite element method (FEM) is best suited for analysis of the structural part and boundary element method (BEM) is adept for the analysis of acoustic part as it reduces the dimensionality of the system by one degree. Here the review of literature is presented under the following heads.

i. Free Vibration Analysis of Composite Plate Using FEM
ii. General Acoustic Analysis
iii. Boundary Element (BE) Analysis of Acoustic Domain
iv. Coupled Structural Acoustics (CSA) Analysis
v. Interior Acoustics with Multi-domain
vi. Exterior Acoustic Analysis

2.1 Free Vibration Analysis of Composite Plate Using FEM

The classical plate theory (CPT) [1], was developed in 1850 without the impact of transverse shear deformation, making it unsuitable for analysing multilayer orthotropic composites, even though it is effective for homogeneous materials. The transverse shear deformation in 1945 by Reissner [2] and by Mindlin [3] in 1951 was introduced with first-order shear deformation theory (FSDT). These theories provide foundational approaches for understanding the behaviour of such materials as laminated composite folded plates. In 1966, YNS theory (Yang, Norris, and Stavsky theory) [4] was used as a basis for the study of transverse shear deformation and rotary inertia. In 1967, Raville et al. [5] investigated the natural frequencies of sandwich plates through experimental tests and theoretical analysis, highlighting the influence of material and geometric properties. In 1979, Reddy [6] used the quadratic isoparametric element to study the free vibration of antisymmetric angle-ply laminated plates, including transverse shear deformation and rotary inertia. Chen et al. (1990) [7] analysed the static deflections and natural frequencies of various composite plates using a Levy-type solution and state-space formulation, examining the impact of geometric and material parameters on their behaviour. In 1992, Sai Ram et al. [8] studied the free vibration and buckling characteristics of laminated composite plates with the influence of moisture. In 1996 Bathe [9] provided a comprehensive overview of the finite element method, covering fundamental concepts and advanced topics, including formulation techniques, solution procedures, and practical applications in engineering analysis. Meunier et al. (2001) [10-11] studied the dynamic behaviour of fibre-reinforced plastic (FRP) composite materials using Reddy's first and higher-order shear deformation theories and Jones [12] published a comprehensive textbook that serves as an essential resource for understanding the mechanical behaviour of composite materials. Kant et al. (2001) [13] demonstrated that higher-order refined theories provide more accurate vibration analysis for isotropic, orthotropic, and multilayer plates. Nayak et. al. (2002) [14] presents an in-depth analysis of the free vibration characteristics of composite sandwich plates using Reddy's higher-order theory. This study offers valuable insights for the design and optimization of sandwich structures in engineering applications. In 2002 Cook et al. [15] published a widely acclaimed textbook that offers in-depth coverage of finite element analysis (FEA). Reddy (2003) [16] provided a comprehensive analysis of the behaviour and theory of laminated composite structures, with a focus on advanced topics like smart materials and functionally graded materials. Kumar et al. (2005) [17] explored the free vibration behaviour of square laminates with delamination around a central cutout using higher order shear deformation theory (HSDT). Shivakumar's (2006) [18] study focused on developing a lightweight, fire-

resistant core material for sandwich structures using syntactic foam made from fly ash and phenolic resin binders. Ovesy et al. [19] (2012) investigate the buckling and free vibration behaviour of composite plates with cutouts using two distinct modelling approaches in finite strip analysis.

Several works of literature are evaluated for stiffened plate constructions. Olson et al. (1977) [20] focused on the vibration characteristics of integral rib-stiffened plates. Deb et al. [21] (1988) presented a comprehensive analysis of finite element models for stiffened plates under transverse loading. Mukherjee et al. [22] (1988) introduced an isoparametric stiffened plate element for analysing the free vibration of eccentrically stiffened plates. Attaf et al. [23] (1990) explored the dynamic response of rectangular composite plates, both stiffened and unstiffened, under static in-plane compressive loads. Chattopadhyay et al. [24] (1993) conducted a finite element analysis of blade-stiffened composite plates subjected to transverse loads. Lee et al. [25] (1995) conducted a comprehensive vibration analysis of anisotropic plates with eccentric stiffeners, providing significant insights into the dynamic behaviour of anisotropic materials when reinforced with eccentrically placed stiffeners. Qing et al. (2006) [26] presented a novel mathematical model for the free vibration analysis of stiffened laminated plates, providing insights into the dynamic behaviour and stability of these composite structures under various conditions.

Many scientists have made contributions to folded plate structures. In 1957, Goldberg et al. [27] solved folded plate structures using the method of elasticity. In 1969, Cheung et al. [28] used the finite strip method to analyse folded box girder and prismatic plate structures. Irie et al. [29] (1984) performed dynamic analysis of isotropic folded plate structures. Liu et al. [30] (1992) analysed one and two-fold plates using the finite element transfer matrix method. In 1999, Niyogi et al. [31] conducted finite element-based free vibration analysis of laminated composite folded plate structures using first-order shear deformation theory. Lee et al. (2004) [32] investigated the dynamic behaviour of folded composite plates using third-order plate theory. In 2005, Lee et al. [33] analysed the dynamic response of a pre-stressed concrete box girder bridge subjected to moving loads using folded plate elements. Haldar et al. (2005) [34] analysed the free vibration behaviour of isotropic and composite folded plates using a shear flexible element. In 2006, Liew et al. [35] investigated the elastic buckling behaviour of stiffened and un-stiffened folded plates under partial in-plane edge loads using the mesh-free Galerkin method. In 2006, Peng et al. [36] analysed stiffened and un-stiffened folded plates using the mesh-free Galerkin method. Pal et al. (2007) [37] effectively used folded plate

formulation and Lagrangian plate elements to analyse the transient vibration behaviour of stiffened laminated composite and sandwich folded plates, accurately predicting their dynamic response. Singh et al. (2012) [38] utilize an efficient C0 finite element model based on higher-order zigzag theory to perform a detailed buckling analysis of laminated composite plates behaviour. Barbero et al. (2014) [39] introduced a mixed isostatic 24-degree-of-freedom element for the static and buckling analysis of laminated folded plates, demonstrating its accuracy and efficiency in handling complex structural behaviours. Peng (2015) [40] introduced an element-free Galerkin method for analysing the free vibration of symmetrically laminated folded plate structures, demonstrating its effectiveness through numerical examples. Le-Anh et al. (2015) [41] presented an adjusted Differential Evolution algorithm combined with a smoothed triangular plate element for optimizing the static and frequency responses of folded laminated composite plates. Xiangying et al. (2019) [42] investigated the nonlinear vibration behaviour of Z-shaped folded plates with inner resonance, combining theoretical analysis and experimental validation to reveal complex dynamic responses. Das et. al (2020) [43] analysed the free vibration behaviour of epoxy-based cross-ply laminated composite folded plates under hygro-thermal loading, revealing that increased hygro-thermal loads significantly reduce structural stiffness. Peng et al. (2022) [44] analysed the flexural vibration of CSP-RHC using 2D-HPM, showing that its natural frequencies are lower than traditional honeycomb plates due to the NPR effect, with variations influenced by aspect ratio, thickness, and cell angle. Song et al. (2024) [45] presented a method using Donnell's shell theory and the Rayleigh-Ritz technique to study vibration in composite fuselage battery compartments of hydrogen-electric aircraft, considering hygrothermal effects and validating results through experiments and finite element analysis. Salehipour et al. (2024) [46] investigated the free vibration behaviour of folded sandwich plates with a porous core and functionally graded carbon nanotube-reinforced composite coatings using FSDT and the two-dimensional generalised differential quadrature method.

2.2 Acoustic Analysis Books

Several books are available that provide a detailed insight into acoustics. In 1954, Beranek [47] made significant contributions to practical acoustical concepts. Sommerfeld (1967) [48] provides a unified approach to PDEs, emphasizing Green's functions, eigenvalue problems, and the method of characteristics for solving complex physics and engineering problems. It applies these methods across fields like wave propagation, heat conduction, and quantum mechanics. Later, in 1968, Morse and Ingard [49] made notable advancements in theoretical

acoustics. In 1971, Skudrzyk [50] and Seto [51], bridged the gap between theoretical understanding and analytical computations and made exemplary contributions to this field in the same year. In 1973, Kuttruff [52] contributed to understanding room acoustics. Porges [53] 1977, Pierce (1981) [54] and Kinsler et al. (1982) [55], published works that made the understanding of acoustic analysis more accessible. Dowling and Williams [56], in 1983, further contributed to the ease of reading and comprehension of acoustic concepts. Fahy (1985) [57] in his monograph, gave a revealing note on the sound-structure interaction problem. Later, in 1989, Norton et. al. [58] provided a comprehensive discussion on the gradual emergence of structural acoustics, starting from the basics of structural dynamics and engineering acoustics. In 1991, Turner et al. [59] explored noise control methods for cost-effective insulation and practical solutions using modern measurement techniques and applied acoustics. Another set of monumental contributions is furnished in the four volumes of the Encyclopedia of Acoustics edited by Crocker [60] in 1997, where theories, applications, measurement techniques, and noise abatement techniques are elaborately discussed. Marburg et al. [61] published a book in 2008 with focusing on FEM for interior problems and BEM for exterior problems, covering numerical aspects, convergence, multi-frequency solutions, efficient methods, absorbing boundaries, non-uniqueness in BEM, fluid-structure interaction, and transient problems. In 2016, Hambric et al. [62] discussed a different range of analytical and computational methods for vibroacoustic analysis, including classical modal synthesis, FEM, BEM, SEA (Statistical Energy Analysis), EFEA (Energy Finite Element Analysis), hybrid methods, and wave-based methods, and provides theoretical formulations, practical applications, and guidance on noise and vibration control, optimization, and uncertainty estimation.

2.3 Boundary Element Analysis of Acoustic Domain

The Boundary Element Method (BEM), regarded as an integral method, has a long history dating back to 1903 when Fredholm [63] published his seminal work on integral equations in potential theory. This early research provided the groundwork for developing and applying BEMs to acoustic radiation problems. The classical works of Muskhelishvili [64] in 1958 and Kupradze [65] in 1965 in elastostatics, and Kellogg [66] in 1967 on potential theory, represent applications of integral equations in continuum mechanics. During this period, Zienkiewicz et al. [67] in 1977 derived techniques to couple FEM and BEM based on variational methods. The term ‘boundary element method’ was first coined by Brebbia [68] in 1978. Later, the term was used by Banerjee et al. [69] in 1981 and Brebbia et al. [70] in 1989, who showed that the method could also be derived from the weighted residual technique like FEM, making the name

boundary element method (BEM) preferred over boundary integral equation method (BIEM). In 1992, Becker [71] presented a detailed formulation process, complete with computer listings, for practical applications like potential problems, elastostatics, and acoustics. Chen et al. [72] (1993) provided a comprehensive analysis and validation of a boundary element method (BEM) for determining acoustic eigenfrequencies in car compartments, demonstrating its effectiveness in extracting acoustic eigenvalues by unifying Robin, Dirichlet, and Neumann boundary conditions and incorporating acoustic admittance or impedance. This method was shown to be applicable to large-scale problems, even on relatively small workstations. Building on this foundation, Marburg et al. [73] (1997) introduced an optimization method for a vehicle body using a parametric geometry model of the roof under time-harmonic excitation, assuming other parts remain rigid. Their study incorporated admittance boundary conditions to evaluate various loads and frequency domains, with a primary focus on structural harmonic analysis to improve the vehicle's acoustic performance. Kim et al. [74] (1999) presented a compact matrix formulation using impedance and mobility approaches for analysing structural-acoustic systems. This method simplifies the coupling analysis between structural vibrations and acoustic responses, enhancing computational efficiency and accuracy. Furthering this research, Marburg et al. [75] (1999) explored the use of boundary admittance as a Robin-type boundary condition in low-frequency, time-harmonic acoustic problems, detailing methods for determining the complex reflection coefficient and highlighting the sensitivity of higher damped modes to the admittance phase angle. A case study involving a sedan car cabin was presented to demonstrate the practical application of boundary admittance determination. In 2002, Marburg [76] examined the rule of thumb for using six elements per wavelength in linear time-harmonic acoustics, reviews boundary element methods and interpolation functions, compares numerical and analytical solutions in a long duct, evaluates error norms, and analysed a sedan cabin compartment with different mesh types to determine the required elements per wavelength for accurate sound pressure magnitude. Zhang, Z et. al. [77] (2003) emphasized the importance of acoustic sensitivity analysis in reducing structure-borne noise levels and reviews previous methods like finite element method (FEM) and boundary element method (BEM) Li, S. [78] (2005) discusses the conventional BEM formulation and its challenges with frequency dependence, highlighting the time-consuming nature of recalculating matrices for different frequencies. Kirkup's [79] book published in 2007 addresses a range of acoustic or Helmholtz problems, including both interior and exterior acoustic fields, and provides practical examples like vehicle noise analysis and loudspeaker design. In the same year, Shen et al. [80] presented an adaptive fast multipole boundary element method (FMBEM) using the Burton-

Miller formulation to address high costs and non-uniqueness in traditional BEM for 3-D acoustic problems.

2.4 Coupled Structural Acoustics (CSA) Analysis

The first discussion on fluid-structure interaction problem using a BE-FE approach was found in 1970 by Shaw [81]. The author discussed the transient analysis thereafter for an ocean wave-structure interaction problem. Later, in 1973, Shaw [82] reported the FE-BE analysis of three-dimensional scattering and radiation problems for transient and time-harmonic cases by smooth elastic structures. In 1977, Zienkiewicz et al. [83] emphasized the integration of boundary solution procedures into the finite element method (FEM) framework, showcasing its versatility for various engineering problems. In 1989, Suzuki et al. [84] tackled the challenge of coupled interior structural acoustic problems by employing the Boundary Element Method (BEM) to address noise issues in complex-shaped cavities, particularly within vehicle cabins. They introduced a novel formulation to manage intricate boundary conditions, considering the acoustic effects of absorbent materials on vibrating surfaces and the influence of leaks through openings. This method also facilitates the calculation of boundary vibration velocities with structural-acoustic coupling effects. Additionally, it examines sound transmission through a cavity-backed plate and evaluates sound absorption characteristics within a sedan compartment model, demonstrating its practical applications in vehicle noise analysis. In 1990, Jeans and Mathews [85] numerically modelled elasto-acoustic problems in thin shells and curved plates by combining 9-noded isotropic Mindlin plate finite elements for the elastic problem with a variational boundary element solution using nine-noded isoparametric elements for the exterior infinite acoustic domain, enabling them to study far-field normalised radiated pressure for cantilever plates and spherical shells excited by point forces through fully integrated structural and acoustic degrees of freedom. In 1994, Cheng [86] presented a vibroacoustic model for a plate-ended cylindrical shell with an enclosed acoustic cavity, highlighting the weak coupling at low frequencies, the dominance of plate-induced noise, and the effectiveness of reducing joint stiffness in decreasing cavity noise, particularly through diminished translational coupling. Ohayon et al. [87,88] (1995,1998) book covered comprehensively overviews numerical methods used in fluid-structure interaction. It discusses various techniques and applications for analysing the interaction between fluid and structural systems, which is crucial for solving complex engineering problems involving these coupled systems. In 1998, V. Jayachandran et al. [89] highlighted the limitations of Green's function for vibrating boundaries due to Gibbs' phenomenon, proposing a more accurate and faster-converging solution for

inhomogeneous boundary conditions, while noting that both methods yield similar optimal controls and performance indices in simulations. Guha Niyogi et al. (2000) [90] developed a coupled FE-BE approach using 8-noded quadratic boundary elements and serendipity Mindlin elements to model the interaction between acoustic cavities and the laminated composite enclosure surfaces, enhancing the accuracy of structural-acoustic analysis. Gaul et al. (2002) [91] developed a coupled symmetric FE-BE method for linear acoustic fluid-structure interaction in both time and frequency domains using a hybrid boundary element method (HBEM) that leverages Hamilton's principle for a symmetric mass and stiffness matrix formulation. Desmet et al. (2002) [92] introduced a computationally efficient technique for steady-state dynamic analysis of coupled vibroacoustic systems by using global wave function expansions of dynamic field variables that satisfy the governing equations. Li and Cheng's (2007) [93] provided an in-depth analysis of the vibroacoustic behaviour of a system comprising a flexible panel backed by a rectangular cavity with a tilted wall. They developed a fully coupled vibroacoustic model to examine the interactions between the structure and the acoustic field within this configuration. The study specifically explores the impact of the tilted wall's geometrical distortion on the system's overall performance. Key metrics in their analysis include the average sound pressure level inside the cavity and the average quadratic velocity of the vibrating plate. Tong et al. (2007) [94] proposed a direct-BEM/FEM method to analyze the vibration and acoustic radiation characteristics of submerged structures, demonstrating its effectiveness over FEM in computing underwater sound radiation, particularly in applications like submerged cylindrical shells and submarine stern structures. Deu et al. (2008) [95] developed a variational formulation and numerical method for vibroacoustic problems in structural–acoustic coupled systems, introducing an additional unknown field at the fluid–structure interface to incorporate various damping models, which enhances noise reduction techniques by modelling the effects of interface damping layers and allows solutions in both frequency and time domains. In 2008, Warszawski et al. [96] introduced a FEM–BEM coupling procedure for modelling the propagation of interacting acoustic–acoustic and acoustic–elastic waves in axisymmetric media, effectively leveraging the combined strengths of the Finite Element Method (FEM) and the Boundary Element Method (BEM) to address complex wave interactions in these environments. Daneshjou et al. (2008) [97] use first-order shear deformation theory (FSDT) to analyse sound transmission into aircraft interior through laminated composite cylindrical shells, focusing on transmission loss across varying Mach numbers and the effects of the composite plate warp angle at both low and high frequencies. He et al. (2011) [98] introduced a coupled edge-based smoothed finite element method (ES-

FEM) and boundary element method (BEM) for fluid-structure interaction problems, achieving superior accuracy and efficiency, especially in high-frequency ranges. This method's practical application to an automobile passenger compartment demonstrates its effectiveness in predicting sound levels and overcoming traditional FEM limitations, making it suitable for various engineering applications. Jiang and Kam (2013) [99] analysed the vibration of elastically restrained laminated composite plates in flat-panel sound radiators. They emphasized the importance of incorporating elastic restraints and the voice coil assembly in finite element models. Their experimental validation showed that simplified models significantly underpredict natural frequencies and vibration shapes. Sahu et al. (2014) [100] discussed a fully coupled FE-BE vibroacoustic analysis for laminated composite structures with enclosed cavities, enabling accurate modelling of structural vibrations and acoustic interactions within the cavity. Das et al. (2016) [101] presented a detailed study of sound pressure levels in symmetric and anti-symmetric cross-ply laminated acoustic cavities, focusing on how variations in wall thickness and the number of laminates affect acoustic responses. Li et al. (2016) [102] developed and validated a finite element method-boundary element method (FEM-BEM) dynamic model for predicting vibration-acoustic coupling in aircraft, showing strong agreement between simulations and experiments, particularly in low to medium frequencies, to enhance understanding vibroacoustic behaviour of aircraft structure for better design and comfort. Zhang et al. (2018) [103] used simple first-order shear deformation theory tailored for vibroacoustic analysis of laminated rectangular fluid-structure coupling systems, emphasising the importance of fluid-structure interaction. It presents a simplified mathematical model validated through numerical examples, showing improved accuracy and computational efficiency compared to existing methods, with significant engineering applications. Zhang Hong et al. (2019) [104] presented a unified analytical model using simplified plate theory (SPT) for vibroacoustic analysis of laminated rotary plates coupled with impedance cavities, demonstrating superior accuracy and efficiency over other methods. Numerical and experimental results reveal that air-filled systems exhibit weak coupling, while water-filled systems show strong coupling with low-frequency responses significantly influenced by geometric parameters. Kim et al. (2020) [105] investigated the sound transmission loss (STL) of multi-layered infinite micro-perforated plates (MPPs) using a prediction model. It reveals that as perforation ratio increases, the equivalent complex mass decreases, leading to a decrease in STL. Zhong et al. (2022) [106] investigated the vibroacoustic behaviour of a circumferentially coupled laminated annular plate with cylindrical cavities using a unified Ritz energy scheme, integrating shear lamination theory and orthogonal

polynomial expansions, and validated the model with numerical and experimental comparisons to provide insights for low-noise design. Zhang et al. (2022) [107] developed a unified analysis model for a rotary composite laminated plate and conical–cylindrical double cavities coupled system, using isoparametric transformation to determine model parameters. Modified Fourier series are employed to define the displacement and sound pressure functions, while the Rayleigh–Ritz method is used to solve the established energy functional of the structure and acoustic domains. The findings reveal that impedance walls reduce sound pressure amplitude and suppress resonance, and the composite laminated plate exhibits effective noise reduction. AllahTavakoli et al. (2023) [108] introduced a hybrid parameter updating method to enhance vibroacoustic modelling of composite panels, combining hierarchical functions, inhomogeneous wave correlation (IWC) approach, and least squares optimisations. Laboratory experiments validate the method, including Laser Doppler Vibrometry and sound pressure level measurements on composite and isotropic panels. Chen et al. (2023) [109] investigated how thermal effects impact Coupling Loss Factors (CLFs) in vibroacoustic systems using Statistical Energy Analysis, showing CLFs decrease with temperature, influenced more by stress stiffness. Zhang et al. (2023) [110] presented a vibroacoustic analysis of a cavity with ribbed panels, revealing that rib enhancement reduces energy transmission, while multiple ribbed panels with air gaps improve attenuation, with larger gaps resulting in better sound attenuation. Wang et al. (2023) [111] investigates the vibroacoustic behaviour of carbon fibre reinforced composite laminates under transient impact loads, revealing that the [0°/90°] 5s orthogonal lay-up scheme improves acoustic radiation performance. Huang et al. (2023) [112] demonstrate that embedding shape memory alloys (SMAs) in orthogonal antisymmetric composite laminates can significantly enhance vibroacoustic sound quality. By adjusting SMA parameters and matrix material ratios, sound characteristics such as loudness, sharpness, and roughness can be effectively controlled, especially in high-temperature environments. El Kharras et al. (2023) [113] presented a comprehensive study on the vibroacoustic behaviour of multi-layered micro-perforated plates within acoustic enclosures, focusing on sound transmission, absorption, and resonance suppression effectiveness. Tarkashvand et al. (2024) [114] analysed vibroacoustic behaviour in partially filled laminated composite cylinders using two coordinate systems, exploring fluid height, materials, and load distribution effects on structural deformation and acoustic pressure. Zhang et al. (2024) [115] analysed vibroacoustic characteristics in a coupled system of composite laminated rotationally stiffened plates with various acoustic cavities, including cylindrical, spherical, and conical shapes.

2.5 Interior Acoustics with Multi-domain

The multi-domain Boundary Element Method (BEM) is crucial in acoustic analysis because it effectively manages complex geometries, reduces computational effort, and enhances solution accuracy. By dividing a structure into smaller, more manageable subdomains, it tackles intricate acoustic problems where geometry plays a critical role in sound propagation and scattering. This division reduces computational workload, as each subdomain can be solved independently and then combined, making it highly efficient for large-scale problems. Additionally, multi-domain BEM improves accuracy through precise modelling of boundary conditions and interactions within the structure. Its flexibility makes it suitable for both interior and exterior acoustic applications, including noise control, underwater acoustics, and acoustic device design. Furthermore, BEM naturally provides non-reflecting boundaries, which are essential for accurately simulating open-field acoustic scenarios without artificial reflections.

There is limited research available on the analysis of irregularly shaped structures using the multi-domain Boundary Element Method (BEM). A notable study by Lachat et al. [116] in 1976 transformed three-dimensional elastostatic field equations into boundary integral equations, facilitating the analysis of complex structures by dividing them into subregions. This approach employed Gaussian quadrature formulas for accurate evaluation of boundary integrals, demonstrating its practical application in complex engineering scenarios, such as the analysis of a nuclear reactor pressure vessel. In 1977, Rizzo et al. [117] introduced an advanced Boundary integral equation method, highlighting its unique boundary-focused approach and enhanced capabilities. It draws parallels with Finite Element methods and validates its effectiveness through comparisons with existing results on stress and thermal effects. Cheng et al. [118] (1991) introduced a multi-domain BEM to enhance the prediction of acoustic responses and transmission loss in mufflers, effectively handling complex geometries by dividing the domain into subdomains with distinct boundary conditions. Their method, validated against experimental data, proved accurate and efficient for silencers with intricate structures. In 1994, Wu et al. [119] used the Multi-Domain Boundary Element Method (MBEM) to model sound transmission through thin structures. They assume continuity of normal velocity at the interface and introduce an admittance matrix to relate the pressure jump across the structure to the velocity. Their method couples the two fluid domains on either side of the structure, providing a more comprehensive solution than an uncoupled approach. Layton et al. (1997) [120] used symmetric Galerkin multi-zone BEA formulation, which is more computationally efficient than collocation-based BEA for medium-to-large elasticity problems by exploiting block symmetry, though its advantage diminishes with an increasing number of

zones. The method is especially effective for problems with pre-defined or arbitrarily defined zones, such as in composite materials. Lothar et al. (1999) [121] introduced a method for teaching the Boundary Element Method (BEM) by integrating fundamental undergraduate concepts like rod vibrations and finite elements, extending them to acoustics and elastodynamics, and addressing fluid-structure interaction using both unsymmetric and symmetric hybrid BEM approaches, with practical applications such as sound radiation from vibrating structures. In 2001, Ju et al. [122] introduced a method combining boundary element methods (BEM) for acoustics and finite element methods (FEM) for structures, eliminating the need for interface boundary conditions and validating it through experiments that showed good agreement in frequency responses and sound pressure levels. In 2002, Wu et al. [123] introduced a direct mixed-body boundary element method (BEM) for modelling packed silencers without requiring zonal division. By combining integral equations for all subdomains and using normal-derivative integral equations at interfaces, the method functions like a multi-domain BEM but in a single-domain manner. This approach simplifies the modelling process and accurately predicts transmission loss, with results closely aligning with experimental data. In 2003, Jeong et al. [124] investigated the computational characteristics of the multi-domain BEM (MBEM) for interior acoustic fields, demonstrating that with proper division of a single cavity into subdomains, MBEM can achieve more accurate and efficient computation than the single-domain BEM (SBEM), using a two-dimensional long duct as an example. Zeng et al. [125] (2004) introduced multi-domain pseudospectral time-domain (PSTD) method using Chebyshev Lagrange polynomials and an unsplit-field PML is developed for efficient simulation of 2D and 3D acoustic waves in lossy media, validated by analytical solutions, which is effective for complex geometries. In 2005, Jeong et al. [126] demonstrated that using the multi-domain boundary element method (MBEM) for shape optimization in acoustic interior problems, significantly enhances computational efficiency by reducing matrix inversion tasks, especially in iterative processes, as shown through the example of optimising noise reduction in a two-dimensional automotive interior cavity. Hyeon et al. [127] (2005) proposed a new method using multi-domain BEM to overcome the limitations of conventional BEM for 3D silencers, formulating algebraic equations with particle velocities as unknowns. This method, validated by experimental results, offers computational efficiency and accurate transmission loss predictions for complex acoustic structures. In 2007, Ju et al. [128] introduced a multi-domain BEM for calculating transmission loss in 3D silencers with complex connections, validated by experimental results for a splitter silencer model. Wu (2008) [129] illustrated the significance of the multi-domain boundary element method (MBEM) in

acoustics combined with the direct mixed-body boundary element method (DMBEM), enables efficient solutions to complex problems involving multiple media and thin bodies. This approach is memory-efficient and versatile, making it particularly valuable for applications like muffler and silencer analysis. In 2009, Cheng et al. [130] highlighted the use of multi-domain boundary element method (MBEM) for acoustic sensitivity analysis in optimising vibrating structures. MBEM improves computational efficiency by reducing repetitive calculations, making it ideal for large-scale problems and practical engineering applications. Soares (2011) [131] explored multi-domain decomposition techniques for modelling interacting acoustic-elastic waves using various numerical methods, emphasising the flexibility and efficiency of explicit and implicit coupling algorithms. The study demonstrates the effectiveness of independent spatial and temporal discretisation in improving the accuracy and robustness of the coupled numerical models. Larbi et al. (2015) [132] presented a finite element model for analysing sound transmission through double sandwich panels with a viscoelastic core. Using a reduced-order approach and the Rayleigh Integral, the model efficiently calculates radiated sound power, validated by accurate results. Zhang et al. (2020) [133] proposed a multi-domain spectral approach for vibroacoustic analysis of interior structural-acoustic problems with discontinuous boundaries, offering high accuracy and computational efficiency at higher frequencies. The method is validated through finite element simulations, demonstrating significant computational advantages over traditional finite element methods for complex systems. Wang et al. (2022) [134] investigated the vibroacoustic behaviour of a coupled cavity-panel-cavity system using the Spectro-Geometric method, which employs Fourier series for efficient modelling. Factors like panel size, position, and boundary conditions are analysed, showing the method's computational advantage over FEM/BEM in complex geometries and its impact on modal shapes and natural frequencies. Preuss et al. (2022) [135] provide a comprehensive review of modern applications of acoustic boundary element methods (BEM), focusing on advancements such as viscothermal wave propagation and surface contribution analyses. Chai, et al. (2023) [136] introduced the Dual Interpolation Boundary Face Method (DiBFM-HMLS) to improve interpolation accuracy in geometric structures with small chamfers or short edges, and propose a multi-domain method combining DiBFM-HMLS with matrix condensation for precise 3D elasticity modelling. This approach ensures accurate interpolation across multi-domain models and allows for free meshing at interfaces. Tang et al. (2024) [137] introduced a hybrid approach that combines the finite element method (FEM) for complex interior domains with an artificial boundary element method (ABEM) for the exterior. This method improves computational efficiency and accuracy in acoustic scattering problems

by simplifying the fluid domain, reducing calculation time without sacrificing precision, making it ideal for applications like cavity scattering and vibroacoustic analysis.

2.6 Exterior Acoustic Analysis

The early works laid a strong foundation for the development and application of Boundary Integral Methods (BIMs) in addressing acoustic problems for the exterior acoustic. Notably, Fredholm's [63] work on integral equations in 1903 was instrumental in formulating BIMs for acoustic radiation issues. In the early 1960s, classical formulations of acoustic radiation from vibrating bodies using integral equations began to take shape. Beranek's [47] 1954 textbook provided a comprehensive overview of acoustics, covering a range of acoustic radiation problems and the application of BIMs in solving these challenges. In these works, exterior steady-state acoustic radiation problems for bodies of arbitrary shape were investigated. Chen et al. (1963) [138] described the acoustic field by a distribution of surface sources of unknown strength at the shell-fluid boundaries, which led to a set of integral equations. This numerical technique is named Simple Source Formulation (SSF) in which the acoustic pressure at an exterior field point is represented in terms of a surface integral of a source density function. Computational results were given for two-sample problems such as a piston set in a rigid sphere, and a stiffened cylindrical shell of finite length in water. Chertock (1964) [139] developed a numerical method utilizing the discretized Surface Helmholtz Integral (SHIE) for the solution of radiation problems involving surfaces of revolution. Another approximate method was presented by Williams et al. (1964) [140] in which the far-field pressure was approximated by a truncated series of spherical Hankel functions. The method was shown to be most accurate for radiating surfaces that are nearly spherical. Copley [141] (1967) proposed a method applicable to radiation from surfaces of revolution utilizing the Interior Helmholtz Integral Equation (IHIE). All these types of integral formulations for obtaining approximate solutions to the exterior steady-state acoustic radiation problem for an arbitrary surface were discussed by Schenck [142] (1968) by proposing a Combined Helmholtz Integral Formulation (CHIEF) to overcome the deficiencies and computational difficulties in the previous works. Burton and Miller [143] (1971) discussed integral equation methods for exterior problems in Laplace's and Helmholtz equations, addressing non-uniqueness by introducing a second integral equation. Engblom et al. [144] (1975) redefined modal analysis to effectively compute sound pressure levels in infinite acoustic mediums arising from harmonic vibrations within enclosed structures. Their study focuses on cylindrical cavities and elastic spheres, illustrating the method's versatility in handling complex structures like solid isotropic, hollow isotropic,

and laminated orthotropic spheres in acoustic environments. Employing a finite element approach, they integrate velocity mobility and impedance matrices to investigate the responses of closed structures. Bell et al. [145] (1977) presented an integral approach for predicting the acoustics of arbitrarily shaped bodies in deriving a new boundary integral equation for predicting the acoustics of arbitrarily shaped bodies. Stepanishen [146] (1977), studied the radiation impedance of a rectangular piston to calculate the radiation impedance of a rectangular piston. Meyer et al. [147] (1978) explored the development of a technique for generating sound fields radiated by three-dimensional bodies with arbitrary shapes. They utilised the solutions from the Helmholtz equation and implemented the Burton and Miller method to address non-uniqueness in the external Helmholtz formulas, particularly focusing on the internal eigenfrequencies of the geometry under examination. Watson [148] (1979) proposed an advanced implementation of the boundary element method for two and three-dimensional elastostatics. In his publication he proposed subdividing elements into sub-elements for integration, thereby enhancing the accuracy of the results obtained. Koopman et al. [149] (1982), presented a method for computing the sound power of machines based on the Helmholtz integral. In 1982, Kinsler et al. [55] published the fourth edition of their book which provided an in-depth understanding of acoustics and is considered a standard reference in the field. Seybert et al. [150] (1983) applied the BIE method to sound radiation problems using a new method for solving sound radiation problems using the boundary integral equation method and an isoparametric element. The BEM was used to obtain numerical solutions to the same classical radiation problems. Levine, H. et al. [151] (1983) established single integral representations for the resistive and reactive components of the radiation impedance of a rectangular piston, allowing for systematic refinement of estimates at both short and long wavelengths. They introduced an isoparametric element formulation in which both the surface geometry and the acoustic variables on the surface of the radiating body were represented by quadratic shape functions. In addressing challenges associated with the application of the Boundary Element Method (BEM) to acoustic radiation at characteristic frequencies, Amini's [152,153] work during 1982 and 1983 played a particularly influential role, focusing on highly accurate numerical methods specifically tailored for boundary integral formulations of the Helmholtz equations in the exterior domain. Piaszczyk et al. [154] (1984), proposed an iterative overdetermination scheme to address non-uniqueness issues in the study of acoustic radiation from vibrating surfaces at characteristic frequencies. This approach significantly enhances the understanding of this phenomenon. Concurrently, Brod [155] (1984) demonstrated the uniqueness of solutions for all wavenumbers in acoustic radiation, highlighting the

effectiveness of “null-field” equations derived from Green’s function. These contributions provide valuable insights into overcoming complexities in BEM applications for acoustic scenarios. These publications significantly advance the field of acoustic radiation problems, offering a deeper understanding and leading to the development of new and improved solution methods. Imai et al. (1985) [156] explored holographic interferometry and boundary element calculation to assess the radiation efficiency of engine structures, providing valuable insights into practical applications. Seybert et al. (1986) [157] developed a specialized integral equation formulation for acoustic radiation and scattering, focusing on axisymmetric bodies and unique boundary conditions. Seybert et al. 1985 [156] and 1986 [158] significantly advanced computational methods for radiation and scattering of acoustic waves in three dimensions, contributing to the broader understanding of these phenomena. Amini et al. (1986) [159] further investigated boundary element methods, specifically addressing exterior acoustic problems. Seybert et al. (1987) [160] applied the Boundary Element Method (BEM) to interior acoustic problems using the Helmholtz equation, avoiding the non-uniqueness issues found in exterior problems. They demonstrated accurate solutions for cavity response and muffler transmission loss, validated against analytical and finite element method (FEM) results. Seybert et al. (1987) [161] employed the CHIEF algorithm to obtain unique solutions for acoustic radiation using boundary integral equations, showcasing the practical applications of these numerical techniques. Amini (1987) [162] made noteworthy contributions by developing an iterative method specifically tailored for the boundary element solution of exterior acoustic problems. Concurrently, Croker (1987) [163] delved into experimental work on the Ricardo crankcase simulation rigs, offering valuable insights into the practicalities and prediction of engine noise. Concurrently, Cunefare et al. (1989) [164] developed a boundary element method for acoustic radiation that remained valid across all wavenumbers, further expanding the applicability of these methods. Brebbia et al (1989) [70] served as an introductory guide to boundary elements, offering valuable insights into the theory and applications of this computational method. It is designed to provide a simple and comprehensive understanding of boundary elements, making it a valuable resource for those venturing into the field or seeking foundational knowledge in computational mechanics. Kirkup (1989) [165] furthered the field by introducing a boundary element method for acoustic radiation based on a hybrid formulation. The work of Seybert et al (1990) [166] represented a significant advance in the development of BEM methods for solving coupled interior/exterior acoustic problems. The new BEM developed by the authors is accurate, efficient, and easy to implement. It is expected to be a valuable tool for solving a wide range of coupled interior/exterior acoustic problems. Stanton's (1990) [167] work utilized

the boundary element method to explore sound scattering by spherical and elongated shelled bodies, adding depth to the understanding of acoustics. Juhl (1993) [168] contributed a comprehensive textbook on the boundary element method for sound field calculations. Stewart et al. (1996) [169] developed an adaptive finite element method for the Helmholtz equation in exterior domains. This method is more efficient than traditional finite element methods for solving acoustic radiation problems with complex geometries. Stewart et al. (1997) [170] developed an H-adaptive finite element method for the time-harmonic exterior acoustics problem in two dimensions. This method is even more efficient than the method developed in their previous paper. Zaman (2000) [171] conducted a comprehensive review of boundary integral formulations of acoustic scattering problems. This review provides a valuable resource for researchers and practitioners who are interested in using BIMs to solve acoustic scattering problems. Lee's [172] (2002) pivotal study of the nonlinear natural frequency of a rectangular box with one flexible plate and five rigid plates, analyses the structural-acoustic coupling between the flexible plate and the air cavity using a finite element modal method. Schuhmacher et al. (2003) [173] developed a sound source reconstruction method using inverse boundary element calculations, while Visser (2004) [174] introduced a boundary element approach to acoustic radiation and source identification. Marburg et al. [175] collaborative study in 2005 that conducted a comparative analysis of the treatment of irregular frequencies for cat's eye radiation using boundary elements. Wright et al. (2005) [176] applied boundary element methods to near-field acoustic measurements on cylindrical surfaces. Guha Niyogi (2006) [177] investigated interconnected structural acoustic concerns in laminated composite enclosures by employing an isoparametric quadratic boundary element formulation that is coupled to structural properties via mobility relations. The results demonstrate frequency-dependent impacts of absorbent layers, thereby implying the possibility of enhancing performance through adjustments in structural damping. Denli et al. (2007) [178] reviewed the composite sandwich modelling and optimisation techniques for structural acoustic problems, emphasising the lack of experimental work on vibration and acoustic transmission through the multilayered sandwich plate. Wu [179] (2008) demonstrated the multi-domain boundary element method in muffler and silencer analysis to demonstrate the effectiveness of this method in thin-body radiation and scattering coupled with the direct mixed-body method. Marburg et al. [180] (2008) comprehensive exploration of Finite Element Method (FEM) and Boundary Element Method (BEM) applications in computational acoustics serves as a pivotal resource, providing theoretical foundations and practical insights into noise propagation in fluids. Marburg et al. (2008) [181] contributed to the discourse by discussing methods for addressing

irregular frequencies in boundary element approaches. These collective efforts during this period significantly enriched the understanding and application of boundary element methods in solving various acoustic challenges. Biermann et al. (2009) [182] contributed by developing higher-order finite and infinite elements, specifically tailored for solving Helmholtz problems. Wright et al. (2009) [183] utilised a distributed computing system to predict acoustic radiation from axisymmetric surfaces with arbitrary boundary conditions, employing the boundary element method. Venkatesham et al. [184,185] (2008,2010) provided an analytical method for predicting breakout noise from a rectangular plenum with four flexible walls, incorporating the modal characteristics of the uncoupled structural and acoustical systems. Yang et al. (2010) [186] took a multifaceted approach, coupling the finite element method with the boundary element method to simulate the vibroacoustic response of an elastic target.

Thomas et al.'s [187] (2011) groundbreaking research introduces the Sound Quality Contribution Factor (SQCF), revolutionising electric vehicle interior sound design through a two-level optimisation scheme. Meanwhile, Butkus et al. (2011) [188] delved into acoustic investigations focusing on both the exterior and interior walls of a log house. Zhou et al. [189] (2012) analysed automobile passenger compartment acoustics using frequency response analysis and the Boundary Element Method (BEM), focusing on modifying panel properties and seat cushion materials to reduce acoustic pressure at the driver's and passenger's ears, thereby influencing purchasing decisions. Qian et al. [190] (2012) presented an efficient method for simulating seismo-acoustic scattering in multilayered media using global matrix propagators to overcome memory constraints, accurately modelling seismic wave propagation and underwater explosive sources, which is essential for deep ocean acoustic experiments. D'Alessandro et al. [191] (2013) reviewed the acoustic properties of sandwich panels, emphasizing validated sound transmission models and the critical role of incorporating the radiation loss factor for accurately evaluating the panel's loss factor. Zhou et al. [192] (2014) proposed an efficient method to uncover nonlinear phenomena in vibroacoustic systems, showing that manipulating excitation frequency near the oscillator's natural frequency significantly affects vibration and acoustic radiation, particularly third-harmonic generation, with implications for designing and controlling nonlinear oscillators. Ramesh et al. (2015) [193] conducted a comparative analysis, contrasting constant and discontinuous quadratic boundary elements for exterior axisymmetric acoustic-wave propagation problems. Praveena et al. [194] (2016) studied breakout noise in flexible rectangular ducts using an analytical model validated with FEM and BEM, considering coupled acoustic-structural behaviour to

identify efficient radiating modes by analysing duct acoustic and structural modes. Jin et al. [195] (2016) proposed a modelling method for predicting 3D rectangular opened enclosure acoustic responses with a rectangular opening of arbitrary size and general wall impedance. They utilise a convenient analytical approach, addressing the lack of studies on coupled acoustic problems in 3D opened cavities. Recently Ouedraogo et al. [196] (2016) investigated further diverse realms, from circular multi-cavity mufflers for noise reduction in a circular duct to utilising perforated screens and air cavities to enhance scattering mechanisms, aiming to identify optimal configurations for reducing exhaust noise from helicopter turboshaft engines. The work of Das et al. (2016) [197] provided valuable insights into the vibroacoustic characteristics of acoustic cavities confined inside cross-ply laminated composite enclosures. This work can be used to design and optimise these structures for improved acoustic performance. The authors' work also highlights the potential of BIMs for solving vibroacoustic problems in composite structures. Galgalikar et al. [198] (2016) developed an optimisation method for honeycomb unit cells in sandwich panels to enhance sound transmission loss (STL) while maintaining mass and dimensional constraints. Using structural acoustic finite-element modelling and MODEL FRONTIER software, they identified optimal geometric parameters, achieving at least a 20% improvement in STL over standard hexagonal honeycomb panels. The study highlighted the significant impact of cell wall angle and unit cell count on acoustic performance. Shen et al. [199] (2017) comparative study evaluated algorithms for enhancing acoustic attenuation in reactive mufflers, highlighting GA and PSO algorithms as particularly effective. Sedaghatjoo et al.'s [200] (2017) exploration focused on the uniqueness of numerical solutions for boundary integral equations with 3-times monotone radial kernels. Marburg (2017) [201] offered insights into recent developments and opportunities in conventional boundary element techniques. Du, J.et al.[202] (2018) used the Improved Fourier series method for acoustic-vibroacoustic modelling of combustion systems, verified through numerical examples and analysis of boundary conditions. The comprehensive review by Fahy et al. [203] in 2018 covered the modelling and prediction of acoustic coupling between vehicle interiors and exteriors, considering factors such as geometry, material properties, and environmental conditions. Marburg's [204] (2018) chapter introduced the boundary element method for solving time-harmonic acoustic problems. Shi et al.'s [205] (2018) work outlined a method for vibroacoustic modelling of a coupled acoustic system, with a focused on partially opened cavities and flexible plates. Li et al. [206] (2018) proposed a Modified Dual-Level Fast Multipole BEM (MDFMA) to tackle storage and ill-conditioning issues in BEM. By using a locally supported sparse matrix and a dual-level structure, MDFMA achieves O(N) efficiency

in operations and memory, significantly accelerating computations, especially for high condition number interpolation matrices. Singh et al. [207] (2018) paper explored the use of sustainable materials, such as jute felt and waste cotton, for HVAC noise control in vehicles, demonstrating a reduction in annoyance through effective treatment and human-subject evaluation. Zhong et al.'s [208] (2019) study explored predicting aerodynamic noise in passenger vehicles, identifying key contributors and applying statistical energy analysis. Shi et al. [209] (2019) studied the vibroacoustic behaviours of an L-shaped plate–cavity coupling system using the Fourier series method. They found that the natural frequency increases with spring stiffness, and resonance is effectively attenuated by a cuboid acoustic cavity with an impedance wall, with material properties significantly influencing displacement response and sound pressure. Kirkup [210] (2019) reviewed the application of the boundary element method (BEM) in acoustics, focusing on its use for problems governed by the Helmholtz equation and extending to vibroacoustic and aero-acoustic challenges. The paper also highlights computational improvements and the potential for a software library approach to enhance BEM efficiency. Sami et al.'s (2019) [211] work highlighted the importance of integrating acoustic considerations into interior design, which can significantly enhance both the aesthetic and functional aspects of a space. Han et al.'s [212] (2020) research offers a holistic approach to studying vibration and noise in multibody systems under impact loading. Zhao et al.'s [213] (2020) presentation introduces a novel approach to topology optimization for acoustic-structure interaction systems, addressing challenges in interface variation. Wang et al.'s [214] (2020) paper proposes an efficient method for acoustic topology optimization using Vibroacoustic Coupled Craig–Bampton Mode Synthesis, significantly reducing computation time. Qian et al.'s [215] (2021) contributions focus on electric vehicle sound design, introducing Transfer Path Analysis and Synthesis to optimise interior noise. Li et al.'s [216] (2021) application of the Elman neural network algorithm predicted vehicle noise levels, providing an effective optimisation method for Noise, Vibration, and Harshness (NVH) performance. Kun et al.'s [217] (2021) method predicts the dynamic behaviour of 3D coupled acoustic systems, emphasizing partially opened cavities and flexible plates. In recent years, the field of vehicle acoustics has witnessed significant advancements, as evidenced by a collection of influential research studies. Tang et al.'s [218] (2022) computational method studied acoustic interaction with large underwater structures, leveraging the physical mechanisms of structural acoustics. The collective findings contribute to a deeper understanding of the complex dynamics involved in enhancing vehicle sound quality and comfort, paving the way for future innovations in the field. Münder et al. (2022) [219] conducted a literature review, particularly focusing on

perceptual parameters of interior soundscapes in electrified vehicles. Recent developments include Fakhraei et al. (2023) [220], who developed modified 2.5D singular boundary methods to address spurious eigen solutions in exterior acoustic problems. Gonçalves et al. (2023) [221] contributed by developing an optimisation strategy for the precise placement of CHIEF points in boundary-element acoustic problems. Collectively, these studies represent a diverse and dynamic landscape of research endeavours in the field of acoustics.

2.7 Research Gap

The above comprehensive overview highlights the dynamic evolution of research in structural-acoustic interaction using advanced BEM, reflecting diverse methodologies and applications. However, it has been observed that there is still a dearth of research on structural acoustic analysis for lightweight structures that are coupled to the external environment. As, vehicular cavities are made up of light weight structures with openings, this research is crucial for assessment of sound pressure level both inside and outside the cavity. The development of BEM in a multi-domain environment is essential to analyse irregular, complex-shaped cavities. After careful investigation of existing literatures, it is observed that there is no integrated coupled analysis approach where a general complicated-shaped flexible composite enclosure with opening at the boundary wall can be analysed for acoustic pressure both inside and outside the cavity, with or without application of absorbent coatings on multiple walls, utilising multi-domain coupled BE-FE method. This is the motivation behind this research.

2.8 Objective

It is evident from the literature review above that while there is a lot of research on the subject of interior and exterior acoustic analysis of vehicles, the structures that are employed in these studies are often simple in shape. Few studies have been conducted on interior coupled structural acoustic problems using laminated composite materials to determine the acoustically soft areas of irregularly shaped acoustic cavity boundaries with openings.

Hence, the proposed research aims to examine the vibroacoustic response of a complicated-shaped composite acoustic cavity, having a combination of rigid and flexible panels and windows, by analysing the flexible laminated composite structure using the finite element method and the internal fluid domain by boundary element method. Multi-domain boundary element approach has been resorted to ensure accurate computation of sound pressure level when the source and the observation points are not interconnected inside domain. A versatile

program is developed in MATLAB to handle cavities of any shape and multiple interacting boundary panels with arbitrary positions of opening. Coupling of FEM and BEM has been performed using the mobility relation and coupling of the interior and exterior domain has been performed by using continuity condition at the windows to obtain the sound pressure level in and outside the cavity. Various parametric studies have been conducted to analyse the impact of varying flexibility and damping in the boundary wall, placement of absorbent layers etc., to control the acoustic response using passive means. The effect of applying stiffeners judiciously in altering the sound pressure level at our desired frequency range has also been investigated.

2.9 Scope of the Present Work

The scope of the present research may be defined in the following steps:

i. An eight-noded Mindlin plate element with five degrees of freedom (u, v, w, θx, θy) per node, excluding the in-plane rotation θz has been used to analyse composite stiffened folded structures with multiple flexible walls. YNS theory with first-order shear deformation and rotary inertia is adopted to accommodate wide variation between E1 and E2.

ii. Folded plate transformations have been applied by incorporating a very small value of θz to convert the element stiffness and mass matrices from local to global axes before assembling.

iii. A finite element code is developed in MATLAB for the free vibration analysis of the laminated composite/sandwich stiffened folded enclosure. This code has been used to generate the mobility relationship correlating the nodal pressures with nodal velocities normal to the cavity surface.

iv. A multi-domain boundary element code with isoparametric eight-noded serendipity elements has been developed to analyse an acoustic cavity where the nodal pressures and the fluid particle velocities normal to the boundary are the basic variables. The analysis is done in the frequency domain only to solve the Helmholtz equation.

v. The vehicular cavity is divided into several domains with intermediate imaginary interface layers where the continuity conditions of the pressure and the velocity have been taken into consideration, such that $P_1 = P_2;\ V_1 = -V_2$.

vi. The acoustic boundary, S, is assumed to have four different types of boundary conditions.

a. **Rigid boundary,** where the amplitude of normal velocity V=0 at rigid walls and takes some specified value at the exciting wall.
b. **Interaction Boundary,** where at the interacting surface between flexible structure and acoustic domain, neither p nor v is known. Mobility matrix [Q] developed in part iii is used to couple the FEM and BEM and relate normal particle velocity and pressure as shown.
$\{v\} = \{\dot{d}\} = [Q]\{P\}e^{i\Omega t}$
c. **Boundary with absorbent layer,** where the fluid particle velocity V and the structural velocity V_s is related using the acoustic admittance Y and acoustic pressure P as shown.
$V = YP + V_s$
d. **Boundary with opening,** where the exact analysis is done by coupling the interior and exterior domains.

vii. The coupled analysis for an acoustic cavity inside a partly rigid and partly flexible containing structure, along with a window opening, is developed by eliminating the velocity terms at the interaction boundaries from the BE equation.

viii. This code has been validated, mesh convergence is tested, and set to generate new results by inflicting
a. Variation of flexible wall thickness
b. Variation of stiffener position
c. Variation of modal damping ratio
d. Variation in the placement of the absorbent layer
e. Presence of opening
f. Variation of SPL at different locations
g. Variation in the shape of the cavity
h. Variation in SPL pattern for rigid and partially flexible cavity

ix. The feedback from the acoustic responses at the boundary of the structure is used to compute the structural displacement amplitudes and stress amplitudes.

x. Finally, the interpretation of the obtained results is presented, and suitable conclusions have been drawn.

3

Theoretical Formulation

In the vibroacoustic analysis, the cavity structure has been modelled using an orthotropic laminated composite material. To evaluate the coupled acoustic behaviour of this cavity, a free vibration analysis is necessary to obtain the natural frequencies and modal data of the partially flexible cavity. The cavity is modelled as a folded plate structure using finite element analysis (FEA), and the derived modal characteristics are employed in the mobility matrix, which is used in coupled structural acoustic analysis for single-domain or multi-domain cases. Sometimes, to change the acoustic output favorably, stiffeners have been used in the cavity. These stiffeners can be modelled as part of a folded plate too.

Hence, the formulation can be divided mainly in three parts.

I) Finite element analysis of folded composite structure
II) Development of mobility matrix
III) Structural acoustic analysis
    a. Single-domain acoustic analysis
    b. Multi-domain acoustic analysis

3.1.Formulation for Laminated Composite Folded Plate Structure

An acoustic cavity is essentially a special kind of folded plate forming an enclosure. The stiffeners added to the exterior of the cavity walls too are modelled as plate elements. In the finite element analysis of the cavity wall, the first order transverse shear deformation has been employed, which follows the Yang-Norris-Stavsky theory [4] and includes the effect of rotary inertia in the mass matrix formulation.

The displacements of a flat Mindlin plate are fully described by three displacements (u, v, w) and two rotations (θ_x , θ_y) components that follow right-hand cork screw rule as shown in Figure. 3.1.a through 3.1.d. The generalized displacements are as follows [8]

$$
\begin{aligned}
&u(x,y,z) = u_0(x,y) + z\theta_y, \\
&v(x,y,z) = v_0(x,y) - z\theta_x, \\
&w = w_0 \\
&\emptyset_x = \theta_y + w_{,x}, \text{ and} \\
&\emptyset_y = -\theta_x + w_{,y}
\end{aligned}
\qquad (3.1.1)
$$

Generalized linear strains in terms of mid-plane strains are expressed as

$$
\begin{aligned}
&\epsilon_x = u_{,x} = u_{0,x} + z\theta_{y,x} = \epsilon_x^0 + zK_x \\
&\epsilon_y = v_{,y} = v_{0,y} - z\theta_{x,y} = \epsilon_y^0 + zK_y \\
&\gamma_{xy} = u_{,y} + v_{,x} = u_{0,y} + v_{0,x} + z(\theta_{y,y} - \theta_{x,x}) = \epsilon_{xy}^0 + zK_{xy} \\
&\gamma_{xz} = \emptyset_x,\ \gamma_{yz} = \emptyset_y,\ \varepsilon_z = 0
\end{aligned}
\qquad (3.1.2)
$$

where, K_x and K_y are the curvatures along x and y axes and K_{xy} is the cross curvature in xy plane. $\emptyset_x$ and $\emptyset_y$ are the shear rotations in x-z and y-z planes, respectively.

The nodal displacements of a plate finite element are approximated as

$$
\begin{aligned}
&u_0 = \sum_{i=1}^{8} N_i(\xi,\eta)u_{o_i},\ v_0 = \sum_{i=1}^{8} N_i(\xi,\eta)v_{o_i},\ w = \sum_{i=1}^{8} N_i(\xi,\eta)w_i \\
&\theta_x = \sum_{i=1}^{8} N_i(\xi,\eta)\theta_{x_i}, \text{ and} \\
&\theta_y = \sum_{i=1}^{8} N_i(\xi,\eta)\theta_{y_i}
\end{aligned}
\qquad (3.1.3)
$$

in which u_{0_i},v_{0_i}, w_{0_i}, θ_{x_i}, $\theta_{y_i}$are the displacements at node i and N_i are serendipity interpolation functions [8].

The stiffness matrix of a plate element of size a × b assumes the form

$$[K'_e] = \int_{-1}^{1}\int_{-1}^{1}[B]^T[D][B]|J|d\xi\, d\eta \qquad (3.1.4)$$

where,

$$\{\varepsilon\} = \begin{bmatrix} {\varepsilon^0}_x \\ {\varepsilon^0}_y \\ {\gamma^0}_{xy} \\ K_x \\ K_y \\ K_{xy} \\ \gamma_{yz} \\ \gamma_{xz} \end{bmatrix} = \sum_{j=1}^{8} \begin{bmatrix} N_{j,x} & 0 & 0 & 0 & 0 \\ 0 & N_{j,y} & 0 & 0 & 0 \\ N_{j,y} & N_{j,x} & 0 & 0 & 0 \\ 0 & 0 & 0 & 0 & N_{j,x} \\ 0 & 0 & 0 & -N_{j,y} & 0 \\ 0 & 0 & 0 & -N_{j,x} & N_{j,y} \\ 0 & 0 & N_{j,x} & -N_j & 0 \\ 0 & 0 & N_{j,y} & 0 & N_j \end{bmatrix} \begin{bmatrix} u_{0j} \\ v_{0j} \\ w_{0j} \\ \theta_{xj} \\ \theta_{yj} \end{bmatrix} = [B]\{\delta\} \qquad (3.1.5)$$

Here, $\{\varepsilon\}$ is the strain vector, and $\{\delta\}$, the nodal displacement vector, $[B]$ is the strain-displacement matrix, and [D] is the stiffness matrix, given by

$$[D] = \begin{bmatrix} A_{11} & A_{12} & A_{16} & B_{11} & B_{12} & B_{16} & 0 & 0 \\ A_{12} & A_{22} & A_{26} & B_{12} & B_{22} & B_{26} & 0 & 0 \\ A_{16} & A_{26} & A_{66} & B_{16} & B_{26} & B_{66} & 0 & 0 \\ B_{11} & B_{12} & B_{16} & D_{11} & D_{12} & D_{16} & 0 & 0 \\ B_{12} & B_{22} & B_{26} & D_{12} & D_{22} & D_{26} & 0 & 0 \\ B_{16} & B_{26} & B_{66} & D_{16} & D_{26} & D_{66} & 0 & 0 \\ 0 & 0 & 0 & 0 & 0 & 0 & A_{44} & A_{45} \\ 0 & 0 & 0 & 0 & 0 & 0 & A_{45} & A_{55} \end{bmatrix}$$

In [D],

$$(A_{ij}, B_{ij}, D_{ij}) = \sum_{k=1}^{n} \int_{z_{k-1}}^{z_k} {c'^{k}}_{ij} [1, z, z^2]_k \mathrm{dz} \qquad (i, j = 1, 2 \text{ and } 6)$$

$$\text{and } (A_{ij}) = \alpha \sum_{k=1}^{n} \int_{z_{k-1}}^{z_k} {c'^{k}}_{ij} \mathrm{dz} \qquad (i, j = 4, 5) \qquad (3.1.6)$$

Here shear correction factor α= 5/6 and index k indicates loop over the layers of the composite. The mass matrix of the plate element is given by

$$[M'_e] = \int_{-1}^{1} \int_{-1}^{1} [N]^T [\rho] [N] \, |J| d\xi \, d\eta \qquad (3.1.7)$$

$[\rho]$ being the density matrix and $|J|$ being the Jacobian of transformation for integrating numerically between ±1.

A 3-point Gauss quadrature is applied for computation of the bending stiffness of the elements, whereas a 2-point integration is adopted [31] to compute the shear stiffness and the mass matrix to avoid shear locking.

(a) Local axes

Global axes

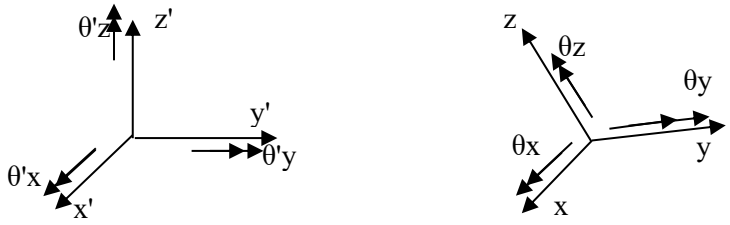

(b) Local axes

Global axes

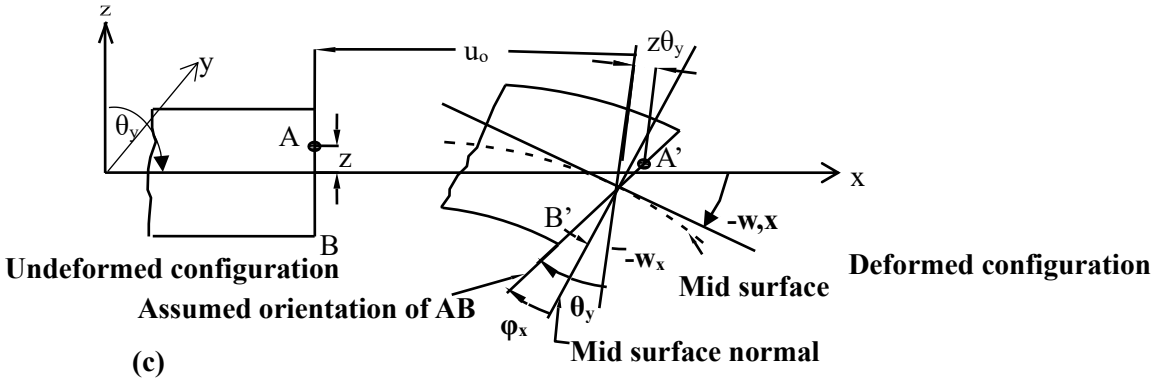

(c)

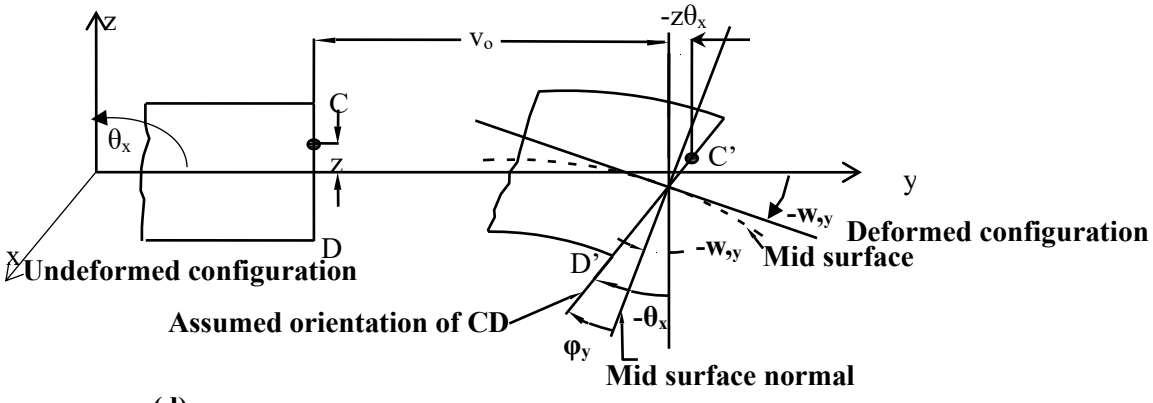

(d)

Fig. 3.1.1: Transformation of (a) translations and (b) rotation from local xi′-axes to global x_i-axes. Detail deformation of the laminated composite plate in (c) x-z plane and (d) y-z plane

For stiffened cavity, the stiffeners are modelled as plate elements appended to the main cavity structure. Hence, for stiffened cavity and folded cavity structure a transformation is applied to convert the stiffness and mass matrices from local (x'_i) to global axes (x_i) (Fig. 3.1.1). The relations between local and global displacements are given in [8]

$$\{u'\} = [T]\{u\}$$

Here,

$$[T] = \begin{bmatrix} \cos(x,x') & \cos(y,x') & \cos(z,x') & 0 & 0 & 0 \\ \cos(x,y') & \cos(y,y') & \cos(z,y') & 0 & 0 & 0 \\ \cos(x,z') & \cos(y,z') & \cos(z,z') & 0 & 0 & 0 \\ 0 & 0 & 0 & \cos(x,x') & \cos(y,x') & \cos(z,x') \\ 0 & 0 & 0 & \cos(x,y') & \cos(y,y') & \cos(z,y') \\ 0 & 0 & 0 & \cos(x,z') & \cos(y,z') & \cos(z,z') \end{bmatrix}$$

= Transformation Matrix (3.1.8)

Finally, the global stiffness and mass matrices are expressed as,

$$[K]_e = [T]^T[K']_e[T], \quad (3.1.9)$$

$$[M]_e = [T]^T[M']_e[T], \quad (3.1.10)$$

To apply the transformation, the stiffness and mass matrices are expanded to fit the sixth drilling degrees of freedom per element. A very small positive number (nearly 1000 times smaller than the smallest leading diagonal) is used at the corresponding leading diagonal terms [9] whereas the off-diagonal terms corresponding to the θ_z are set to zero.

Applying the minimization of total potential energy Π, the equilibrium equation for the free vibration (Eq. 3.1.11) is developed and the undamped natural frequencies of the structure are extracted.

$$([K] - \omega_n{}^2[M])\{\delta\} = 0, \quad (3.1.11)$$

By solving this eigen equation in MATLAB program natural frequency ω and mode shape Φ has been extracted and used in the mobility relation.

3.2.The Mobility Relation

A relation between nodal velocities and nodal forces is obtained from the governing equation of motion for the multi-degree of freedom (MDOF) system, subjected to harmonic loading

$$[M']\{\ddot{d}\}+C\{\dot{d}\}+[K']\{d\}=F_0e^{i\Omega t} \quad (3.2.1)$$

Ω being the forcing frequency in radians per second

Since the problem involves a time-harmonic forcing function, the modal solution technique is chosen for the solution. The solution of Eq (3.2.1) for the displacements is given by [90]

$$\{d\} = [\,[\Phi]\,\{diag\,(\frac{1}{\omega_k^2-\Omega^2+2i\Omega\xi_k\,\omega_k})\}\,[\Phi]^T]\,F_0e^{i\Omega t} \quad (3.2.2)$$

$$\{d\}=[\alpha]\,F_0e^{i\Omega t} \quad (3.2.3)$$

Here, ξ_k and [Φ] denote the modal damping ratio and mass-normalized set of eigenvectors for the uncoupled structure, respectively, while *diag(i)* indicates leading diagonal terms of receptance matrix [α], the off-diagonal terms being zero.

The matrix [Q'], required for the structural-acoustic coupling is obtained by differentiating the above relation with respect to time, to obtain modal velocity terms for the structure:

$$\{v\} =\{\dot{d}\}=[\Omega(\Phi)[\mathrm{diag}\left(\frac{2\Omega\omega_k\,\xi_k+i(\omega^2-\Omega^2)}{(\omega_k^2-\Omega^2)^2+4(\Omega\xi_k\omega_k)^2}\right)]\Phi^T]F_0e^{i\Omega t} = [Q']F_0e^{i\Omega t} \quad (3.2.4)$$

Only the normal-to-the-boundary components of the velocity and forces are retained in the [Q'] matrix while coupling the structural and acoustic domains. In the case of stiffeners, the component of velocity and forces normal to the base plate on which the stiffeners are attached are accounted for and added to the combination of the finite element attached to the boundary element node of the acoustic cavity to account for the contribution of stiffeners in the cavity wall.

The coupled velocity terms can be expressed in the form of pressure terms at the interacting interfaces through an area matrix [A] as given below:

$$\{f\}^e = [A]^e\{p\}^e \quad (3.2.5)$$

$$\text{Here, } A_{ij}^e = \int_{S_e} N_i\,N_j\,dS_e,\ i,j=1\sim8 \quad (3.2.6)$$

In component form, Equation (3.2.4) may be written as

$$f_i^e = \sum_{j=1}^{8} (\int_{S_e} N_i N_j) p_j^e dS. \quad (3.2.7)$$

where N_i are the shape functions for any boundary element. For a constant element, the area matrix would have been a scalar term equal to the area of the element. Combining Equations (3.2.4) and (3.2.7), and selecting only the normal velocity and pressure components on the interacting zone, the final mobility relation can be expressed as

$$\{\boldsymbol{v}\} = [Q']\{p\} \quad (3.2.8)$$

$$[Q'] = \left[\Omega[\Phi]\left[diag\left(\frac{2\Omega\omega_k\xi_k + i(\omega_k^2 - \Omega^2)}{(\omega_k^2 - \Omega^2)^2 + 4(\Omega\xi_k\omega_k)^2}\right)\right][\Phi]^T[A]\right]$$

where $[Q']$ is the desired mobility matrix, while $\{\boldsymbol{v}\}$ and $\{p\}$ are the nodal velocities and pressures, respectively, at the flexible interacting zones of the boundary.

3.3.Analysis of the Acoustic Domain

3.3.1. Single-domain Acoustic Analysis

The governing equation of a time-harmonic acoustic problem is given by the reduced wave (Helmholtz) equation [55]

$$\nabla^2 p + k^2 p = 0 \quad (3.3.1)$$

Here, *p* stands for the acoustic pressure while *k* represents the wave number given by the ratio *ω/c* with *ω* being the radian frequency of the harmonic sound wave and *c* the speed of the sound through the acoustic medium.

The corresponding boundary integral equation is given by [160]:

$$C(P)p(P) = \int_S p\frac{\partial G(P,Q)}{\partial n} ds_Q - \int_S G\frac{\partial p(P,Q)}{\partial n} ds_Q \quad (3.3.2)$$

The fundamental solution *G (P, Q)* in Equation (3.3.2) is the solution to the non-homogeneous Helmholtz equation, the non-homogeneous term being the Dirac delta function:

$$\nabla^2 p^* + k^2 p^* = \delta\{r(P,Q)\} \quad (3.3.3)$$

The free space Green's function, *G*, is given by [160]

$$G = e^{-ikr(P,Q)}/4\pi r(P,Q) \quad (3.3.4)$$

Here, *P* is a source point that may be inside the acoustic domain, *V*, or, on the boundary, *S*, of the acoustic domain, *Q* is a field point that lies on the boundary, *S,* while *r* (*P*, *Q*) is the distance between the points *P* and *Q* (Figure 3.3.1). For interior problems, where the acoustic fluid domain lies inside the bounding surface, the direction of the unit normal *n* on *S,* is directed outwards with respect to the confined fluid domain. *C* (*P*) is a constant depending upon the location of point *P.* If P is inside the domain, then *C* (*P*) assumes a value of unity, while if *P* is on *S,* and if a unique tangent plane to *S* exists at point *P*, then *C* (*P*) has a value of 0.5. The general expression for *C* (*P*) is, however [160]:

$$C(P) = \int_S -\frac{\partial}{\partial n}\left(\frac{1}{4\pi r(P,Q)}\right) ds_Q \tag{3.3.5}$$

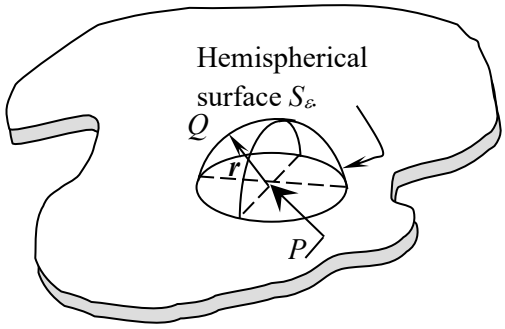

Fig. 3.3.1: Schematic Diagram for source (P) and sink (Q) point

Equation (3.3.2) is now modified to replace the pressure derivative with a more meaningful normal particle velocity term. For the time-harmonic cases, the momentum-balance equation relates the normal velocity and the normal pressure derivative on the boundary as follows [55]:

$$\frac{\partial p}{\partial n} = -i\Omega\rho v \tag{3.3.6}$$

Where, Ω is forcing frequency and ρ is density of acoustic medium. Equation (3.3.2) thus, modifies to

$$C(p)P(p) + \int_S P(q)\frac{\partial G(p,q)}{\partial n_q} dS_q = \int_S v(q)(-i\Omega\rho G(p,q))\, dS_q \tag{3.3.7}$$

Assuming that, the surface is discretized into M eight-noded surface elements, the discretized form of Equation (3.3.7) is given as

$$C(P)p(P) + \sum_{m=1}^{M}\sum_{l=1}^{8}\int_{-1}^{+1}\int_{-1}^{+1}\frac{\partial G}{\partial n}(P,Q)N_l(\xi_1,\xi_2)\,p_l\,J(\xi_1,\xi_2)d\xi_1\,d\xi_2 =$$

$$\sum_{m=1}^{M}\sum_{l=1}^{8}\int_{-1}^{+1}\int_{-1}^{+1}-i\Omega\rho G(P,Q)]N_l(\xi_1,\xi_2)\,v_l\,J(\xi_1,\xi_2)d\xi_1\,d\xi_2 \qquad (3.3.8)$$

Each node of the BE mesh is used once as an observation point and a boundary element equation is generated. Upon assembly of these equations the system equation for the acoustic enclosure is found in the form of a set of linear simultaneous algebraic equations, given below:

$$[H]\{p\} = [G]\{v\} \qquad (3.3.9)$$

At a node, connected to *r* number of elements, there are essentially *r* velocity terms whose magnitude and direction may be independent. The pressure terms are, however, scalar quantities, and unique at a node. Hence, though $[H]$ is a fully populated square matrix due to full assembly, $[G]$ remains a rectangular one, that has to be selectively assembled.

3.3.2. Multi-domain Acoustic Analysis

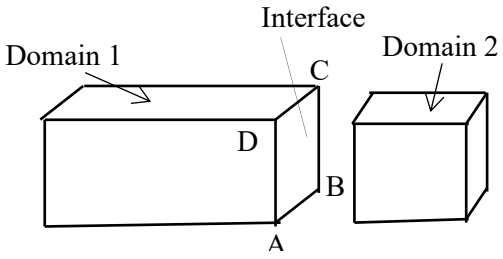

Fig. 3.3.2: Rectangular cavity with subdomain

For multi-domain case as shown in Fig. 3.3.2, the coefficients of $[H]$ and $[G]$ matrices of equation 3.3.9, are calculated [118] for each domain and assembled with proper nodal connectivity. The interface layer ABCD between two domains is common for both. Acoustic pressure p and normal velocity v are continuous across the interface. Thus,

$$p_1 = p_2;\;\; v_1 = -v_2 \qquad (3.3.10)$$

The subscripts signify the boundary sides the variables belong to.

Equation 3.3.9 when combined for both domains take the form:

$$\begin{bmatrix} H^1 & H^{1i} & 0 \\ 0 & H^{2i} & H^2 \end{bmatrix}\{p\} = \begin{bmatrix} G^1 & G^{1i} & 0 \\ 0 & -G^{2i} & G^2 \end{bmatrix}\{v\} \tag{3.3.11}$$

$H^{1i}, H^{2i}, G^{1i}, G^{2i}$ indicates the coefficient matrix at interface for domain 1 and domain 2 respectively. Negative sign indicates that the normal directions are opposites at the interface. Applying suitable boundary conditions, all nodal pressure and velocity components are solved and the domain sound pressure has been calculated from the known sound field after post processing.

3.3.3. Exterior Acoustic Analysis

The Sommerfeld [48] radiation condition at infinity is inherently satisfied for the exterior acoustic domain field. However, a notable issue arises with the exterior boundary integral formulation, whether direct or indirect, as it fails to yield a correct solution at certain irregular frequencies corresponding to the eigenfrequencies of the interior domain. In the direct BEM formulation, this issue is known as the "non-uniqueness difficulty," while in the indirect BEM formulation, it is referred to as the "non-existence difficulty."

To address this problem, the CHIEF method proposed by Schenck [142] in 1968 has been discussed in the literature. This method involves modelling the exterior domain along with a corresponding (imaginary) interior domain that shares the same boundary as shown in Fig. 3.3.3. In the figure, B and B' denote interior and exterior domain respectively. n is the outward normal for interior domain B and n' is the normal for exterior domain B' pointed inside. P and Q denotes the source point and observation point having a distance r. The integral equation for exterior domain is same as Eq. 3.3.2. The direct boundary integral equations for the exterior and interior problems differ slightly in two key aspects:

1. Their normal directions are opposite to each other as shown in Fig. 3.3.3.
2. Their solid angles differ at corners and edges. For exterior acoustics the solid angle is expressed as

$$C(P) = 1 - \int_S \frac{\partial}{\partial n}\left(\frac{1}{4\pi r(P,Q)}\right) ds_Q \tag{3.3.12}$$

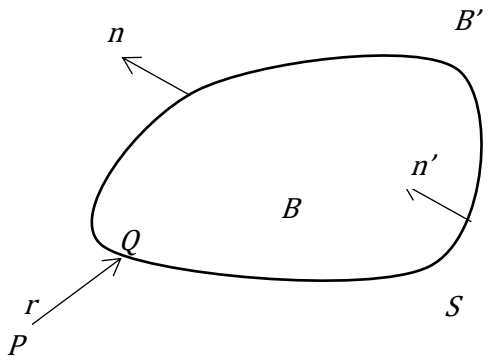

Fig.3.3.3: Graphical representation of the interior-exterior acoustic domain

To overcome the non-uniqueness problem, m collocation points located in the enclosed cavity need to be chosen [161]. These points usually referred to as CHIEF points. The system matrix H corresponding to the CHIEF method takes the form.

$$H = \left| \begin{array}{ccc} c1+\bar{h}11 & \bar{h}12 \ \ldots & \bar{h}1n \\ \bar{h}21 & c2+\bar{h}22 \ \ldots & \bar{h}2n \\ : & : & : \\ \bar{h}n1 & \bar{h}n2 \ \ldots & cn+\bar{h}nn \\ \hline \bar{h}n+11 & \bar{h}n+12 & \bar{h}n+1n \\ : & : & : \\ \bar{h}n+m1 & \bar{h}n+m2 & \bar{h}n+mn \end{array} \right| \qquad (3.3.13)$$

The rectangular system reflects an over-determined linear system of algebraic equations for the n-dimensional vector of unknowns, p. This system is solved in a least square sense, where the unknown solution is formally given by

$$p = (H^H H)^{-1} H^H G v \qquad (3.3.14)$$

with superscript H denoting Hermitian, i.e. transposed conjugate complex matrix.

3.4.Multi-domain interior-exterior Coupling Formulation

The combined multi-domain interior- exterior coupling condition is explained in the Fig. 3.4.1. The interfaces between the domains are denoted as i1, i2 and i3 respectively where i1

is the interface between domain 1 (interior) and domain 2 (interior), i2 is the interface between domain 2(interior) and domain 3(exterior) and i3 is the interface between domain 3(exterior) and domain 1(interior). In this interface layer pressure for domain 1(p_{i1}^1) is the same as that for domain 2 (p_{i1}^2). Also, the normal velocity at interface nodes for domain 1 (v_{i1}^1) is equal but opposite to that of the of domain 2 (v_{i1}^2). Similarly,

$$p_{i1}^1 = p_{i1}^2 \text{ and } v_{i1}^1 = -v_{i1}^2$$

$$p_{i2}^2 = p_{i2}^3 \text{ and } v_{i2}^2 = -v_{i2}^3;$$

$$p_{i3}^1 = p_{i3}^3 \text{ and } v_{i3}^1 = -v_{i3}^3 \quad (3.4.1)$$

The subscripts denote the interface layer and the superscript denotes the domain number.

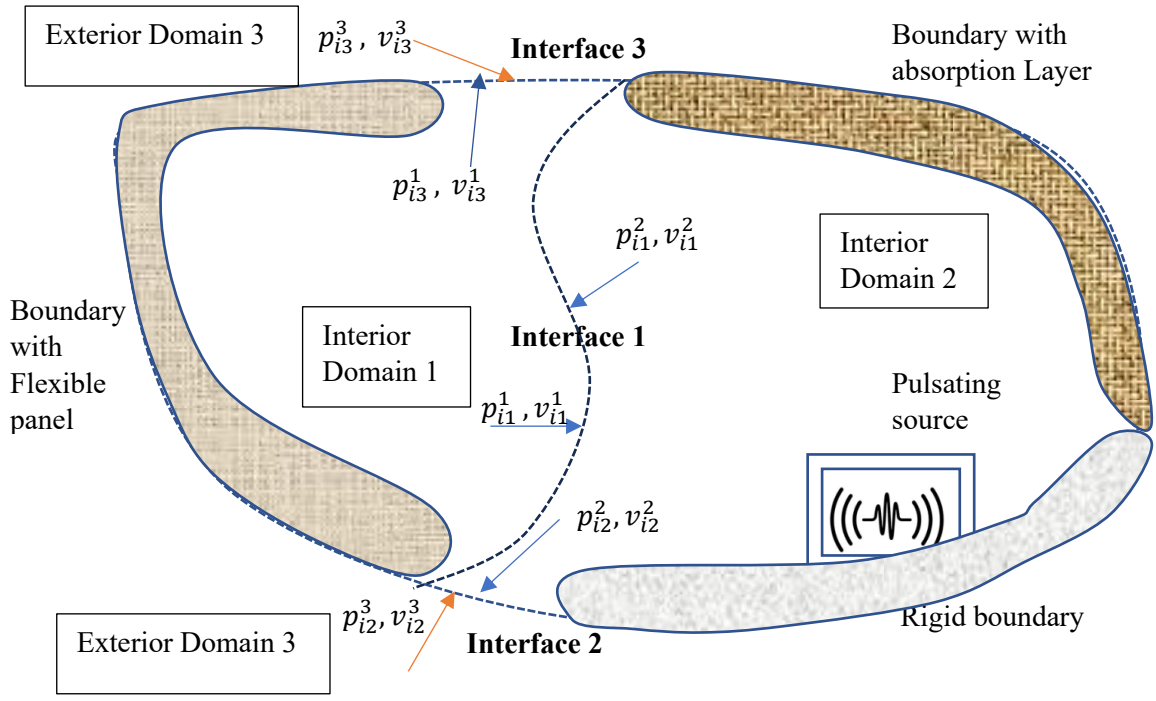

Fig. 3.4.1: The schematic diagram for Multi-domain Interior Exterior acoustic problem

The element nodal connectivity has been devised in such a way that the normal direction of the plane enclosing the interior cavity points outward for domain 1 and domain 2, while for domain 3, the normal direction points inward as shown in Fig. 3.3.3. For the multi-domain interior-exterior coupling case $[H]$ and $[G]$ matrices are calculated for every domain and assembled with proper nodal connectivity.

$$\begin{bmatrix} H^1 & H_{i1}^1 & 0 & 0 & 0 & H_{i3}^1 \\ 0 & H_{i1}^2 & H^2 & H_{i2}^2 & 0 & 0 \\ 0 & 0 & 0 & H_{i2}^3 & H^3 & H_{i3}^3 \end{bmatrix} \begin{Bmatrix} p_1 \\ p_{i1}^1 \\ p_2 \\ p_{i2}^2 \\ p_3 \\ p_{i3}^3 \end{Bmatrix} = \begin{bmatrix} G^1 & G_{i1}^1 & 0 & 0 & 0 & -G_{i3}^1 \\ 0 & -G_{i1}^2 & G^2 & G_{i2}^2 & 0 & 0 \\ 0 & 0 & 0 & -G_{i2}^3 & G^3 & G_{i3}^3 \end{bmatrix} \begin{Bmatrix} v_1 \\ v_{i1}^1 \\ v_2 \\ v_{i2}^2 \\ v_3 \\ v_{i3}^3 \end{Bmatrix} \tag{3.4.1}$$

Rearranging the unknown quantity in the left side the modified equation (3.4.1) in given in equation (3.4.2).

$$\begin{bmatrix} H^1 & H_{i1}^1 & 0 & 0 & 0 & H_{i3}^1 & -G_{i1}^1 & 0 & G_{i3}^1 \\ 0 & H_{i1}^2 & H^2 & H_{i2}^2 & 0 & 0 & G_{i1}^2 & -G_{i2}^2 & 0 \\ 0 & 0 & 0 & H_{i2}^3 & H^3 & H_{i3}^3 & 0 & G_{i2}^3 & -G_{i3}^3 \end{bmatrix} \begin{Bmatrix} p_1 \\ p_{i1}^1 \\ p_2 \\ p_{i2}^2 \\ p_3 \\ p_{i3}^3 \\ v_{i1}^1 \\ v_{i2}^2 \\ v_{i3}^3 \end{Bmatrix} =$$

$$\begin{bmatrix} G^1 & 0 & 0 & 0 & 0 & 0 \\ 0 & 0 & G^2 & 0 & 0 & 0 \\ 0 & 0 & 0 & 0 & G^3 & 0 \end{bmatrix} \begin{Bmatrix} v_1 \\ 0 \\ v_2 \\ 0 \\ v_3 \\ 0 \end{Bmatrix} \tag{3.4.2}$$

In the modified equation unknown nodal boundary pressure $(p^1, p^2, p^3,\ p_{i1}^1, p_{i1}^2, p_{i1}^2)$and the velocity at the interface zone $(v_{i1}^1, v_{i1}^2, v_{i1}^2)$ are unknown so these terms are taken in right hand side and can be solved with unknown boundary pressure p. The total number of elements is denoted as ne, where $ne = ne1 + ne2 + ne3 + \ldots$. The total number of boundary nodes is represented by nn, where $nn = nd1 + nd2 + nd3 + \ldots$ Common interface nodes are used to model the interface, but the element connectivity is opposite. As a result, the dimension of the H matrix is $nn \times nn$, and the dimension of the G matrix is $nn \times 8ne$. Here, $ne1, ne2$, and $ne3$ refer to the number of eight-node elements, and $nd1, nd2$, and $nd3$ represent the number of nodes in domain 1, domain 2, and domain 3, respectively, which are used to model the boundary.

3.5.Different boundary conditions

After formulating the system matrices, the boundary conditions are incorporated to solve the coupled acoustic problem. Four types of boundary conditions have been considered here.

i. Rigid Boundary: The velocity (Neumann) boundary conditions, where the amplitude of normal velocity v=0 at rigid walls and takes some specified value at the exciting wall.

ii. Interaction Boundary: At the interacting surface between flexible structure and acoustic domain neither p nor v is known. Mobility matrix $[Q']$ as shown in Eq. 3.2.8 is used to couple the FEM and BEM [90] and relate normal particle velocity and pressure as shown.

$$\{v\} = \{\dot{d}\} = [Q']\{p\}e^{i\Omega t} \tag{3.5.1}$$

where,

$\{\dot{d}\}$= nodal velocity

$\{p\}$=nodal pressure

$$[Q'] = \left[\Omega[\Phi]\left[diag\left(\frac{2\Omega\omega_k\xi_k + i(\omega_k^2 - \Omega^2)}{(\omega_k^2 - \Omega^2)^2 + 4(\Omega\xi_k\omega_k)^2}\right)\right][\Phi]^T[A]\right] \tag{3.5.2}$$

where,

Ω = forcing frequency in radian per second

[Φ]= mass-normalised set of eigenvectors for the uncoupled structure

ω_k= kth natural frequency in radian/second

ξ_k = damping ratio for kth mode

$[A]$= area matrix for the interaction boundary

iii. Boundary with absorbent layer: When absorbent layers are used at the boundary, the fluid particle velocity v and the structural velocity v_s is related using the acoustic admittance Y and acoustic pressure p as shown in eq. 3.5.3. The value of admittance which is a variable of frequency have been taken from Suzuki et al. (1989) [84] and Niyogi (2006) [177]. Thus, the velocity terms are remodeled before incorporating the boundary values if the structural surface is provided with absorbent layers.

$$v = Yp + v_s \tag{3.5.3}$$

iv. Boundary with opening:

In case of window boundary condition, the exact analysis is done by coupling of interior and exterior domain as shown in Eq. 3.4.2.

In another approach, the approximate solution can be obtained at low frequencies where the square opening has been transformed to an equivalent circle and radiation impedance has been found out. [Kinsler et al. (1982) [55]. The total reaction $f_r = -\,pdS$ acting on the piston is therefore given by

$$f_r = -\frac{i\rho ck}{\pi} U_o e^{i\Omega t}[R_1(2ka) + iX_1(2ka)] \tag{3.5.4}$$

$$Z_r = \frac{-f_r}{U_o e^{i\Omega t}} = \rho cA\{R_1(2ka) + iX_1(2ka)\} \tag{3.5.5}$$

where $R_1(x)$ and $X_1(x)$ are two piston impedance functions defined as

$$\mathrm{R_1\,(x)} = 1 - \frac{2*\mathrm{J}_1(x)}{x} = \frac{x^2}{2.4} - \frac{x^4}{2.4^2.6} + \frac{x^6}{2.4^2.6^2.8} - \cdots \tag{3.5.6}$$

and

$$\frac{2*H(x)_1}{x} = X_1(x) = \frac{4}{3\pi}\left(\frac{x}{3} - \frac{x^3}{3^2.5} + \frac{x^5}{3^2.5^2.7} - \cdots\right) \tag{3.5.7}$$

Here J_1 is first-order first-kind Bessel function and H_1 is first-order Struve function.

The approximated equation given by equation 3.5.8 has been used by Seybert et al. (1990) [161] to the pressure velocity equation.

$$Z_r = \frac{-f_r}{U_o e^{i\Omega t}} = \rho cA\{0.5(ka)^2 + i0.85ka\} \tag{3.5.8}$$

Where, ρ is air density, c is the speed of sound, A is the area of opening surface, k is the wave number and a is the equivalent radius of the opening. After calculating the impedance, the surface velocity terms are expressed by pressure terms and all pressure quantities are evaluated.

3.6. Post processing

After calculating the sound pressure levels at the boundary, the post-processing calculation for structural displacement has been done. The pressure terms computed at the element nodes on the structural boundaries are applied as distributed forces. The global force vector is computed from the local forces using proper transformations as indicated in Eq. (3.1.8) and assembling the element load array thereafter. If the receptance matrix [α] is post-multiplied by this global force vector, the nodal displacement array is obtained along the global coordinates (Eq.3.2.2).

For ease of understanding a flowchart of the algorithm has been incorporated.

FLOW CHART OF THE ALGORITHM

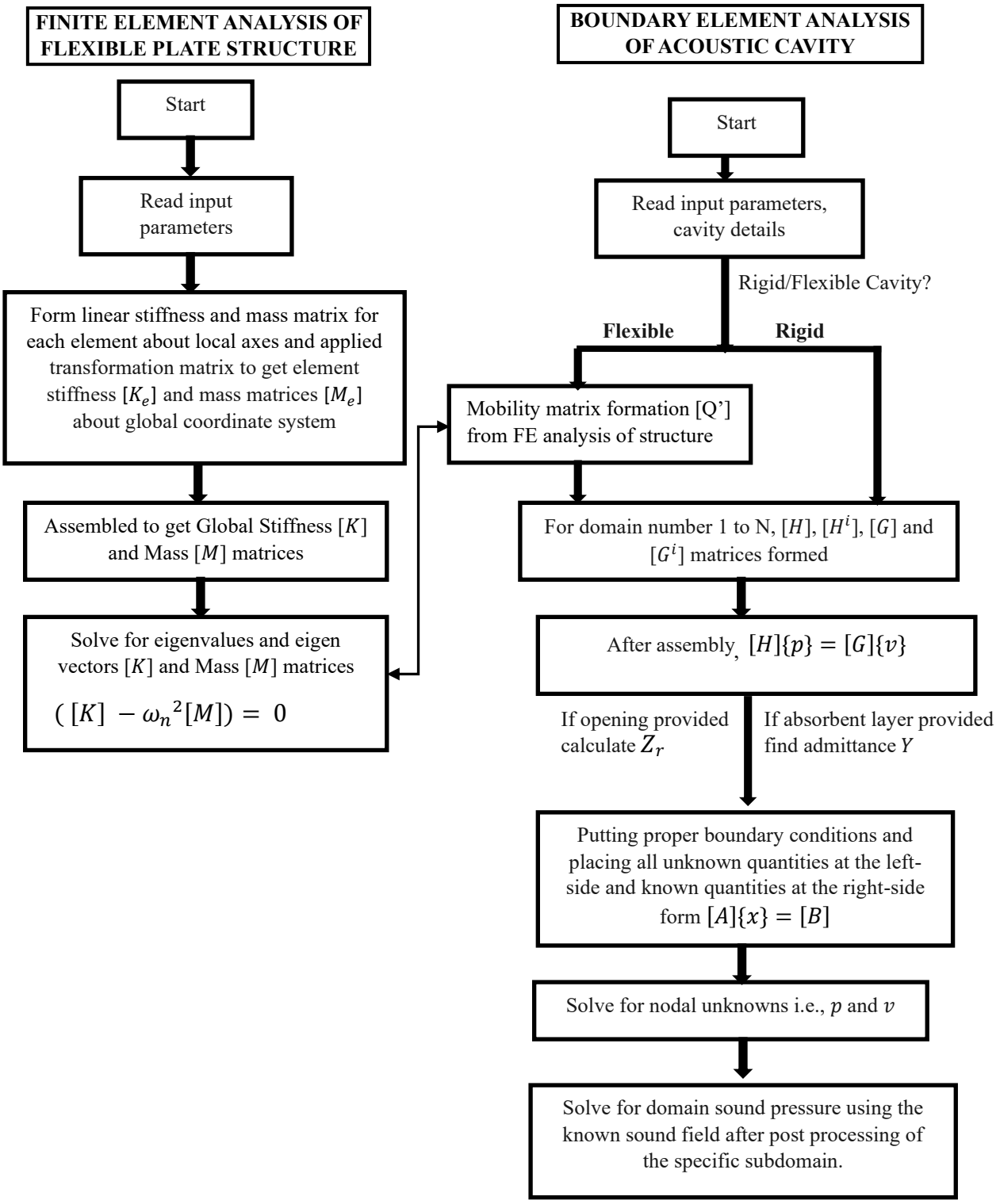

4

Free Vibration Analysis of Composite Folded Plate Structure

Based on the theoretical formulation presented in Chapter 3.1, free vibration analysis of laminated composite folded plate structures has been performed using MATLAB coding. Composite formulation has been used effectively to model sandwich folded structure too. Validation studies have been conducted to show the accuracy of the FEM code in calculating the natural frequencies and mode shapes of the flexible folded structure. Multiple folds have been inserted to evaluate the effect of various parameters such as thickness, fibre angle, fold angle etc. Stiffeners have been added to the flexible folded structure to understand the change in behaviour under free vibration for various stiffener positions.

4.1. Validation Study for Folded Plate Formulation

The validation study has been divided into four parts.

4.1.1. Validation study for stiffened laminated composite plate structure
4.1.2. Validation study for isotropic one-fold plate structure
4.1.3. Validation study for sandwich plate structure
4.1.4. Validation study for sandwich one-fold plate structure

4.1.1 Validation Study for stiffened laminated composite plate structure

To observe the accuracy and reliability of the present code in modelling the stiffeners (as shown in Fig. 4.1), the free vibration analysis of clamped laminated composite stiffened plates built of graphite/epoxy (ASI/3501-6) is analysed numerically and compared with Lee and Lee [25], who have used Timoshenko beam theory to model the stiffeners unlike YNS theory [4] being applied in the present case. Dimensions of the stiffened laminated plate is a × b × h = 500mm × 250mm × 1.04mm. The lamination of the plate is $(0^o/+45^o/-45^o/90^o)_s$ the fibre angles being measured anticlockwise positive with respect to the line AB in Fig. 4.1. The stiffener is 10.5mm wide and 3.64mm thick. The stiffeners have a stacking sequence of $(90^o/0^o)_s$ with respect to the soffit line and placed perpendicular to the lamination of the plate. The ply properties of Lee and Lee [25] are given as follows: E_1=128GPa, E_2=11GPa, G_{12} = G_{13}=4.48GPa, G_{23}=1.53GPa, ν_{12} = 0.25 and density ρ =1500kg/m^3. 8-noded serendipity element has been used with 12 × 6 mesh arrangement. The natural frequencies, obtained from the present code are shown in Table 4.1, which show acceptable degree of conformity with

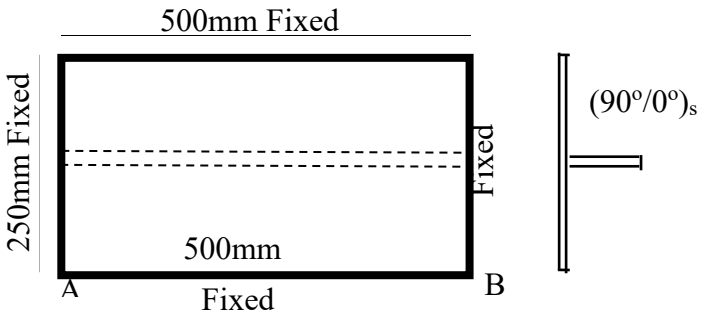

Fig. 4.1: Geometry of the plate with $(0^o/45^o/-45^o/90^o)_s$ stack sequence of graphite/epoxy

results of Lee and Lee [25].

Table 4.1: The first three natural frequencies (Hz) for stiffened laminated plate in Fig. 4.1

Mode	Present study	Ref. [25]	Error (%)
1	216.69	213.8	1.3
2	223.23	229.4	2.7
3	281.13	270.2	4.0

4.1.2 Validation Study for isotropic one-fold plate structure

The validation study for isotropic one-fold cantilever plate with crank angle 90°, as shown in Fig. 4.2 have been performed and compared with ANSYS. The plate dimension is given as follows:

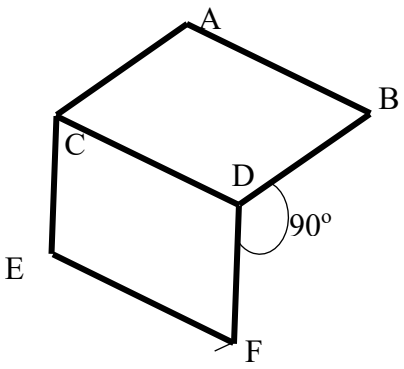

Fig. 4.2. One-fold isotropic plate model for validation study

AB = EF = 1m, AC = CE = BD = DF =0.5m. Thickness h= 0.01m. The plate is clamped along ACE. For isotropic material the properties taken are E = 10.92×10^9 Pa, Poisson's ratio $\upsilon = 0.3$, Density $\rho = 1000$ Kg/m^3. Table 4.2 shows the first three natural frequencies (Hz). The results are compared with results produced through ANSYS 19 R3 academic version. From Table 4.2, it is seen that the result matches very well with ANSYS.

Table 4.2 The first three modes from free vibration isotropic folded plate

Mode Number	MATLAB (Hz)	ANSYS (Hz)
1	13.477	13.456
2	27.099	27.083
3	49.032	48.970

4.1.3 Validation study for sandwich plate structure

For validation of sandwich plate structures a three-layer rectangular simply supported sandwich plate has been taken [5]. The dimension of the plate is 1.83m ×1.22m. Skin plate thickness = 4.06×10^{-4} m, E_s= 68.9GPa, ν = 0.3, ρ_s=2.77×10^3 Ns^2/m^4; For core layer,

thickness=0.0064 m, E=0.134GPa, G=0.052GPa, ρ_c=0.122×10^3 Ns^2/m^4. The results from the current formulation, HSDT [10] and experimental results [5] are given in Table 4.3.

Table 4.3 Natural Frequencies (Hz) of a three-layer simply supported rectangular sandwich plate

Modes	Experimental [5]	HSDT [10]	Present
1	-	23	23.37
2	45	45	44.97
3	69	71	71.93
4	78	80	81.29
5	92	93	93.74
6	129	128	131.38

From Table 4.3, it is seen that the result matches quite well with experiments and with HSDT for three-layer sandwich plate.

4.1.4 *Validation study for sandwich one-fold plate structure*

Since no case of sandwich folded plate was obtained in the open literature, the folded plate model (Fig. 4.2) has been analysed using two layers of e-glass epoxy composites with fiber angle ($0^o/90^o$) and HEREX C70.130 PVC foam core with the following properties:

For the Face sheet: Thickness = 2mm, E_1= 24.51 GPa, E_2= 7.71 GPa, G_{12} = G_{13} =G_{23}=3.34 GPa, ν_{12} = ν_{21}= 0.078 and ρ= 1800 Kg/m^3. For the Core layer: Thickness= 6mm, E_1= E2= 0.104 GPa, G_{12} = G_{13} = G_{23}= 0.05 GPa, ν_{12} = ν_{21}= 0.33 and ρ= 130 Kg/m^3.

In Table 4.4, the first three natural frequencies (Hz) are tabulated and compared with ANSYS using SHELL281 layered element. From the results, it is noticed that MATLAB formulation provides slightly conservative results. It could be since the present element is based on an equivalent two-dimensional formulation with five degrees of freedom (DOF) per node, whereas in ANSYS, SHELL281 allows six DOF per node and used with layered shell definition with definable number of integration points through the thickness of the layers.

Table 4.4. The first three modes of free vibration (Hz) for the sandwich folded plate

Mode Number	MATLAB (Hz)	ANSYS (Hz)
1	13.170	12.713
2	28.300	27.560
3	52.821	50.334

4.2. Mesh Convergence Study

The corrugated plate of thickness 10mm as shown in Fig. 4.3 has been analysed. Length of the inclined stretch (=AB=CD=EF=GH) of the folded plate is taken as 0.5m and that of horizontal part (=BC=DE=FG) is 1m. Let the number of elements along local X direction be denoted by N_x and that along Y by N_y. The edge along Y=1 plane is taken as clamped. All other sides are set free. Sandwich plates with fibre-reinforced plastic face sheets, made of glass polyester resins and HEREX C70.130 PVC foam core with properties as follows: Face layer: E_1= 24.51 GPa, E_2= 7.77 GPa, $G_{12} = G_{13}$ = 3.34 GPa, G_{23}= 1.34 GPa, $\nu_{12} = \nu_{21}$= 0.078 and ρ= 1800 Kg/m³. For the Core layer: E_1= E2= 0.104 GPa, $G_{12} = G_{13} = G_{23}$= 0.05 GPa, $\nu_{12} = \nu_{21}$= 0.33 and ρ= 130 Kg/m³ are taken for the present analysis.

Two layers of e-glass epoxy composites with fibre angles ($0^o/90^o$) and ($90^o/0^o$) have been accounted as top and bottom face sheets. The face sheets are assumed to be 2 mm each with a core thickness of 6 mm. First five natural frequencies (Hz) for different N_x and N_y are presented in Table 4.5. From Table 4.5, it is seen that with increase in mesh number, % error reduces. Hence, N_x = 40 (four and eight elements along each inclined and straight stretch respectively) and N_y =4 can be used for further analysis.

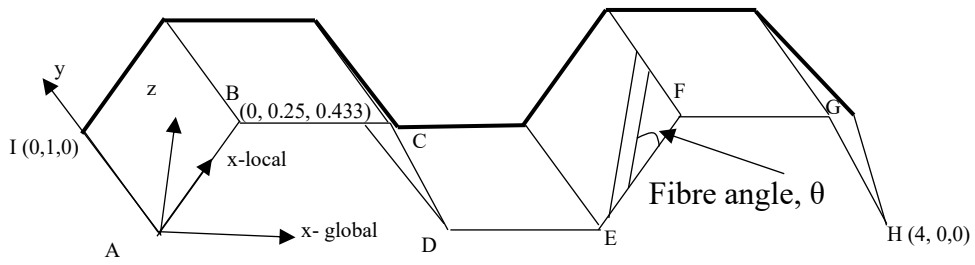

Fig. 4.3 Geometry of corrugated plate

Table 4.5: First five undamped natural frequencies (Hz) computed for different mesh sizes

Mode no	N_x=10, N_y=1	N_x=20, N_y=2	*% error*	N_x=20, N_y=4	*% error*	N_x=40, N_y=4	*% error*
1	20.68	19.47	*6.21*	18.99	*2.53*	18.95	0.21
2	20.77	19.52	*6.40*	19.04	*2.52*	19.00	0.21
3	34.10	32.93	*3.55*	32.22	*2.20*	32.12	0.31
4	38.44	37.02	*3.84*	36.25	*2.12*	36.08	0.47
5	39.74	38.39	*3.52*	37.60	*2.10*	37.39	0.56

4.3. Case Study

4.3.1. Case Study 1: Free Vibration of cantilever one-fold composite plate

The free vibration behaviour of plane one-fold composite plate (Fig. 4.2). with one side clamped and the other side free are conducted. The dimension AB=EF=1.5m, AC = CE = BD = DF =0.75m. The composite material composed of three layers of E-glass epoxy material and the overall thickness are assumed as 20mm (mass = 26 Kg/m^2). The data used for E-glass epoxy surface material is E_1=60.7 x 10^9 N/m^2, E_2 = 24.8 x 109 N/m^2, G_{12} = G_{13} = G_{23} = 12.0 x 10^9 N/m^2, ν_{12} = ν_{21} = 0.23, ρ = 1300 Kg/ m^3. Parametric studies are conducted with reference to fold angle and fibre orientation.

It may be observed from Table 4.6, that the fundamental frequencies of the single-fold folded plates are very nearly identical for different crank angles, but the remaining frequencies change. It may also be seen that with increase of fibre angle the frequency decreases for a particular crank angle.

Table 4.6: Effect of different fibre angle and fold angle (α) on Natural Frequency (Hz) of Composite One-fold Folded Plate Structure

Mode	90 Degree			120 Degree			150 Degree		
	(30/-30/30)	(45/-45/45)	(60/-60/60)	(30/-30/30)	(45/-45/45)	(60/-60/60)	(30/-30/30)	(45/-45/45)	(60/-60/60)
1	19.417	18.994	18.250	19.421	18.998	18.256	19.408	18.984	18.248
2	35.654	37.765	40.339	35.324	37.288	39.612	33.584	34.794	35.894
3	73.547	70.247	66.641	73.530	70.207	66.583	73.323	69.847	66.128
4	82.637	80.309	78.764	82.396	80.007	78.395	80.728	77.985	76.108
5	135.158	146.771	152.348	135.537	146.429	145.901	107.548	104.653	101.338

4.3.2. Case Study 2: Free Vibration Study of the Sandwich Corrugated Plate

Free vibration analysis of the sandwich folded plate (Fig. 4.3) made up of material as explained in mesh convergence study in the previous section, is conducted and reported in Table 4.7. The total thickness is kept as 10 mm. The lay up for the sandwich is taken as 0/θ/core/θ/0 where θ is the inclination of fibres with respect to local X axis (Fig. 4.3). θ is varied as 30^o, 45^o, 60^o, 75^o and 90^o and the boundary conditions taken are as follows.

a) CCCC - Clamped at all edges
b) SSSS - Simply supported at all edges
c) FCFC - Clamped along two opposite straight edges i.e., along y direction of Fig. 4.3 at x=0,4.
d) CFCF - Clamped along two opposite folded edges i.e., along x direction of Fig. 4.3 at y=0,1
e) CFFF - Clamped along folded edge along y=1 plane only of Fig. 4.3

Variation of natural frequency for various boundary conditions with respect to fibre angle θ has been plotted for 6 mm thick core in Fig. 4.4.

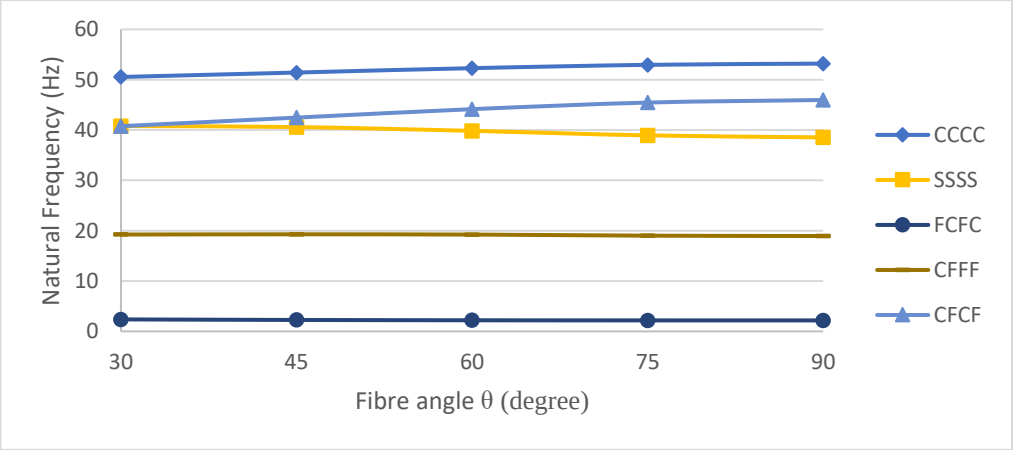

Fig. 4.4 Fundamental Frequencies (Hz) plotted against changing θ for core thickness of 6mm

From Table 4.7 and Fig. 4.4 the following observations can be made:

1. With increase in core thickness, natural frequency increases. However, the gain in frequency drops as core thickness rises. When the core thickness is 6mm, the face thickness is 2mm each. Gradual increase in core thickness to 7mm or 8mm increases the lever arm distance at the cost of face sheet thickness. The mass drops linearly as core widens. Thus, there is a rise that shows a negative gradient.
2. It is evident that for CCCC and CFCF cases, the natural frequency increases with increase in θ (Fig. 4.4). But for all other boundary conditions the changes in natural frequency are very nominal. For CCCC and CFCF case the structure spans in shorter direction and as θ rises, the fibres too orient themselves along the shorter direction. However, for the remaining cases, just the reverse holds true.
3. From Table 4.7, it is observed that CCCC boundary condition makes the structure stiffest followed by CFCF, SSSS, CFFF, FCFC conditions. In case of CFCF condition, the unsupported length is 1m thus providing higher stiffness than FCFC condition where unsupported length is 4m.

First three mode shapes of corrugated roof model with 6mm core thickness and stack sequence $0^o/90^o$/core/$90^o/0^o$ for different boundary conditions are plotted in Fig 4.5. It shows in all mode shapes the horizontal plates have deformed predominantly leaving the

Table 4.7: First three natural frequencies (Hz) for different boundary conditions and θ

Ply Angle	Mode No	CCCC			SSSS			FCFC			CFCF			CFFF		
		Core Thickness (mm)			Core Thickness (mm)			Core Thickness (mm)			Core Thickness (mm)			Core Thickness (mm)		
θ		6	7	8	6	7	8	6	7	8	6	7	8	6	7	8
30°	1	50.5	52.1	52.5	40.8	42.0	42.3	2.4	2.4	2.4	40.8	42.1	42.6	19.2	19.7	19.8
	2	52.4	53.9	54.3	42.5	43.8	44.0	3.0	3.1	3.1	40.8	42.2	42.6	20.8	21.4	21.6
	3	54.0	55.6	55.9	44.7	46.0	46.2	5.2	5.3	5.4	51.3	52.9	53.3	34.6	35.4	35.4
45°	1	51.4	53.1	53.5	40.6	41.8	42.1	2.3	2.3	2.3	42.5	44.0	44.6	19.3	19.8	19.8
	2	53.0	54.7	55.1	42.2	43.4	43.6	3.1	3.2	3.2	42.5	44.0	44.6	20.6	21.2	21.4
	3	54.5	56.1	56.5	44.2	45.4	45.6	5.0	5.1	5.1	52.1	53.8	54.2	33.6	34.3	34.2
60°	1	52.3	54.1	54.6	39.8	41.0	41.2	2.2	2.2	2.2	44.2	45.9	46.6	19.2	19.7	19.8
	2	53.8	55.6	56.1	41.4	42.5	42.7	3.0	3.0	3.1	44.2	45.9	46.6	20.0	20.6	20.8
	3	55.2	56.9	57.4	43.3	44.4	44.5	4.8	4.9	4.9	53.0	54.7	55.3	32.8	33.4	33.2
75°	1	53.0	54.8	55.4	38.9	40.0	40.1	2.2	2.2	2.2	45.5	47.4	48.2	19.0	19.5	19.5
	2	54.5	56.3	56.9	40.5	41.5	41.6	2.8	2.9	2.9	45.5	47.4	48.2	19.4	19.9	19.9
	3	55.8	57.6	58.2	42.5	43.5	43.6	4.8	4.9	4.8	53.6	55.5	56.1	32.3	32.8	32.6
90°	1	53.2	55.1	55.8	38.5	39.5	39.6	2.2	2.2	2.2	46.0	48.0	48.8	18.9	19.4	19.4
	2	54.7	56.6	57.2	40.1	41.1	41.2	2.7	2.8	2.8	46.0	48.0	48.9	19.0	19.5	19.5
	3	56.1	57.9	58.5	42.1	43.1	43.1	4.8	4.8	4.8	53.9	55.8	56.4	32.1	32.6	32.4

ridge and the inclined plates undeformed. The first mode in CFFF is antisymmetric, unlike CCCC case.

	MODE 1	MODE 2	MODE 3
CCCC	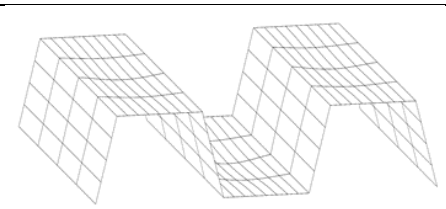	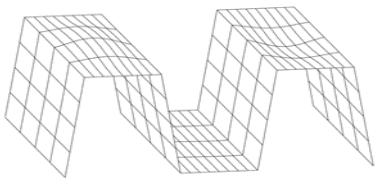	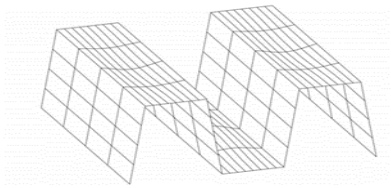
CFFF	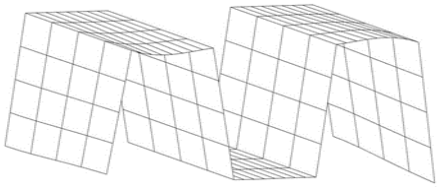	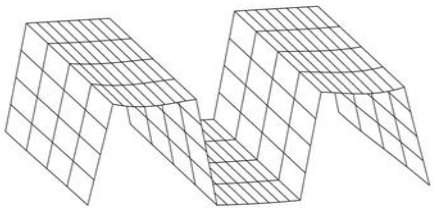	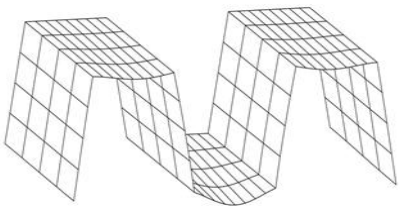
FCFC	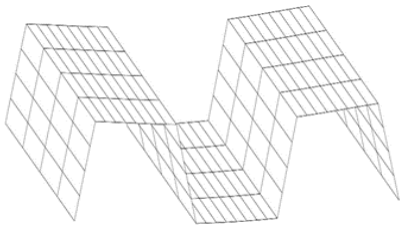	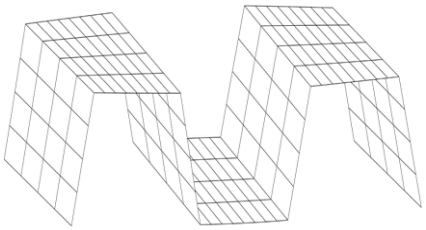	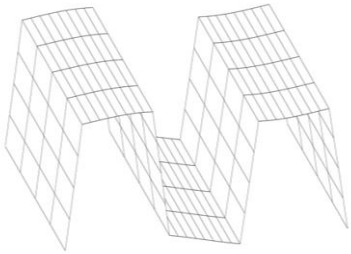
CFCF	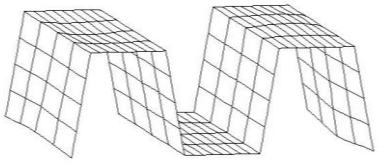	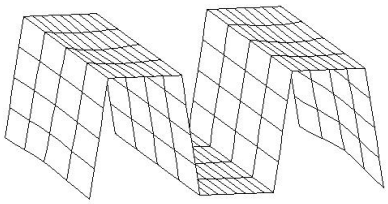	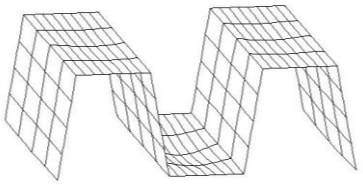
SSSS	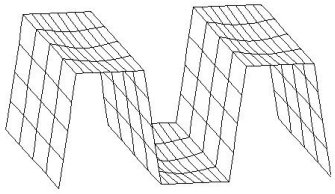	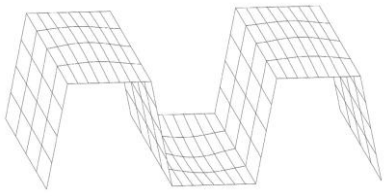	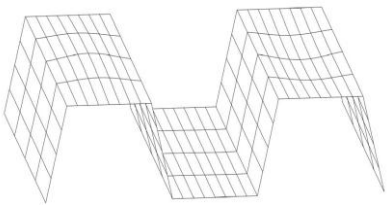

Fig 4.5. First three mode shapes of corrugated roof model (0º/90º/core/90º/0º), with core thickness 6mm, for free vibration analysis (Case study 2)

The tip of the central flat element in CFFF shows out of the plane deformation only in the third mode. FCFC condition is the weakest with two further ends clamped and the longer sides free, showing one-way bending in first mode, torsion in the second and a wavy form in the third mode. In SSSS boundary conditions, the horizontal plate elements are most disturbed,

with symmetry in first and second modes, antisymmetry in third. In CFCF case the mode shape comes quite similar to CFFF case.

4.3.3. Case Study 3: Analysis of the Sandwich Corrugated Plate with Stiffener

Here the corrugated folded plate is stiffened with two 0.1m wide stiffeners in the X-Z plane as shown in Fig. 4.6. The stiffeners are assumed to have the same property as of the main plate. Three cases have been studied with cantilever boundary condition (CFFF).

a. Stiffener is attached at y = 0.5 m (position 1) with increase in mass by 10%
b. Stiffener is attached at y = 0.0 m (position 2) with increase in mass by 10%
c. Both stiffeners are attached with increase in mass by 20%

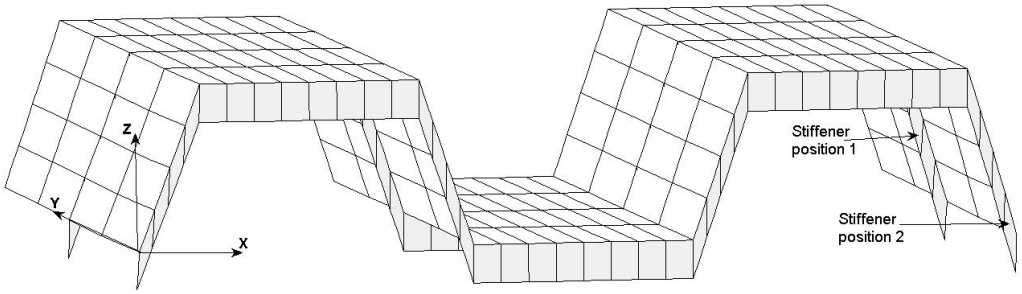

Fig.4.6 Geometry of stiffened corrugated plate

The thickness of the plate is taken as 10 mm with core thickness 6 mm. 0/θ/core/θ/0 layup sequence is used once again. The natural frequencies in Hz for different layup arrangements are tabulated in Table 4.8 First three mode shapes for free vibration and buckling mode shapes have been plotted in Fig. 4.7.

Comparing columns 3 and 6 of Table 4.8, one can see that a 20% rise in mass in the form of stiffeners increased fundamental frequencies to the tune of 260-275%, which is quite commendable. When the stiffener is attached at the free end, the change in stiffness is maximum (70% to 80%). Applying both stiffeners simultaneously increases stiffness above 100%.

From Fig. 4.7, no prominent changes are found in first two mode shapes of the stiffened sandwich folded plate. Only the central flat plate is subjected to bending deformation in the

third mode. Comparing with Fig. 4.5, it may be inferred that the stiffeners at position 2 have resisted flat plate displacements to a great extent.

Table 4.8: Natural Frequencies (Hz) of stiffened cantilever sandwich corrugated plate

		Natural Frequency (Hz)			
Ply Angle θ	Mode No	No Stiffener	Stiffener Position 1	Stiffener Position 2	Stiffener Position 1 And 2
30°	1	19.25	27.68	32.59	52.03
	2	20.78	29.81	32.93	52.34
	3	34.59	41.24	45.54	73.34
45°	1	19.29	27.89	33.05	51.86
	2	20.61	30.07	33.81	52.62
	3	33.56	40.80	45.68	74.82
60°	1	19.24	27.64	33.33	51.85
	2	20.05	29.45	34.34	52.80
	3	32.77	40.09	45.49	75.60
75°	1	19.02	27.27	33.67	52.00
	2	19.37	28.35	34.42	52.66
	3	32.28	39.40	45.16	75.78
90°	1	18.95	27.43	34.10	52.26
	2	19.00	27.48	34.13	52.35
	3	32.12	39.10	45.01	75.75

	Stiffener Position 1(Y=0.5)	Stiffener Position 2(Y=0.0)	Stiffener Position 1 and 2
Mode 1	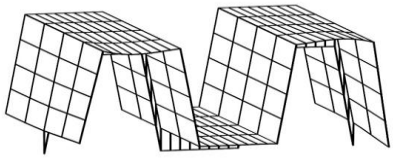	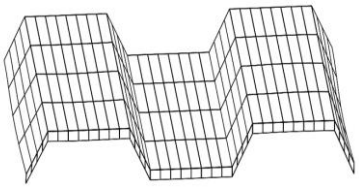	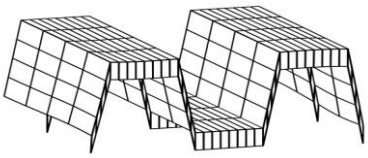
Mode 2	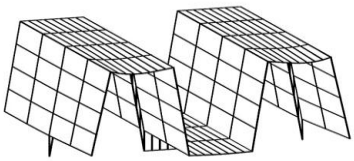	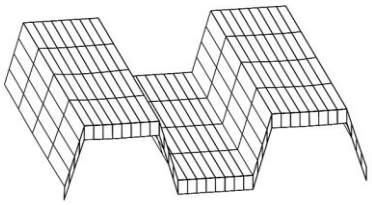	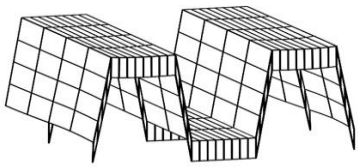
Mode 3	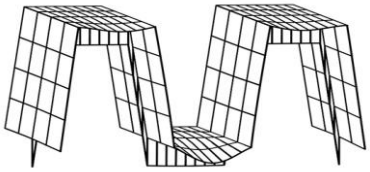	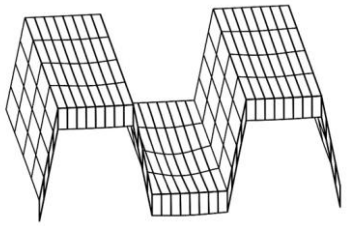	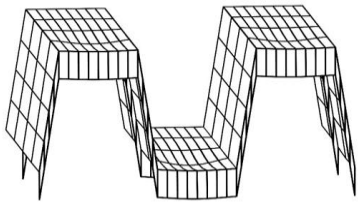

Fig 4.7: First three mode shapes (free vibration) stiffened sandwich corrugated folded plate with 6mm core and lay up $0^o/90^o$ /core/ $90^o/0^o$ for different stiffener position (Case study 2)

4.4. Conclusion

This study deals with the free vibration of sandwich-folded plates of self-replicating nature with and without stiffeners. An eight-noded regular five degrees of freedom per node element considering first-order transverse shear deformation theory and rotary inertia has been used. This has been converted into a six degree of freedom per node by introducing a small θ_z seed in the otherwise blank θ_z locations to apply the full three-dimensional transformation applicable to folded plate elements.

From the studies, it is observed that with an increase in core thickness, the stiffness of the structure decreases but mass decreases even more rapidly for the cases considered. As a result,

fundamental frequency has increased for the case studies presented. However, the gain in natural frequency reduces asymptotically since frequencies have the joint contribution of stiffness and mass. Natural frequencies depend on the boundary condition and the layup sequence of face sheets too. As expected, when the folded plate is clamped on all edges the stiffness of the structure increases radically. Also, in this case at fibre angle $\theta = 90^{o}$, fundamental frequency attained maxima. For stiffened corrugated plates proper selection of stiffener location could enhance performance of the structure and thus judicious use of stiffeners could be quite lucrative in boosting mass-specific stiffness.

5

Acoustic Response within Thin Laminated Composite Stiffened Cavities

Based on the theoretical formulation presented in section 3.1, 3.2 and 3.3.1, the acoustic analysis of a laminated composite interior cavity has been studied. This study explores how the acoustic response inside a vehicular cabin can be modified by introducing composite stiffeners at various locations, thickness, and orientations. By carefully planning the arrangement of these stiffeners, it is possible to control the acoustic output of the cabin and suppress sharp crests within the intended working frequency range for which the cabin is designed. The folded plate acoustic cavity with stiffeners has been modelled using common FEM and BEM meshing techniques. This chapter focuses specifically on the single-domain acoustic behaviour in the presence of stiffeners.

A MATLAB program has been developed for the present analysis subsequently to plot the model figure, mode shape and sound pressure level (SPL) 4D plot. The main program has two slaves: A finite element tool, to conduct free vibration analysis of the stiffened folded plate structure and generate the mobility relation, and a boundary element method solver, for the acoustic cavity. The main routine, first calls the finite element module to generate requisite eigen-solutions and then for each forcing frequency, invokes the boundary element module to conduct the internal coupled structural acoustic (ICSA) analysis using Eq. (3.3.8) and store the results in data files to generate graphical outputs subsequently. All SPL graphs have been plotted in Microsoft Excel.

5.1.Studies on the Finite Element Mesh Convergence

Following reference Niyogi et al. (2000) [90], the problem domain in this study is taken to be a box structure of dimension 1.8m × 0.6m × 0.6m as shown in Fig. 5.1 The top and the right walls are assumed to be flexible and the rest is taken to be rigid.

The flexible walls are assumed to comprise of E-glass/epoxy laminated composite material with material properties provided in Table 5.1. A stacking sequence of $(0^o/90^o)_s$ is used while the flexible walls are taken to be 0.004 m thick. A mesh convergence study for the free vibration response of dry structure is reported in Table 5.2. The length of 1.8 m is divided into n_1 elements, and the smaller lengths (0.6 m) are modelled by n_2 elements. From Table 5.2 it is seen that a mesh with $n_1 = 9$ and $n_2 = 3$ can be accepted for subsequent studies without compromising accuracy.

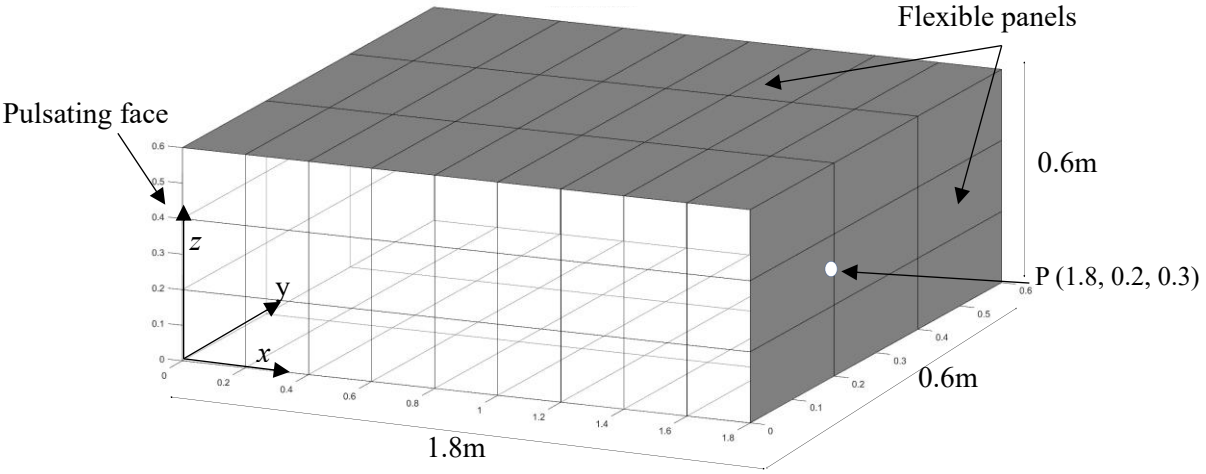

Fig. 5.1: Geometry of the acoustic container with flexible walls at the top and right with rigid piston to the left

Table 5.1: Material properties used in the study

Material	E_1 GPa	E_2 GPa	$G_{12} = G_{13}$ GPa	G_{23} GPa	ν_{12}	ρ kg/m^3
Aluminium [74]	71	71	26.692	26.692	0.33	2770
E-glass/epoxy laminated composite [90]	60.7	24.8	12	12	0.23	1300
Graphite/epoxy laminated composite ASI/3501-6 [25]	128	11	4.48	1.53	0.25	1500

Table 5.2: Natural frequencies (Hz) for different mesh size in one-fold folded plate

Mode	Mesh size			
	n_1=6, n_2=2	n_1=8, n_2=2	n_1=9, n_2=3	n_1=10, n_2=3
1	63.54	63.04	62.65	61.84
2	77.90	79.01	84.30	81.84
3	104.86	104.18	110.78	107.59
4	107.39	111.26	132.08	129.40
5	141.33	152.79	155.02	151.86

5.2. Validation Study

The validation for the code has two parts, namely

a. Validation of the ICSA analysis using isotropic rectangular cavity
b. Validation of the ICSA analysis using laminated composite rectangular cavity

5.2.1. Validation for Internal Coupled Structural Acoustic (ICSA) Formulation Using Isotropic Rectangular Cavity

To validate the ICSA code with experimental data, a rectangular cavity of dimensions 1.5m × 0.3m × 0.4m [74,184,185] with a 5mm thick, simply supported aluminium [ref. Table 5.1] plate at the top, as shown in Fig. 5.2, has been modelled numerically. The speed of sound, c, is taken as 340m/s and the density of air, ρ, is 1.225 kg/m^3. A damping ratio of 0.01 has been used. A pulsating source was placed at the left most panel at X=0. A meshing of 10 × 5 × 5 have been used in the FE and BE model to optimize the time of computation. First seven dry structural frequencies are tabulated in Table 5.3. The sound pressure level (dB) has been calculated at (0.6m, 0.15m, 0.2m) inside the cavity and compared in Fig. 5.3 with the experimental result [74] and numerical result using commercial software package SYSNOISE as in [184,185]. In Fig. 5.3, a good agreement with the experimental as well as numerical data can be observed and thus can be used for further numerical studies.

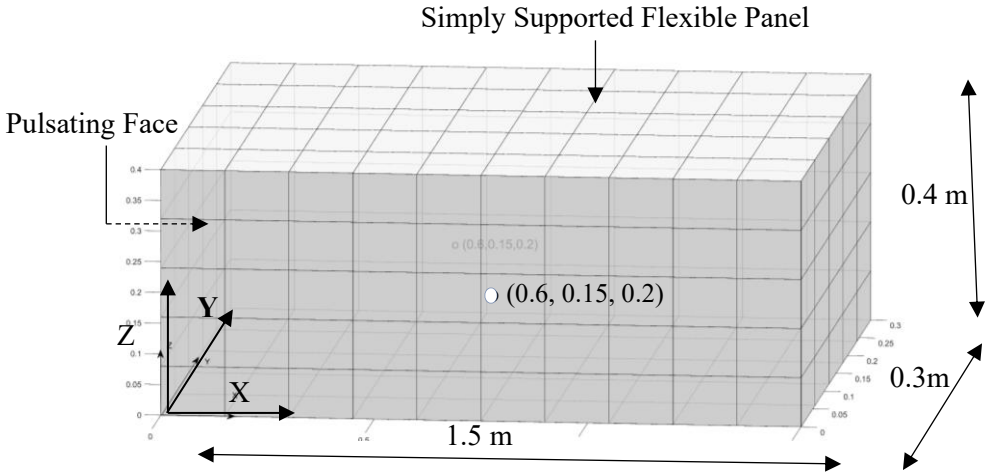

Fig. 5.2: Geometry of the box as in validation study 2

Table 5.3: Natural Frequency (Hz) for Topside Flexible Panel

Kim et al. [74]	Venkatesham et al. [184,185]	Present
141	142.1	140.36
157	158.2	156.37
184	185.5	183.71
222	224.1	224.60
270	275	281.37
330	338.8	358.17
-	416.7	456.69

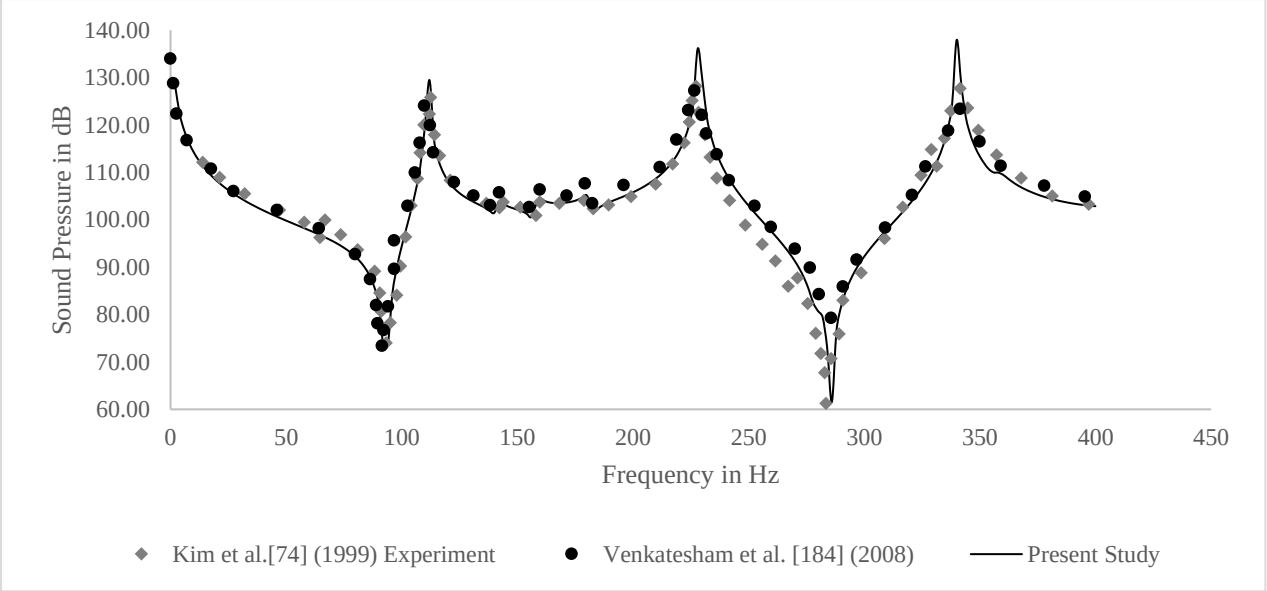

Fig.5.3: Comparison of Coupled SPL at domain point (0.6m, 0.15m, 0.2m)

5.2.2. Validation for Internal Coupled Structural Acoustic (ICSA) Formulation Using Laminated Composite Rectangular Cavity

To validate the ICSA code, a box structure of dimensions 1.8m×0.6m×0.6m having flexible top and right walls, is considered and the result of sound pressure level at the boundary and at the centre of the domain have been compared with Niyogi et al. (2000) [90]. The flexible walls are taken as 2.5mm thick and made up of E-glass epoxy laminated composite with the properties shown in Table 5.1 with the lay-up sequence $(30^o/-30^o)_s$. The remaining four walls are taken as acoustically rigid. The density of air, ρ, is taken as 1.20 kg/m^3. The medium is excited by a sinusoidal motion imparted to the left wall, acting as a rigid piston, with velocity amplitude of 0.001m/s. The acoustic responses are computed between a range of 0.001 rad/s to 1800.001 rad/s at an interval of 2 rad/s. The meshing is taken as 8×2×2 as in [90]. First twenty structural modes have been used in the present study to compute the mobility relation. The modal damping is taken as 0.1% for each structural mode. First ten dry natural frequencies of the cabin structure obtained from the finite element free vibration analysis of the container are shown and compared with [90] in Table 5.4. The sound pressure level at the centre of the right boundary and at the centre of the domain have been plotted in Figs. 5.4(a) and (b) respectively. From Table 5.4 and Figs. 5.4 it is evident that present study gives exact sound pressure both at the boundary and at the centre of the domain.

Table 5.4: First ten natural frequencies (rad/s) of the box with 2.5 mm flexible walls

Mode	2.5mm thick cavity (present model)	2.5mm thick cavity Niyogi et al. (2000) [90]
1	266.77	266.7666
2	337.61	337.6062
3	438.41	438.4063
4	465.12	465.1226
5	632.49	632.4927
6	819.34	819.3376
7	1012.41	1012.4053
8	1174.88	1174.8832
9	1526.88	1526.8841
10	3517.80	3517.8012

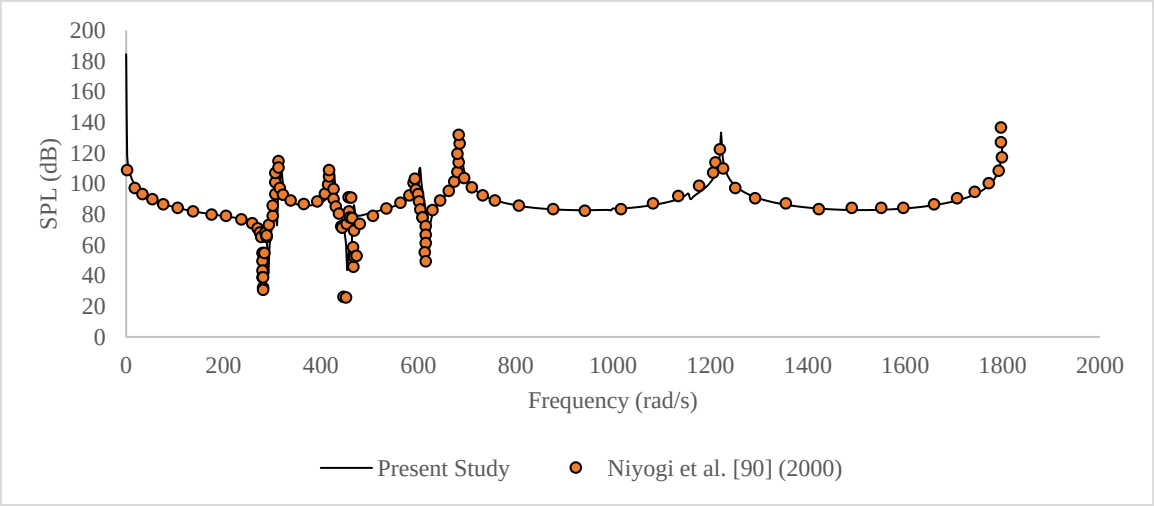

(a)

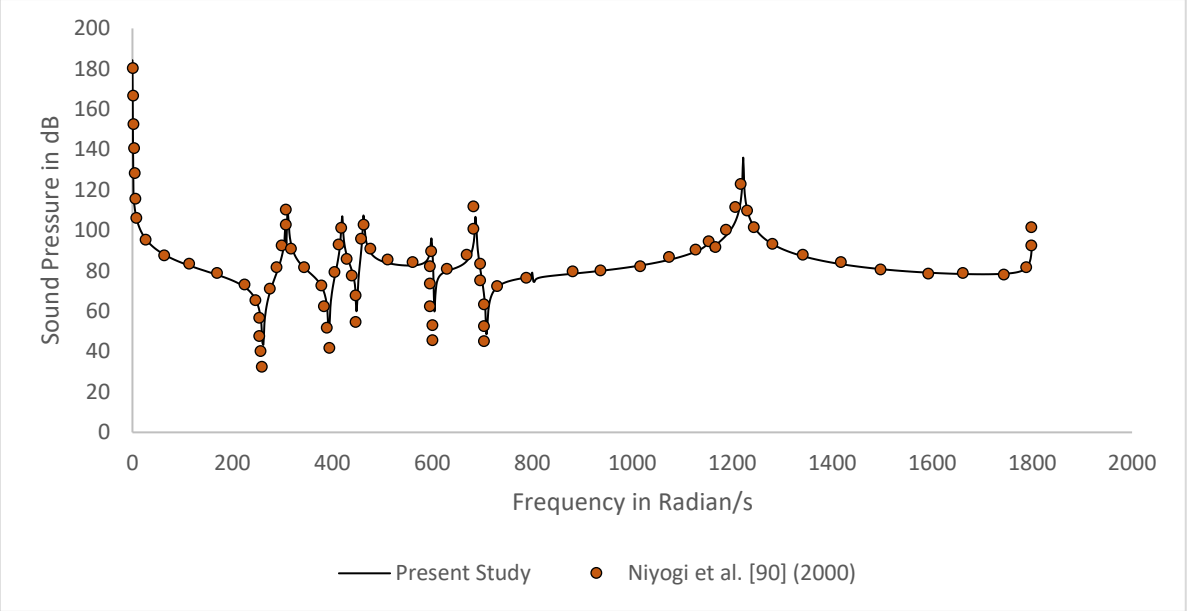

(b)

Fig. 5.4: SPL (dB) (a) at centre of the right boundary wall and (b) at the centre of the domain

5.3.Numerical Case Studies

5.3.1. Case Study 1: Variation of Sound Pressure Level for Stiffened and Unstiffened Acoustic Cavities

In this study, the variations of SPL (dB) for stiffened and unstiffened acoustic cavities are compared. Use of stiffener increases the stiffness of the structure and hence the dynamic behaviour of the dry cavity gets modified. As a result, a variation in SPL in the ICSA problem is only natural. The basic cavity selected for the research is as shown in Fig. 5.1, with flexible top and right walls. In the corresponding stiffened acoustic cavity shown in Fig. 5.5, the top flexible wall of 1.8m×0.6m is stiffened by two transverse stiffeners with same material properties. Three different widths of stiffeners have been taken into consideration.

Case-I: 4mm thick cavity with 4mm thick and 75mm wide stiffeners
Case-II: 4mm thick cavity with 4mm thick and 100mm wide stiffeners
Case-III: 4mm thick cavity with 4mm thick and 150mm wide stiffeners

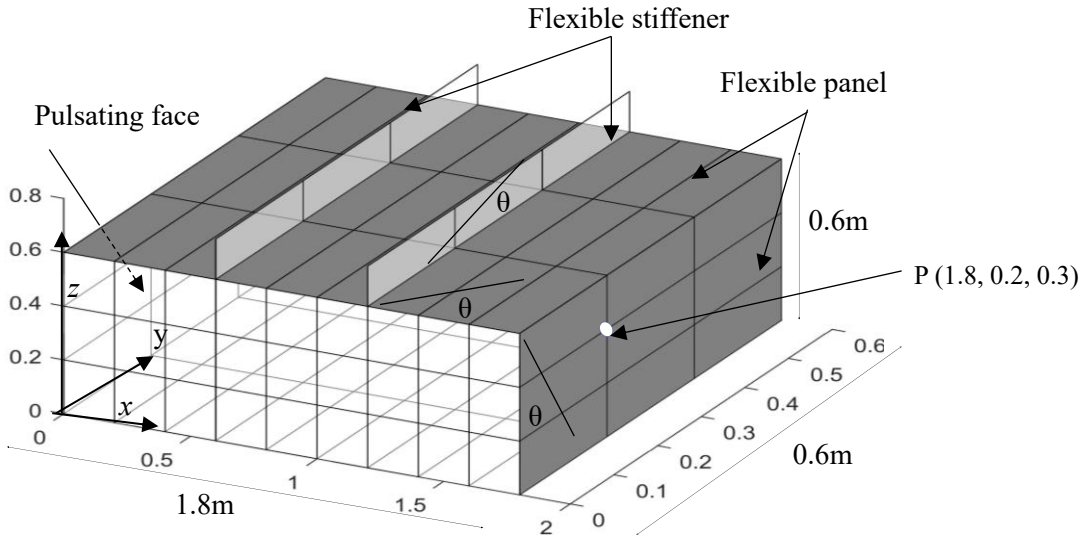

Fig. 5.5: Geometry of stiffened acoustic container, θ shows the definition of fibre angles

The thickness of the flexible walls and stiffeners are taken as 4mm while the stack sequence is $(0^o/90^o)_s$. The material and layup sequence of the stiffeners are kept same as that of original cavity. For the stiffeners, the extreme edges at the two ends have been kept free.

Table 5.5 shows the first twenty undamped natural frequencies of unstiffened and stiffened enclosures. Fig. 5.6 shows graphical representation of corresponding dry natural frequencies. These structural modes have been taken in the analysis to calculate the mobility relation for both the cavities.

Table 5.5 reveals that the fundamental frequency for stiffened structure is nearly 72% more than the unstiffened cavity. However, the percent increase has dropped in the higher modes. In comparison, the percentage increase in the total mass of the flexible walls is only 12.5% for case III, computed based on the top and right flexible walls, ignoring other four walls.

The cavity is excited as stated earlier in validation study 2 and the variation above SPL (dB) is shown graphically for point P (Fig. 5.7) at the boundary in Fig. 5.7.a and at the centre of the cavity in Fig. 5.7.b. The damping ratio, ξ, for all the participating modes has been taken as 0.1% in all the four cases.

Table 5.5: First twenty natural frequencies (rad/s) of the 4mm thick stiffened and unstiffened acoustic cavities

Mode	Unstiffened	Stiffened-Case-I	Stiffened-Case-II	Stiffened-Case-III
1	393.36	678.66	679.33	679.16
2	528.93	780.05	781.87	782.07
3	701.18	873.52	875.91	876.88
4	866.30	896.69	898.06	899.12
5	959.92	1333.72	1334.52	**1218.19**
6	1072.05	1386.40	1387.41	**1225.26**
7	1161.19	1405.04	1405.21	1336.39
8	1265.63	1433.19	1434.53	1388.77
9	1346.62	1581.13	1585.81	1405.59
10	1413.51	1636.31	1641.87	1435.70
11	1620.06	1677.85	1677.79	1592.84
12	1648.66	1688.40	1688.40	1655.94
13	1690.49	2271.85	2116.94	1686.10
14	1951.02	2300.09	2127.00	1688.41
15	2036.76	2314.53	2273.83	2119.92
16	2308.56	2319.79	2301.54	2123.92
17	2316.90	3378.17	2314.66	2275.42
18	2353.57	3398.09	2319.95	2302.89
19	2680.64	4326.37	3020.18	2314.79
20	2822.27	4360.03	3034.17	2321.02

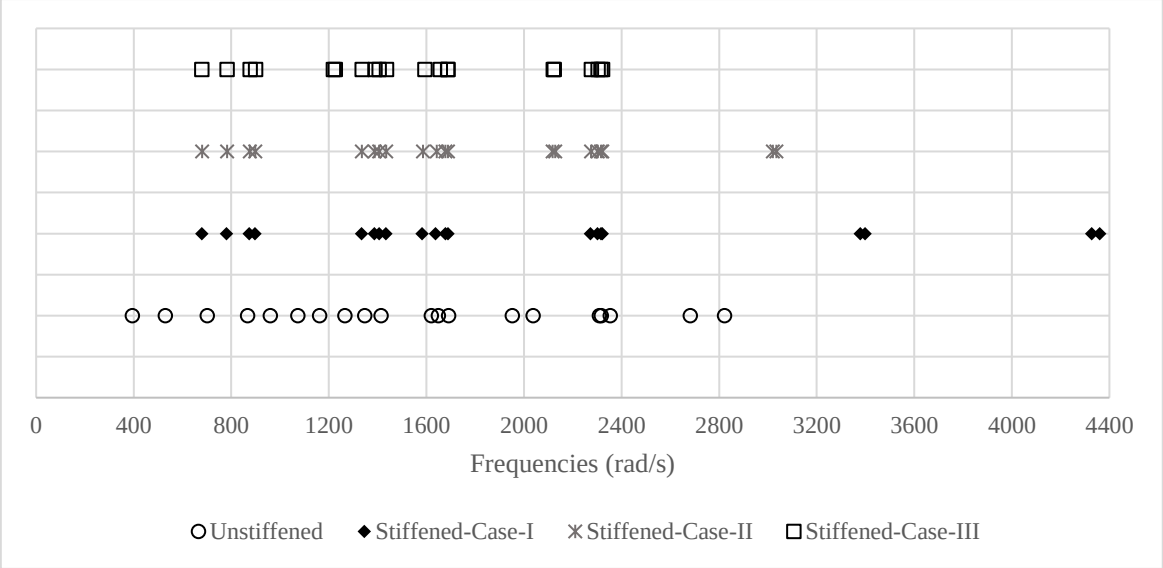

Fig. 5.6: Graphical comparison of dry natural frequencies (Case Study 1)

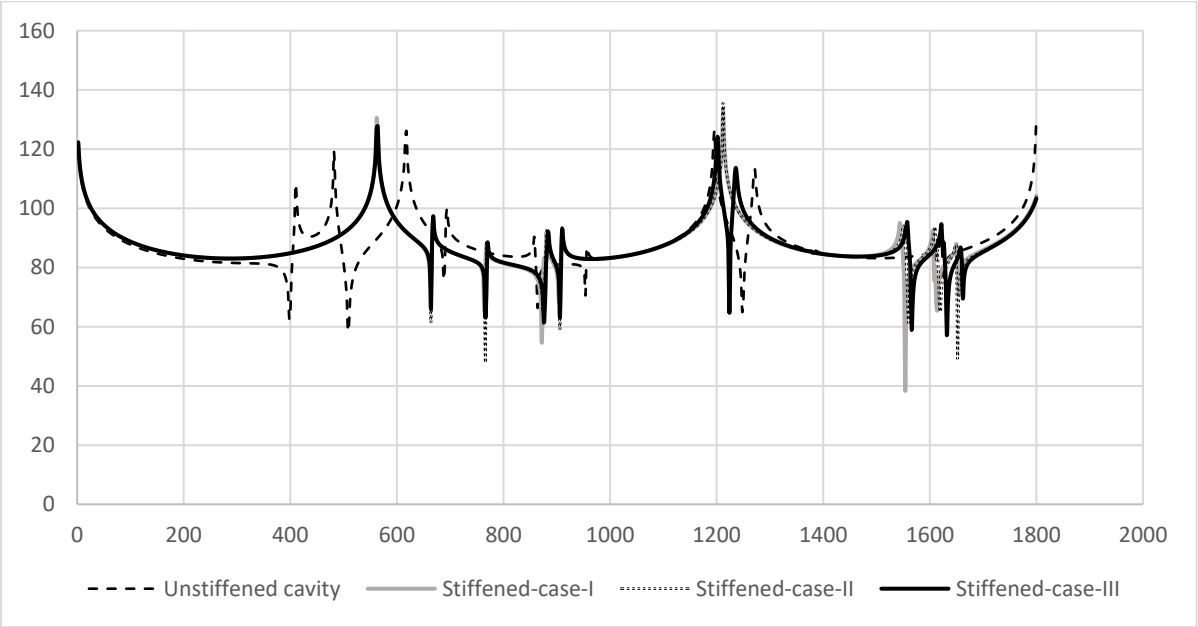

(a)

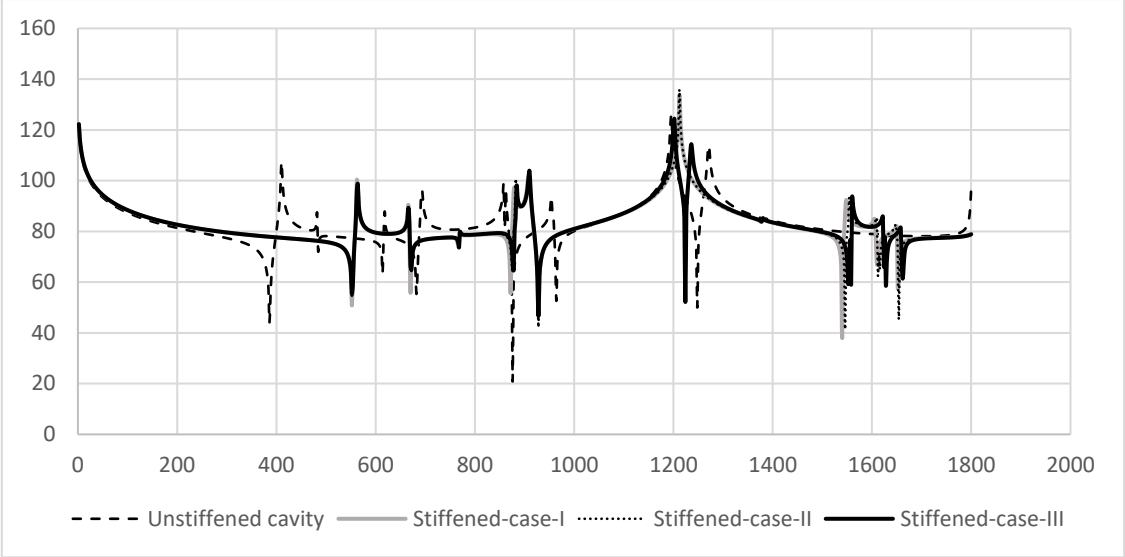

(b)

Fig. 5.7: Variation of SPL (dB) (a) at boundary point P (**Fig**. 5.5) on the right wall and (b) at the centre of the domain for 4mm thick flexible walls of stiffened and un-stiffened cavities with ξ = 0.1% for each structural mode

From Fig. 5.6, it is observed that for the unstiffened case, the dry natural frequencies are more evenly distributed throughout the range of frequency, unlike the stiffened cases, where the natural frequencies are clustered in narrow bands. This implies that the stiffeners suppress certain modes those are visible in unstiffened cavities. The fundamental frequency increases due to increase in stiffness when stiffeners are added. However, interestingly, the value of first natural frequencies suggest that the width of the stiffeners have very small contributions on structural stiffnesses. This might be due to the edges of the stiffeners being left free and unconnected. The effect of these natural frequencies is prominent from the SPL plot at the boundary and at centre of domain as shown in Fig. 5.7.a and b, respectively.

From Fig. 5.7.a, it is observed that the first acoustic peak of 108 dB for the unstiffened cavity appears at 410 rad/s after a trough of 62.6dB at 398 rad/s whereas the first structural mode of the dry cabinet appears at 393.36 rad/s while the computed first rigid acoustic mode is at $\Omega = c\pi/L =$ 593.4 rad/s. The next acoustic peak is induced at 482 rad/s (119 dB) followed by a 58 dB trough at 508 rad/s. The effect of acoustic mode is shifted at 618rad/s with a 126dB peak. The second rigid acoustic mode is prominent at 1200 rad/s (125dB). Another short peak of 112.6dB is produced which could be induced by the presence of some structural modes of dry cavity. Intermediate kinks are developed at nearly all structural frequencies though the effects are not equally intense.

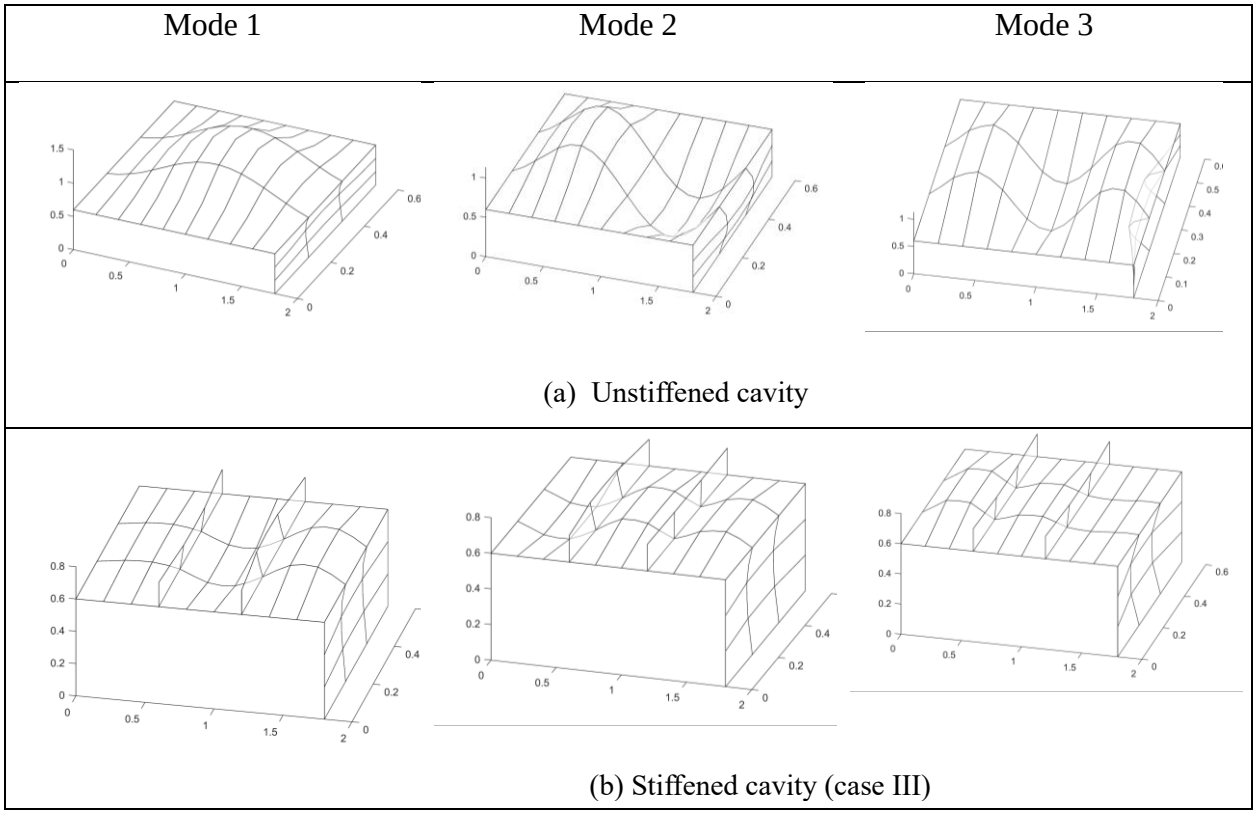

Fig. 5.8: First three mode shapes of the unstiffened and stiffened cavities

When the transverse stiffeners are attached at the top face, the stiffness of the flexible wall is enhanced with non-uniform distribution of natural frequencies. As a result, though the fundamental frequency of the dry stiffened cavity is approximately 679 rad/s for all three cases of stiffened cavity (Table 5.5) and the first acoustic mode is at 593.4 rad/s, Fig. 5.7.a reveals that the first acoustic peak appears at 562 rad/s (126dB), lower than either, manifesting dominance of the local variation of cavity stiffness due to the stiffeners. However, the second peak shows up at 1200 rad/s, a bit higher that the expected second rigid acoustic mode ($2c\pi/L$ =1186.8 rad/s).

For stiffened case I, II and III, the natural frequencies are similar in values and distribution except at the region of 1200 rad/s where, case III with stiffener width 150mm, two frequencies, 1218 rad/s and 1225 rad/s exist. As a result, a shorter peak is visible near second acoustic mode for case-III following a dip of 52dB at 1224 rad/s both at boundary and centre of domain (Fig. 5.7.a and b). At the lower structural frequencies, prominent kinks are visible due to presence of structural modes whereas, at higher natural frequencies, effects of structural modes are nominal. Application of stiffener has quite efficiently truncated the acoustic peaks visible at the centre of the domain of the unstiffened cavity near 410 rad/s. Also, an inverted

nature of SPL is observed in the range of 670 to 870 rad/s. For the stiffened cavities, three structural modes are present in this region.
First three mode shapes of the unstiffened and stiffened cavities have been shown in Fig. 5.8. The patterns are quite different. It is evident that presence of structural modes in a particular region, and rather intuitively, mode shapes play important roles in variation of the SPL pattern.

5.3.2. Case Study 2: Variation of Sound Pressure Level for Stiffened Acoustic Cavity Due to Variation in Flexible Wall Thickness

In this study, the variation of SPL (dB) within the stiffened acoustic cavity is performed for variation in the thickness of flexible skin and stiffeners. Five cases have been studied.

Case I: Cavity with 3mm skin and 3mm thick stiffener
Case II: Cavity with 4mm skin and 4mm thick stiffener
Case III: Cavity with 5mm skin and 5mm thick stiffener
Case IV: Cavity with 4mm skin and 3mm thick stiffener
Case V: Cavity with 4mm skin and 5mm thick stiffener

Stiffener width taken is 150mm for all the cases. Table 5.6 shows first twenty natural frequencies for the structure for different thicknesses. Graphical representation of natural frequencies of dry cavities are plotted in Fig. 5.9. Table 5.6 shows that there are clusters of natural frequencies in each of the cases.

For proper understanding in Fig. 5.10 we plot SPL at boundary point P and centre of domain for cases I, II and III wherein both stiffeners and the flexible walls have 3, 4 and 5mm thicknesses and compare the results. In a second case, in Fig. 5.12 we compare results of cases II, IV and V, where the stiffener thicknesses are varied from 3 to 4 to 5mm keeping cabin wall thickness 4mm. The damping ratio, ξ is taken as 0.1% for all participating modes.

From Fig. 5.9, it could be observed that with increase in thickness, the stiffness of the structure increases which in turn alter the SPL patterns.

Table 5. 6: First twenty natural frequencies (rad/s) of the stiffened cabin for Case Study 2

SL	Case-I	Case-II	Case-III	Case-IV	Case-V
1	533.10	679.16	817.14	673.12	686.59
2	607.66	782.07	945.43	777.42	786.07
3	670.02	876.88	1073.62	873.37	878.19
4	683.85	899.12	1105.84	898.74	899.35
5	922.74	1218.19	1504.84	942.07	1341.22
6	925.97	1225.26	1519.13	947.13	1391.63
7	1027.61	1336.39	1639.14	1331.62	1404.67
8	1058.69	1388.77	1712.48	1385.62	1436.51
9	1073.60	1405.59	1726.78	1405.40	1458.34
10	1088.62	1435.70	1776.19	1434.50	1469.61
11	1226.76	1592.84	1948.69	1590.23	1599.23
12	1268.94	1655.94	2030.44	1621.87	1665.07
13	1285.05	1686.10	2072.95	1624.76	1688.42
14	1290.47	1688.41	2086.78	1651.15	1693.95
15	1607.76	2119.92	2623.45	1683.30	2276.00
16	1611.66	2123.92	2628.07	1688.42	2303.36
17	1726.97	2275.42	2808.61	2274.44	2314.84
18	1740.13	2302.89	2854.42	2302.02	2320.21
19	1746.32	2314.79	2873.98	2314.70	2593.52
20	1749.54	2321.02	2883.91	2320.27	2600.07

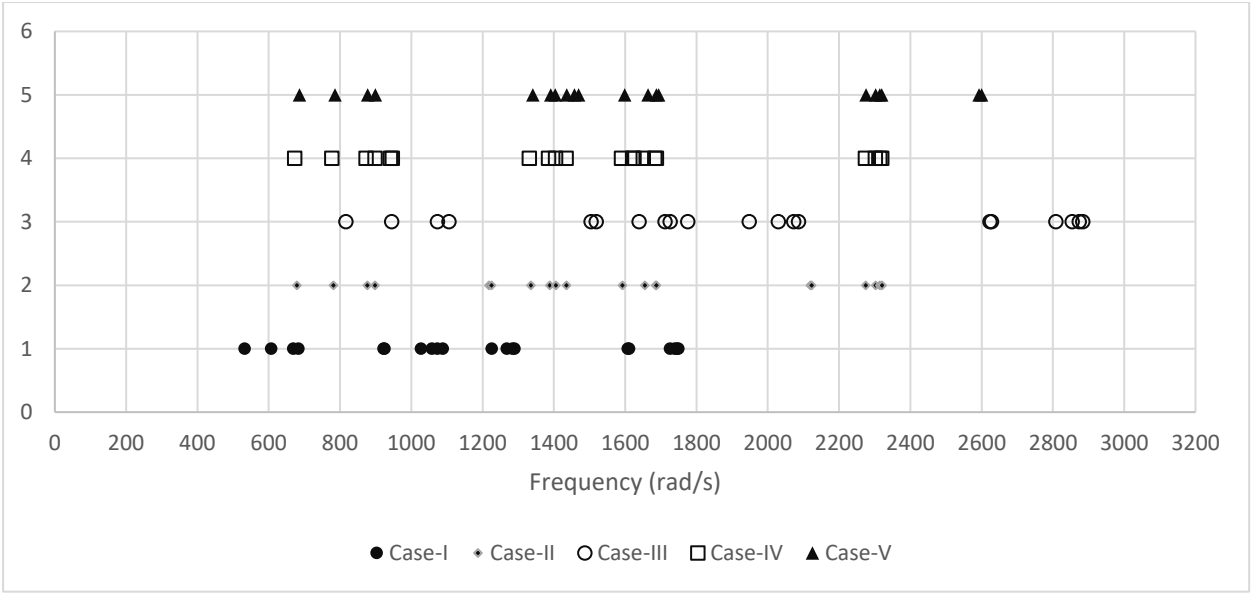

Fig. 5.9: Graphical comparison of dry natural frequencies (Case study 2)

Though the fundamental frequency of cavity in case I is 533rad/s (refer Table 5.6) and the first rigid acoustic peak is at 593.4rad/s, case study I shows first crest at 500rad/s (Fig. 5.10a). In unstiffened cavities the first peak appeared after the first structural or rigid acoustic mode. This variation occurs because of stiffeners present over the cavity that alters the mode shape which is equivalent to 3 by 1 mode for the unstiffened top plate.

Presence of peak has been observed at 598rad/s which is near the first acoustic mode for rigid cavity i.e., 593.4 rad/s. Due to presence of close third and fourth natural frequencies, a combined peak has formed at 692 rad/s with a dip in SPL at 668rad/s. As several natural modes are present near the second rigid acoustic mode, a set of peaks and troughs have developed around 1200 rad/s. At lower frequencies, existence of two peaks in quick succession, reduces individual SPLs compared to the case where there is only one peak. For 4mm and 5mm thick cavities (case II and III) the first peaks are manifested at 562 rad/s and 580rad/s, respectively, which are slight behind of the first rigid acoustic modes. At nearly all natural frequencies of the dry cavity and rigid acoustic frequencies a sudden jerk is observed in the curve. From Fig. 5.9, it is observed that near the second rigid acoustic mode, dry frequencies exist for 3mm and 4mm thick cavity (case I and II) with stiffener of same thicknesses. This results in successive troughs in this frequency zone. For case III, absence of dry frequency near rigid second acoustic mode produces a clear peak of 131dB at 1226rad/s. It is also observed that the maximum SPL value in dB exceeds 140dB for this case at the first acoustic mode. Overall, it

can be said that the acoustic peaks are smallest for the thinnest enclosure and largest for the thickest one.

From Fig. 5.10b, it is observed that interaction kink is present at same frequencies in domain as well as on the boundary point P. Looking into Fig. 5.10a and b, it may be noticed that the thinner cavities have lower closely spaced peaks than the thicker one.

Looking into Figs. 5.9 and 5.11, it is observed that the overall pattern of SPL remains same irrespective of the stiffener thicknesses for cases II, IV and V respectively except only at the region of second rigid acoustic mode where the cavity with 4mm thick stiffener (case II) shows a dip due to presence of dry structural frequencies. The cavity with 3mm thick stiffener (case III) being softer than case II and V, shows lesser SPL values at crests and troughs in certain regions than others. Hence, it can be said that presence of structural modes near rigid acoustic mode provides a control in the SPL both at the boundary and at the domain centre.

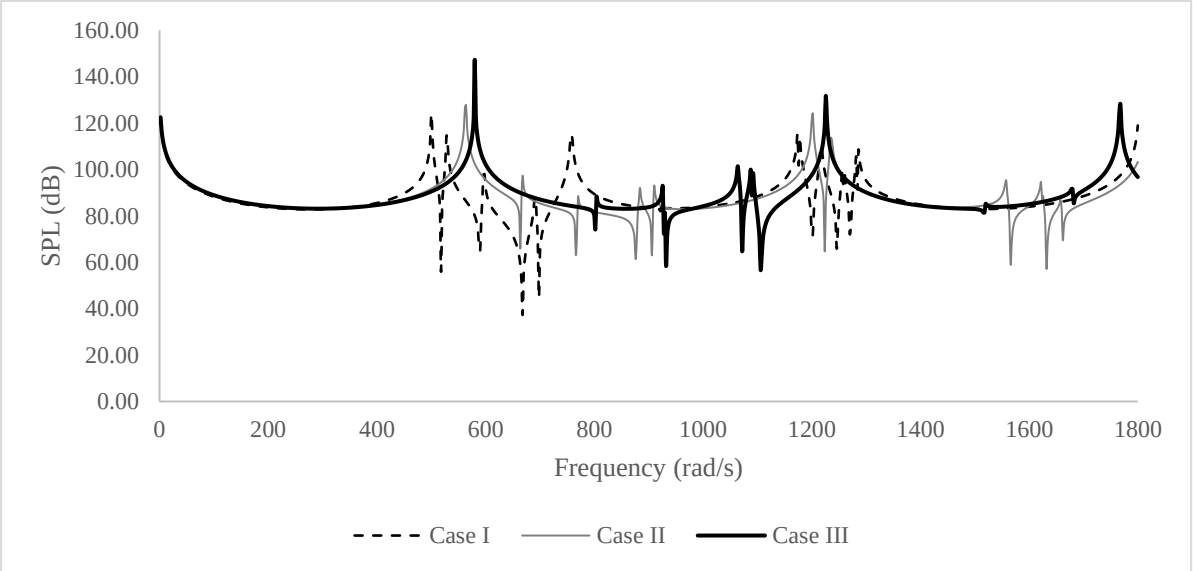

(a)

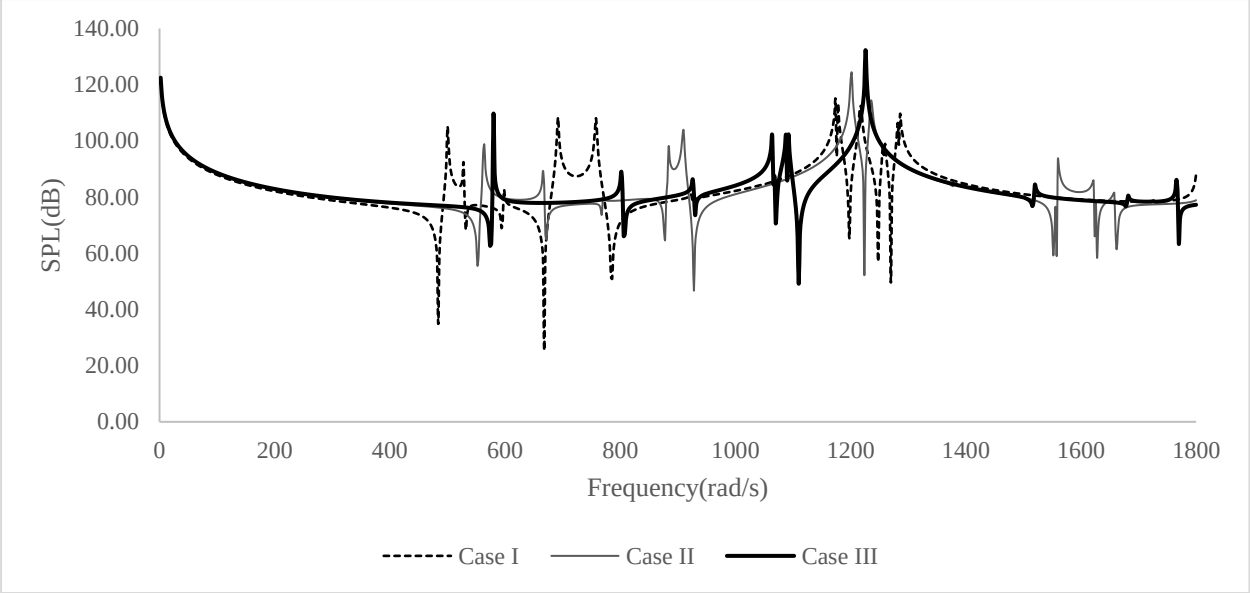

(b)

Fig. 5.10: Variation of SPL (dB) (a) at boundary point P in right wall and (b) at the centre of the domain due to variation in thickness of the flexible skin and stiffener

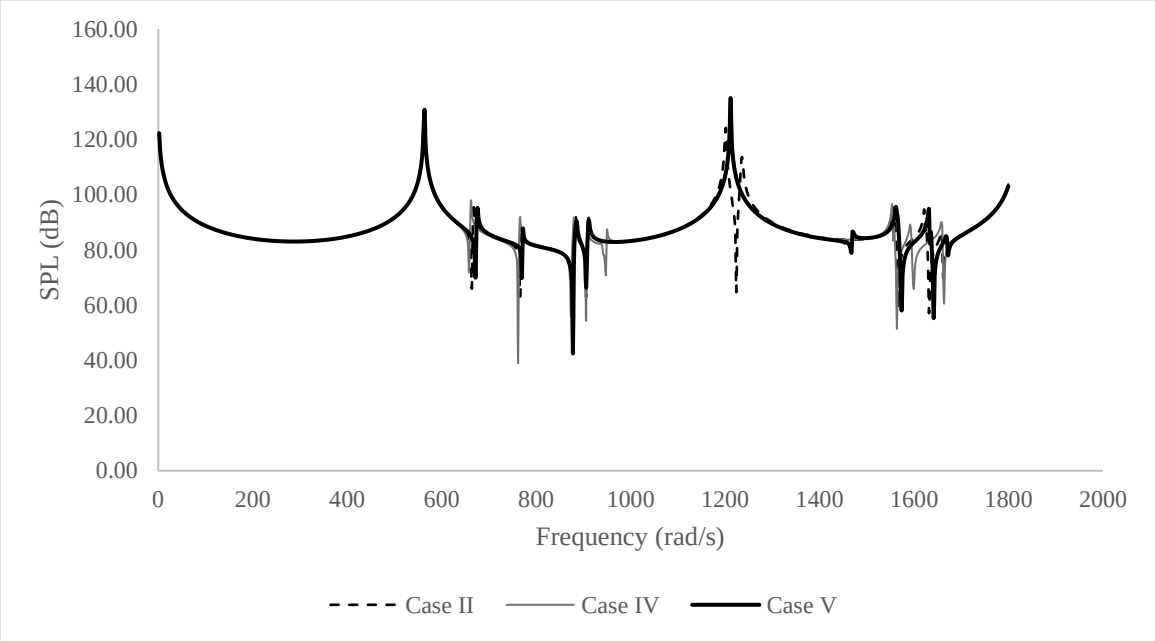

(a)

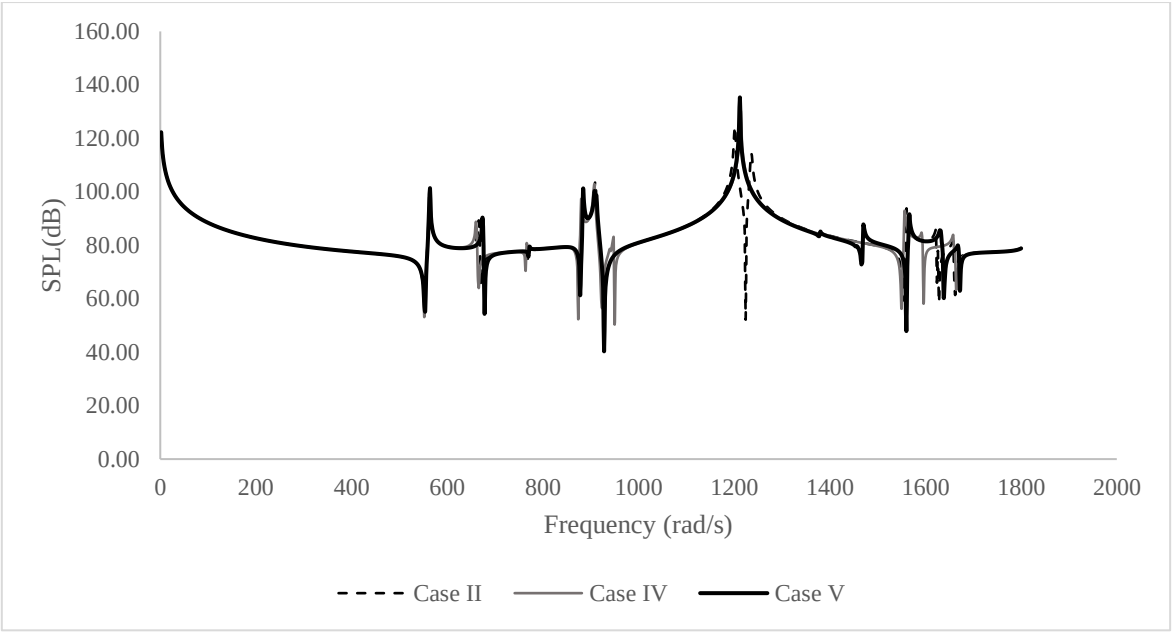

(b)

Fig. 5.11: Variation of SPL (dB) (a) at boundary point P in right wall and (b) at the centre of the domain due to variation in thickness of stiffeners

5.3.3. Case Study 3: Variation of Sound Pressure Level in Stiffened Acoustic Cavities Due to Change in Damping Ratios, ξ

In this study, the variation of SPL (dB) for stiffened acoustic cavity shown in Fig. 5.5 is studied due to imposed variation in viscous damping of the cabin structure. Three case studies are presented with structural damping ratios set at 0.1%, 0.5% and 1% for all participating modes of the containing structure wherein the thickness of the flexible walls and the stiffeners are kept 4mm for E-glass epoxy composites (ref. Table 5.1). The variation of sound pressure level in dB is plotted at the boundary point P and at centre of the domain in Fig. 5.12a and 12b respectively.

From the inspection of Fig. 12a and 12b, it is seen that the three cases provide identical plots except at the acoustic crests and troughs. In other words, the change in damping ratio is manifested only at the crests and troughs and nowhere else. Most importantly, the introduction of higher damping ratio unfailingly truncates the peaks producing a relatively shorter crest and trough thus making the SPL curve relatively dwarf, but has no influence on the SPL in the saddles. The effect of changing damping ratio is, however, prominent after the first rigid acoustic peak of Fig. 5.12a. The first peak point is observed at 564 rad/s for the rigid acoustic mode.

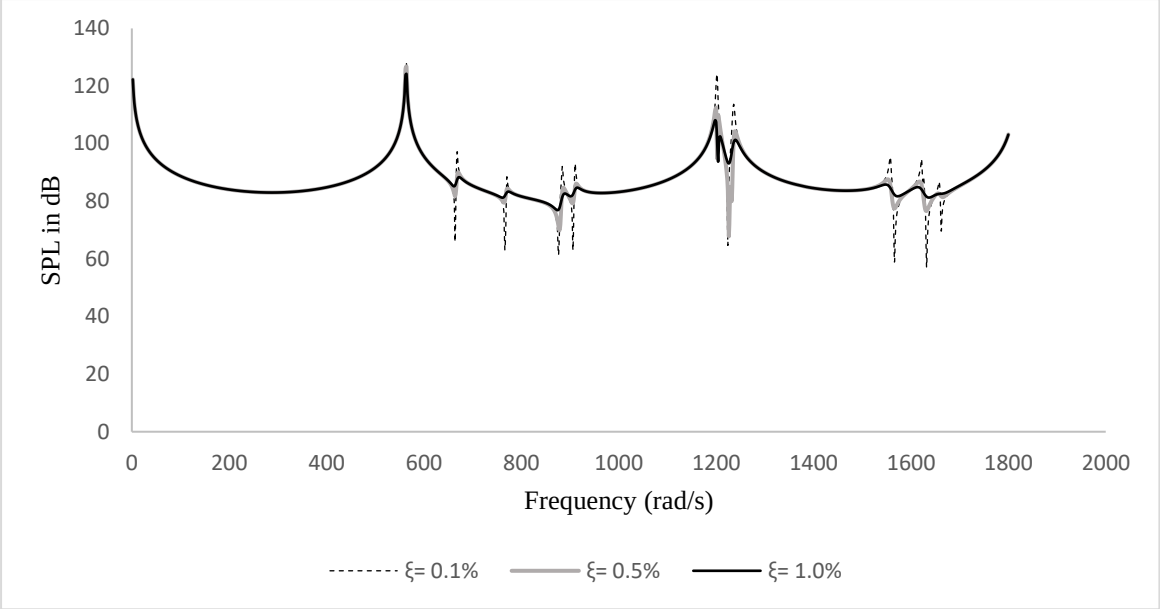

(a)

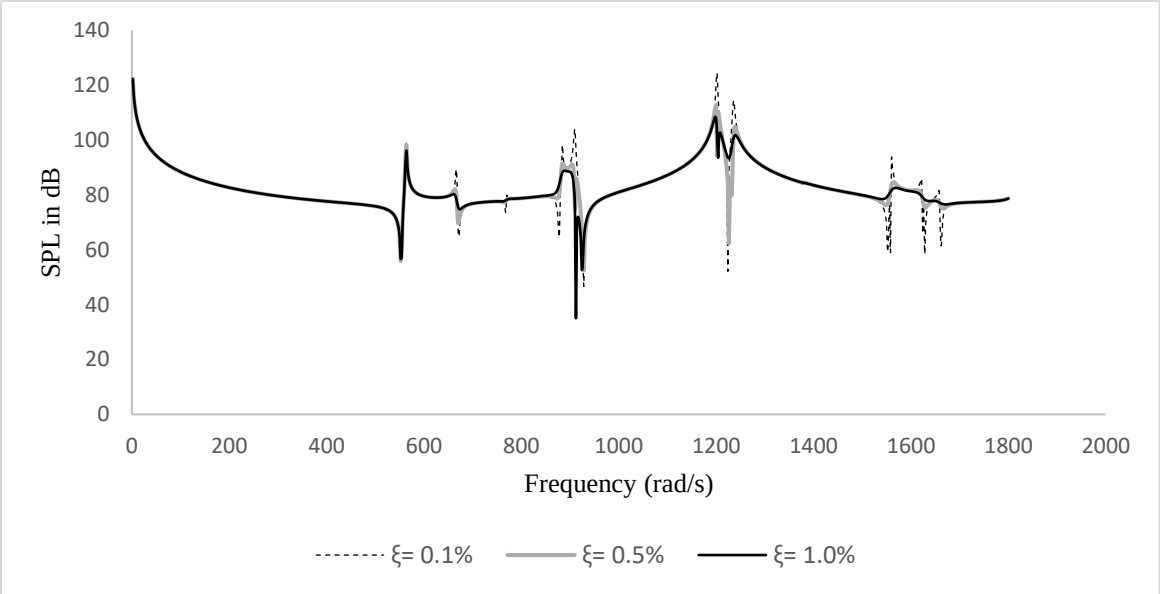

(b)

Fig. 5.12: SPL (dB) (a) at boundary point P and (b) at the centre of the domain for different damping with 4mm thick flexible walls in the stiffened cavity

Then second peak at 668 rad/s has been steadily truncated with damping ratio gradually increasing from 0.1% to 0.5% to 1%. In the second rigid acoustic peak near 1200 rad/s higher damping ratio reduces the peak value to a large extent from 122dB to 107dB at boundary as well as at the centre of the domain.

5.3.4. Case Study 4: Variation of Sound Pressure Level in Stiffened Acoustic Cavities Due to Change in Position and Number of Stiffeners

To observe the effect of adding stiffeners with different orientations, three case studies, as listed below, have been conducted with cavities shown in Fig. 5.13.

Case I: Cavities with two transverse stiffeners at one-third and two-third positions of the top plate (Fig. 5.5)

Case II: Cavities with two longitudinal stiffeners at one-third and two-third positions of the top plate (Fig. 5.13a)

Case III: Cavities with two longitudinal and two transverse stiffeners (Fig. 5.13b)

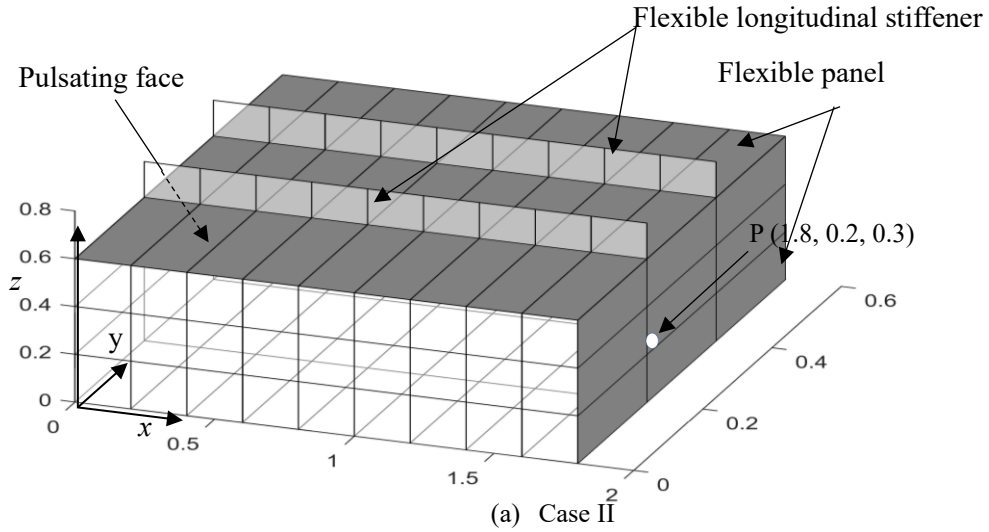

(a) Case II

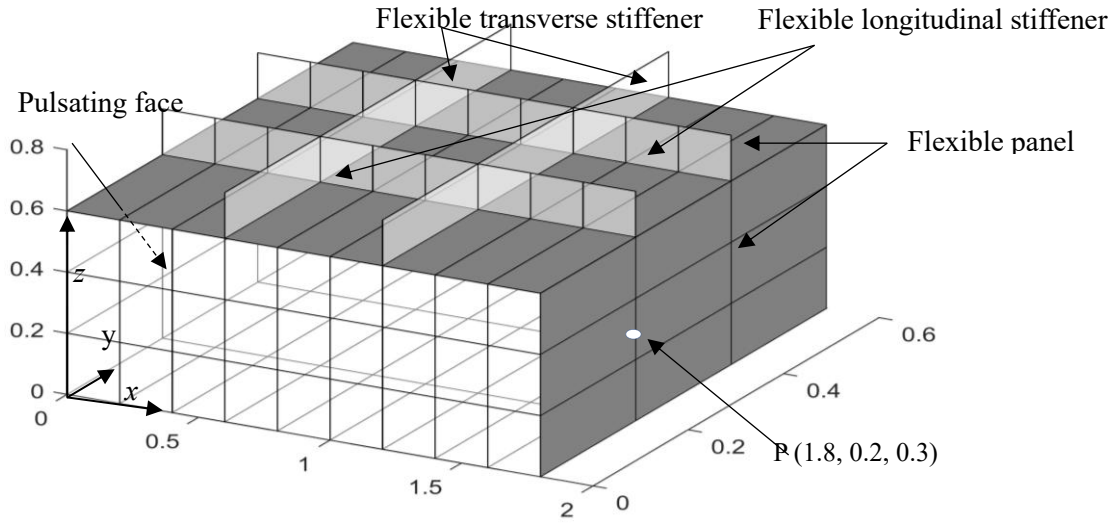

(b) Case III

Fig. 5.13: Arrangement of the stiffened cavities for (a) Case II and (b) Case III

The flexible walls are 4mm thick with $(0^o/90^o)_s$ lay-up made up of E-glass/epoxy composites as detailed in Table 5.1. The modal damping ratio is taken as 0.1% for all modes. Twenty structural modes have been used to compute the mobility for the cavity for all the cases listed above. First twenty undamped natural frequencies have been tabulated in Table 5.7. The sound pressure level (SPL) at the boundary point P (1.8, 0.2, 0.3) (refer Fig. 5.13) and at centre of domain (0.9, 0.3, 0.3) in dB is plotted in Fig. 5.14 (a) and (b) respectively. First three mode shapes for all cases have been shown in Fig. 5.15. It can be seen from Table 5.7, that first few frequencies are very close for cases I and II. Whereas the frequencies for case III are sufficiently large.

Table 5.7: First twenty undamped natural frequencies (rad/s) of the stiffened cavities for cases I, II and III

Mode	Case I	Case II	Case III
1	679.16	675.37	893.15
2	782.07	737.16	1140.09
3	876.88	851.76	1176.90
4	899.12	866.31	1196.44
5	1218.19	895.91	1216.47
6	1225.26	1061.50	1230.48
7	1336.39	1112.19	1238.45
8	1388.77	1354.04	1422.93
9	1405.59	1387.02	1693.63
10	1435.70	1422.46	2089.43
11	1592.84	1675.57	2097.55
12	1655.94	1692.46	2115.06
13	1686.10	1714.37	2124.76
14	1688.41	1727.82	2133.24
15	2119.92	2089.40	2141.34
16	2123.92	2117.70	2314.99
17	2275.42	2123.95	4544.94
18	2302.89	2314.98	5603.53
19	2314.79	2526.77	5949.85
20	2321.02	2531.22	6019.70

However, from Fig. 5.14a and 14b, it has been noticed that the SPL curve at boundary for case II and III are similar though some differences are noted for SPL at the domain mid-point. This signifies that mode shapes have significant role in coupled behaviour just as the effect of frequencies corresponding to rigid acoustic modes and natural frequencies of the dry cabin. Number of interaction kinks are more in case I compared to other two cases at boundary. For case I, the plate in between the stiffeners has some deflection as seen in the mode shape Fig. 5.15. For cases II and III, the longitudinal stiffeners suppress the plates from bending and hence no significant deflections have been observed. Fig. 5.16a plots the SPL at the boundary point P and inside the domain at the horizontal and vertical planes through the mid-point, at a particular exciting frequency of 750rad/s for cases -I, II and III. It is seen that at this frequency a low-pressure zone is created at 1.2m from left side both at the boundary and at the domain irrespective of number of stiffeners or their positions. At the extreme left, the SPL at boundary and domain for cases II and III are slightly higher than that of case I. Fig. 5.16b shows the SPL distribution on the boundary for case III at frequencies 750 rad/s, 900 rad/s and 1050 rad/s, respectively. It is observed that the position of low-pressure zone shifts with change in frequency. At 900 rad/s a low-pressure zone is developed at the right flexible plate element. At 1050rad/s, presence of two low pressure zones travelling can be observed.

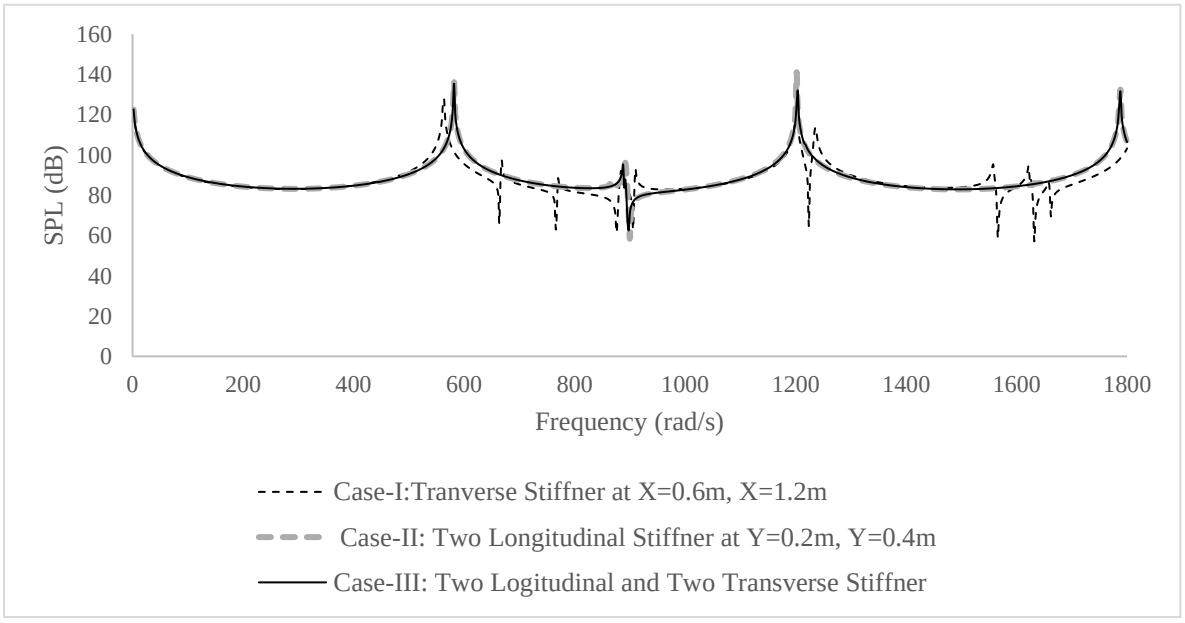

(a)

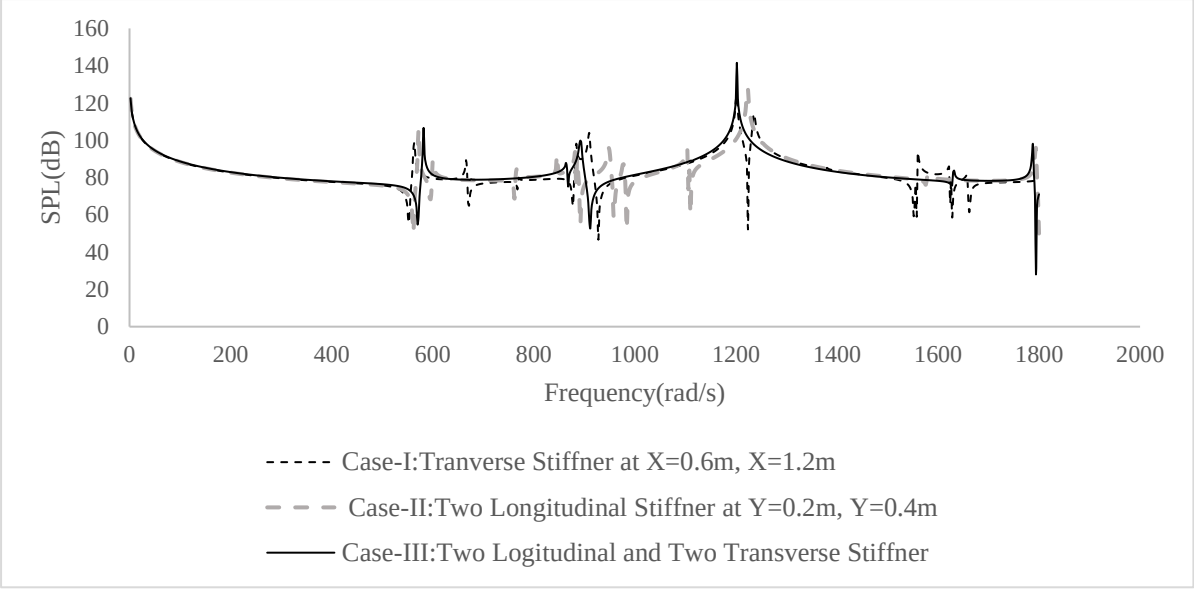

(b)

Fig. 5.14: SPL (dB) (a) at boundary point P on the right wall and (b) at the centre of the domain with 4mm flexible walls of the two stiffened cavities with $\xi = 0.1\%$

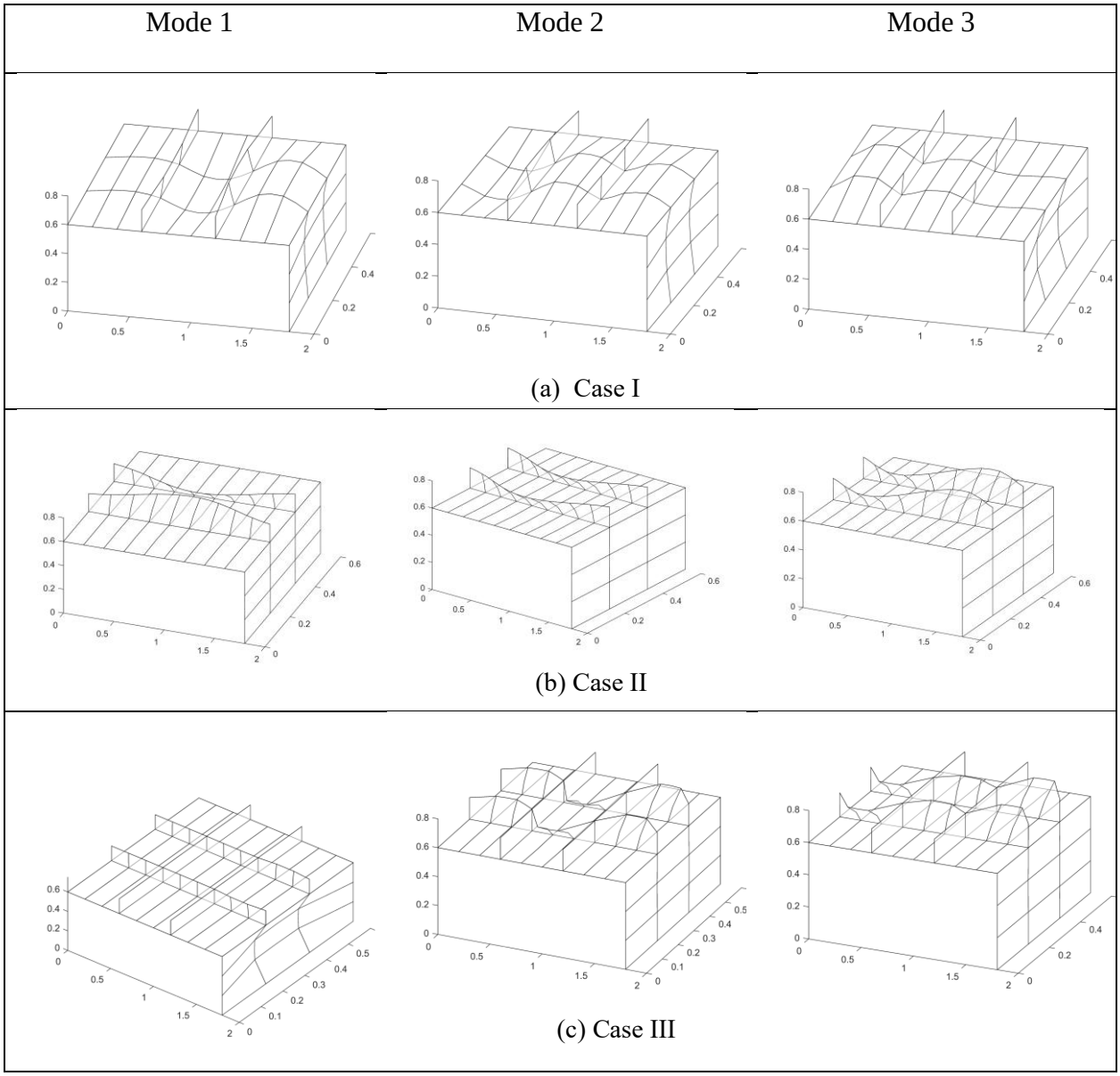

Fig. 5.15: First three mode shapes for (a) unstiffened cavity, (b) stiffened cavity with two transverse stiffeners and (c) stiffened cavity with two transverse and two longitudinal stiffeners

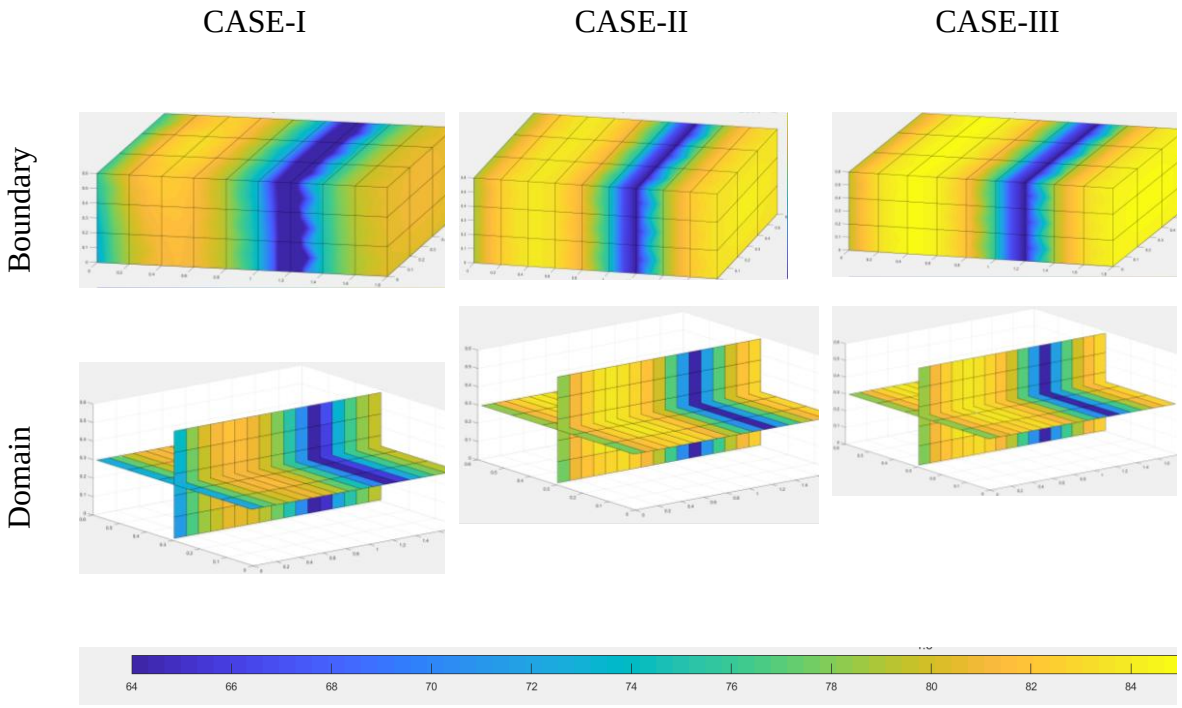

Fig. 5.16a: Sound pressure level (dB) on the boundary and domain at the horizontal and vertical plane through domain centre at 750 rad/s

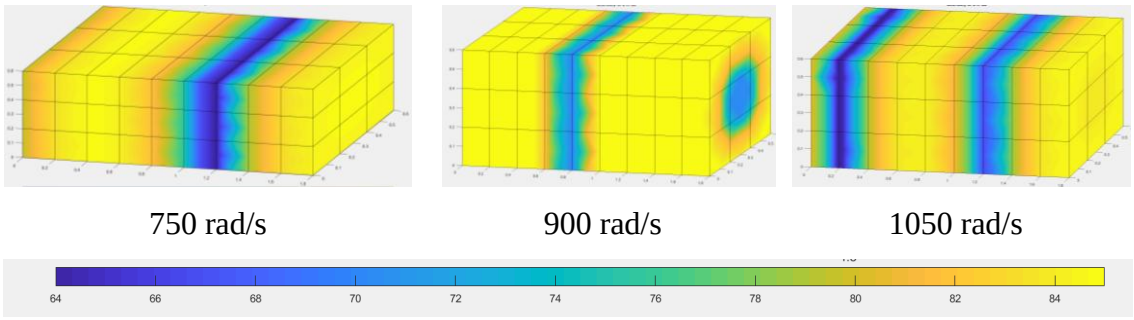

Fig. 5.16b: Sound pressure level (dB) on the boundary for case-III at different forcing frequencies

5.3.5. Case Study 5: Comparison of Displacement at the Boundary of the Cavity

In this study, in-plane and out of plane structural displacements on the flexible panel at location (1.8m, 0.2m, 0.3m) have been computed and plotted in Fig. 5.17a to 17c for unstiffened and transversely stiffened cavity (case-I) as given in case study 4 with same thickness and material properties. The acoustic pressure terms computed at the element nodes on the structural boundaries are applied as distributed forces. The global force vector is computed from the local ones by applying transformations in Eq. (8) to compile the element

load arrays. If the receptance relation (Eq. 13) is post multiplied by this global force vector, the nodal displacement array is obtained along the global co-ordinates. The displacement inflexion for the structures can be observed from Figs. 5.17(a), (b) and (c) which replicate each other very closely.

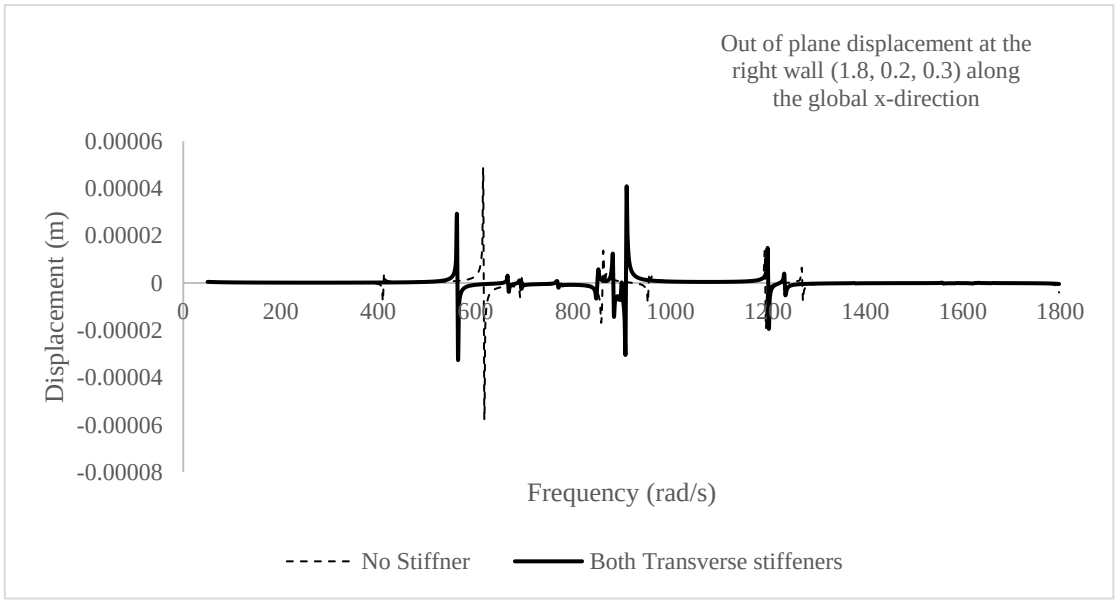

(a)

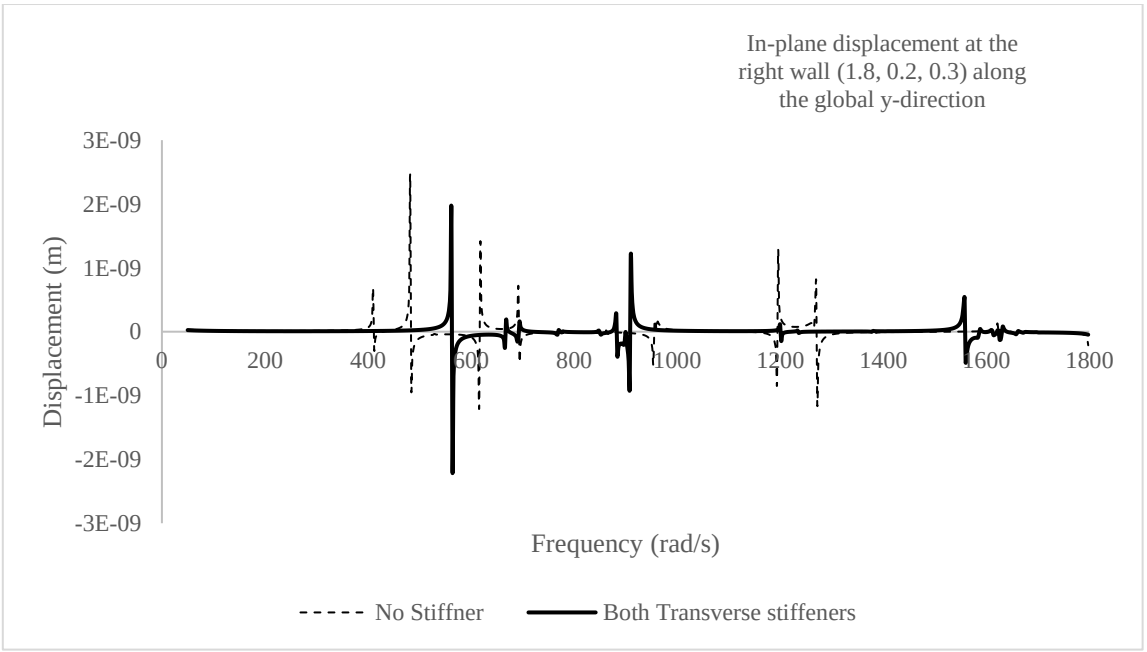

(b)

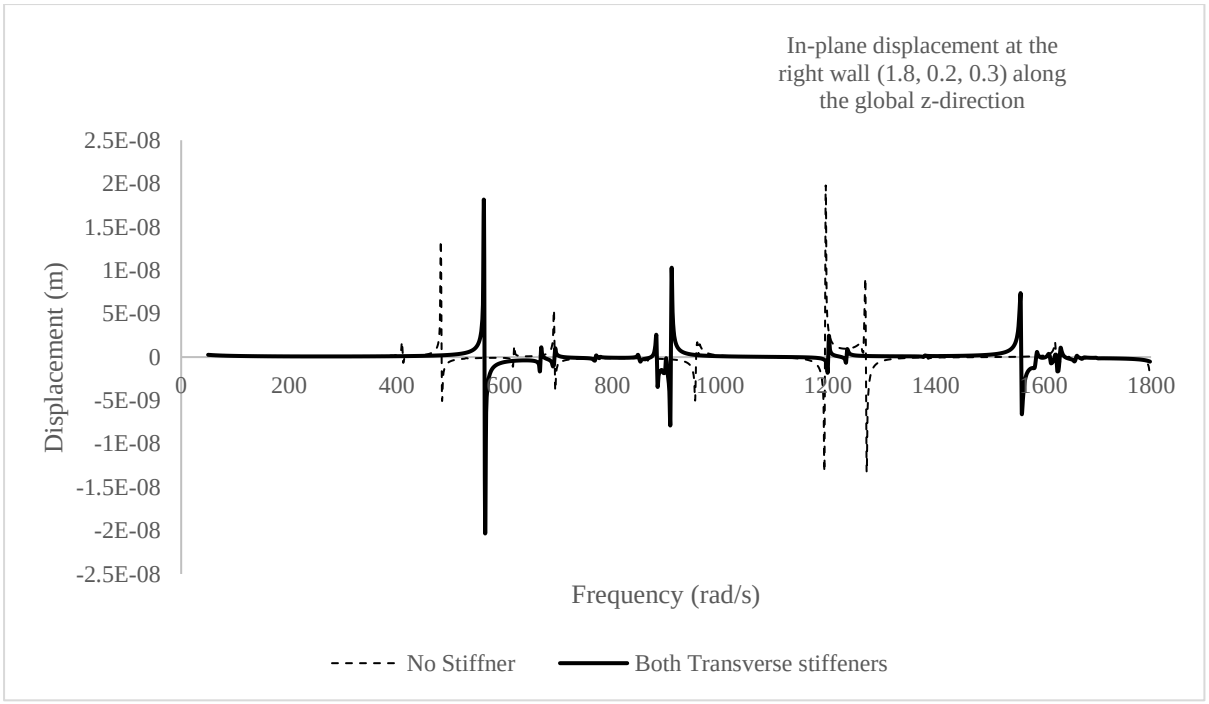

(c)

Fig. 5.17: (a) Out of plane displacement along x direction, (b) In plane displacement along y direction and (c) In plane displacement along z direction on the right flexible wall at (1.8, 0.2, 0.3)

For the unstiffened cavity, a small kink is visible at 414rad/s which is slightly higher than the first mode frequency (393.36rad/s) of the dry structure as given in Table 5.5. At 618rad/s acoustic resonance occurs with maximum displacement whereas the first rigid acoustic mode is at 593.4 rad/s. Other displacement kinks are short and are formed near the natural frequencies of the uncoupled structure (ref. Table 5.5). For stiffened cavity, first displacement kink is visible at 566 rad/s. Next large inflexion is visible near the fourth natural frequency at 910rad/s (ref. Table 5.5). Presence of stiffener modifies the stiffness of the structure and hence such large kink is observed. All the displacement kinks have occurred near the uncoupled frequencies of the dry structure, but large deflection did not necessarily form at all those frequencies.

The sound pressure level (dB) and the displacement(m) at P (Fig. 5.5) simultaneously with respect to the frequencies are plotted both for unstiffened and transversely stiffened cavities in Fig. 5.18a and 18b respectively. It is noticed that the displacement kinks triggered by structural modes are small compared to those by rigid acoustic modes in general, which instigates to investigate acoustic responses considering structural displacements.

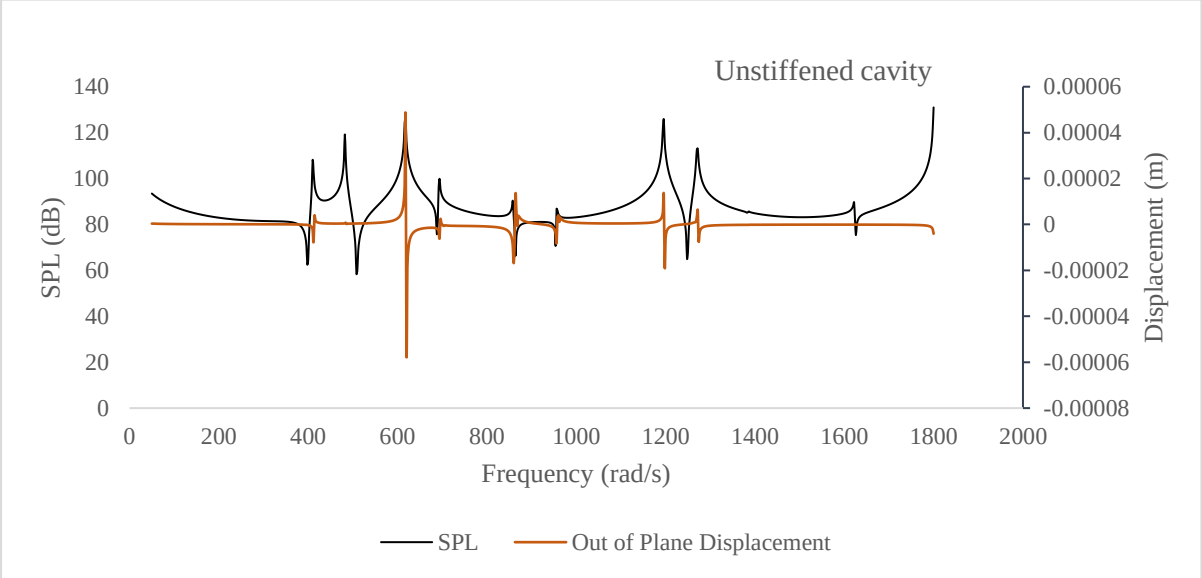

(a)

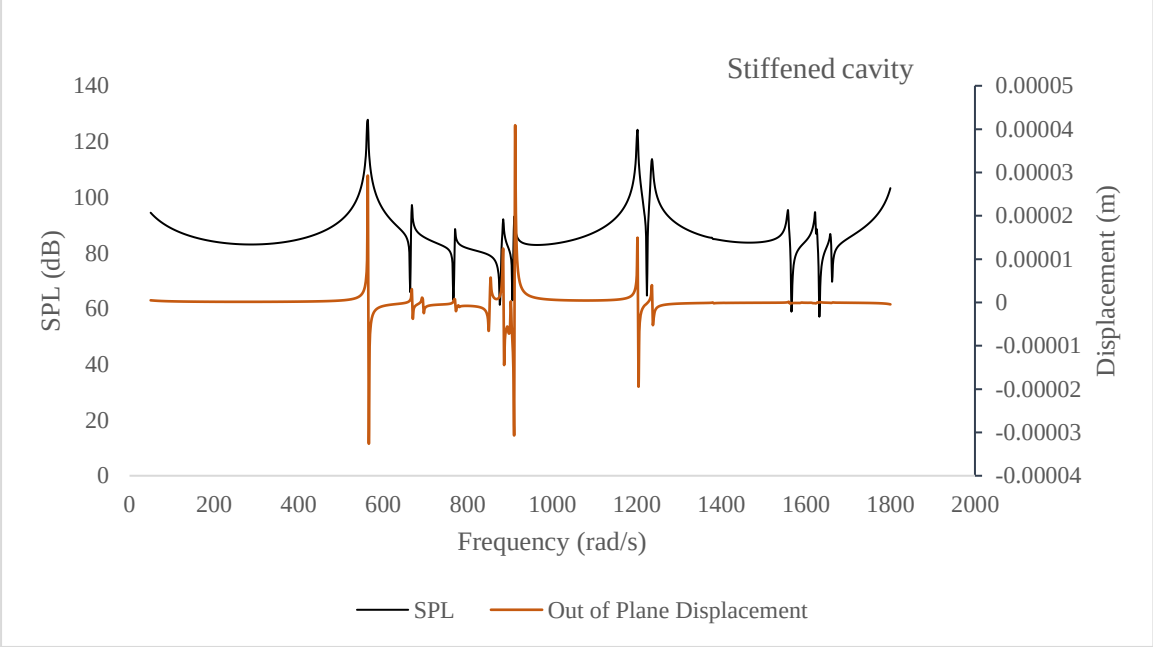

(b)

Fig. 5.18: The displacement along the global x direction (out of plane) and the SPL at the

right wall at 1.8, 0.2, 0.3 for (a) unstiffened and (b) stiffened cavity (case-III)

Fig. 5.19 depicts the displacements along x direction and along z direction for the boundary nodes at a particular forcing frequency 1200rad/s for unstiffened and transversely stiffened cavities (Case-I, in case study 4) respectively. To make the displacement clear, the stiffeners

are not shown. From Fig. 5.19, it can be observed that the x and z displacement values are nominal in case of stiffened cavity at the specified frequency.

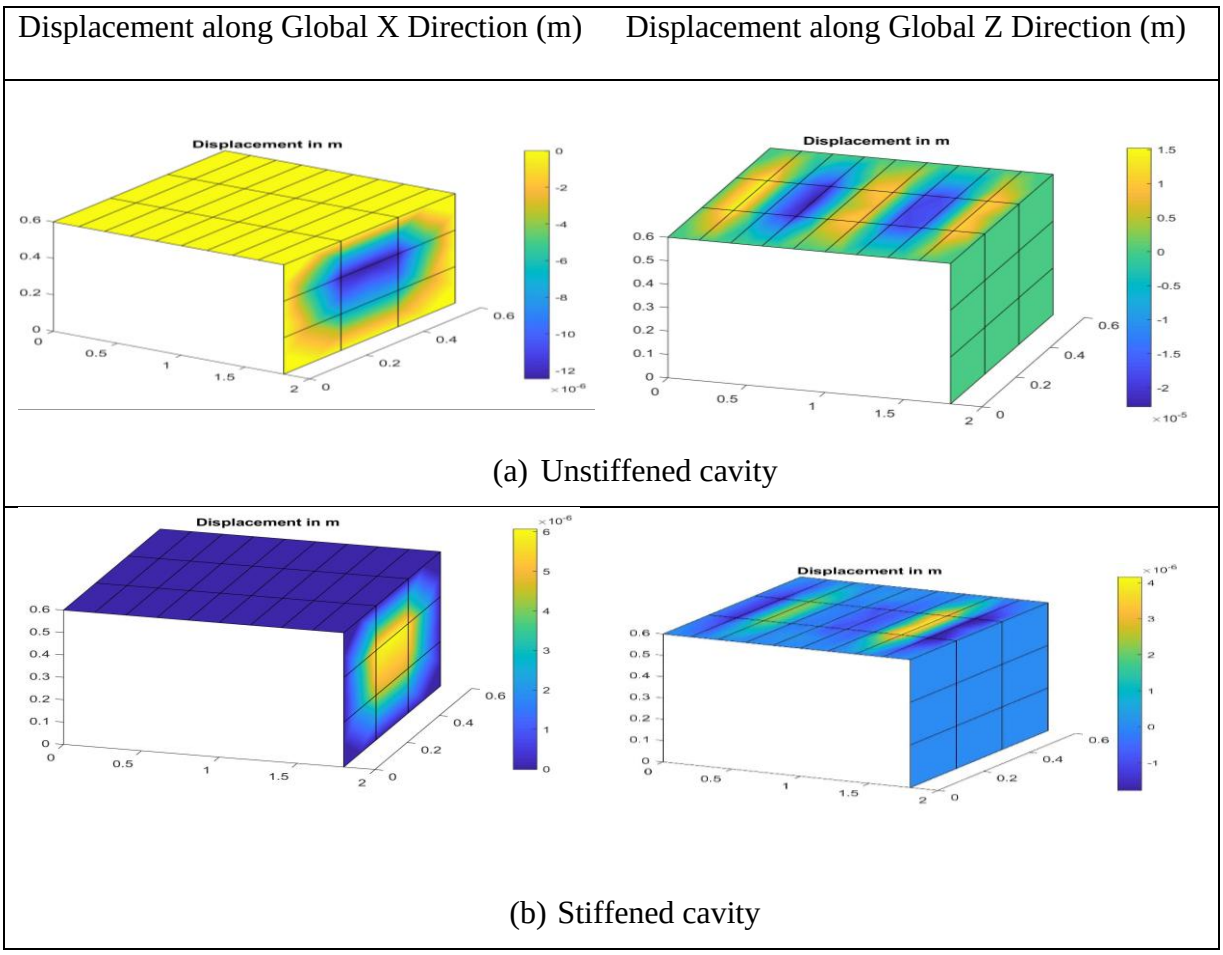

Fig. 5.19: Displacement of Flexible Panel along Global X and Global Z Directions for (a) unstiffened cavity, (b) stiffened cavity with two transverse stiffeners for 1200 radians/s

5.4.Discussion

In this study, sound pressure levels and structural displacements for unstiffened and stiffened acoustic cavities have been studied with variation in modal damping ratio, wall thicknesses and various stiffener arrangements. The following observations can be made.

1. Stiffeners enhance the natural frequencies of the overall structure and shifts the acoustic peaks implying supremacy of local variation of cavity stiffness.

2. At higher natural frequencies of the dry cavity, reduced amplitude of kinks imply that the effects of structural modes get subdued at high forcing frequencies.

3. Case study 2 reveals that peak acoustic responses are bigger in thicker enclosures and vice versa.

4. Higher damping ratio truncates the peak SPL value efficiently, without changing the SPL distribution at the saddle.

5. In case study 4, number of interaction kinks observed are more for transversely stiffened cavity (case I) than longitudinally stiffened ones (cases II and III) as the bending of plate have been more efficiently supressed by the longitudinal stiffeners.

6. Case study 5 reveals that all the displacement kinks have occurred near dry natural frequencies of the box structure, although presence of larger deflections are visible only at certain initial natural frequencies.

To conclude, in a large cavity with thin walls, it is usual to add stiffeners to enhance structural stability. However, the case studies show that the acoustic peaks are usually smaller in thin unstiffened cavities related to the stiffened ones. In contrary to unstiffened cavities, in case of stiffened cavities it has been observed that the dry natural frequencies are clustered with intermittent blanks. Thus, limited control is exerted by the structural modes in delimiting acoustic responses in the cavity in those blank frequency zones. Hence, it is essential to tailor-make the positions, thickness, and width of such stiffeners to suppress the acoustic peaks efficiently, introducing acoustic troughs instead of peaks.

Further, if physical experiments were conducted as an alternative, huge amount of non-biodegradable waste would have been formed giving rise to a separate problem of managing the waste. Numerical experiments are, therefore, a welcome substitute in figuring out prospective quiet cabins before conducting physical experiments. Shape optimization and use of absorbent layers has not been tried in this research.

6

Vibroacoustic Analysis of Laminated Composite L-shaped Acoustic Cavity Using Multi-Domain Method

In this chapter, a vibroacoustic analysis of an L shaped acoustic cavity, consisting of rigid and laminated composite thin flexible walls with an opening, has been conducted. The analysis utilizes a coupled multi-domain boundary element (BE) method with a finite element (FE) method. The cavity is divided into multiple domains with intermediate interface layers, and continuity conditions are established at the interfaces, as discussed in Chapter 3.4 of the theoretical formulation. A robust numerical model is required to describe complex vibroacoustic behaviour for complicated shape of domain, both for rigid and flexible. In simple cavity structure, where the source and the observation points are interconnected inside domain, the single domain boundary element method can be applied suitably as demonstrated in chapter 5. However, in complex boundary configurations, the generation of sound fields may be prone to errors where this direct connection is disrupted. Hence, multi-domain boundary element analysis is a must, where an interface layer between two domains is used ensuring that every point within each domain behaves consistently as either a source or an observation point to avoid erroneous results. Multi-domain formulation generates sparse system matrices thus reducing memory space required, too. After careful investigation of existing literatures discussed in section 2.5, it is observed that there is no integrated coupled analysis approach where a general complicated-shaped flexible composite cavity with opening at the boundary wall can be analysed for acoustic pressure with or without application of absorbent coatings on multiple walls utilizing multi-domain coupled BE-FE method. This research aims at developing an inhouse software using mobility relationship for interior

coupled structural analysis (CSA) with laminated composite panels that could further be associated with absorbent layers, windows and multi-domain acoustic coupling so as to solve a practical vibroacoustic engineering problem and here lies the uniqueness of this work.

Hence, our objective is to investigate vibroacoustic response of an L-shaped three-dimensional acoustic cavity, having a combination of rigid and flexible panels, with complex boundaries involving absorbent layers and opening, using coupled finite element and multi-domain boundary element analysis. Though, the program developed is versatile enough to handle cavities of any shape and multiple interacting boundary panels with arbitrary positions of opening. The program has been verified with analytical and experimental data available in the literature to ensure accuracy. The cavity is divided into several smaller domains, linked by an imaginary interface layer and the continuity conditions have been established. The finite element analysis of the flexible panels is done using first order shear deformation theory with eight noded isoparametric element and folded plate transformations **[**8**]** are applied to modify the structural stiffness and mass matrices from local to global coordinates prior to assembly. The nodal sound pressure levels at flexible boundaries are determined using mobility relationship obtained from the finite element structural analysis. A MATLAB program has been developed for the analysis. Eight-noded isoparametric serendipity elements are used to model the boundary. The FEM model is executed only once to obtain the mobility relationship, while the BEM module is executed repeatedly for each forcing frequency level to conduct the internal acoustic analysis and store the results in data files to generate graphical outputs at a later stage.

The numerical work is divided into two parts.

- Analysis of a rigid L-shaped cavity
- Analysis of a flexible L-shaped cavity

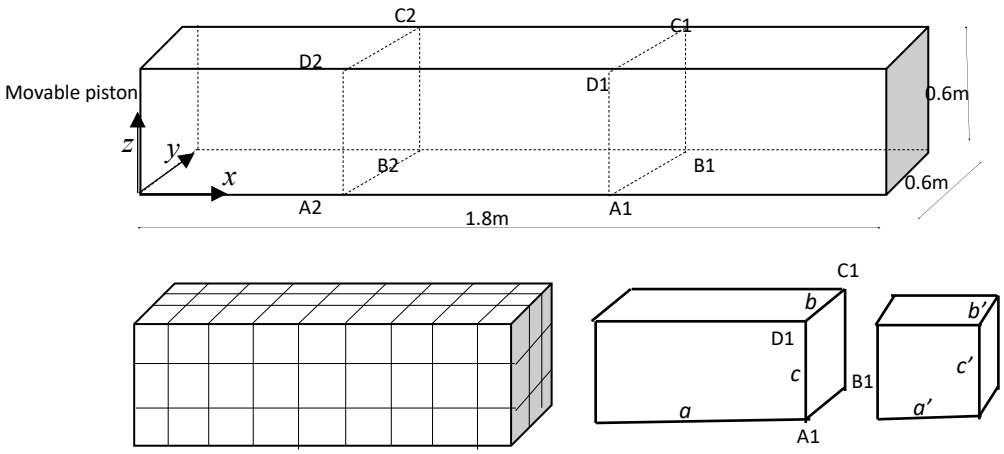

Fig. 6.1: Rectangular Cavity with subdomains

6.1 Analysis of a Rigid L-shaped Cavity

In this analysis, the validation of the multi-domain program has been performed by comparing the sound pressure level with theoretical values. Two validation studies have been performed.

- Validation and Mesh Convergence Study for Multi-domain Acoustic Analysis
- Validation Study for Multi-Domain Rigid Acoustic Analysis with Absorbent Layer

After successful validation, analysis of L-shaped cavity has been done using absorbent layer. Effect of presence of opening has also been shown.

6.1.1. Validation Studies

6.1.1.1. Validation and Mesh Convergence Study for Multi-domain Acoustic Analysis

A rigid container of dimensions 1.8m × 0.6m × 0.6m (Fig. 6.1) is taken in the study. The air inside the cavity is excited by a sinusoidal motion of the left wall with a velocity amplitude of 0.001m/s. The analysis is shown for single domain, two domains (interface at A1-B1-C1-D1 at X=1.2m) and three domains (interfaces at A1-B1-C1-D1 and A2-B2-C2-D2 at X=1.2m and 0.6m respectively) (ref. Fig. 6.1). Mesh sizes of 0.2m and 0.15m square grids are taken following **[**90**]**. The number of elements along x axis is taken is nine (mesh size 0.2m x 0.2m) and twelve (mesh size 0.15m x 0.15m) respectively. In Fig. 6.2a and 2b, the notation used are (a x b x c, a' x b' x c') where a, b, c denote number of elements along x, y and z axes respectively in domain 1 and a', b', c' denote number of elements along x, y and z axes respectively in domain 2. The sound pressure level (SPL) at the boundary and at the center of the domain has been calculated theoretically. The speed of sound, c, is taken to be 340m/s and

the density of air, ρ, is 1.20 kg/m^3. The analytical solution of sound pressure at an axial position *x* is given by equation 6.1 assuming plane wave propagation **[**55,89**]**.

$$p(x) = \frac{Acos(kL-kx)-\mathrm{Bcos}(kx)}{\mathrm{ksin}(kL)} \tag{6.1}$$

where A and B are the normal gradient of the acoustic pressure on the rigid piston and opposite wall of the piston, *k* the wave number, and *L* the duct length and x is the point location from the piston.

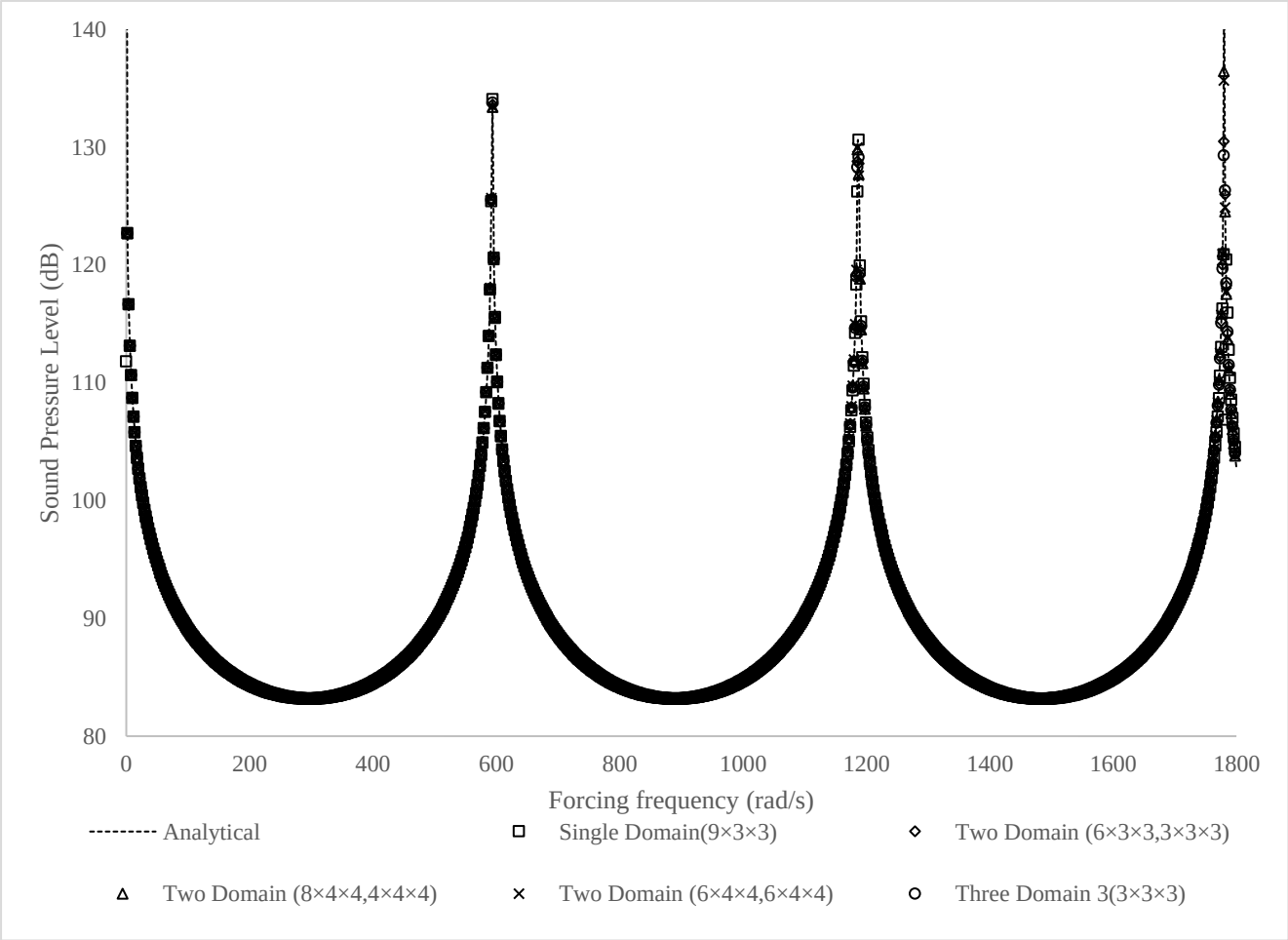

Fig. 6.2a: Sound Pressure Level (SPL) at Boundary Point P_1 (X=1.8)

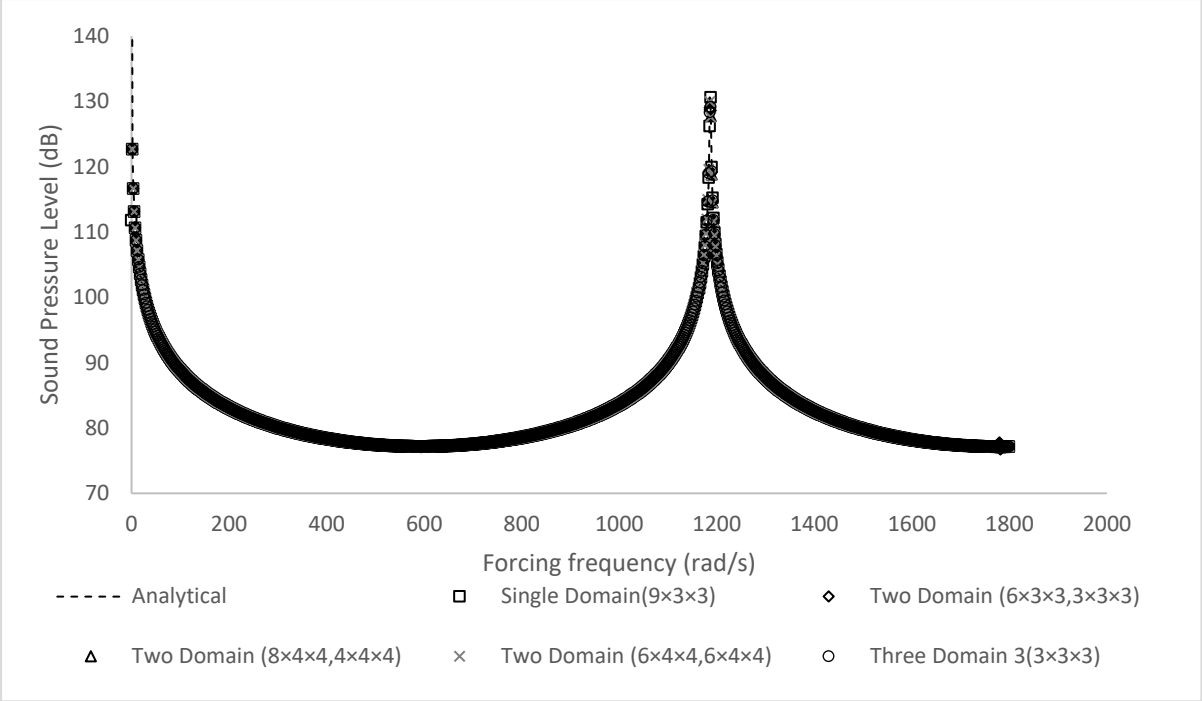

Fig. 6.2b: Sound Pressure Level (SPL) at Center of Domain (X=0.9)

The responses at the right boundary wall (X=1.8m) and at the center of the domain (X=0.9m) has been plotted in Fig. 6.2a and 2b respectively. Analytically acoustic resonance is scheduled to occur at frequency $\Omega=n\,c\pi / L$ and $\Omega=2n\,c\pi / L$ [89] at the right boundary and at the center of the domain respectively, where L is the length of the duct.

In our cavity, the acoustic resonance should occur at 593 rad/s, 1186 rad/s and 1780 rad/s for the boundary wall. That for domain centre is 1186 rad/s, 2372 rad/s. It has been observed from the figures that the results match exactly with the analytical one for all three cases, without subdomain and with two and three subdomains respectively. Hence, it can be concluded that the multi-domain formulation is correct and can be carried out for further analysis taking element size 0.2m × 0.2m for up to 1800 radian/s frequency range. It is also noticed that change of interface position does not alter the SPL at the boundary and domain for this cavity.

6.1.1.2. Validation Study for Multi-Domain Rigid Acoustic Analysis with Absorbent Layer

The effect of adding absorbent layers at the inner surface of the cavity has been considered. The validation study has been performed on the same rectangular cavity as shown in Fig. 6.3 with absorbent lining of 30mm thick polyurethane foam [84,177] at the right and left panel simultaneously. The excitation is taken same as described in previous case. Two equal subdomains have been considered with mesh size 0.225m × 0.3m as followed in Niyogi et al.

[177]. The sound pressure level (dB) has been plotted at the centre of right wall and at centre of domain and compared with [177] in Fig. 6.3. It is observed that the result matches well with the available literature.

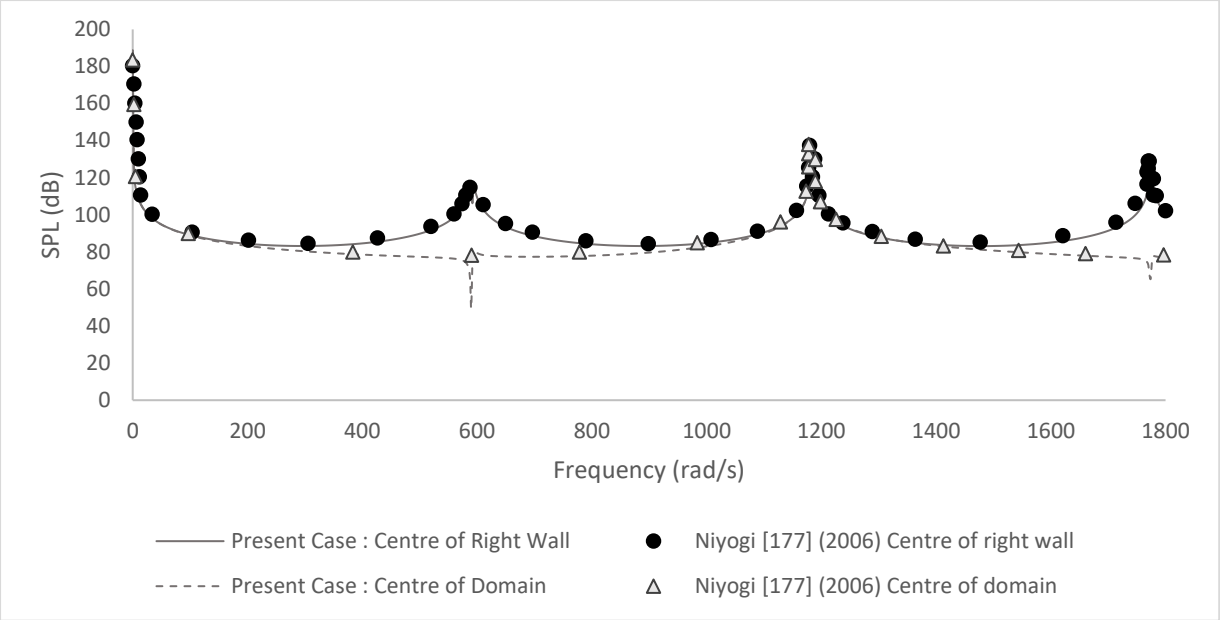

Fig. 6.3: Comparison of SPL at centre of right wall and at centre of boundary with absorbent lining present in the left and rightmost panel

6.1.2 Numerical Case Studies

6.1.2.1 Case Study 1: Analysis of an L shaped rigid Cavity

Here the L-shaped box cavity (mesh size 0.2m × 0.2m) has been divided in two domains with changing the interface layer position. In the first case, the imaginary interface layer has been taken at X=1.2m on the YZ palne as shown in Fig. 6.4a. In this case the first domain is 1.2m × 0.6m × 0.6m and second domain is 0.6m ×1.8m × 0.6m. In the second case, imaginary interface layer has been taken at Y=0.6m on XZ plane as shown in Fig. 6.4b. Here, the first domain is 1.8m × 0.6m × 0.6m and second domain is 0.6m × 1.2m × 0.6m. The left most face acts as a piston with velocity amplitude 0.001m/s. It will be has used errorneous to find the appropriate sound field inside the entire domain without taking multi-domain formulation because of the path discontinuity of source and observation points.

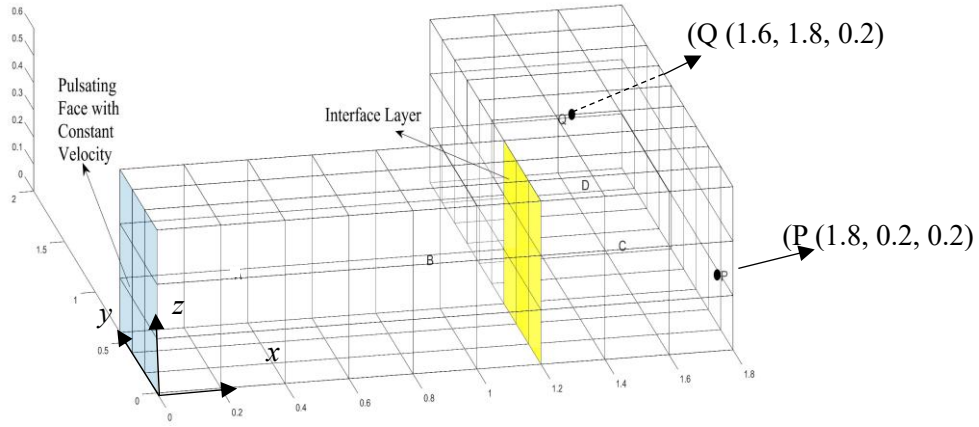

Fig. 6.4a: Geometry of Multi-domain L Box Cavity with Interface layer at X=1.2 m

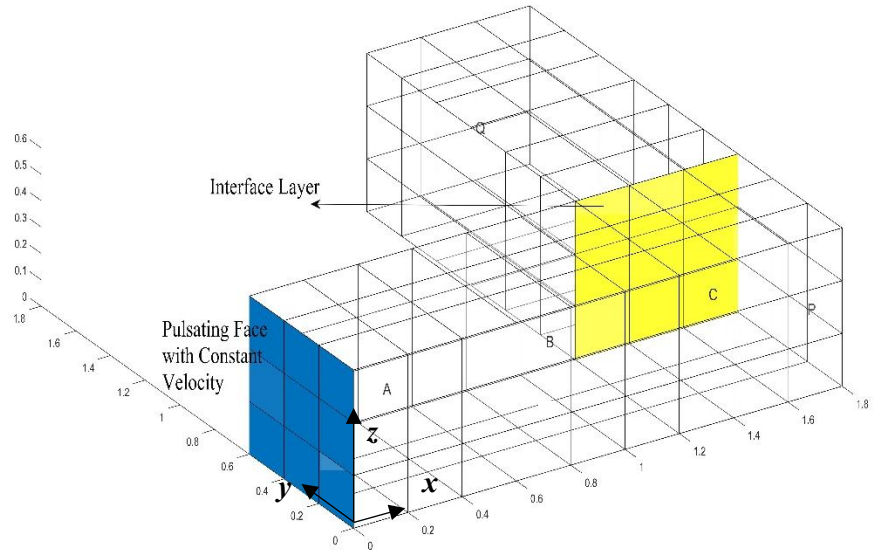

Fig. 6.4b: Geometry of Multi-domain L Box Cavity with Interface layer at Y=0.6 m

The SPL at the boundary at point P (1.8, 0.2, 0.2) and at Q (1.6, 1.8, 0.2) has been plotted in Fig. 6.5a. From Fig. 6.5a, the acoustic mode has been observed at 696, 1282 and 1780 rad/s respectively for both points. At 386 and 1146 rad/s, peaks have been observed only at point Q while at P we see sharp troughs. Shape of acoustic domain plays a significant role in the vibroacoustic response largely affecting the SPL pattern. From the Fig. 6.5a it is clear that wherever is the position of the interface region at the junction, the SPL patterns at the boundary remains the same. Hence, we have plotted the next results taking the interface at X=1.2m (ref. Fig. 6.5a)

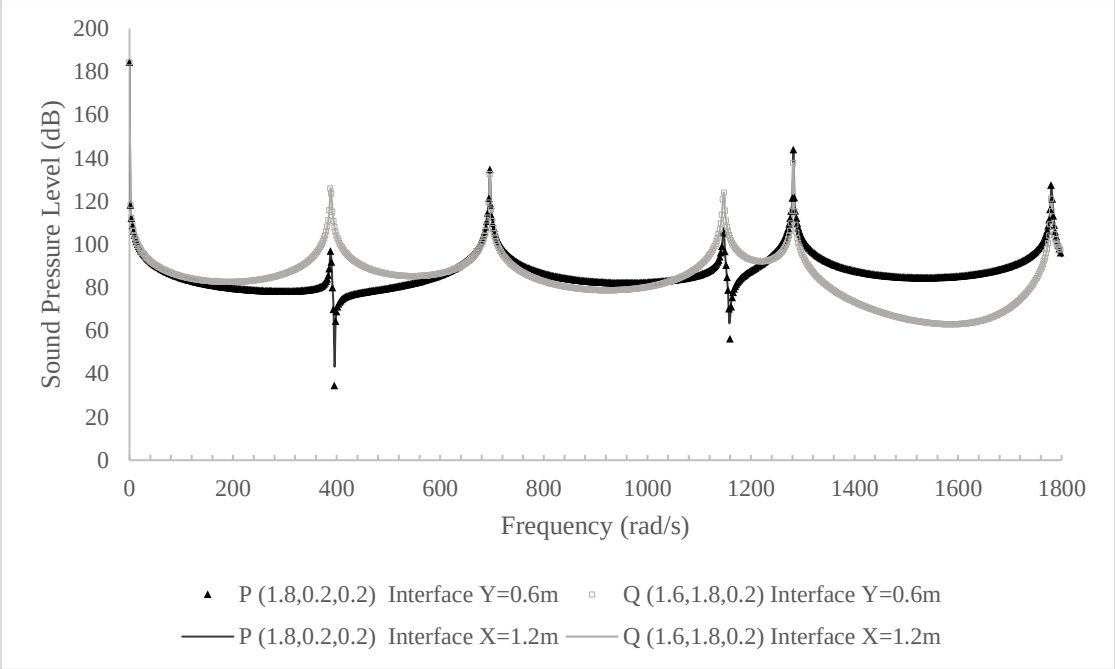

Fig. 6.5a: Sound pressure level in dB at boundary point P and Q

The domain SPL have been plotted at three different points B (0.9,0.3,0.3), C (1.5, 0.3, 0.3) and D (1.5, 1.2, 0.3) in Fig. 6.5b. From the figure, it is observed that, acoustic resonance has occurred at 696 rad/s and 1282 rad/s at all locations. For points B and D intermediate peaks are observed at 386 rad/s and at 1146 rad/s respectively. For point D, low pressure zone is created at 902rad/s and 1586rad/s with SPL values 21dB and 2dB respectively. Comparing Fig. 6.5a with Fig. 6.5b, a shift in acoustic mode has been observed. Also, the arrangement of peaks and troughs are altered which is due to the change in geometry of the acoustic cavity.

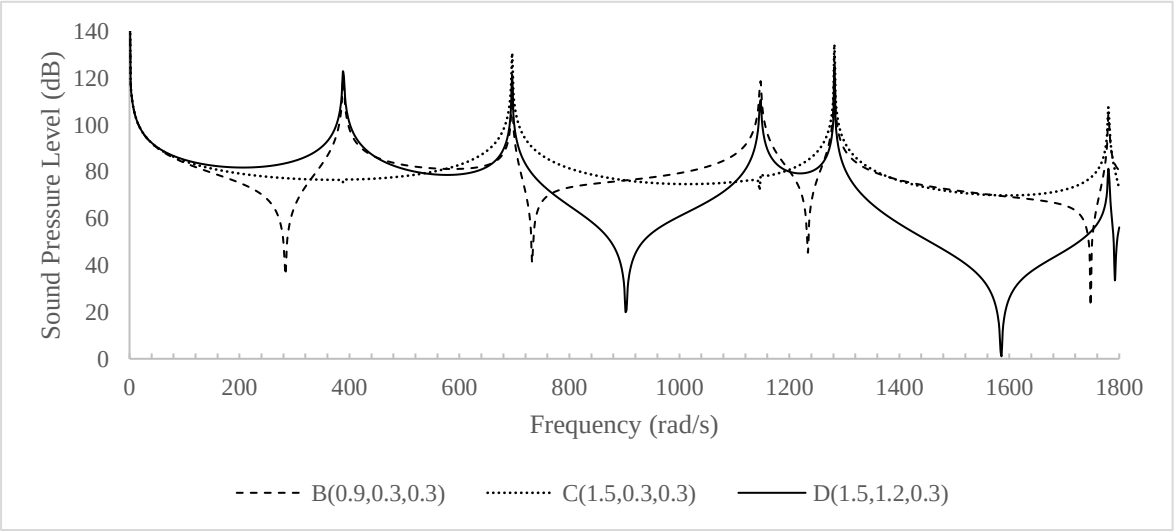

Fig. 6.5b: Sound pressure level in dB at domain points

6.1.2.2 Case Study 2: Analysis of a Rigid L Shaped Box with Absorbent Layer

In this case, Absorbent layers are provided in the L box at the boundary faces. The 30mm thick polyurethane foam's frequency-dependent admittance is taken from Suzuki et al.'s studies [84] and Niyogi [177]. Zero acoustic admittance indicates a boundary without any absorbent layer. The following cases have been considered and compared with cases with no absorbent layer.

1. Case-I: Absorbent layer at both side faces of the cavity
2. Case-II: Absorbent layer at both side faces and top of the cavity

The SPL at boundary point P and Q and at interior point (1.5, 0.3, 0.3) have been plotted in Figs. 6.5a, 5b and 5c, respectively. Also, the SPL at selected frequencies has been tabulated in Table 6.1 for better understanding. From Fig. 6.5, it is observed that the action of absorbent layer is frequency dependent and manifests itself only at the resonant frequencies. Table 6.1 shows that at 696 rad/s and 1282 rad/s the SPL is reduced at all points in boundary and domain both for case I and II. The absorbent layer effect is not noticeable in the domain at 386 rad/s or 1146 rad/s because of absence of peaks in this region. Compared to case I, the position of absorbent layer in case II offers a lower SPL in the working frequency region.

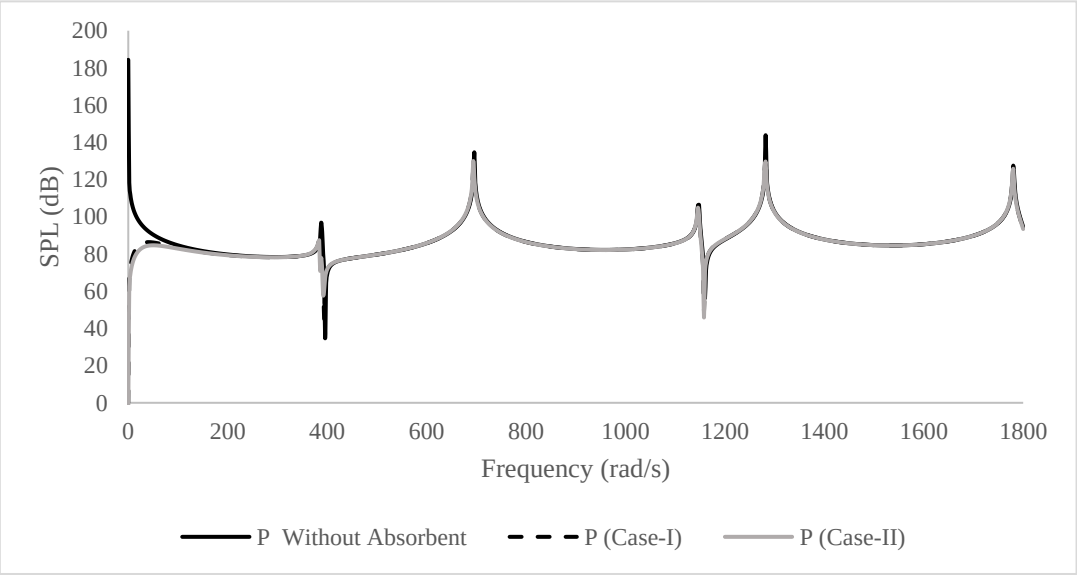

(a)

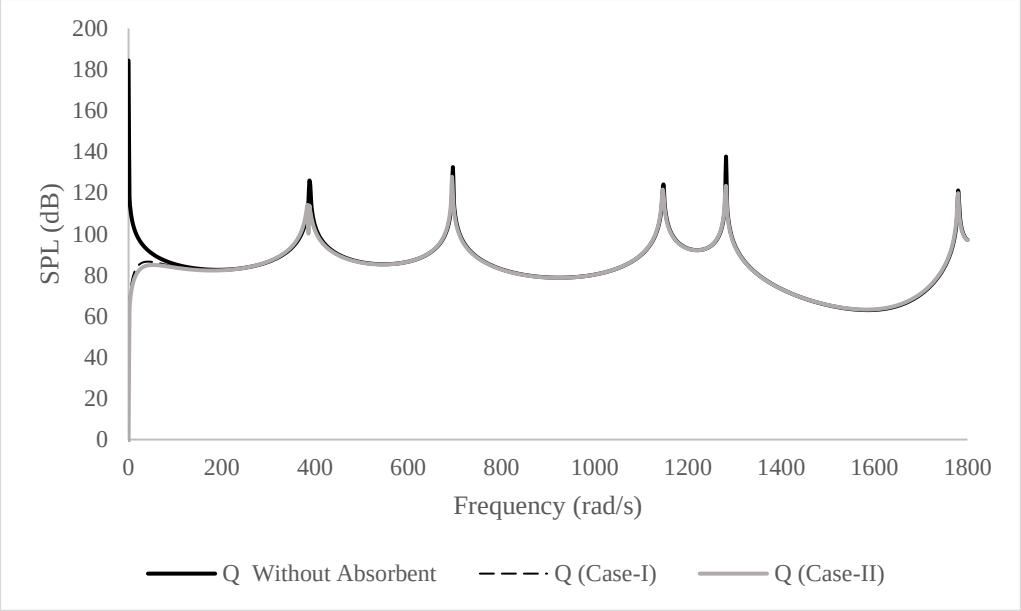

(b)

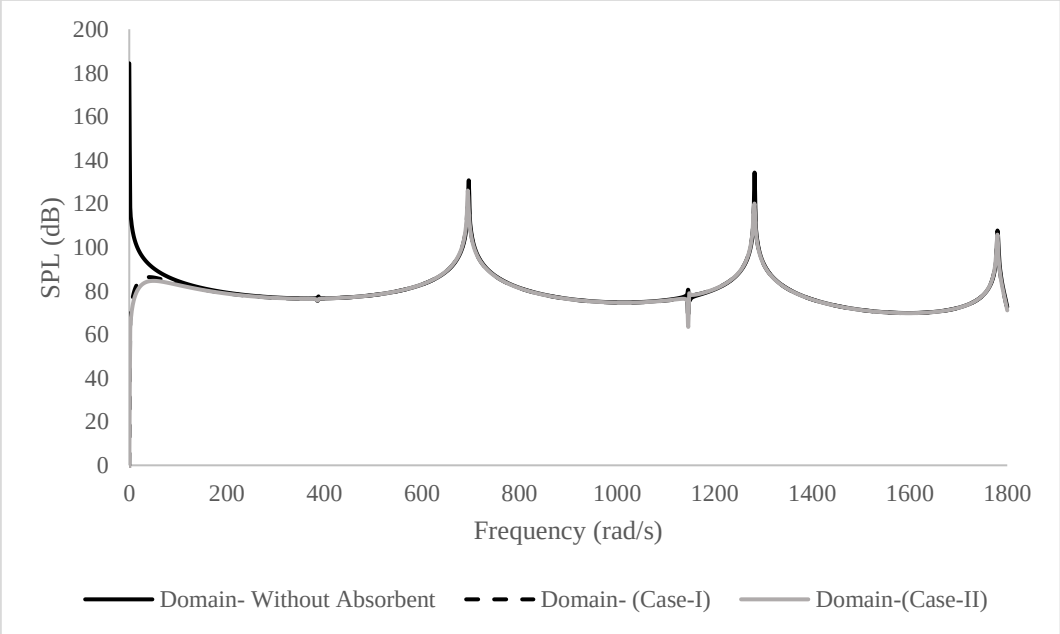

(c)

Fig. 6.5. SPL at boundary Point (a) P (1.8, 0.2, 0.2), (b) Q (1.6, 1.8, 0.2) and domain point (1.5,0.3, 0.3) with and without absorbent layer

Table 6.1: Sound pressure level (dB) at peak frequencies

Frequency (rad/s)	P Without Absorbent	P absorbent (Case-I)	P absorbent (Case-II)	Q Without Absorbent	Q absorbent (Case-I)	Q absorbent (Case-II)	Domain (1.5, 0.3, 0.3) Without Absorbent	Domain-absorbent (1.5, 0.3, 0.3) (Case-I)	Domain-absorbent (1.5, 0.3, 0.3) (Case-II)
386	88.73	88.11	70.86	115.86	115.31	100.17	76.75	75.36	75.52
696	134.65	124.06	121.21	132.55	121.91	119.05	130.72	120.11	117.26
1146	106.33	102.09	100.54	123.96	120.49	119.16	75.39	79.08	78.85
1282	143.84	132.65	129.43	137.68	126.39	123.15	134.26	123.05	119.83

6.1.2.3 Case Study 3: Analysis of a Rigid Partly Opened L Shaped Box

In this case study, an L-shaped box with a square opening of size 0.2m × 0.2m as shown in Fig. 6.6 is taken for study. The radiation impedance from equation (3.5.6 & 3.5.10) has been calculated following Kinsler *et al.* [55] and applied as known boundary condition. The SPL at boundary points P and Q and inside the domain at (1.5, 0.3, 0.3) have been plotted in Figs. 6.7a, 7b and 7c respectively.

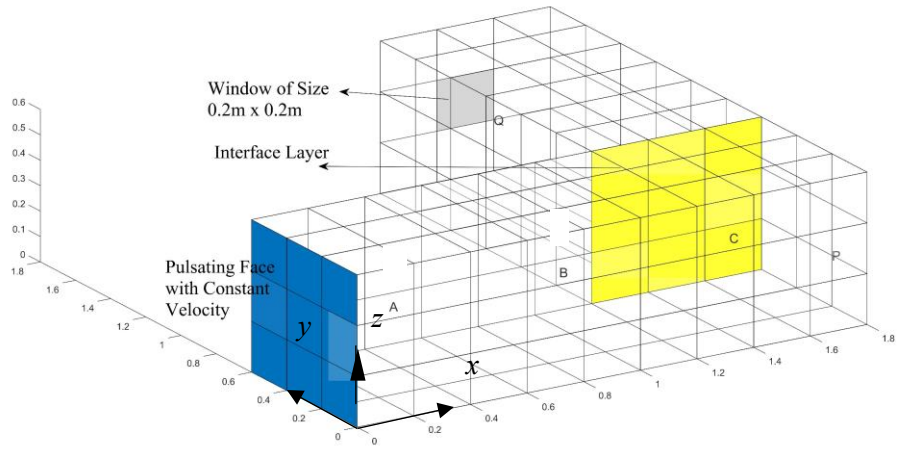

Fig. 6.6: L-shaped box with square opening at Y=1.8 m at the centre on XZ plane

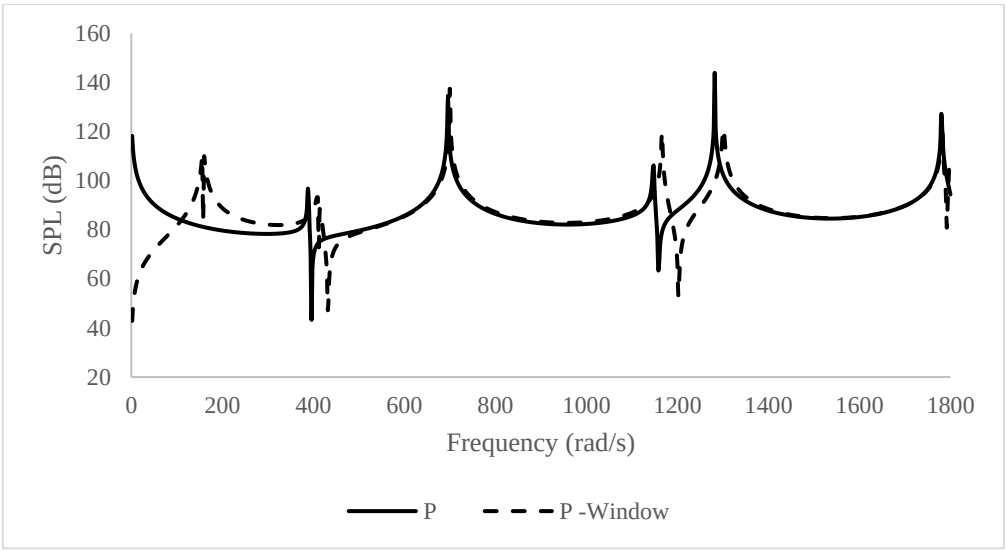
160
140
120
100
80
60
40
20
SPL (dB)
0
200
400
600
800
1000
1200
1400
1600
1800
Frequency (rad/s)
P
P -Window

(a)

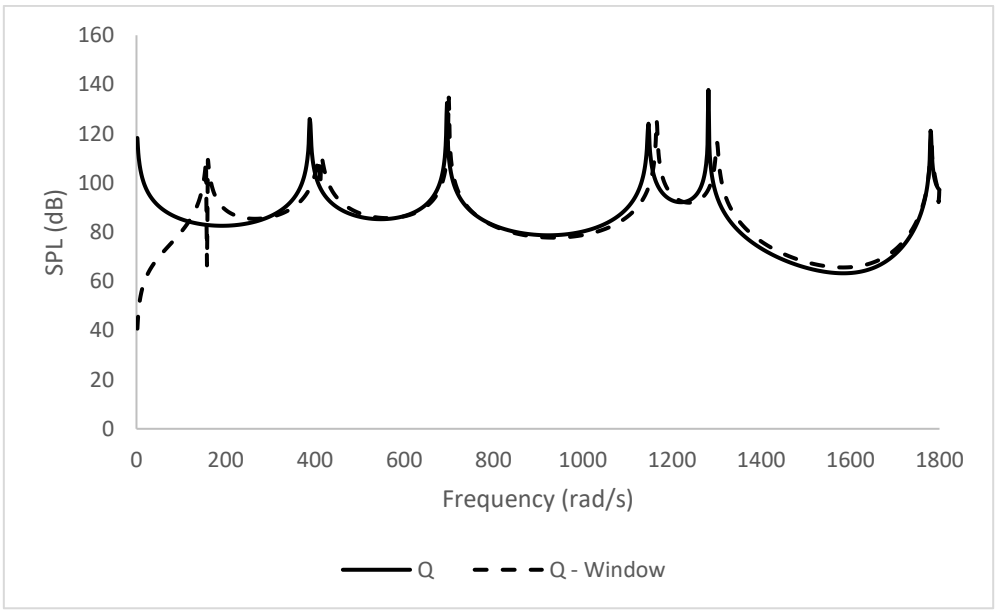
160
140
120
100
80
60
40
20
0
SPL (dB)
0
200
400
600
800
1000
1200
1400
1600
1800
Frequency (rad/s)
Q
Q - Window

(b)

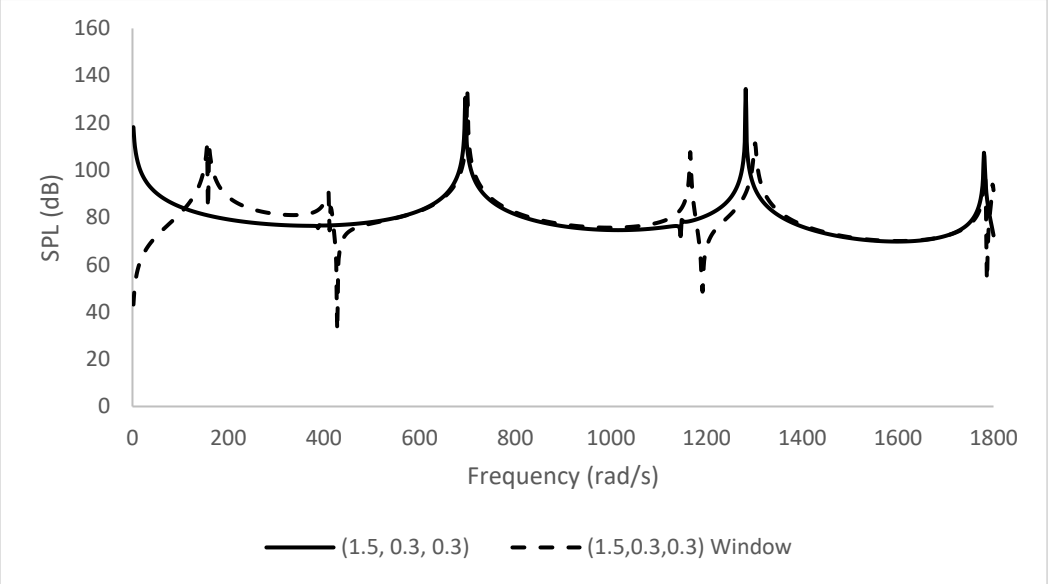

(c)

Fig. 6.7: SPL at boundary Point (a) P (1.8, 0.2, 0.2), (b) Q (1.6, 1.8, 0.2) and domain point (1.5,0.3, 0.3) with and without opening

It can be observed that an additional peak of 108dB is developed due to presence of the opening at 156rad/s and 160rad/s following a sharp dip at 158rad/s for all cases. The magnitude of the dip is 83dB at boundary point P and at the domain, whereas, the value is 66dB for boundary point Q as it is located at the corner of the opening. It has been noticed that the resonant frequencies have been shifted slightly to the right when an opening is provided, due to the coupling effect. At first acoustic mode of frequency, 696 rad/s, the SPL level remain unaltered. Because of their close proximity, a peak and trough are formed at boundary P and within the domain at 1166 rad/s, which lowers the SPL in the region of 1180 rad/s to 1300 rad/s.

6.2 Analysis of Flexible Laminated Composite L-Shaped Cavity

In this coupled structural acoustic analysis, FEM is used to find modal characteristics of laminated composite flexible cavity structure and a pressure-velocity formulation is adopted to model the acoustic domain using BEM. A coupled FE-BE code has been developed in MATLAB environment and the program is validated for flexible cavity using multi domain analysis technique.

6.2.1 Validation Study

Two sets of validation studies have been considered.

- Validation study for interior coupled structural acoustic (ICSA) analysis for flexible cavity has been discussed in section 5.2.
- Validation study for multi-domain acoustic analysis in flexible cavity with absorbent layer

6.2.1.1 Validation Study for Multi-Domain Acoustic Analysis in Flexible Cavity with Absorbent Layer

A cavity of dimensions 1.8m × 0.6m × 0.6m (Fig. 6.1) is taken in the validation study with flexible top and right-side wall keeping other panels rigid. The flexible panels are made up of E-glass epoxy (material 1 ref. Table 5.1) [90] laminated composite material (ref. Table 5.1 for material properties of E-glass epoxy surface material is E_1=60.7 x 10^9 N/m^2, E_2 = 24.8 x 109 N/m^2, $G_{12} = G_{13} = G_{23}$ = 12.0 x 10^9 N/m^2, $\nu_{12} = \nu_{21}$ = 0.23, ρ = 1300 Kg/ m^3) with layup sequence $(30^o/-30^o)_s$ and the thickness is taken as 2.5mm. 30mm thick polyurethane foam is used as absorbent layer at left and right panels [84,90]. The modal damping is taken as 0.1% for each structural mode. First ten natural frequencies are presented and compared with Niyogi et al. [90] in Table 6.2. The air inside the cavity is excited by a sinusoidal motion of the left wall with velocity amplitude of 0.001m/s up to 1800 rad/s forcing frequency with interval 2 radian/s. The speed of sound, *c*, is taken to be 340m/s and the density of air, ρ, is 1.20 kg/m^3 as earlier. The number of elements along length is taken as eight and that along width and height is taken as two respectively (8×2×2) as provided in [90]. Two cases have been taken for study.

a. Single domain without interface (8×2×2)
b. Two domains with interface region at X= 0.9m (4×2×2, 4×2×2)

The sound pressure level at the boundary (1.8, 0.3, 0.3) and at the domain (0.9, 0.3, 0.3) has been plotted and compared in Fig. 6.8a and 8b, respectively. From Table 6.2 and Fig. 6.8, it is observed that the natural frequencies and corresponding SPL at the boundary and at the domain matches well with Niyogi et al. [90] in the presence of absorbent layer. Hence this multi domain coupled interior acoustic formulation can be used effectively for further analysis of complex L-box structure.

Table 6.2: First ten natural frequencies (rad/s) of the box with 2.5 mm flexible walls

Mode	2.5mm thick cavity (present model)	2.5mm thick cavity [177]	Mode	2.5mm thick cavity (present model)	2.5mm thick cavity [177]
1	266.87	266.77	**6**	819.43	819.34
2	337.76	337.61	**7**	1012.45	1012.41
3	434.42	438.41	**8**	1174.90	1174.88
4	465.95	465.12	**9**	1526.96	1526.88
5	632.68	632.49	**10**	3519.21	3517.80

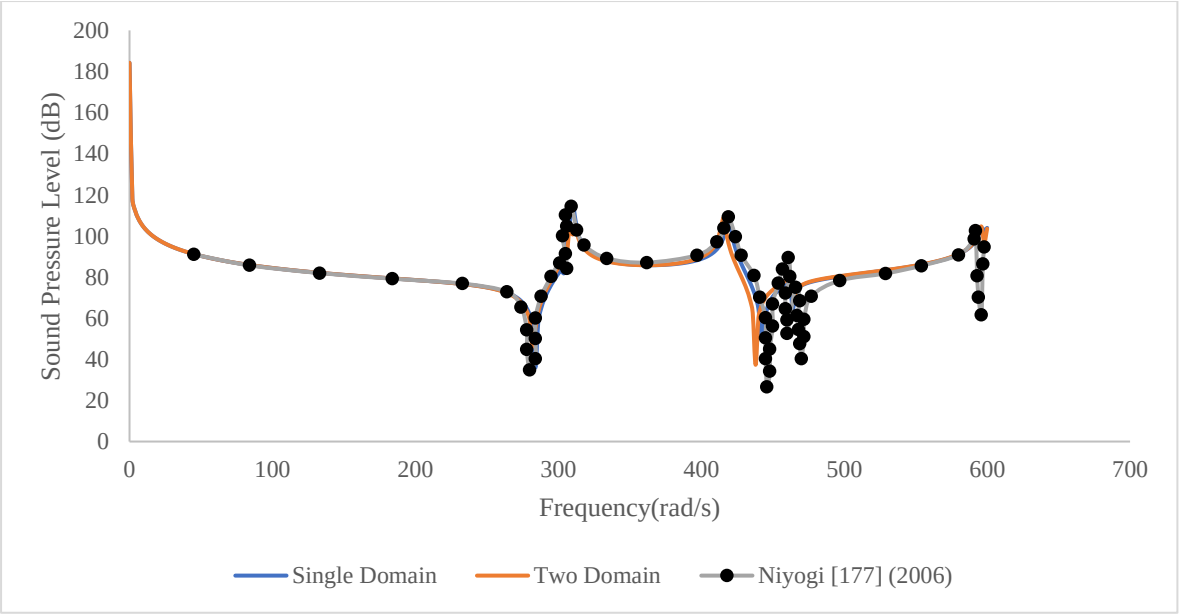

(a)

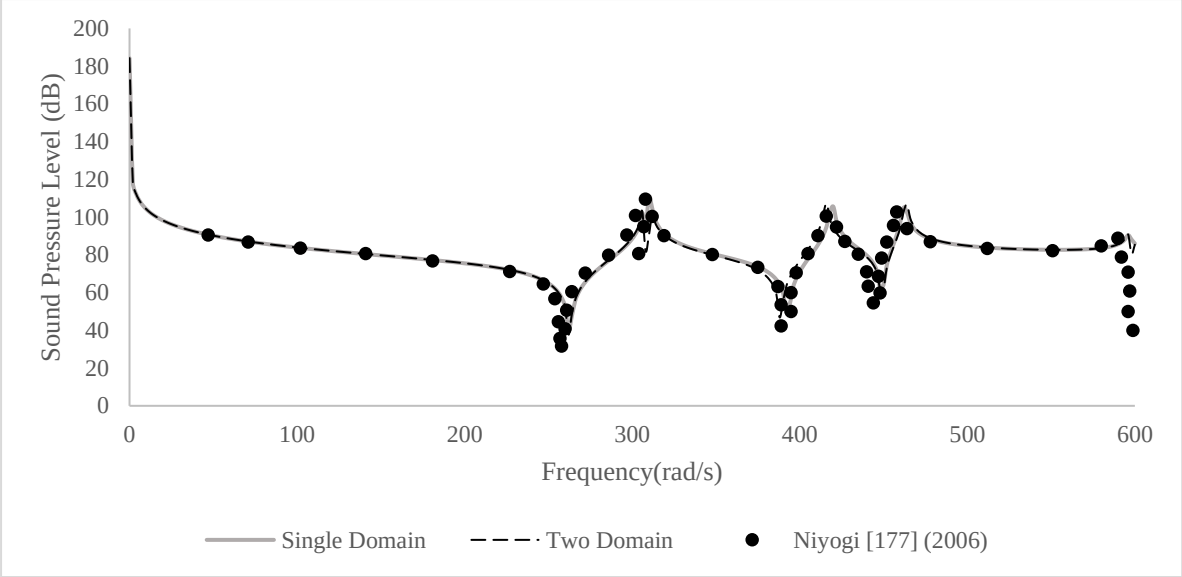

(b)

Fig. 6.8: SPL at (a) boundary Point (1.8, 0.3, 0.3) and at (b) domain point (0.9,0.3, 0.3)

6.2.2 Study of Mesh Convergence

A mesh convergence study for the free vibration response of flexible dry L-box structure (ref. Fig. 6.4a) has been reported in Table 6.3. The top (*xy* plane; *z*=0.6m) and the extreme face (*xz* plane; *y*=1.8m) are taken as flexible panel made with graphite epoxy composite material (ref. Table 4.2.1) with fiber orientation ($0^o/90^o/90^o/0^o$) and the thickness of the panel is 4 mm. The length of 1.8 m is divided into n_1 elements, and the smaller lengths (0.6 m) are modelled by n_2 elements. From Table 6.3 it is seen that a mesh with $n_1 = 9$ and $n_2 = 3$ can be accepted for subsequent studies with reasonable computation time without compromising accuracy.

Table 6.3: Natural frequencies (rad/s) for different mesh size in L-shaped partly flexible box

Mode No	Meshing			Mode No	Meshing		
	8×2	8×3	9×3		8×2	8×3	9×3
1	337.85	315.64	313.85	6	730.80	821.46	809.78
2	446.97	428.70	419.91	7	786.53	878.20	875.81
3	645.72	607.45	588.99	8	886.75	899.12	892.02
4	663.50	640.26	636.24	9	959.57	955.55	933.37
5	706.10	721.12	709.31	10	1233.70	983.13	969.06

6.2.3 Case Studies

6.2.3.1 Case Study 1: Analysis of an L-Shaped Flexible Cavity

Using the multi-domain coupled FEM-BEM program the partially flexible L-shaped cavity, as discussed in previous study, has been analysed. The interface region is taken at y=0.6m plane, ref. Fig. 6.4b). The cavity is excited at the left most face which acts as a piston with a constant velocity amplitude of 0.001m/s. The damping ratio is taken as 0.01 for all modes. The first twenty undamped natural frequencies, which have been used to find the mobility matrix, have been tabulated in Table 6.4. The sound pressure level (dB) is plotted at boundary points P (1.8, 0.2, 0.2) and Q (1.6, 1.8, 0.2) and domain (1.5, 0.3, 0.3) and compared with rigid one in Fig. 6.9a, b and c respectively. Plotting the first twenty natural frequencies in the same plots allows one to see how the modal frequency affects the cavity's SPL at various locations. The combined influence of the structural and acoustic coupling is prominent in this case. At the acoustic peak zone, where the SPL values sharply decline, the impacts become more noticeable. Presence of modal frequency near acoustic peaks causes an inversion around these modes thus reducing the SPL. SPL are comparatively lower in case of flexible panel cavity compared to rigid one at the resonance points. The reduced amplitude of kinks at higher natural frequencies of the dry cavity indicates that the impacts of structural modes become less pronounced at high forcing frequencies. First six dry structural mode shapes have been plotted in Fig. 6.10. Bending modes have been observed in the flexible panels in these modes which affects the acoustic pressure at different points.

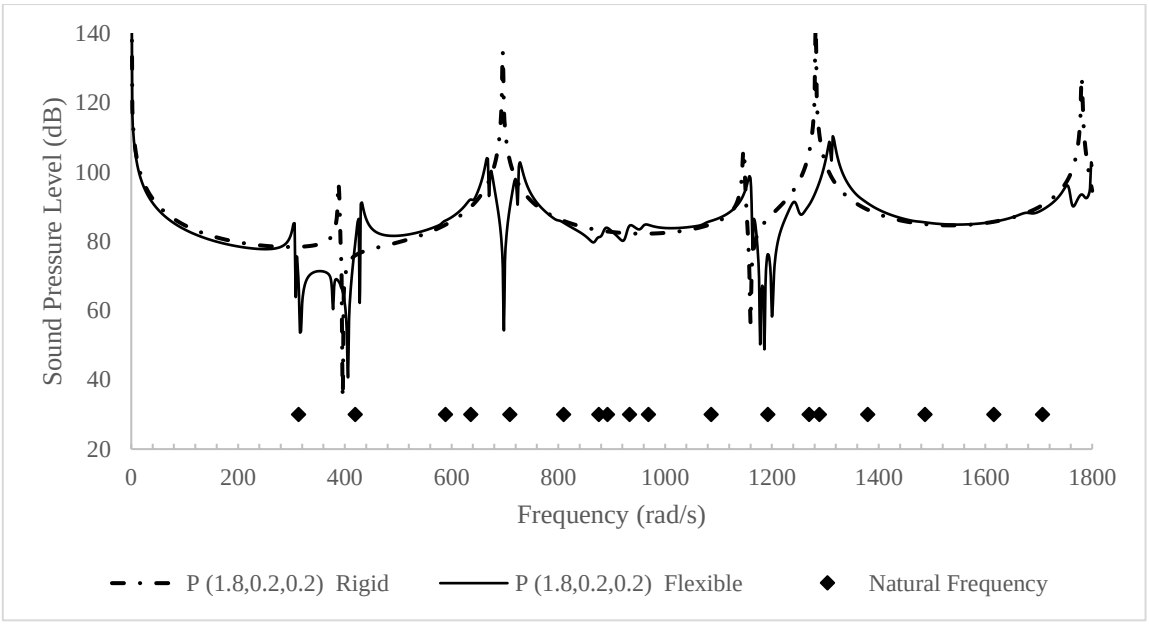
Sound Pressure Level (dB)
140
120
100
80
60
40
20
0
200
400
600
800
1000
1200
1400
1600
1800
Frequency (rad/s)
P (1.8,0.2,0.2) Rigid
P (1.8,0.2,0.2) Flexible
Natural Frequency

(a)

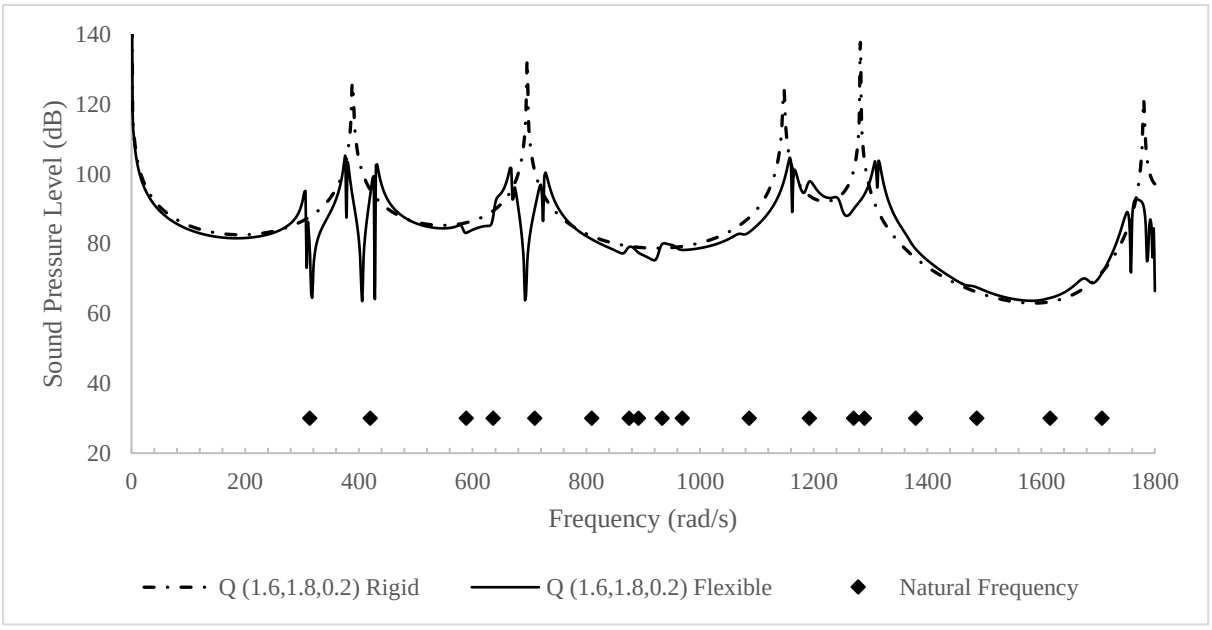
Sound Pressure Level (dB)
140
120
100
80
60
40
20
0
200
400
600
800
1000
1200
1400
1600
1800
Frequency (rad/s)
Q (1.6,1.8,0.2) Rigid
Q (1.6,1.8,0.2) Flexible
Natural Frequency

(b)

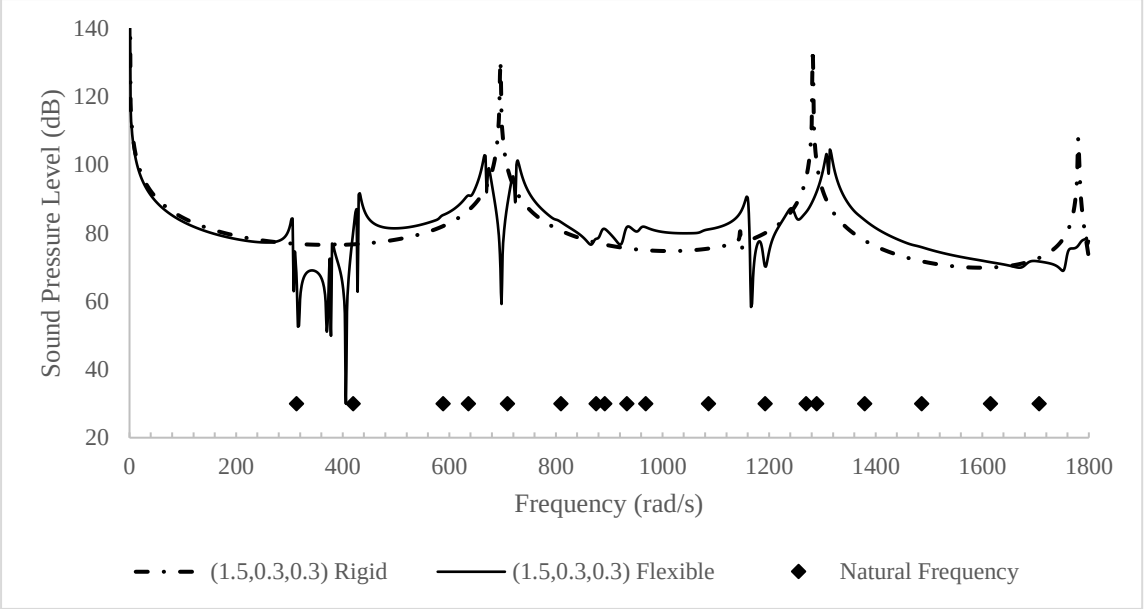

(c)

Fig. 6.9: SPL at boundary Point (a) P (1.8, 0.2, 0.2), (b) Q (1.6, 0.3, 0.2) and domain point (1.5,0.3, 0.3) for flexible L box cavity

Table 6.4: Natural frequencies (rad/s) of the flexible L-shaped cavity

Natural Frequencies (rad/s) for 4mm							
Mode No	**Frequency**	**Mode No**	**Frequency**	**Mode No**	**Frequency**	**Mode No**	**Frequency**
1	313.85	6	809.78	11	1086.74	16	1486.85
2	419.91	7	875.81	12	1192.61	17	1615.78
3	588.99	8	892.02	13	1270.02	18	1707.08
4	636.24	9	933.37	14	1289.44	19	1812.13
5	709.31	10	969.06	15	1379.47	20	1855.86

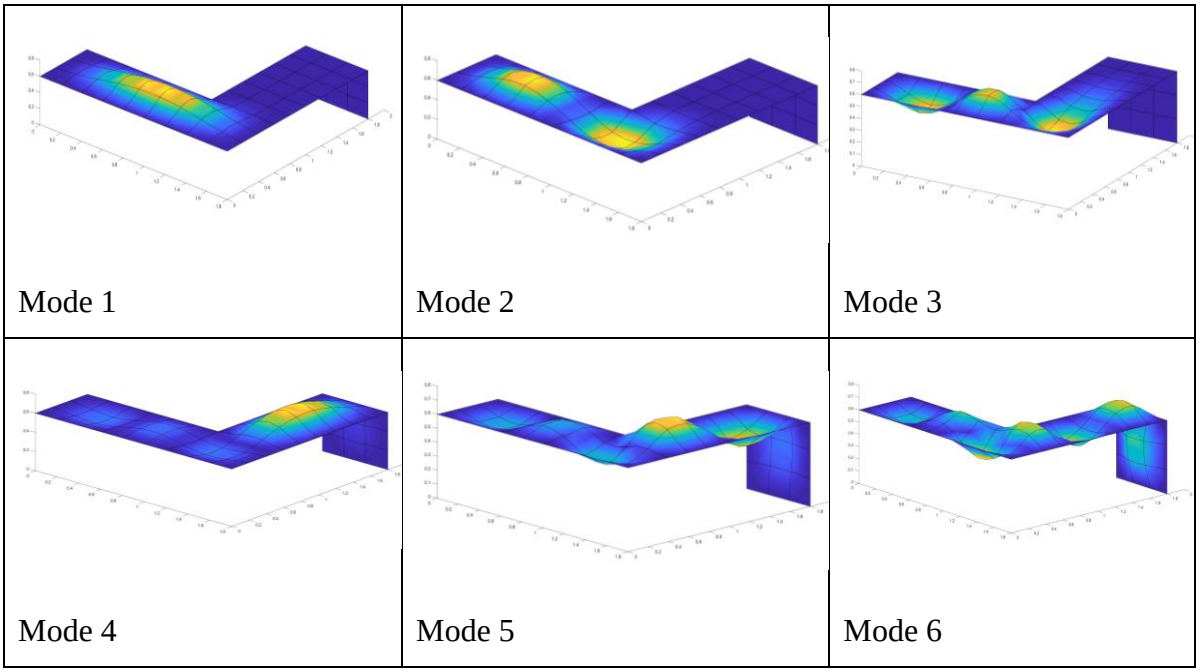

Fig. 6.10: First six mode shapes of L-Box

The sound pressure level distribution at the boundary wall at frequencies 200, 600 and 1200 rad/s has been plotted in Fig. 6.11. It is observed that a low-pressure zone is formed at 0.4m from left side at 200rad/s. Shift in the position of low-pressure zone is detected with change in frequency. At 600 rad/s and at 1200rad/s, the number of low-pressure zones developed are two and three, respectively. This is corroborated with the general understanding of the process since with increase in frequency, wavelength of sound wave reduces and thus the number of low-pressure zones increases.

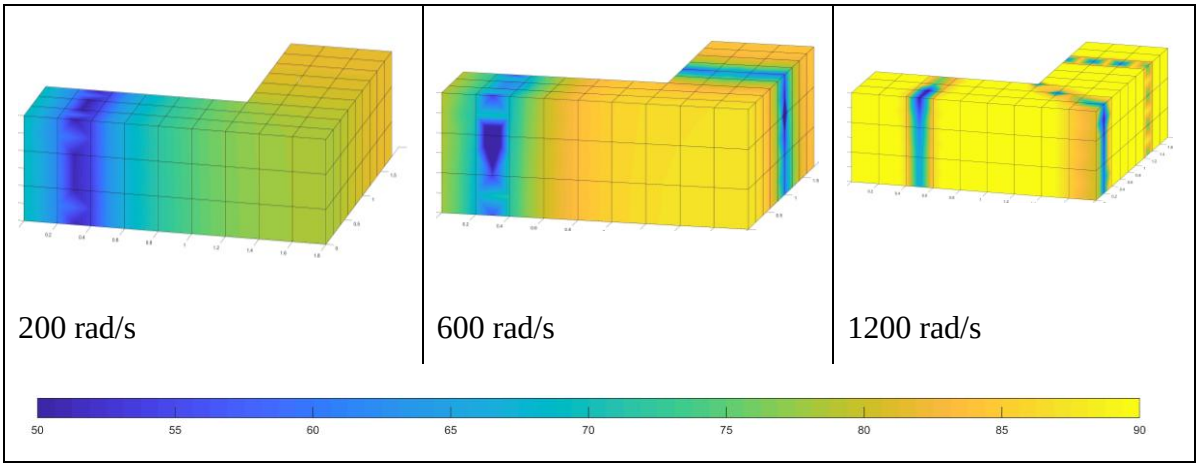

Fig. 6.11: Sound pressure level (dB) on the boundary for partially flexible L-box at different forcing frequencies

6.2.3.2 Case Study 2: Analysis of a Partially Opened L-Shaped Flexible Cavity with Absorbent Layer

In this study, a square opening of size 0.2m × 0.2m is provided at Y = 1.8m at the centre on *XZ* plane (refer Fig. 6.6) keeping the boundary of the opening rigid. 30mm thick polyurethane foam [177] is provided as absorbent layers at both sides of the boundary panels only. First twenty natural frequencies for flexible L shaped plate with opening are tabulated in Table 6.5. The SPL at boundary points P and Q and at interior point (1.5, 0.3, 0.3) for flexible L box with opening and absorbent layers along with the modal frequencies are plotted in Fig. 6.12a, 12b and 12c respectively. Fig 6.13 shows first six mode shapes of the flexible cavity with opening.

Table 6.5: Natural frequencies (rad/s) of the flexible L-shaped cavity with opening

Natural Frequencies (rad/s) for 4mm							
Mode No	**Frequency**	**Mode No**	**Frequency**	**Mode No**	**Frequency**	**Mode No**	**Frequency**
1	313.82	6	821.14	11	1194.31	16	1707.07
2	419.91	7	883.62	12	1273.56	17	1812.13
3	588.96	8	931.36	13	1378.03	18	1857.18
4	638.04	9	963.80	14	1486.52	19	1905.60
5	715.58	10	1086.71	15	1615.55	20	2003.54

Comparing Tables 6.4 and 6.5, it is observed that there is nominal variation in the natural frequencies for the first three modes. Differences have started to appear since the fourth mode. The reason may be attributed to the mode shape as seen in Fig. 6.12. Bending mode is observed at the farthest flexible plate (*xz* plane), following the third mode in Fig. 6.10, whereas, because the boundary of the opening is taken rigid, the same plate is stiffer (Fig. 6.12), which causes the natural frequency to rise starting in the fourth mode. The SPL values at both boundary points P, Q and at the interior point of the flexible cavity with opening and with or without absorbent layer is shown for selected frequencies and compared in Table 6.6.

From Figs. 6.12a, 12b and 12c it has been noticed that significant changes occurred when an opening is provided in the flexible box. Presence of opening inverts the peaks at the resonant points. The effect of absorbent layer is restricted to resonance frequencies only. Additionally, it smoothened the pronounced highs and lows in a frequency range. The location of observation points also plays a crucial role in reducing the SPL. At 146 rad/s, an inverted peak

is visible at boundary point P and at domain, but absent in boundary point Q due to presence of opening. From Table 6.6, it is observed that, at 380 rad/s, the SPL reduces considerably for boundary point Q. No such effect has been observed for point P or at the domain. Whereas, at 648rad/s the effect of using absorbent layer is prominent at point P and at the domain compared to point Q. Similar effect has been observed at 1216 rad/s. The close proximity of boundary point P and the domain point (1.5, 0.3, 0.3) may be the reason. At 1298 rad/s and 1796 rad/s, the reduction in SPL is observed at all three observation points. This is due to the presence of acoustic modes near these regions. It is observed that presence of modal frequencies increases the number of crests and troughs in the lower frequency zone which becomes nearly flat at the higher frequency zone after 1300 rad/s.

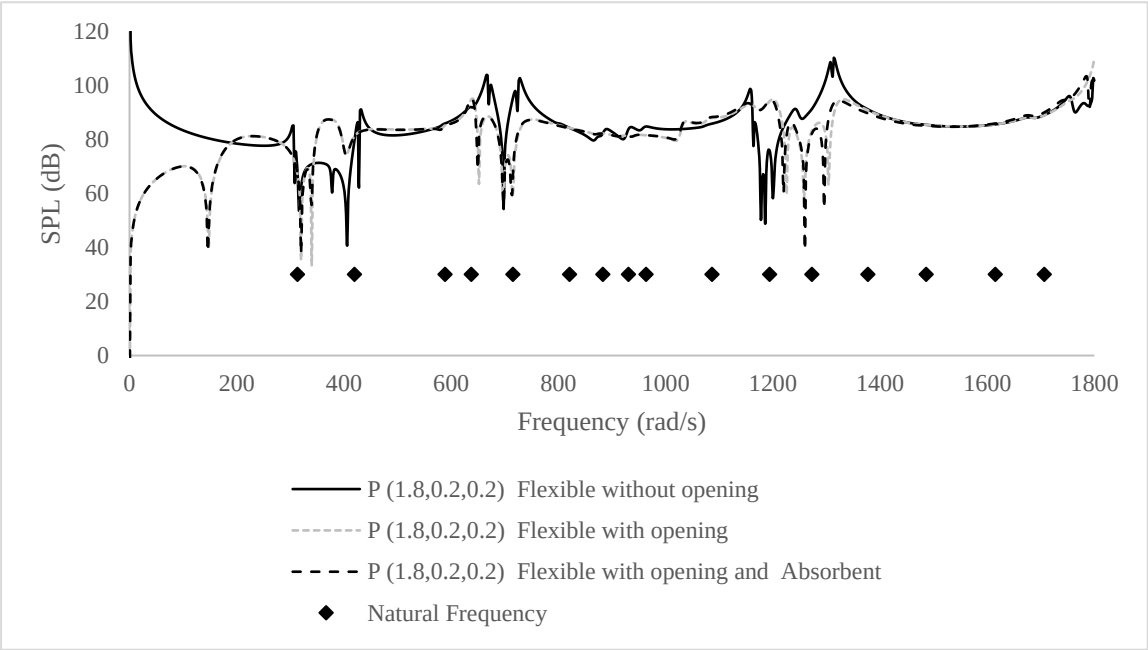

(a)

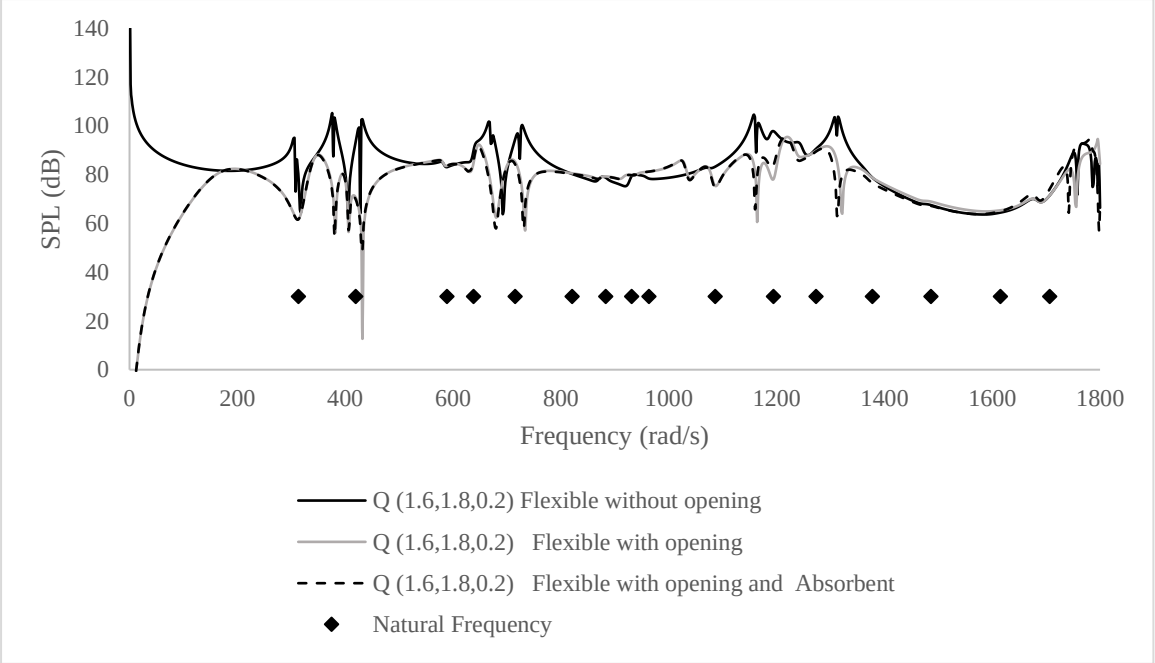

(b)

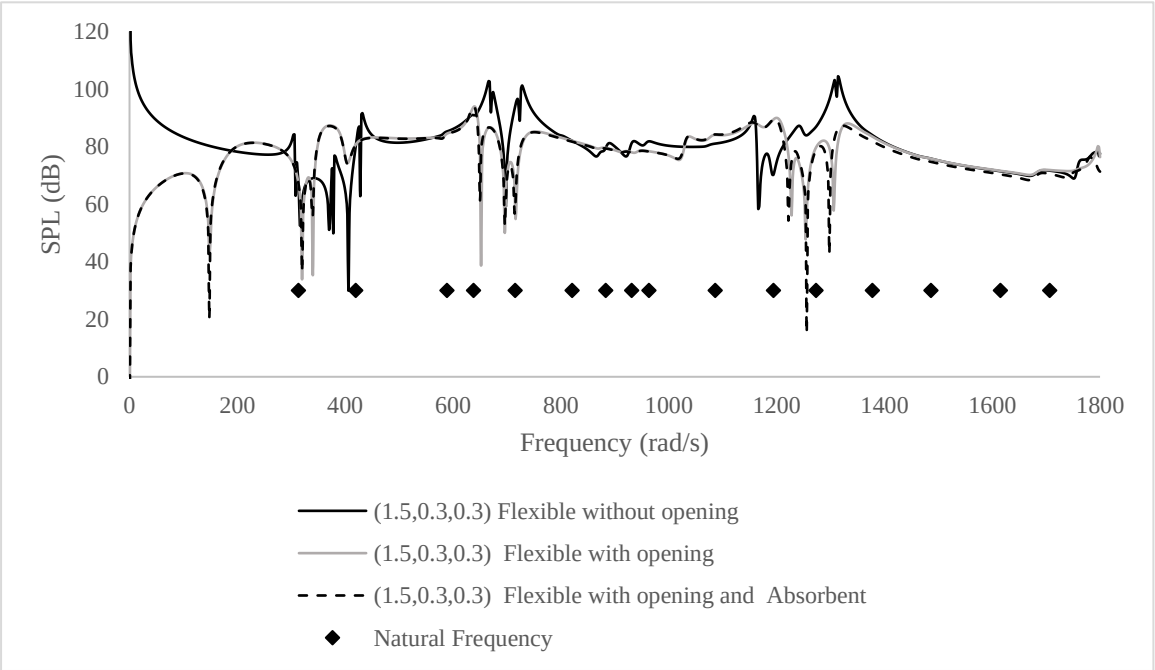

(c)

Fig. 6.12: SPL at boundary Point (a) P(1.8, 0.2, 0.2), (b) Q (1.6, 0.3, 0.2) and domain point (1.5,0.3, 0.3) for flexible L box cavity with square opening and absorbent layer

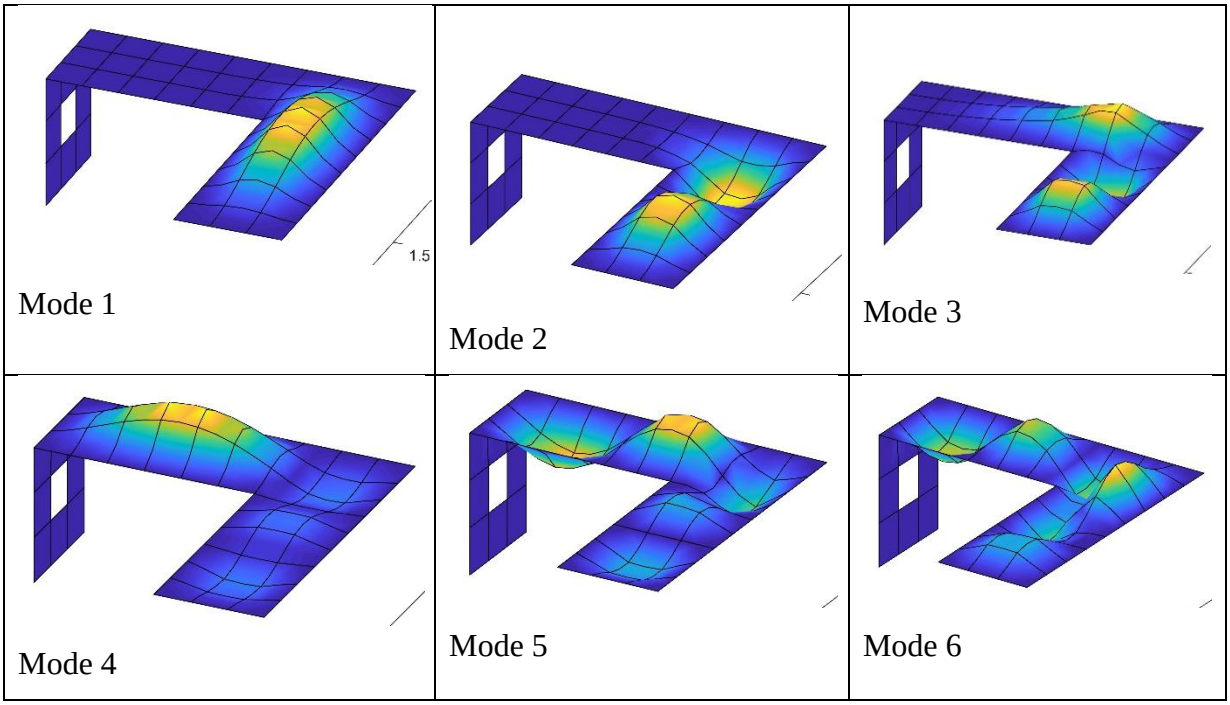

Fig. 6.13: First six mode shapes for L box flexible cavity with opening

Table 6.6: SPL (dB) at boundary point P (1.8,0.2,0.2) and Q (1.6,1.8,0.2) and at domain (1.5,0.3,0.3)

Frequency	P		Q		Domain	
	Partly flexible with opening	Partly flexible with opening with absorbent	Partly flexible with opening	Partly flexible with opening with absorbent	Partly flexible with opening	Partly flexible with opening with
146	47.20	38.52	77.39	77.49	53.67	50.49
338	62.71	59.05	83.86	84.08	62.53	58.92
380	87.30	87.04	62.74	54.71	86.99	86.71
430	82.96	82.84	55.62	50.20	82.45	82.30
648	86.19	77.91	92.33	91.72	85.33	77.91
676	87.61	87.34	66.43	61.97	85.77	85.45
712	68.76	60.56	86.03	85.28	71.31	67.26
728	83.45	84.29	74.00	68.65	80.67	81.59
1160	92.96	93.05	81.17	65.94	88.16	88.21
1216	88.01	80.64	95.11	95.25	83.76	77.86
1260	62.60	39.09	88.01	87.36	69.15	66.47
1298	82.59	75.17	91.44	88.64	79.48	42.80
1312	87.24	92.86	85.36	63.17	78.82	85.50
1742	92.92	94.60	82.06	64.38	71.51	69.72
1796	106.10	101.88	94.50	69.98	80.18	72.40

6.3 Conclusions:

In this research, an in-house program has been developed to analyze L-shaped three-dimensional cavity with complex boundaries for sound pressure levels using coupled multi-domain BE-FE method using MATLAB. Both rigid and partially flexible cavity with or without opening and absorbent layers were considered and the sound pressure levels at the boundary and within the domain have been evaluated. For complex geometry of domain, the sound field generation can encounter significant errors in boundary element analysis if the source and the observation points are not connected directly. Therefore, use of multi-domain technique is a necessity. Finite element structural analysis of the partly flexible composite enclosure has been conducted using folded plate transformation and the mobility relationship between pressure and velocity at the interacting walls has been extracted and applied subsequently to the pressure-velocity boundary element formulation of the interior acoustic

multi-domain cavity. To assure correctness, the current formulation has been validated using analytical and experimental data from the literature. From the case studies, following inferences can be drawn.

1. In multi-domain analysis, there is no change in SPL pattern if the interface is positioned at the junction so that all source and observation points are connected directly.
2. Comparing rectangular (Fig. 6.8) and L-shaped cavities (Fig. 6.9), it can be concluded that the shape of acoustic domain greatly influences the SPL pattern at various locations by altering the arrangements of peaks and troughs. Fig. 6.9 illustrates that presence of dry natural frequencies of the flexible panels near rigid acoustic modes provides control in the SPL both at the domain and at boundary. The mode shapes have a significant role in coupled behaviour of irregular cavity, too.
3. The peak acoustic responses of partially flexible cavity are comparatively lower at the resonance point than that of the rigid one.
4. At higher natural frequencies of the dry cavity, the lower amplitude of kinks suggests that the effects of structural modes get subdued at high forcing frequencies.
5. As demonstrated in Fig. 6.11, the number of low-pressure zones grows as forcing frequencies rise as increased frequencies reduces the wavelength thus increasing the number of low-pressure zones.
6. Presence of opening at the boundary wall also plays a crucial role in changing the sound pressure level pattern at a frequency range. For a rigid cavity, the peaks have been shifted slightly to the right and lowered in value due to the coupling effect of opening except at the first acoustic mode. An opening in a partly flexible L-shaped cavity inverts the peak at all the structural and acoustic modes.
7. The effect of absorbent layers is limited to resonant frequencies. It smooths out the highs and lows in certain frequency band. In case study 2 (refer sec 6.1.4), it has been observed that when the absorbent coating is placed at the top and at side walls, the SPL value reduces more at resonant frequencies. Therefore, by appropriately adding absorbents, one can limit the audio output at the resonant frequencies.

To conclude, complicated shaped flexible laminated composite acoustic cavity has many practical engineering applications and hence, vibroacoustic analysis is very crucial to predict the SPL for efficient acoustic design and noise control.

7

Vibroacoustic Analysis of Laminated Composite Car-shaped Acoustic Cavity Using Multi-Domain Method

In this chapter, a vibroacoustic analysis of a car shaped acoustic cavity, consisting of rigid and laminated composite thin flexible walls with an opening, has been conducted. The analysis utilizes a coupled multi-domain boundary element (BE) method with a finite element (FE) method. The cavity is divided into multiple domains with intermediate interface layers, and continuity conditions are established at the interfaces, as discussed in Chapter 3.4 of the theoretical formulation. A robust numerical model has been developed to describe complex vibroacoustic behaviour for complicated shape of domain, both for rigid and flexible along with opening. The model is tried to made as practicable as possible with generalized boundary conditions. Seat positions along with seat cover (absorbent layer) has been used in the model.

7.1. Validation Studies

For completeness, the validation study should be divided in three parts.

i. Validation study of rigid interior-exterior coupling
ii. Validation study of interior coupled structural acoustic analysis for flexible cavity
iii. Validation study for multi-domain acoustic analysis in flexible cavity with absorbent layer

Among these, case ii and case iii are already discussed in section 5.2.1 and section 6.1.1.2 respectively.

7.1.1. Validation Studies for Rigid Interior Exterior Coupling

In this section, the interior and exterior coupling formulation has been validated with Seybert et al. [166] for a rigid cavity as shown in Fig. 7.1. A cubical box of size 0.5m × 0.5m × 0.5m have been modelled with 5×5×5 boundary mesh and the central sphere of 0.1m radius are modelled with 26 elements. Two 0.1m × 0.1m openings have been kept on two opposite sides one at the bottom corner of left-side panel and the other is at the upper corner of right-side panel. Continuity of pressure and velocity at the openings has been assumed. The sphere is pulsating with a normal velocity 0.2m/s. The boundary surface of the box is taken rigid i.e., the normal velocity is zero. The sound pressure level at the centre of the opening has been plotted in Fig. 2 with 10 Hz interval and compared with Seybert et al. [166]. Fig.7. 2 indicates that the SPL matches well with [166] in the lower frequency region up to 750 Hz. The current analysis includes certain highs and lows that Seybert did not have. This is due to the analysis using a smaller frequency interval than Seybert's.

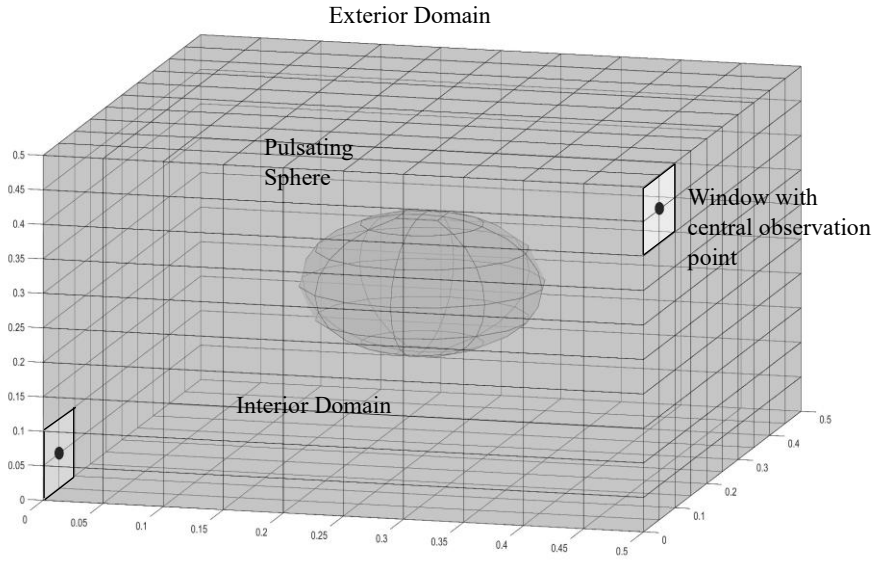

Fig 7.1: Cube Box with central sphere and window

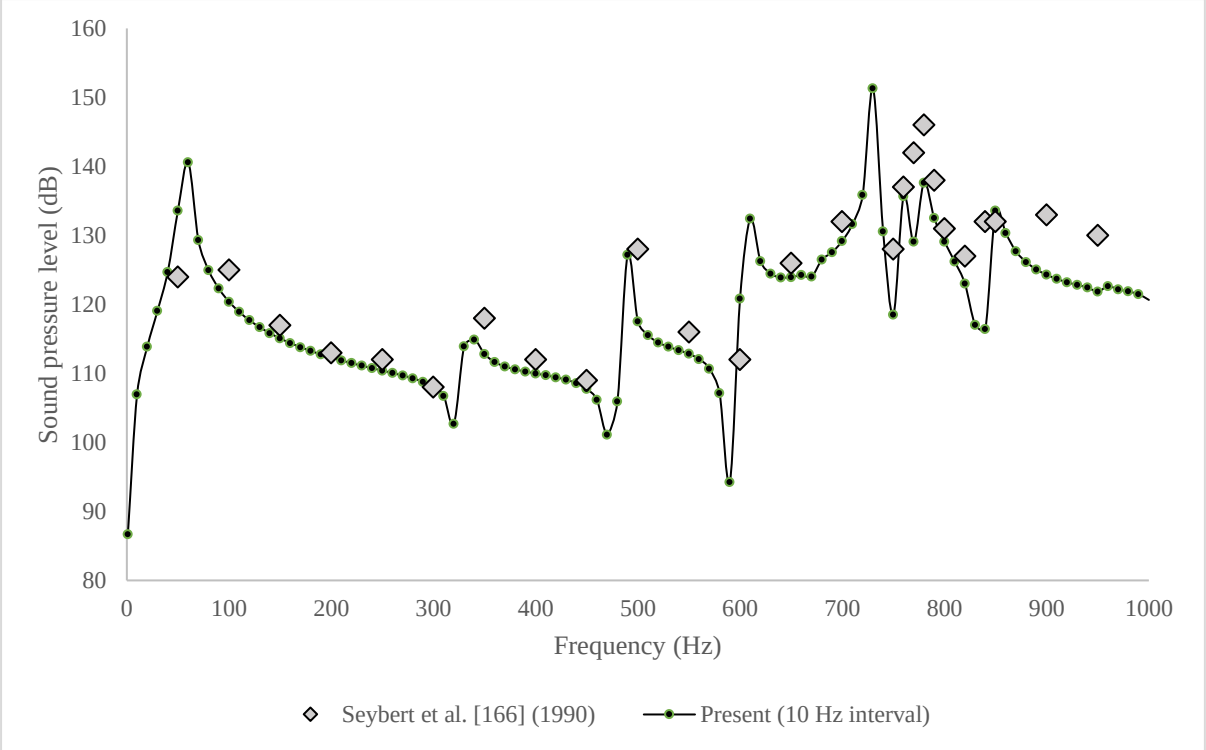

Fig. 7.2: Comparison of SPL at centre of opening with Seybert

7.2. Case Studies:

Two car models are analysed for vibroacoustic problem. Model 1 is a simple structure with the dimensions as given in Fig. 7.3. The car model has window openings at both sides of the cavity. The interior of the model is denoted as domain 1 and the exterior part is denoted as domain 2. Domain 1 and domain 2 is connected through the opening. Two cases have been done:

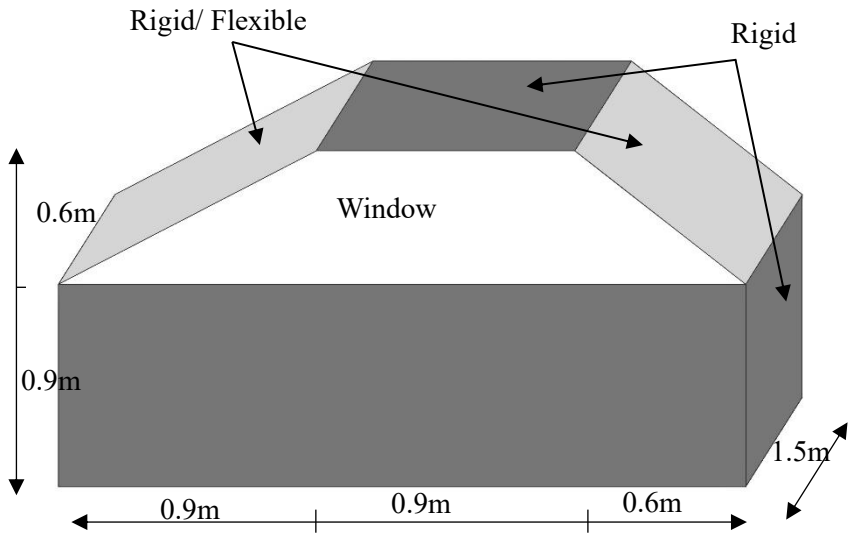

Fig. 7.3: Geometry of simple car model 1

a. Vibroacoustic analysis of car shaped model 1: rigid cavity
b. Vibroacoustic analysis of car shaped model 1: partially flexible cavity

7.2.1. Vibroacoustic analysis of Car Shaped Model 1: Rigid Cavity

In this case, the cavity is fully rigid with window openings at both sides. Fully closed window denotes rigid cavity without opening. For this case no interaction with exterior domain is performed. Fully open window necessitates coupling between interior and exterior domain. The sound pressure level (SPL) inside the domain at driver position A (0.75, 0.45, 1.1) and at passenger position C (1.8,0.3,1.1) has been plotted up to 300Hz with 1 Hz interval for both window closed and window open conditions in Fig. 7.4a and 7.4b. SPL has been plotted at the side boundary point Q (1.3, 0, 1.3) and at roof boundary of the car S (1.35,0.75,1.5) in Fig. 7.4c and 7.4d respectively.

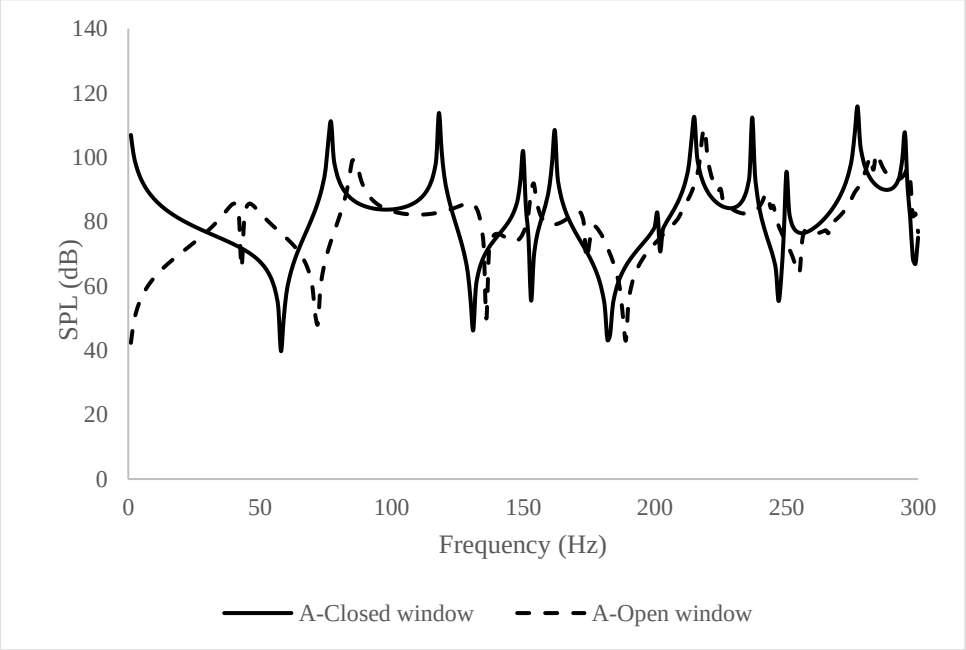

(a)

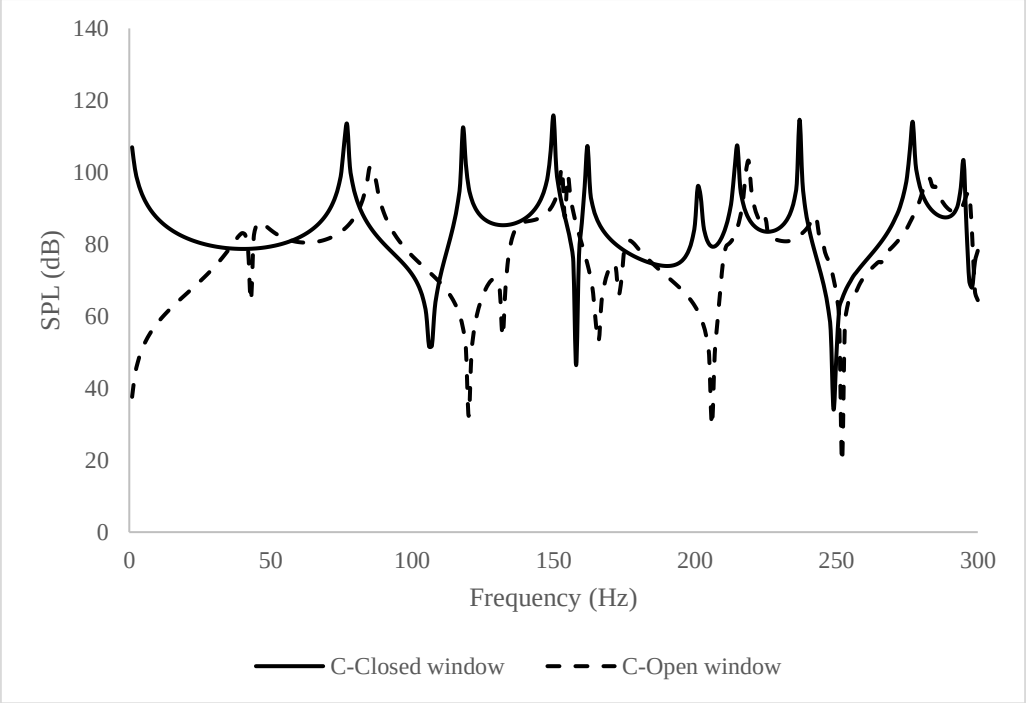
140
120
100
80
60
40
20
0
SPL (dB)
0
50
100
150
200
250
300
Frequency (Hz)
C-Closed window
C-Open window

(b)

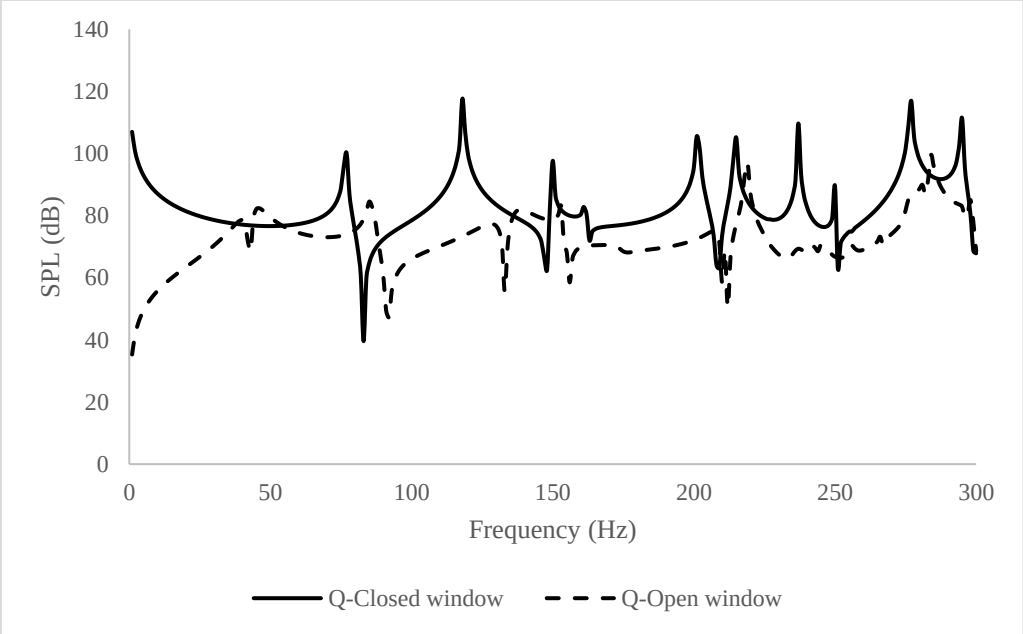
140
120
100
80
60
40
20
0
SPL (dB)
0
50
100
150
200
250
300
Frequency (Hz)
Q-Closed window
Q-Open window

(c)

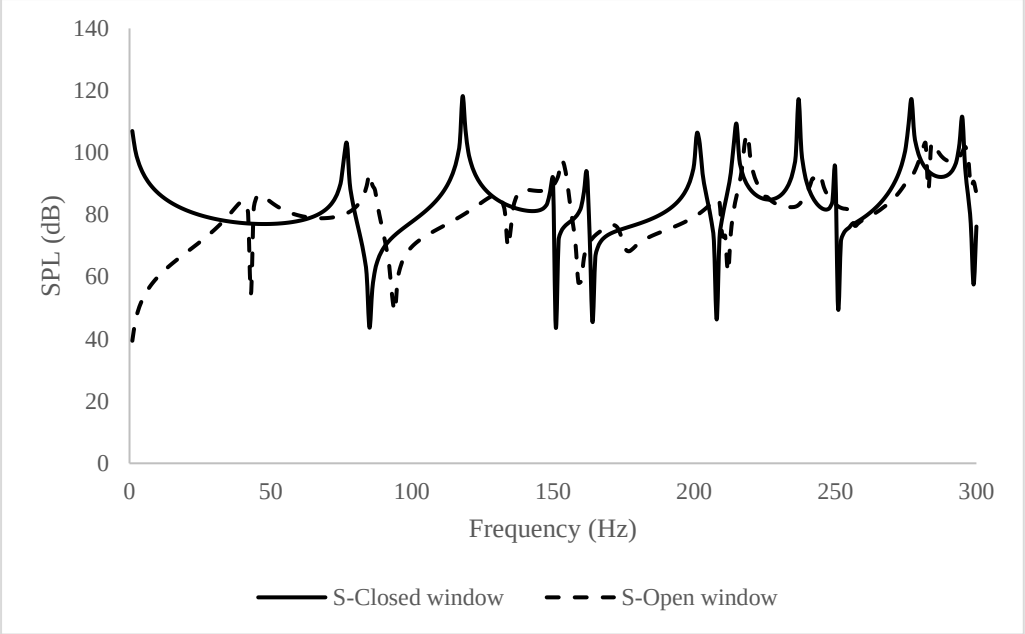

(d)

Fig. 7.4: Comparison of SPL for window closed and open condition at a) point A and b) point C at interior of domain 1 c) point Q and d) point S at the boundary of domain 1 (Rigid Cavity)

From the Figures 7.4a to d, it is noticed that when the window is in open condition, an inverse peak has been developed at first at 43Hz. This is due to interior-exterior coupling of acoustics. For window closed condition, the acoustic resonance occurred at 77Hz and then at 118Hz. Window open condition considerably reduces the SPL values at these frequencies.

7.2.2. Vibroacoustic analysis of Car Shaped Model 1: Partially flexible Cavity

In this study, the car model 1 is made partially flexible by making the slanting edges made up of orthotropic cross ply laminated composite of 6mm thick plate. The material properties of E-glass epoxy composite are as follows:

E_1= 60.7 Gpa, E_2=24.8 Gpa, G_{12}= G_{13}= G_{23}= 12.0 Gpa, ρ = 1300 kg/m^3, υ_{12}= 0.23, υ_{21}= 0.094, Fibre Orientation $0^0/ 90^0 / 90^0 / 0^0$.

All other panels of the interior domain are considered as rigid. The damping ratio is taken as 0.01. The boundary surface is discretized using eight noded isoparametric elements. The first twenty natural frequencies have been shown in Table 7.1 and the first six mode shapes are drawn in Fig. 7.5. From the figure, bending mode shapes are observed for first six natural frequencies.

Table 7.1: First Twenty Natural Frequency in Hz

Mode Number	Frequency in Hz	Mode Number	Frequency in Hz	Mode Number	Frequency in Hz	Mode Number	Frequency in Hz
1	54.58	6	121.97	11	190.63	16	310.57
2	75.64	7	141.91	12	192.93	17	465.31
3	80.90	8	144.10	13	200.24	18	560.57
4	104.45	9	168.27	14	247.28	19	831.19
5	109.86	10	172.62	15	250.92	20	976.71

Using the natural frequencies and modal vectors in the mobility relation as indicated in Eq. 3.2.8, the sound pressure level at driver position A, passenger position C and at the cavity boundary Q and S have been plotted in Fig. 7.6a to 7.6d for the completely closed and fully opened window respectively.

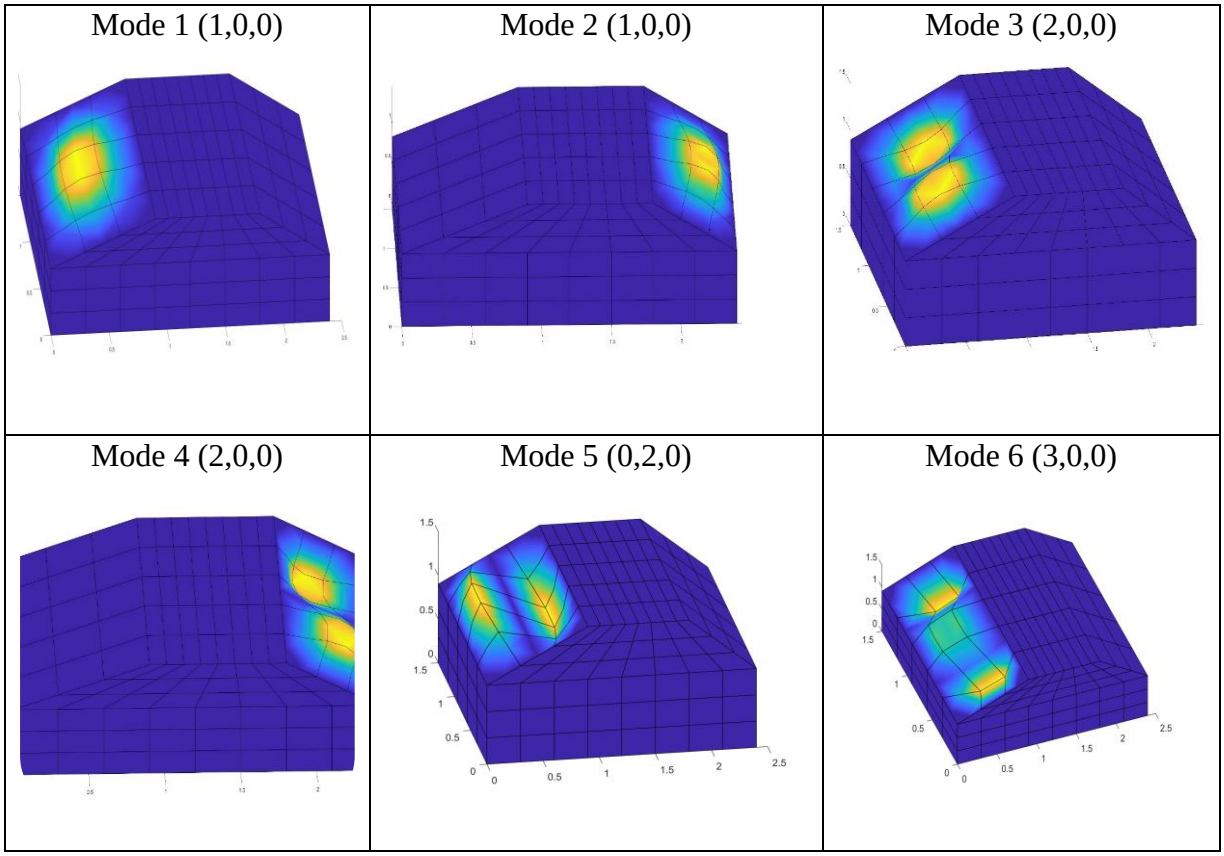

Fig. 7.5: First six mode shapes for flexible panel

For closed window case, the acoustic problem becomes an interior problem and only interaction between flexible membrane with internal cavity have been taken place. The above-

mentioned interaction and interior-exterior coupling have been taken place for fully open window condition. It is observed that for window open condition, the general SPL pattern is at lower value than that of closed window case. Also, at first a dip is observed in the open window case. The peaks are shifted to some extent for open window case. Fig. 7.7 compares SPL at an external domain point X (5,1,1) for both rigid and partial flexible cavity. It is observed that the SPL pattern is identical except in the range 50 Hz to 80 Hz where few peaks and troughs are visible for partly flexible model, which is due to the interaction between flexible surface and interior acoustic domain. It is observed that at 21 Hz, the SPL at 'X' becomes negative indicating that the sound pressure reduces below the reference sound pressure that is audible for human being.

(a)

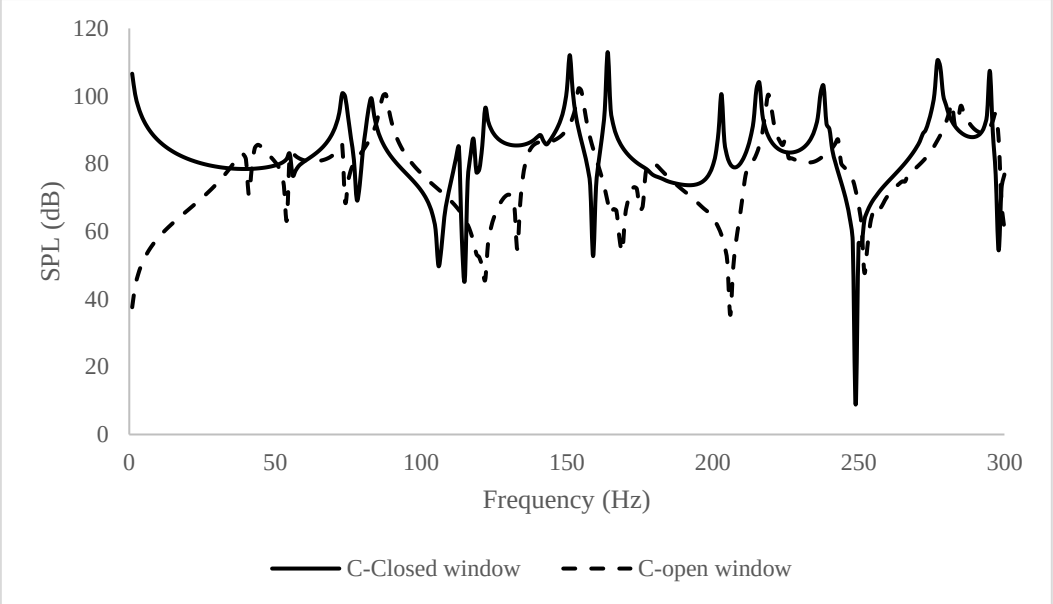
120
100
80
60
40
20
0
SPL (dB)
0
50
100
150
200
250
300
Frequency (Hz)
C-Closed window
C-open window

(b)

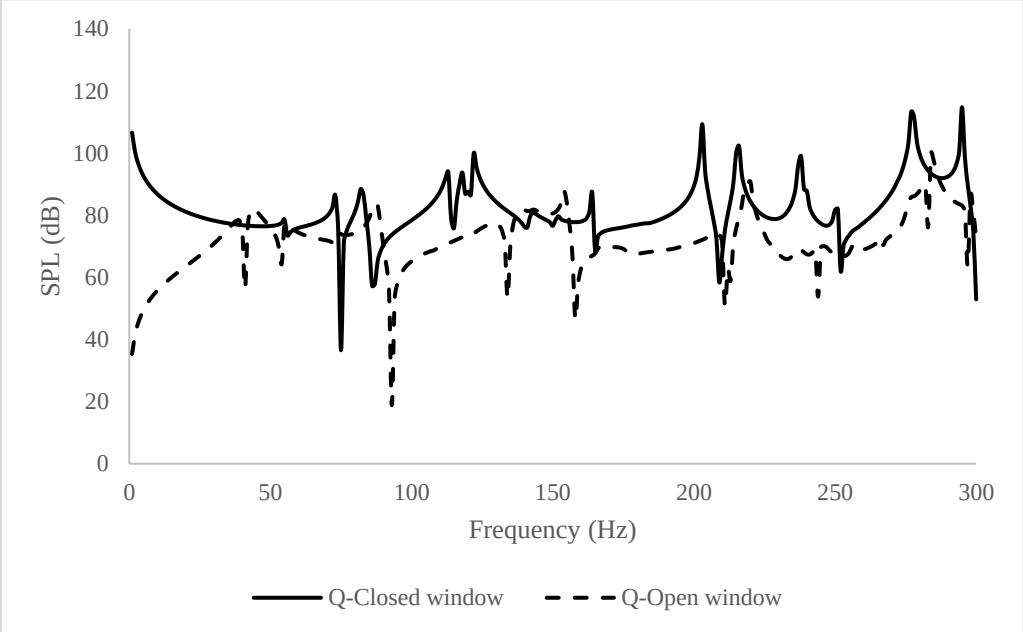
140
120
100
80
60
40
20
0
SPL (dB)
0
50
100
150
200
250
300
Frequency (Hz)
Q-Closed window
Q-Open window

(c)

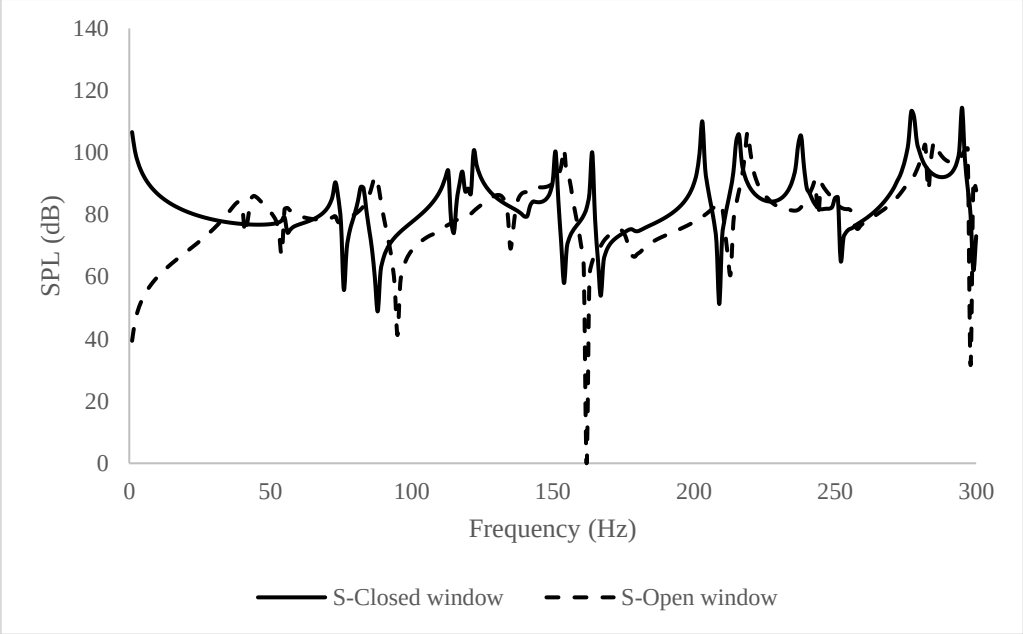

(d)

Fig. 7.6: Comparison of SPL for window closed and open condition at a) point A and b) point C at interior of domain 1 c) point Q and d) point S at the boundary of domain 1 (Partial Flexible Cavity)

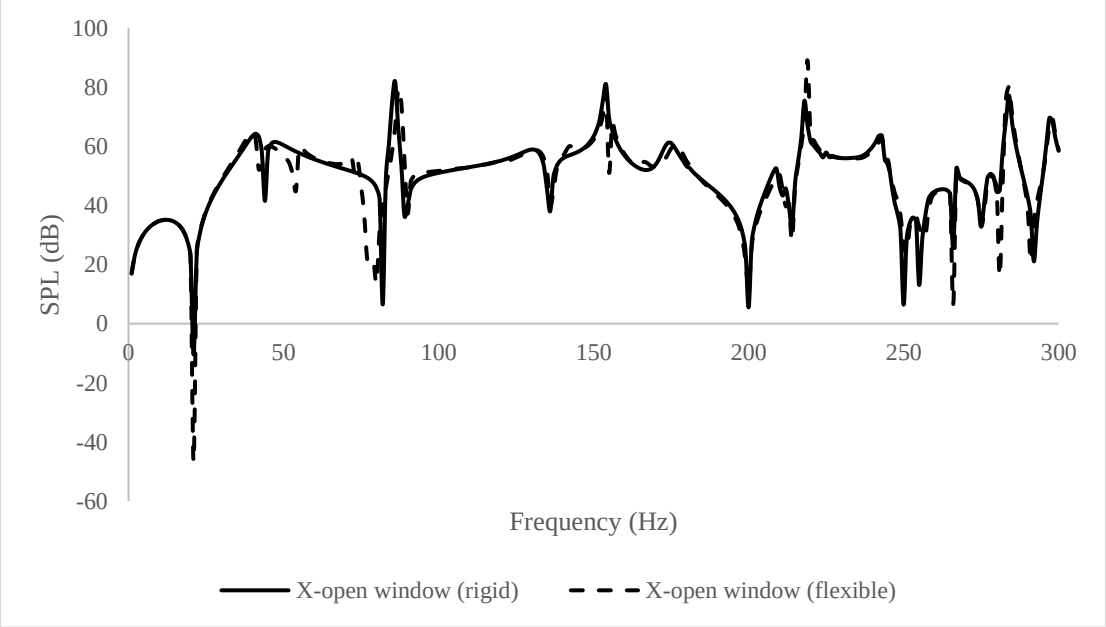

Fig. 7.7: Comparison of SPL at an outside point X (5,1,1) in the exterior domain 2

In Figure 7.8, boundary SPL at the inside of interior domain and external side of exterior domain has been plotted for the frequency 50 Hz both for rigid and flexible model for window

open condition. From the figures 7.8 (a) and 7.8 (c), we can observe that SPL is lower on the region of the window at the interior boundary, compared to other boundary points because of radiation of sound energy from the interior to the exterior domain. For the exterior domain boundary (Fig. 7.8 (b) and (d)) the SPL at the window location is greater in comparison to the other exterior boundary points. Both domains have the same sound pressure at the window position.

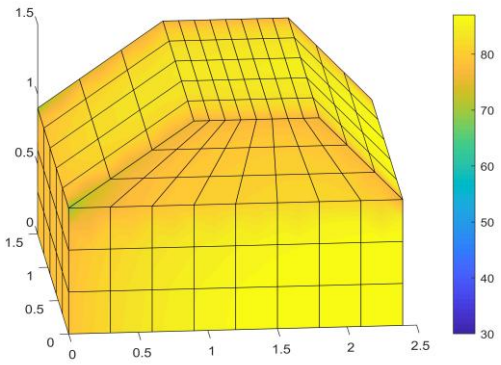

(a) 4D SPL plot at the boundary of interior domain (Rigid model)

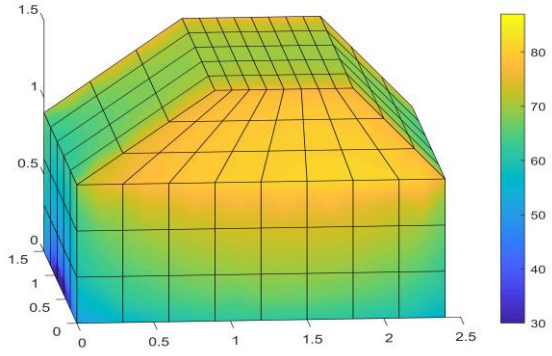

(b) 4D SPL plot at the boundary of exterior domain (Rigid model)

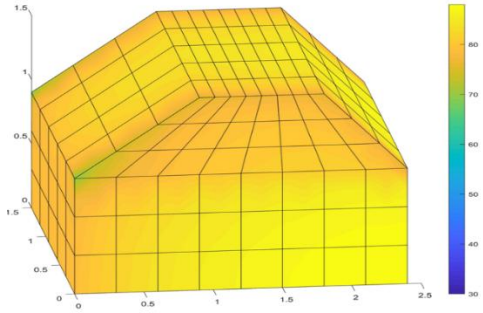

(c) 4D SPL plot at the boundary of interior domain (Flexible model)

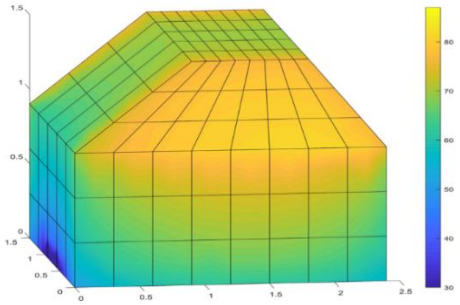

(d) 4D SPL plot at the boundary of exterior domain (Flexible model)

Fig. 7.8: 4-dimensional SPL plot at 50 Hz

An SPL contour has been plotted in Fig. 7.9(a), 7.9 (b) 7.9(c) and 7.9 (d) at 50Hz frequency on the XY plane at the mid height at Z=0.75m from the base of the cavity and on the XZ plane at Y = -0.05m in front of the window panel respectively. It is observed that within the interior car cavity, SPL is highest. With increase in distance, the overall SPL reduces with an alternate

high pressure and low-pressure region in the exterior domain due to presence of compression and rarefaction, respectively. The comparison of the SPL (Fig. 7.9) contours across the figures indicates that the exterior SPL distribution is significantly influenced by the flexibility of the cavity structure.

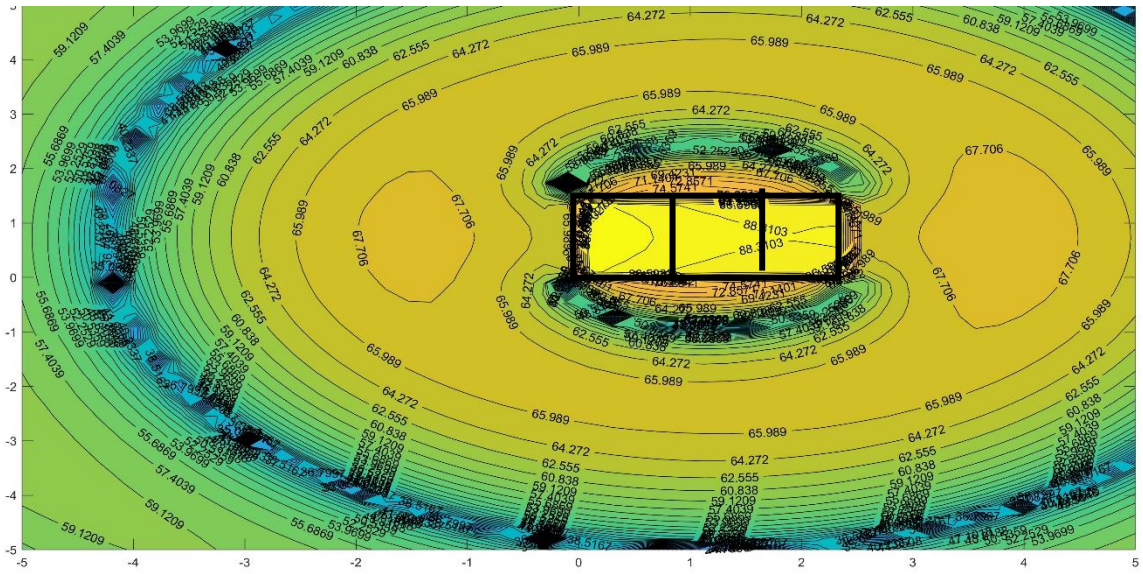

(a)

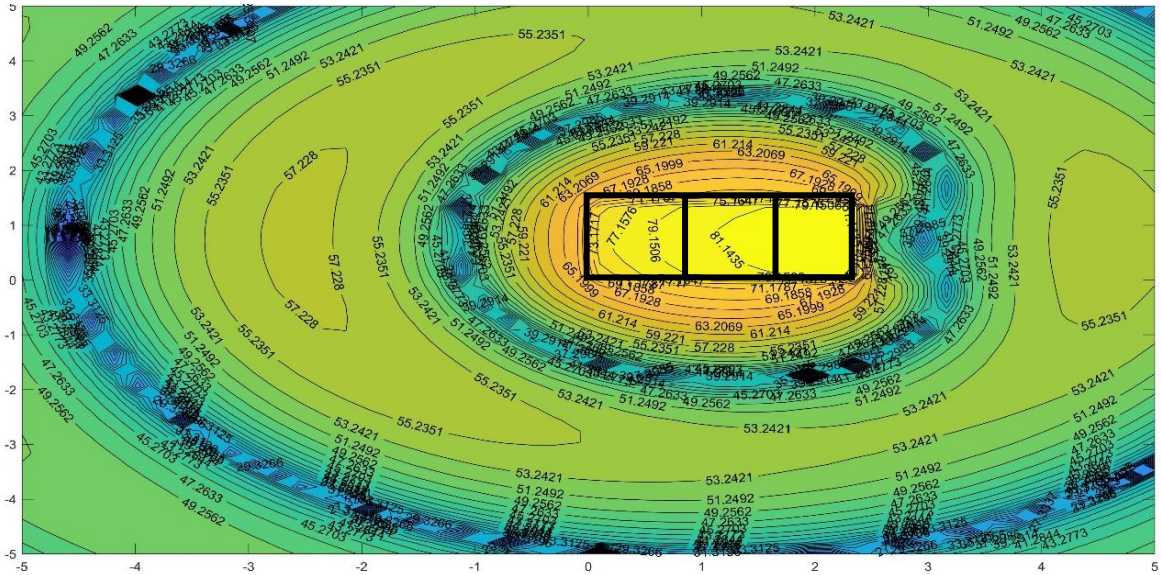

(b)

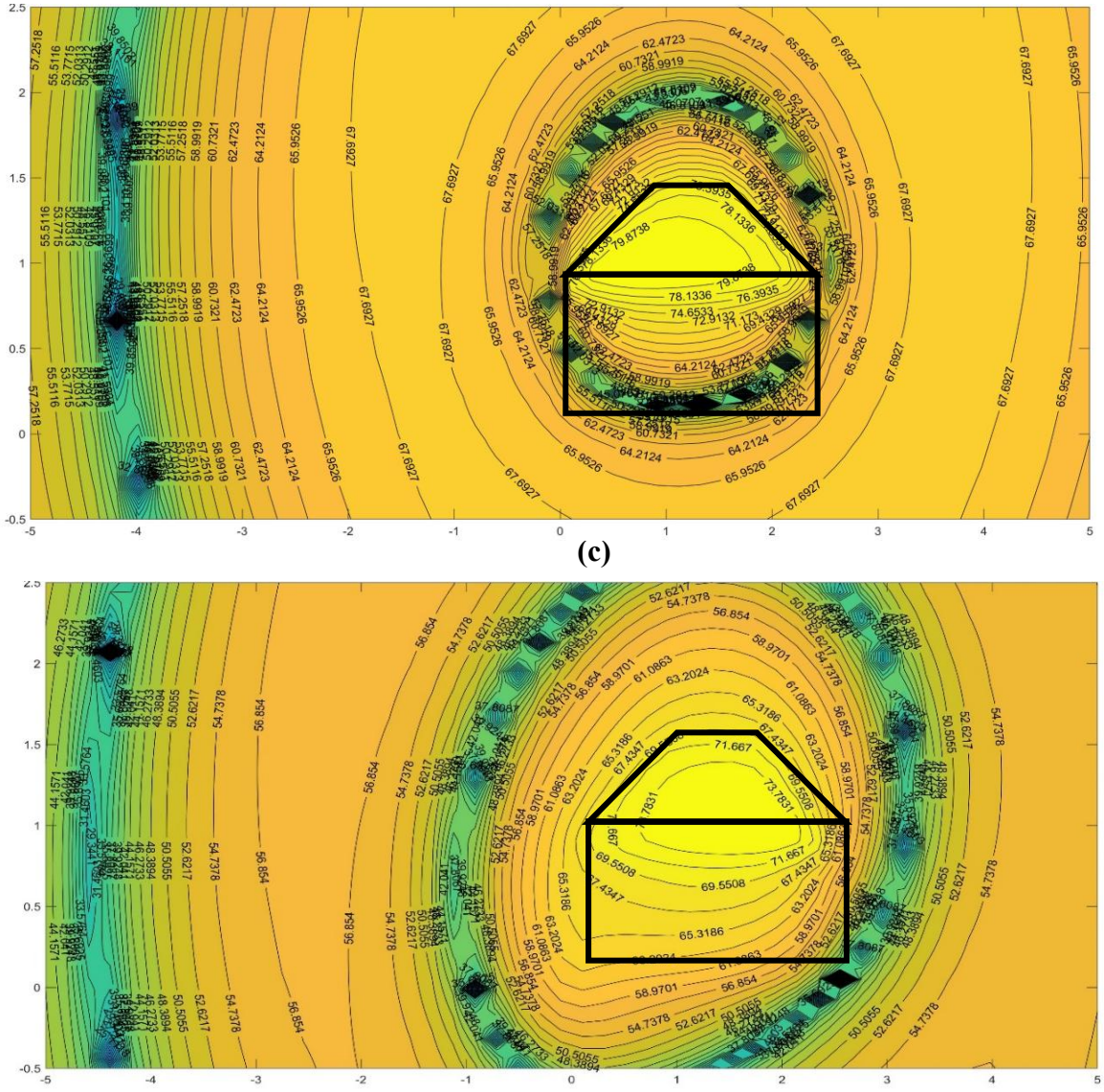

(c)

(d)

Fig.7.9: Contour SPL for 50Hz frequency on the (a) XY plane at height Z=0.75m for rigid (b) XY plane at height Z=0.75m for flexible cavity, (c) XZ plane at Y= -0.05m for rigid cavity
and (d) XZ plane at Y= -0.05m for flexible cavity

7.2.3. Vibroacoustic analysis of Car Shaped Model 2: Interior-Exterior Multi-Domain Coupling Analysis of Partially Flexible Cavity

In this study, the cavity is made as practical as possible with a partially flexible interior of size 2.4m × 1.5m × 1.2m, which has been divided into two domains named domain 1 and 2 and the exterior domain (domain 3) as shown in Figure 7.10. Domain 1 has two window panels at

both sides (white colour) and one flexible panel (green colour) at one end. Two chairs have been placed in domain 1 as shown in Fig. 7.10.a. The seat cushions are modelled as boundary with absorption layer (blue colour). The interface region between domain 1 and 2 has been colored as yellow for clear understanding. As the engine is placed at the front of a car, the pulsating panel has been provided at the front in Domain 1 with a constant velocity amplitude of 0.001 m/s. Similarly, domain 2 has two windows at both sides and it is connected by the interface layer (yellow colour) with domain 1. One flexible panel has been provided at the back side. All other panels of the interior domain are considered as rigid boundary (magenta colour). In the case of the exterior domain, the window panel is common with the interior acoustic cavity and other panels are considered as rigid.

Two interaction couplings have been performed for this car model. One is the interaction between the flexible panels with interior cavity and second one is the coupling between interior and exterior domains.

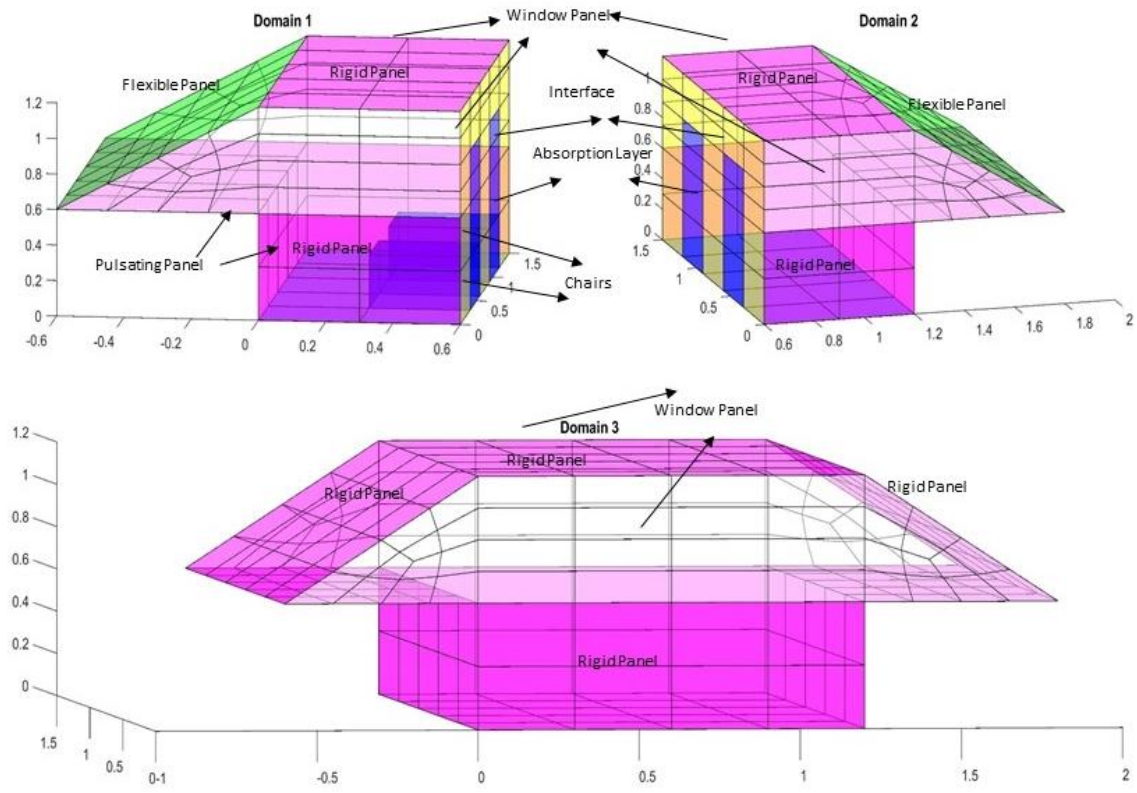

Fig.7.10: Geometry of car model-2

As in section 7.2.2, the flexible panels have been modelled using E-glass epoxy composite with the same material properties as mentioned. The thickness and fibre angle variation have also been kept same. A damping ratio of 0.01 has been taken in the study. The first twenty

natural frequencies have been shown in Table 7.2. Two natural frequencies that are next to each other appear to be the same. This is due to symmetrical geometry of the flexible panels. Plotting of a few mode shapes in Fig. 7.11 makes it evident that bending modes predominate.

Table 7.2: First Twenty Natural Frequency in Hz

Mode Number	Frequency in Hz	Mode Number	Frequency in Hz	Mode Number	Frequency in Hz	Mode Number	Frequency in Hz
1	71.49	6	152.98	11	223.25	16	314.92
2	71.49	7	182.47	12	223.25	17	354.75
3	109.54	8	182.47	13	266.22	18	354.75
4	109.54	9	199.34	14	266.22	19	388.15
5	152.98	10	199.34	15	314.92	20	388.15

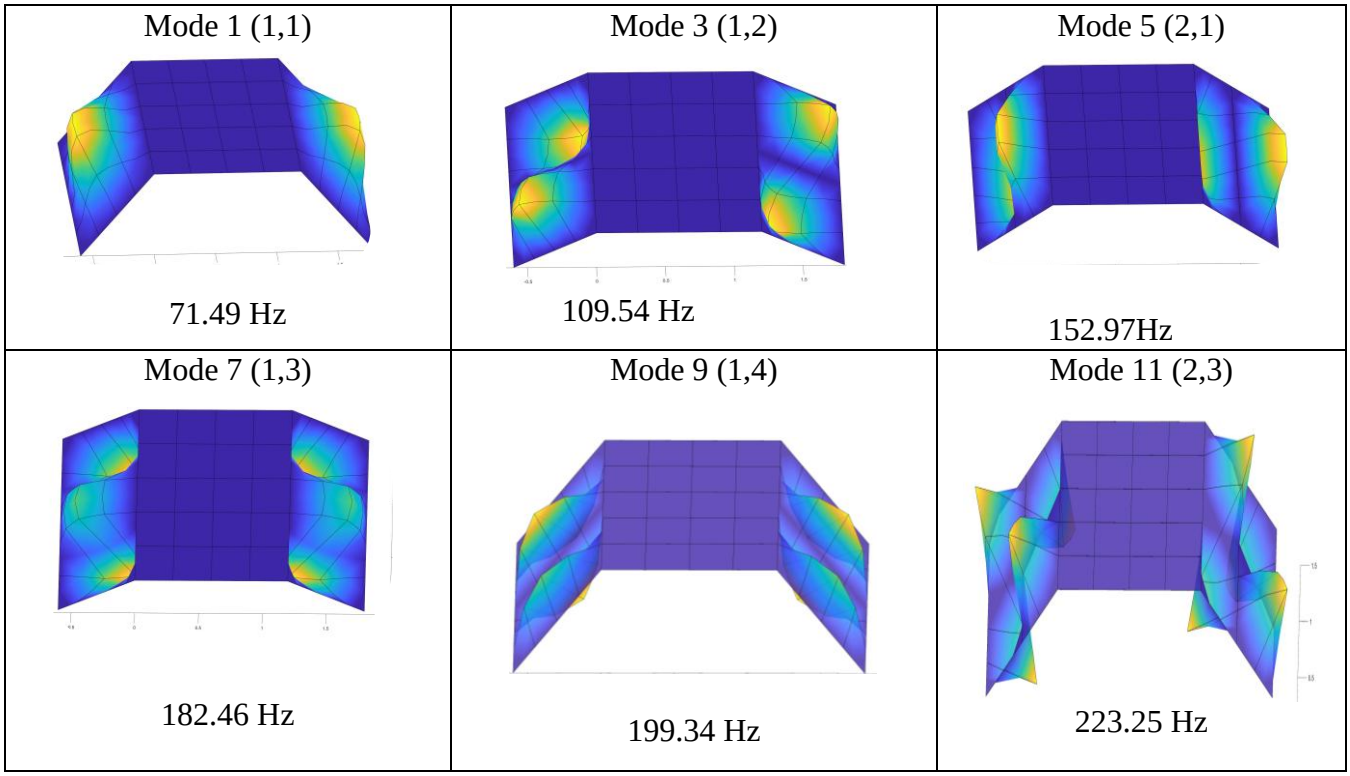

Fig. 7.11: Six mode shapes for flexible panel

The modal parameters thus obtained are then used in the mobility matrix to calculate the acoustic pressure and the interface velocity at different interior and exterior points. The study compares two interior points: the driver's position P1 (0.45, 0.45, 0.9) in domain 1 and the passenger's position P2 (1.05, 0.45, 0.9) in domain 2. One exterior point P3 (5,1,1) in domain

3 has been examined too. For all cases, it is assumed that the window is kept fully open. The following cases have been analysed.

a. Effect of Flexibility
b. Effect of Absorbent Layer
c. Effect of different damping ratios
d. Effect of different locations

7.2.3.a. Effect of Flexibility

i. Domain Point

The domain SPL at points P1, P2 and P3 in domain 1, domain 2 and domain 3, respectively, have been plotted in Fig. 7.12 a and 7.12b for rigid and flexible cases, where flexibility of front and backside panels are ignored in rigid case.

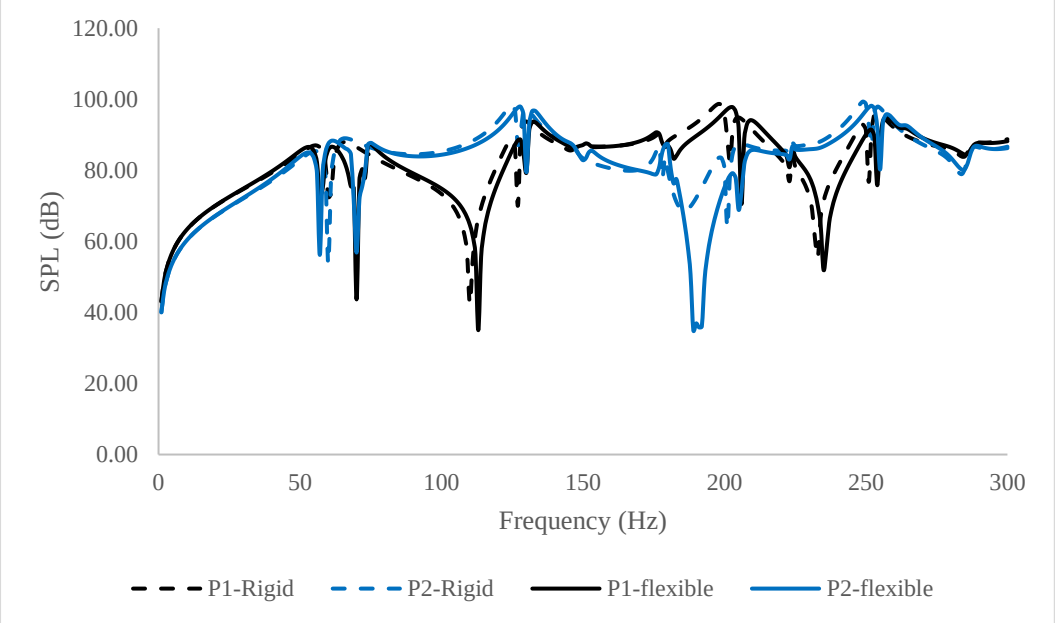

Fig. 7.12a: SPL at interior point at P1 and P2

From the figure, it is observed that at 60Hz, 127Hz, 201Hz and 252 Hz, for both P1 and P2, sharp dips are present, which may be the effect of geometry of the cavity. An extra dip at 110Hz and 233Hz are observed at point P1. At P2, the SPL reduces to 35dB at 190Hz which is due to the combined effect of modal frequency at 182 Hz and 199 Hz. When flexible panels are considered, the overall pattern shifts slightly to the right after 80 Hz. A sharp dip of 44dB is present at 70Hz which is due to the presence of modal frequency at 71.49Hz.

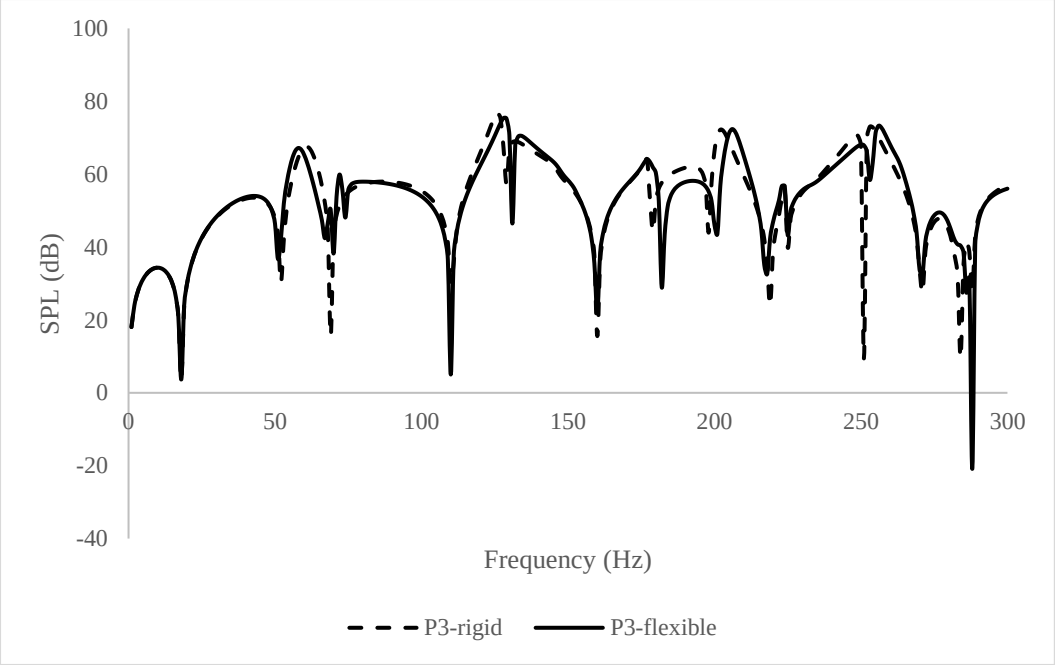

Fig. 7.12b: SPL at exterior point P3 (5,1,1)

From Fig. 7.12b, similar shifting of SPL pattern has been noticed. At 288Hz, a negative SPL is observed at P3 denoting reduction of sound pressure level below reference pressure i.e., $2x10^5$ Pa.

ii. Boundary Point

The SPL at interior boundary B (0.6, 0, 0.3) and at exterior boundary B′(0.6, 0, 0.3) also have been plotted in Fig. 7.12c.

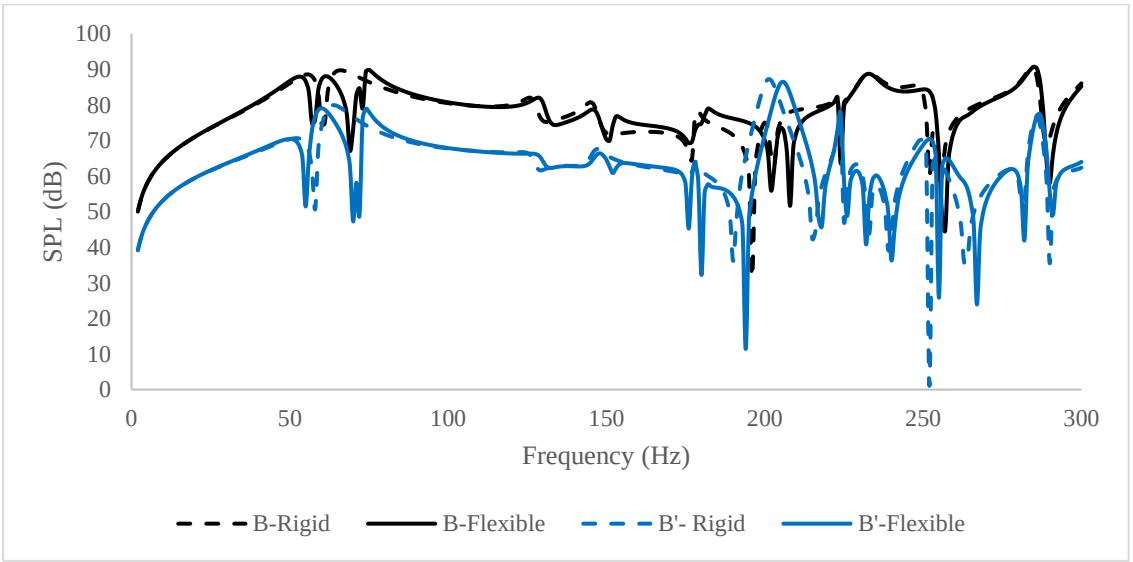

Fig. 7.12c: SPL at interior boundary point B and exterior boundary point B′ (0.6, 0, 0.3)

Figure 7.12c shows that, except for a shifting, a similar pattern is seen at boundary point B and B′ for the rigid and flexible cases. Additionally, the SPL steadily decreases at exterior boundary B', which is precisely on the other side of the internal domain. Several kinks are found after 200 Hz for the exterior boundary point B' when contrasted to B.

7.2.3.b. Effect of adding absorbent layers

In this study, the effect of adding absorbent layers have been found. The absorbent layer is added at the Top, Bottom, Side, and on the Chair and compared with NO absorbent case. The damping ratio is taken as 0.01 for all cases. The sound pressure level has been plotted and compared at P1, P2, P3 and B without and with application of absorbent layers as in Fig. 7.13 a to 7.13d.

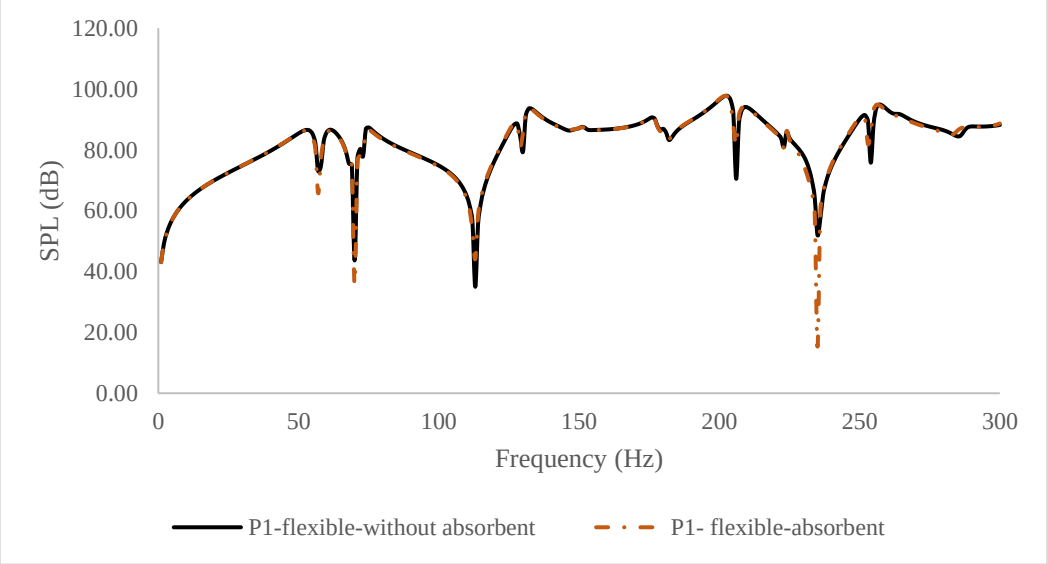

Fig. 7.13a: SPL at interior domain point P1 with and without absorbent layer

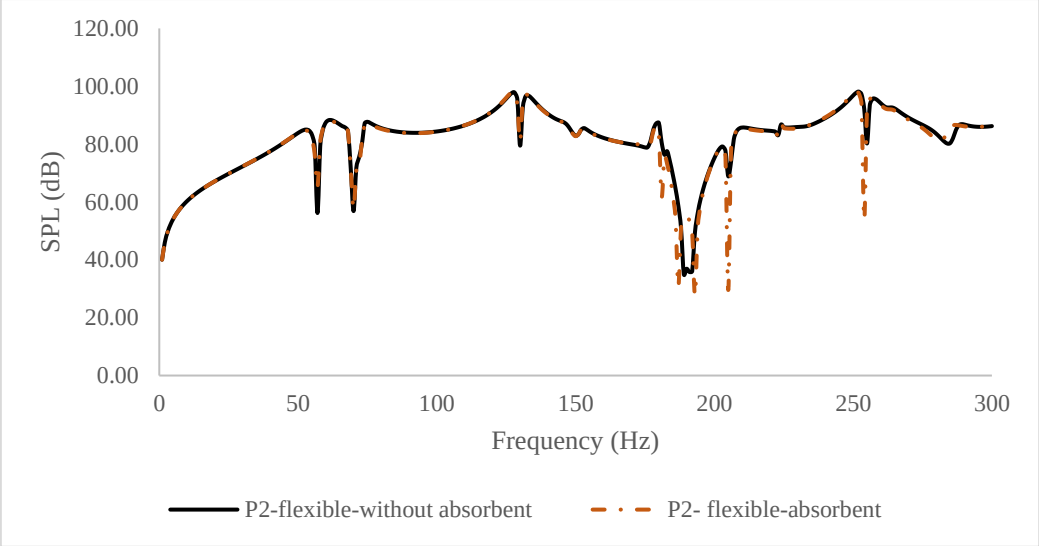

Fig. 7.13b: SPL at interior domain point P2 with and without absorbent layer

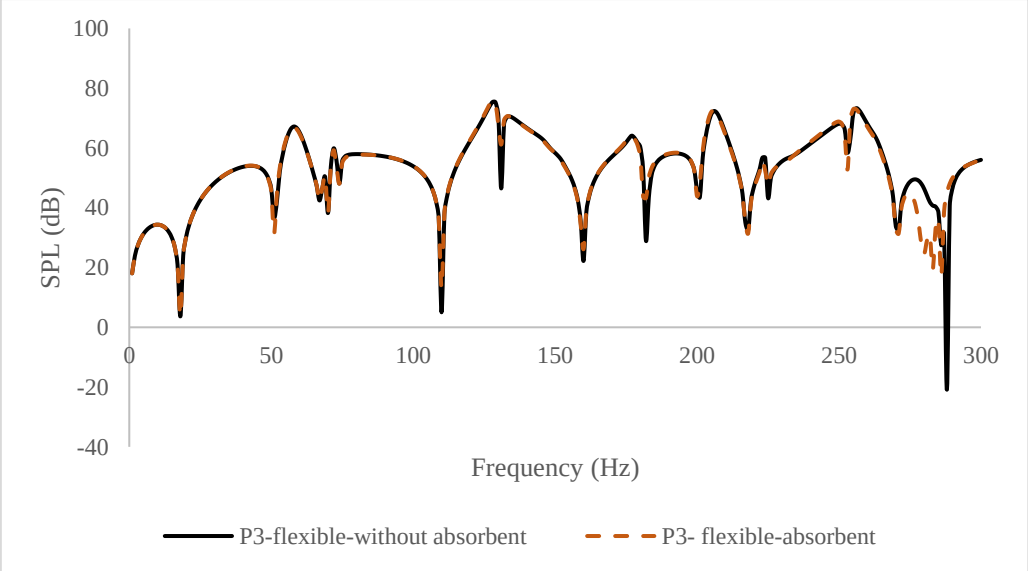

Fig. 7.13c: SPL at exterior domain point P3 with and without absorbent layer

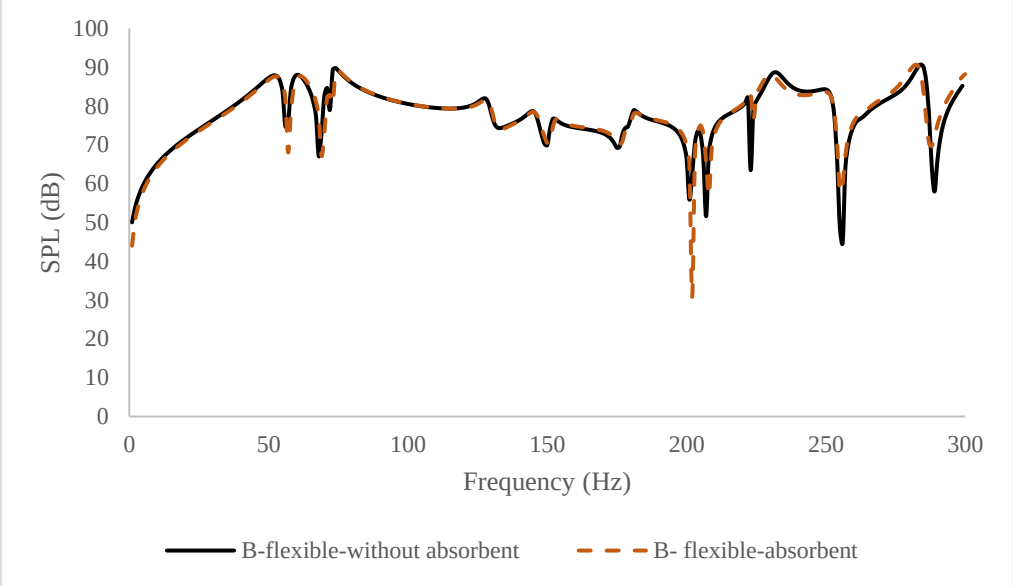

Fig. 7.13d: SPL at interior boundary point B with and without absorbent layer

It is observed that the pattern remains same when absorbent layer is added. At the trough position, however, the effect is more noticeable. To clearly understand the effect of adding absorbent layers SPL values at some frequencies are tabulated in Table 7.3. It is observed that the effect of absorbent layer is location and frequency specific. For example, at 70Hz, the SPL reduces much at P1 and B, but the effect is negligible at P2 and P3 at the same frequency. On the contrary, at 113Hz, the SPL increases after addition of absorbent at P1.

Table 7.3: SPL (dB) at Observation Point P1, P2, P3 and B with and without absorbent layer

Frequency (Hz)	SPL (dB) at Observation Point P1		SPL (dB) at Observation Point P2	
	P1-without absorbent layer	P1-with absorbent layer	P2-without absorbent layer	P2-with absorbent layer
57	73.05	**65.74**	56.18	65.23
70	43.66	**35.70**	56.84	57.70
113	35.00	44.07	87.54	87.60
130	79.37	85.57	79.47	80.94
181	85.76	83.27	80.63	**61.80**
193	91.41	91.56	49.48	**27.63**
205	92.09	**87.93**	68.90	**29.56**
206	70.49	81.57	73.80	77.62
235	52.03	**15.32**	86.71	86.89
254	75.79	86.05	92.08	**53.88**

Frequency (Hz)	SPL (dB) at Observation Point P3		SPL (dB) at Observation Point B	
	P3-without absorbent layer	P3-with absorbent layer	B-without absorbent	B-with absorbent layer
51	**36.73**	**31.46**	87.69	87.23
57	66.49	66.46	75.82	**68.05**
69	50.29	50.32	73.16	**67.18**
70	38.24	38.29	82.60	**72.98**
200	**46.09**	**43.88**	66.44	69.73
202	56.89	59.18	62.23	**30.77**
223	**56.75**	**55.70**	63.47	83.06
253	**58.46**	**52.84**	77.56	78.60
271	**32.57**	**31.34**	81.35	82.30
288	-20.89	44.93	64.20	**69.69**

7.2.3.c. Effect of various damping ratio

In this study, the damping ratio has been changed from 0.1% to 1% and compared with and without addition of absorbent layers at bottom, top, side and on the chairs. The SPL at the interior domain point P1 and at exterior domain point P3 have been compared in 7.14a and b.

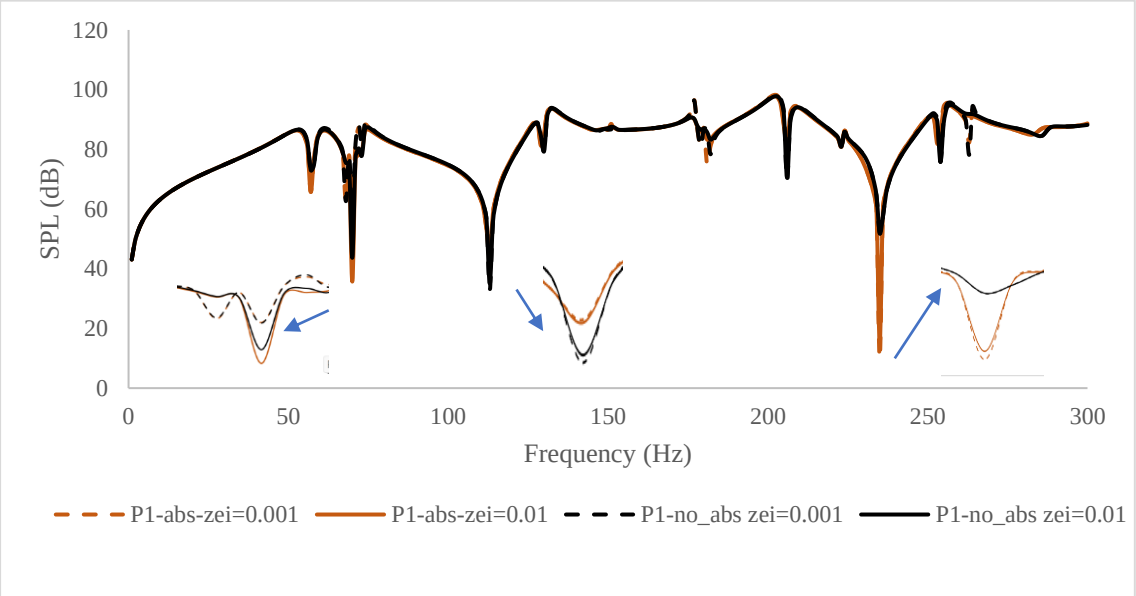

Fig. 7.14a: SPL at interior domain P1

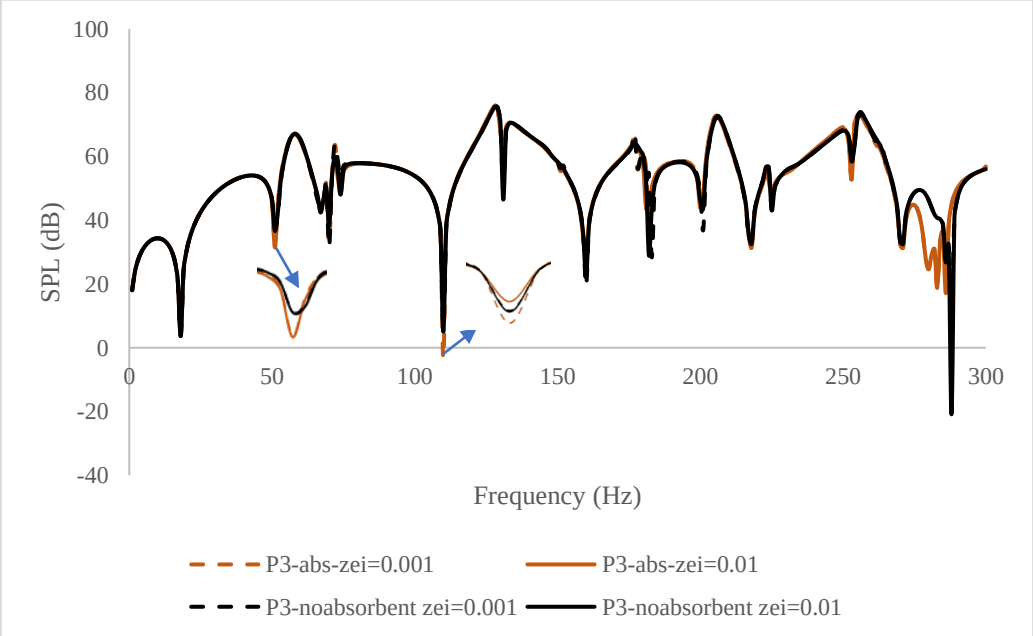

Fig. 7.14b: SPL at exterior domain P3

The effect of damping is restricted to the peaks or troughs, as we have observed in other prior instances. Overall, as shown in Fig. 7.14a, the damping smoothed out the curve's undulations

between 175 and 185 Hz and between 260 and 266 Hz at the trough in P1. Damping operates in the lower frequency range at the trough. At 70Hz, damping decreases the SPL further after the absorbent layer lowers the SPL, which does not occur at 235 Hz. When an absorbent layer is applied, the damping effect is obscured, and in certain places, the absorbent layer further lowers SPL. At P3, application of absorbent layer generally reduces the SPL at various trough locations, though no noticeable dampening effect is seen at 110 Hz.

7.2.3.d. Effect of location

In Figure 7.15, the SPL from zero to 300 Hz has been displayed at domain points P1, P2, and P3 in increments of 1 Hz, with the inclusion of an absorbent layer for a partially flexible cavity with a damping ratio of 1%. The SPL values are comparable because P1 and P2 are in the interior domain. The overall SPL level is significantly lower outside the cavity than it is inside because P3 is in the exterior domain. P1, P2, and P3 show a similar dip at 70 Hz and 253 Hz which is essentially a feature of the entire cavity.

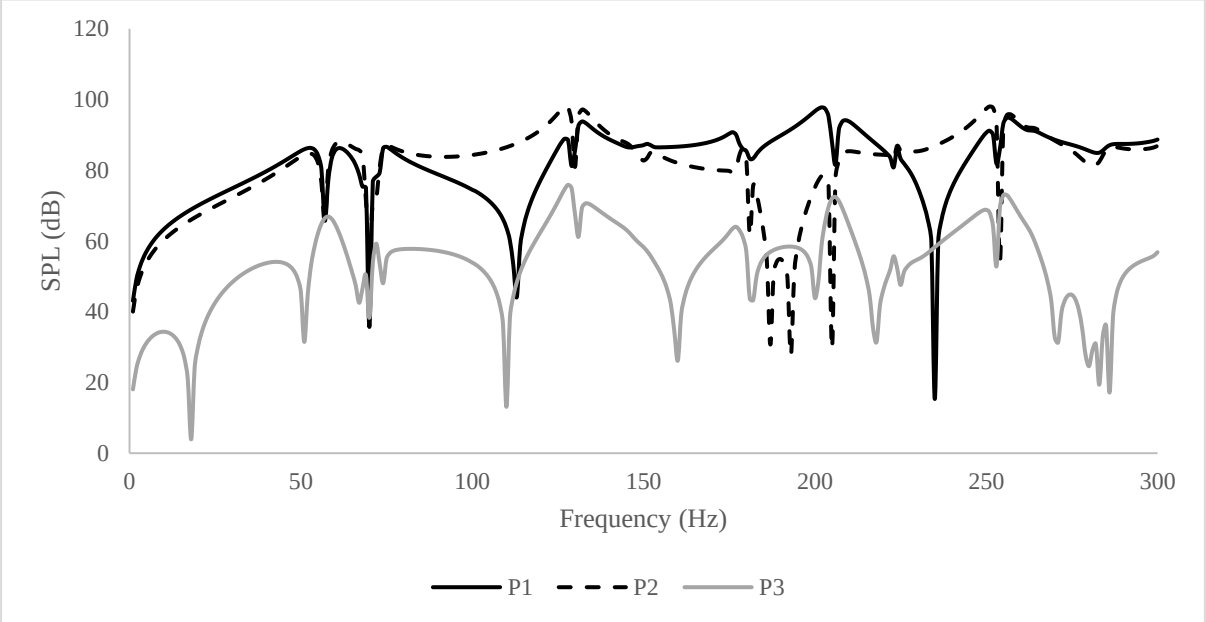

Fig. 7.15: SPL at P1, P2 and P3 at partially flexible cavity with absorbent at 1% damping

A 4-D SPL map of the exterior and interior boundaries of a partially flexible panel with an absorption layer at 100 Hz is shown in Fig. 7.16. The window's SPL for the exterior and interior boundaries is the identical in this instance as well. The outside domain has a lower overall SPL. The front end of the car model has a low-pressure area, and the back end has a high-pressure area.

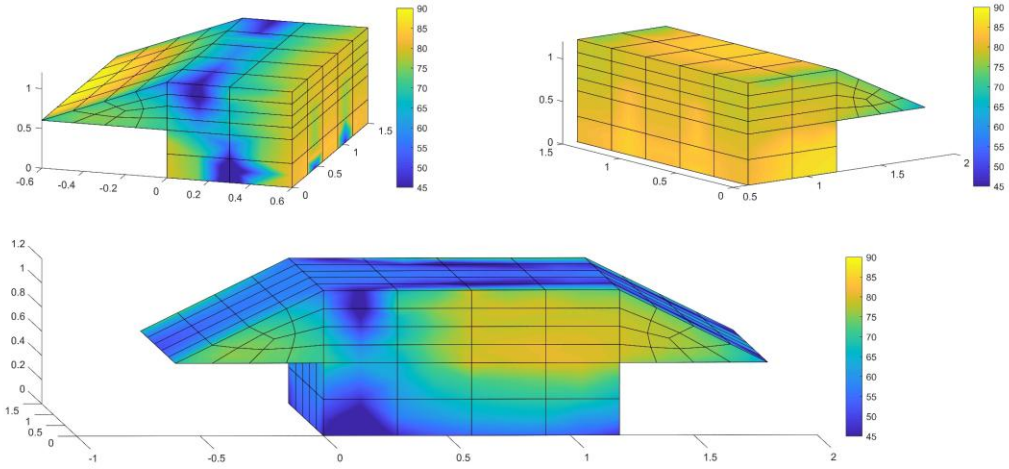

Fig. 7.16: 4D SPL plot at the interior and exterior boundary for 100Hz for partially flexible panel with absorption Layer

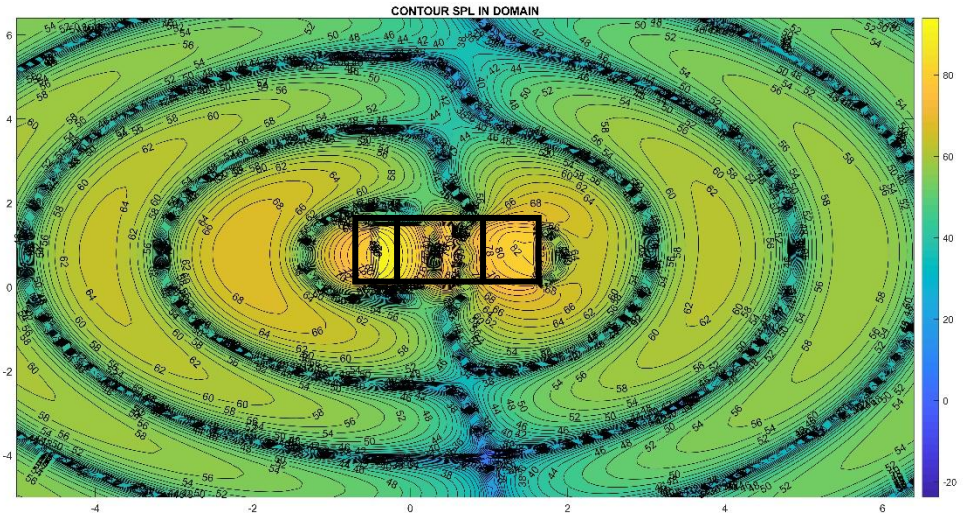

Fig. 7.17a: Contour SPL for 100Hz frequency on the XY plane at height Z=0.75m for the flexible cavity with Absorption Layer

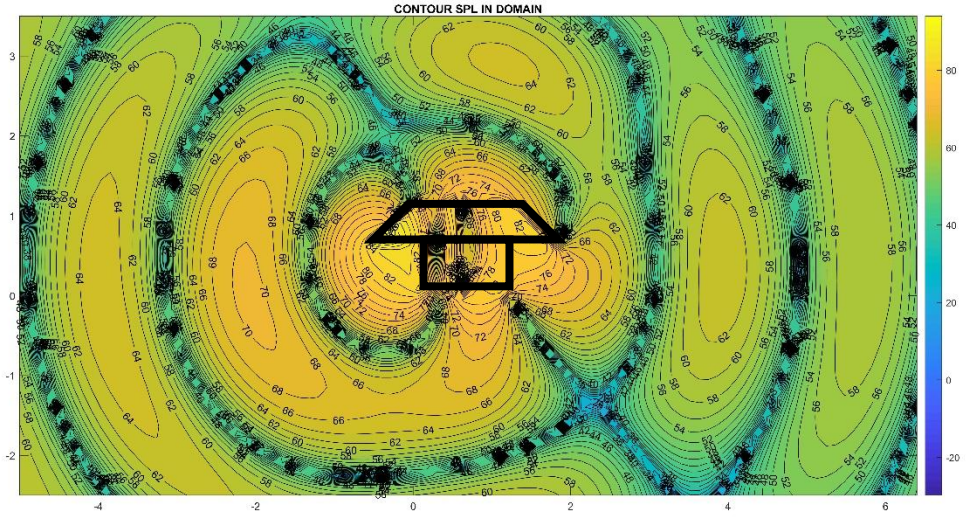

Fig. 7.17b: Contour SPL for 100Hz frequency on the XZ plane at Y=0.75m for the flexible cavity with Absorption Layer

An SPL contour has been plotted in Fig. 7.17(a) and 7.17 (b) at 100Hz frequency on the XY plane at the mid height at Z=0.75m from the base of the cavity and on the XZ plane at Y = 0.75m in the middle of the cavity, respectively. When compared with Fig. 7.9, it is observed that more numbers of compression and rarefaction cycles are visible. This is because, with a driving frequency of 100 Hz, wavelength decreases while velocity stays constant. There are also alternating zones of high and low pressure inside the car's interior. The overall SPL decreases as the distance increases.

7.3. Conclusion:

This research focuses on developing a computer program that simulates sound behaviour in different situations in a partially flexible composite vehicular cavity structure. The program can handle various scenarios like closed spaces with different wall properties, whether rigid or flexible, even accounting for sound absorption materials. Its effectiveness is proven by analysing how sound travels between interiors and exteriors through window.

According to the study, opening has a significant impact on how SPL is distributed. When there is an opening, several inverted peaks are observed, which lowers the overall SPL. The SPL pattern stays the same when the vehicle cavity is partially flexible, except for a small forward shift brought on by the interaction of flexible panels with the interior acoustic cavity.

Plotting SPL at a specific frequency on the cavity's inner boundary reveals that the SPL is lowest at the opening and decreases further with increasing distance from the cavity. Plotting the SPL contour has produced alternating zones of high and low pressure.

Also, as the geometry of the cavity changes, the SPL pattern inside and outside the cavity changes considerably. For model 2 it has been noticed that application of absorbent layer inside the cavity has significant effect on the SPL of a particular point, mainly at the trough position. However, not every trough position exhibits the absorbent layer's action equally. Therefore, it may be concluded that the absorbent layer's influence varies depending on each position and natural frequencies of the structure. The effects of damping and adding an absorbent layer are comparable. The use of absorbent masks the damping effect when both are present, thus lowering the SPL. As the driving frequency increases, the wavelength decreases and the number of high and low pressure zones increases.

The program developed can be used to find solutions for a real-world vehicular problem in structural acoustics. Additionally, the program includes tools to visualise sound levels within the modelled environment. The research plans to further develop the program by analysing more complex situations involving multiple spaces and interior elements.

8

Conclusion

8.1. Summary

Vibroacoustic analysis plays a crucial role across various modern engineering fields, including music, architecture, medical science, and defence, due to its extensive applications in understanding and controlling sound and vibration interactions. The vibroacoustic study of vehicular cavities is one of the main areas of concern for the optimum usefulness of this system's interaction with internal and surroundings. In this thesis, a vibroacoustic analysis of a car shaped acoustic cavity, consisting of rigid and laminated composite thin flexible walls with an opening, has been conducted. The study utilizes coupled multi-domain boundary element method (BEM) with finite element method (FEM). The cavity is divided into multiple domains with intermediate interface layers, and continuity conditions are established at the interfaces, as discussed in Chapter 3. A robust numerical model has been developed to describe complex vibroacoustic behaviour for the complicated shape of the domain, both for rigid and flexible along with opening. Generalized boundary conditions are used to make the model as practicable as possible.

8.2. Discussion

The following conclusions are evident from the studies performed in the thesis.

i. From the study of free vibration of sandwich folded plates, it is observed that geometry plays a very important role in the free vibration analysis of the structure. The fundamental frequency rises as the core thickness increases while maintaining the same overall thickness. Nevertheless, because frequencies have the combined contribution of mass and stiffness, the gain in natural frequency decreases asymptotically.
ii. Both the boundary condition and the face sheet layup sequence affect the stiffness of the structures and hence their natural frequencies. The structure becomes significantly more

rigid when the folded plate is clamped on all sides. In this case, the fundamental frequency reached its maximum at fiber angle θ = 90o.

iii. For stiffened corrugated plates, careful stiffener placement might improve the structure's performance; hence, using stiffeners judiciously could be very profitable in increasing mass-specific stiffness.

iv. From the vibroacoustic analysis it is concluded that a larger acoustic peak response is produced by a thicker flexible cavity than by a thinner one.

v. Within the domain and the boundary, the first few natural frequencies are effective for variation in sound pressure level. At high forcing frequencies, the effects of structural modes become less pronounced.

vi. A higher damping ratio truncates the peak SPL value efficiently, without altering the SPL distribution at the saddle.

vii. From the vibroacoustic analysis of the stiffened cavity, it is concluded that stiffeners improve the natural frequencies of the entire structure and shift the location of acoustic peaks.

viii. The SPL distribution is significantly influenced by the mode shape of the flexible panel of a cavity. The stiffness of the structure increases, and the interaction kink numbers decrease if the stiffeners are arranged to significantly reduce bending in the mode shape.

ix. The displacement kinks have been observed near dry natural frequencies of the box structure, although the presence of larger deflections is visible only at a few initial natural frequencies. Structural modes have less impact at high forcing frequencies.

x. The SPL pattern at different locations is significantly influenced by the shape of the acoustic domain, which modifies the peak and trough arrangements. SPL of both the domain and the boundary is controlled by the dry natural frequencies of the flexible panels that are present close to rigid acoustic modes.

xi. As forcing frequencies increase, the number of low-pressure zones inside and outside the domain increases because higher frequencies produce shorter wavelengths.

xii. The presence of an opening at the boundary wall plays a crucial role in changing the sound pressure level pattern in a frequency range. For a rigid cavity, the peaks have been shifted slightly to the right and lowered in value due to the coupling effect of the opening, except at the first acoustic mode. An opening in a partly flexible cavity inverts the peak at all the structural and acoustic modes.

xiii. Plotting SPL at a specific frequency on the cavity's inner boundary reveals that the SPL is lowest at the opening and decreases further with increasing distance from the cavity.

xiv. The effect of absorbents is not significant throughout the whole range of frequency. Only resonant frequencies are affected by absorbent layers. In a specific frequency range, it evens out the highs and lows. Limiting the audio output at the resonant frequencies and at a particular location can be achieved by adding absorbents judiciously.

xv. The effects of damping and adding an absorbent layer are comparable. The use of absorbent masks the damping effect when both are present, thus lowering the SPL.

8.3. Key Findings

The FE–BE coupled vibroacoustic analysis of a realistic vehicular cavity (Chapter 7), incorporating all practical features, demonstrates that SPL patterns behave fundamentally differently in rigid and flexible cavities, both inside and outside the domain. The SPL contours (Fig. 7.9 and Fig. 7.17) reveal alternating high- and low-pressure zones, with sound pressure naturally decreasing at larger distances. A major finding is that acoustic peak locations in partially flexible cavities can be intentionally shifted by modifying the cavity geometry—such as stiffening specific panels or altering cavity dimensions. Additionally, peak SPL values at resonant frequencies can be significantly reduced by strategically introducing absorbent materials or increasing structural damping. According to the researcher, such comprehensive studies combining peak-shifting and SPL-reduction strategies in flexible cavities have not been previously reported in the existing literature, which ensures uniqueness of this research.

Considering the conclusions drawn from the present research, the scope for future work is identified and stated in the following section.

8.4. Scope for future research

The findings of this study open several avenues for future research.

i. Firstly, further exploration of different materials and configurations for the cavity walls could lead to improved vibroacoustic performance.

ii. Investigating the effects of various absorbent materials and their placement within the cavity could also yield valuable insights.

iii. Additionally, extending the model to include more complex boundary conditions and external factors, such as varying environmental conditions and operational loads, would enhance its applicability.

iv. Future studies could also explore the integration of advanced machine learning techniques to optimize the design and prediction of vibroacoustic behaviour.

8.5. Statement of Contribution

This thesis makes significant contributions to the field of vibroacoustic analysis by developing a robust numerical model that accurately describes the complex behaviour of cavities with complicated shapes. The integration of BEM and FEM techniques provides a powerful toolset for engineers and researchers, offering a balance between computational efficiency and modelling accuracy. The program developed has the capability to simulate both the interior and exterior domain within a single framework. The practical elements incorporated into the model, such as seat positions and absorbent layers, enhance its applicability to real-world scenarios, particularly in the automotive industry.

Major automotive manufacturers typically rely on high-end expensive vibroacoustic software—such as Ansys, ESI VA One, and Simcenter Nastran—to predict noise accurately and analyse vibration early in the design cycle and ensure that performance targets are met. In contrast, the present work develops a coupled boundary element–finite element model within a MATLAB environment to predict and compare SPL patterns at different locations. The model allows the simulation of vibrations originating from either the interior or exterior cavity and enables the computation of the resulting Sound Pressure Levels (SPL) at the internal boundary, external boundary, and multiple points throughout the domain —a capability that, to the best of researcher's knowledge, has not been previously reported. The methodology further incorporates domain contour visualizations to illustrate SPL distribution.

This research expands the existing knowledge base and supports the design of more efficient and effective acoustic systems and control strategies. Since physical experiments often generate considerable non-biodegradable waste, numerical simulations serve as a valuable preliminary tool for deriving meaningful insights. To determine how to reduce SPL at the passenger location, the driver's position, or even for pedestrians outside the vehicle, numerical analysis can be used to identify beneficial geometric modifications, adjust structural damping, or determine the optimal placement of absorbent materials. Once favourable results are achieved computationally, physical testing can then be performed selectively, prior to real-world implementation.

9

References

[1.] Kirchhoff, G. R. (1850). Über das Gleichgewicht und die Bewegung einer elastischen Scheibe. Journal für die Reine und Angewandte Mathematik (Crelle's Journal), 40, 51–88.

[2.] Reissner, E. (1945). The effect of transverse shear deformation on the bending of elastic plates. ASME Journal of Applied Mechanics, 12(2), 69–77.

[3.] Mindlin, R. D. (1951). Influence of rotatory inertia and shear on flexural motions of isotropic, elastic plates. ASME Journal of Applied Mechanics, 18(1), 31–38. https://doi.org/10.1115/1.4010217

[4.] Yang, P., Norris, C. H., & Stavsky, Y. (1966). Elastic wave propagation in heterogeneous plates. International Journal of Solids and Structures, 2(4), 665–684. https://doi.org/10.1016/0020-7683(66)90045-X

[5.] Raville, M. E., & Ueng, C. E. S. (1967). Determination of natural frequencies of vibration of a sandwich plate. Experimental Mechanics, 7, 490–493. https://doi.org/10.1007/BF02326265

[6.] Reddy, J. N. (1979). Free vibration of anti-symmetric angle-ply laminated plates including transverse shear deformation by the finite element method. Journal of Sound and Vibration, 66, 565–576.

[7.] Chen, W., & Liu, W. (1989). Deflections and free vibrations of laminated plates—Levy-type solutions. International Journal of Mechanical Sciences, 32(9), 779–793. https://doi.org/10.1016/0020-7403(90)90028-H

[8.] Sai Ram, K. S., & Sinha, P. K. (1992). Hygrothermal effects on the buckling of laminated composite plates. Composite Structures, 21(4), 233–247. https://doi.org/10.1016/0263-8223(92)90051-d

[9.] Bathe, K. J. (1996). Finite element procedures. Prentice Hall of India.

[10.] Meunier, M., & Shenoi, R. A. (1999). Free vibration analysis of composite sandwich plates. Proceedings of the Institution of Mechanical Engineers, Part C: Journal of Mechanical Engineering Science, 213(7), 715–727. https://doi.org/10.1177/095440629921300707

[11.] Meunier, M., & Shenoi, R. A. (2001). Dynamic analysis of composite sandwich plates with damping modelled using high-order shear deformation theory. Composite Structures, 54(2–3), 243–254. https://doi.org/10.1016/s0263-8223(01)00094-0

[12.] Jones, R. M. (1999). Mechanics of composite materials (2nd ed.). Taylor & Francis.

[13.] Kant, T., & Swaminathan, K. (2001). Free vibration analysis of isotropic, orthotropic, and multilayer plates using higher-order refined theories. Journal of Sound and Vibration, 241(2), 319–327. https://doi.org/10.1006/jsvi.2000.3232

[14.] Nayak, A. K., Moy, S. S. J., & Shenoi, R. A. (2002). Free vibration analysis of composite sandwich plates based on Reddy's higher-order theory. Composites Part B: Engineering, 33(7), 505–519. https://doi.org/10.1016/s1359-8368(02)00035-5

[15.] Cook, R. D., Markus, D. S., & Plesha, M. E. (2002). Concepts and applications of finite element analysis (4th ed.). John Wiley.

[16.] Reddy, J. N. (2003). Mechanics of laminated composite plates and shells: Theory and analysis (2nd ed.). CRC Press.

[17.] Kumar, A., & Shrivastava, R. P. (2005). Free vibration of square laminates with delamination around a central cutout using HSDT. Composite Structures, 70, 317–333. https://doi.org/10.1016/j.compstruct.2004.08.040

[18.] Shivakumar, K. N. (2006). Processing and properties of a lightweight fire resistant core material for sandwich structures. Journal of Advanced Materials, 38(1).

[19.] Ovesy, H. R., & Fazilati, J. (2012). Buckling and free vibration finite strip analysis of composite plates with cutout based on two different modelling approaches. Composite Structures, 94, 1250–1258.

[20.] Olson, M., & Hazell, C. (1977). Vibration studies on some integral rib-stiffened plates. Journal of Sound and Vibration, 50(1), 43–61. https://doi.org/10.1016/0022-460X(77)90550-8

[21.] Deb, A., & Booton, M. (1988). Finite element models for stiffened plates under transverse loading. Computers & Structures, 28(3), 361–372. https://doi.org/10.1016/0045-7949(88)90076-7

[22.] Mukherjee, A., & Mukhopadhyay, M. (1988). Finite element free vibration of eccentrically stiffened plates. Computers & Structures, 30(6), 1303–1317. https://doi.org/10.1016/0045-7949(88)90195-2

[23.] Attaf, B., & Hollaway, L. (1990). Vibrational analyses of stiffened and unstiffened composite plates subjected to in-plane loads. Composites, 21(2), 117–126. https://doi.org/10.1016/0010-4361(90)90003-F

[24.] Chattopadhyay, B., Sinha, P. K., & Mukhopadhyay, M. (1993). Finite element analysis of blade-stiffened composite plates under transverse loads. Journal of Reinforced Plastics and Composites. https://doi.org/10.1177/073168449301200105

[25.] Lee, D., & Lee, I. (1995). Vibration analysis of anisotropic plates with eccentric stiffeners. Computers & Structures, 57(1), 99–105. https://doi.org/10.1016/0045-7949(94)00593-R

[26.] Qing, G., Qiu, J., & Liu, Y. (2006). Free vibration analysis of stiffened laminated plates. International Journal of Solids and Structures, 43(6), 1357–1371. https://doi.org/10.1016/j.ijsolstr.2005.03.012

[27.] Goldberg, J. E., & Leve, H. L. (1957). Theory of prismatic folded plate structures. Journal of the IABSE, 17, 59–86.

[28.] Cheung, Y. K. (1969). Folded plate structures by finite strip method. Journal of Structural Engineering, ASCE, 2963–2979.

[29.] Irie, T., Yamada, G., & Kobayashi, Y. (1984). Free vibration of a cantilever folded plate. Journal of the Acoustical Society of America, 76(6), 1743–1748.

[30.] Liu, W., & Chen, W. (1992). Vibration analysis of skew cantilever plates with stiffeners. Journal of Sound and Vibration, 159(1), 1–11. https://doi.org/10.1016/0022-460X(92)90447-6

[31.] Guha Niyogi, A., Laha, M. K., & Sinha, P. K. (1999). Finite element vibration analysis of laminated composite folded plate structures. Shock and Vibration, 6, Article ID 354234. https://doi.org/10.1155/1999/354234

[32.] Lee, S. Y., Wooh, S. C., & Yhim, S. S. (2004). Dynamic behaviour of folded composite plates analysed by the third order plate theory. International Journal of Solids and Structures, 41, 1879–1892.

[33.] Lee, S. Y., & Yhim, S. S. (2005). Dynamic behaviour of long-span box girder bridges subjected to moving loads: Numerical analysis and experimental verification. International Journal of Solids and Structures, 42(18–19), 5021–5035.

[34.] Haldar, S., & Sheikh, A. H. (2005). Free vibration analysis of isotropic and composite folded plates using a shear flexible element. Finite Elements in Analysis and Design, 42(3), 208–226.

[35.] Liew, K. M., Peng, L. X., & Kitipornchai, S. (2006). Buckling of folded plate structures subjected to partial in-plane edge loads by the FSDT meshfree Galerkin method. International Journal for Numerical Methods in Engineering, 65, 1495–1526.

[36.] Peng, L. X., Kitipornchai, S., & Liew, K. M. (2007). Free vibration analysis of folded plate structures by the FSDT mesh-free method. Computational Mechanics, 39, 799–814.

[37.] Pal, S., & Guha Niyogi, A. (2007). Finite element analysis of free and transient vibration in sandwich folded plates. In Vibration Problems ICOVP-2007 (pp. 315–321). https://doi.org/10.1007/978-1-4020-9100-1_32

[38.] Singh, S. K., & Chakrabarti, A. (2012). Buckling analysis of laminated composite plates using an efficient C^0 FE model. Latin American Journal of Solids and Structures, 1, 1–13.

[39.] Barbero, E. J., Madeo, A., Zagari, G., Zinno, R., & Zucco, G. (2014). A mixed isostatic 24 dof element for static and buckling analysis of laminated folded plates. Composite Structures, 116, 223–234.

[40.] Peng, L. X. (2015). Free vibration analysis of symmetrically laminated folded plate structures using an element-free Galerkin method. Mathematical Problems in Engineering, 2015, Article ID 124296.

[41.] Le-Anh, L., Nguyen-Thoi, T., Ho-Huu, V., Dang-Trung, H., & Bui-Xuan, T. (2015). Static and frequency optimization of folded laminated composite plates using an adjusted Differential Evolution algorithm and a smoothed triangular plate element. *Composite Structures, 127*, 382–394.

[42.] Guo, X., Yang, Z., & Zhang, W. (2019). Theoretical and experimental investigation on the nonlinear vibration behaviour of Z-shaped folded plates with inner resonance. *Engineering Structures, 182*, 123–140. https://doi.org/10.1016/j.engstruct.2018.12.066

[43.] Das, S., & Guha Niyogi, A. (2020). Free-vibration analysis of epoxy-based cross-ply laminated composite folded plates subjected to hygro-thermal loading. *Journal of the Institution of Engineers (India): Series C*. https://doi.org/10.1007/s40032-020-00573-8

[44.] Peng, X., Zhong, Y., Shi, J., & Shi, Z. (2022). Free flexural vibration analysis of composite sandwich plate with reentrant honeycomb cores using homogenized plate model. *Journal of Sound and Vibration, 529*, 116955. https://doi.org/10.1016/j.jsv.2022.116955

[45.] Song, X., Li, H., Zhang, Z., Zang, J., Zhang, Y., & Chen, L. (2024). Vibration of composite open shell of hydrogen-electric fuselage with rectangular cutout in hygrothermal circumstances: Theoretical and experimental research. *Thin-Walled Structures, 205*, 112473. https://doi.org/10.1016/j.tws.2024.112473

[46.] Salehipour, H., Shahmohammadi, M. A., & Civalek, Ö. (2024). Natural frequencies and modal shapes of folded sandwich plates made of porous core and FG-CNTRC coating layers resting on two parameters elastic foundation. *Aerospace Science and Technology, 148*, 109077. https://doi.org/10.1016/j.ast.2024.109077

[47.] Beranek, L. L. (1954). *Acoustics*. McGraw-Hill.

[48.] Sommerfeld, A. (1967). *Partial differential equations in physics*. Academic Press. ISBN 0-12-654656-8

[49.] Morse, P. M., & Ingard, K. U. (1968). *Theoretical acoustics*. McGraw-Hill.

[50.] Skudrzyk, E. (1971). *The foundations of acoustics*. Springer-Verlag.

[51.] Seto, W. W. (1971). *Acoustic theory and problems of acoustics (Schaum's Outline Series)*. McGraw-Hill.

[52.] Kuttruff, H. (1973). *Room acoustics*. Applied Science Publishers.

[53.] Porges, G. (1977). *Applied acoustics*. Edward Arnold.

[54.] Pierce, A. D. (1981). *Acoustics: An introduction to its physical properties and applications*. McGraw-Hill.

[55.] Kinsler, L. E., Frey, A. R., Coppens, A. B., & Sanders, J. V. (1982). *Fundamentals of acoustics* (3rd ed.). John Wiley & Sons.

[56.] Dowling, A. P., & Williams, J. E. F. (1983). *Sound and sources of sound*. Ellis Horwood Ltd.

[57.] Fahy, F. (2007). *Sound and structural vibration: Radiation, transmission and response* (2nd ed.). Academic Press.

[58.] Norton, M. P., & Karczub, D. G. (2003). *Fundamentals of noise and vibration analysis for engineers* (2nd ed.). Cambridge University Press.

[59.] Turner, J. D., & Pretlove, A. J. (1991). Basic concepts of noise and vibration. In *Acoustics for Engineers*. Palgrave. https://doi.org/10.1007/978-1-349-21267-5_1

[60.] Crocker, M. J. (Ed.). (1997). *Encyclopedia of acoustics*. John Wiley & Sons.

[61.] Marburg, S., & Nolte, B. (2008). *Computational acoustics of noise propagation in fluids – Finite and boundary element methods*. https://doi.org/10.1007/978-3-540-77448-8

[62.] Hambric, S. A., Sung, S. H., & Nefske, D. (2016). *Engineering vibroacoustic analysis: Methods and applications*. https://doi.org/10.1002/9781118693988

[63.] Fredholm, I. (1903). Sur une classe d'équations fonctionnelles. *Acta Mathematica, 27*, 365–390.

[64.] Muskhelishvili, N. I. (1958). *Singular integral equations: Boundary problems of function theory and their applications in mathematical physics*. Noordhoff. https://doi.org/10.1007/978-94-009-9994-7

[65.] Kupradze, V. D. (1965). *Potential methods in the theory of elasticity*. Israel Program for Scientific Translations.

[66.] Kellog, O. D. (1967). Foundations of potential theory. Springer-Verlag.

[67.] Zienkiewicz, O. C., Kelly, D. W., & Bettess, P. (1977). The coupling of the finite element method and boundary solution procedures. *International Journal for Numerical Methods in Engineering, 11*(2), 355–375.

[68.] Brebbia, C. A. (1978). *The boundary element method for engineers*. Pentech Press.

[69.] Banerjee, P. K., & Butterfield, R. (1981). *Boundary element methods in engineering science*. McGraw-Hill.

[70.] Brebbia, C. A., & Dominguez, J. (1989). *Boundary elements: An introductory course*. Computational Mechanics Publishers.

[71.] Becker, A. A. (1992). *The boundary element method in engineering: A complete course*. McGraw-Hill.

[72.] Chen, Z. S., Hofstetter, G., & Mang, H. A. (1993). A 3D boundary element method for determination of acoustic eigenfrequencies considering admittance boundary conditions. Journal of Computational Acoustics, 1(4), 455–468. https://doi.org/10.1142/s0218396x93000238

[73.] Marburg, S., Hardtke, H., Schmidt, R., & Pawandenat, D. (1997). Application of the concept of acoustic influence coefficients for the optimization of a vehicle roof. *Engineering Analysis with Boundary Elements, 20*(4), 305–310. https://doi.org/10.1016/S0955-7997(97)00067-2

[74.] Kim, S. M., & Brennan, M. J. (1999). A compact matrix formulation using the impedance and mobility approach for the analysis of structural-acoustic systems. *Journal of Sound and Vibration, 223*(1), 97–113. https://doi.org/10.1006/jsvi.1998.2096

[75.] Marburg, S., & Hardtke, H. (1999). A study on the acoustic boundary admittance: Determination, results and consequences. *Engineering Analysis with Boundary Elements, 23*(9), 737–744. https://doi.org/10.1016/S0955-7997(99)00024-7

[76.] Marburg, S. (2002). Six boundary elements per wavelength: Is that enough? *Journal of Computational Acoustics, 10*(1), 25–51. https://doi.org/10.1142/S0218396X02001401

[77.] Zhang, Z., Vlahopoulos, N., & Raveendra, S. T. (2003). Formulation of a numerical process for acoustic impedance sensitivity analysis based on the indirect boundary element

method. Engineering Analysis with Boundary Elements, 27(7), 671–681. https://doi.org/10.1016/s0955-7997(03)00026-2

[78.] Li, S. (2005). An efficient technique for multi-frequency acoustic analysis by boundary element method. Journal of Sound and Vibration, 283(3–5), 971–980. https://doi.org/10.1016/j.jsv.2004.05.027

[79.] Kirkup, S. M. (2007). The boundary element method in acoustics (2nd ed.). Integrated Sound Software. ISBN: 0953403106

[80.] Shen, L., & Liu, Y. J. (2007). An adaptive fast multipole boundary element method for three-dimensional acoustic wave problems based on the Burton–Miller formulation. Computational Mechanics, 40, 461–472. https://doi.org/10.1007/s00466-006-0121-2

[81.] Shaw, R. P. (1970). The interaction of acoustic waves and elastic structures. In C. Bretchneider (Ed.), Topics in Ocean Engineering (Vol. II, pp. 164–178). Gulf Publishing Co.

[82.] Shaw, R. P. (1973). Integral equation formulation of dynamic acoustic fluid-elastic solid interaction problems. The Journal of the Acoustical Society of America, 53(2), 514–520. https://doi.org/10.1121/1.1913343

[83.] Zienkiewicz, O. C., Kelly, D. W., & Bettess, P. (1977). The coupling of the finite element method and boundary solution procedures. International Journal for Numerical Methods in Engineering, 11(2), 355–375. https://doi.org/10.1002/nme.1620110210

[84.] Suzuki, S., Maruyama, S., & Ido, H. (1989). Boundary element analysis of cavity noise problems with complicated boundary conditions. Journal of Sound and Vibration, 130(1), 79–96. https://doi.org/10.1016/0022-460X(89)90521-X

[85.] Jeans, R. A., & Mathews, I. C. (1990). Solution of fluid–structure interaction problems using a coupled finite element and variational boundary element technique. The Journal of the Acoustical Society of America, 88(5), 2459–2466. https://doi.org/10.1121/1.400086

[86.] Cheng, L. (1994). Fluid-structural coupling of a plate-ended cylindrical shell: Vibration and internal sound field. Journal of Sound and Vibration, 174(5), 641–654. https://doi.org/10.1006/jsvi.1994.1299

[87.] Morand, H. J. P., & Ohayon, R. (1995). Fluid structure interaction: Applied numerical methods. John Wiley & Sons.

[88.] Ohayon, R., & Soize, C. (1998). Structural acoustics and vibration: Mechanical models, variational formulations and discretization. Academic Press.

[89.] Jayachandran, V., Hirsch, S. M., & Sun, J. Q. (1998). The numerical modelling of interior sound fields by the modal function expansion approach. Journal of Sound and Vibration, 210(2), 243–254. https://doi.org/10.1006/jsvi.1997.1328

[90.] Guha Niyogi, A., Laha, M. K., & Sinha, P. K. (2000). A coupled FE–BE analysis of acoustic cavities confined inside laminated composite enclosures. Aircraft Engineering and Aerospace Technology, 72(4), 345–357. https://doi.org/10.1108/00022660010340150

[91.] Gaul, L., & Wenzel, W. (2002). A coupled symmetric BE–FE method for acoustic fluid–structure interaction. Engineering Analysis with Boundary Elements, 26(7), 629–636. https://doi.org/10.1016/s0955-7997(02)00020-6

[92.] Desmet, W., van Hal, B., Sas, P., & Vandepitte, D. (2002). A computationally efficient prediction technique for the steady-state dynamic analysis of coupled vibroacoustic systems. Advances in Engineering Software, 33(7–10), 527–540. https://doi.org/10.1016/s0965-9978(02)00062-5

[93.] Li, Y. Y., & Cheng, L. (2007). Vibroacoustic analysis of a rectangular-like cavity with a tilted wall. Applied Acoustics, 68(7), 739–751. https://doi.org/10.1016/j.apacoust.2006.04.005

[94.] Tong, Z., Zhang, Y., Zhang, Z., & Hua, H. (2007). Dynamic behaviour and sound transmission analysis of a fluid–structure coupled system using the direct-BEM/FEM. Journal of Sound and Vibration, 299(3), 645–655. https://doi.org/10.1016/j.jsv.2006.06.063

[95.] Deu, J. F., Larbi, W., & Ohayon, R. (2008). Vibration and transient response of structural–acoustic interior coupled systems with dissipative interface. Computer Methods in Applied Mechanics and Engineering, 197, 4894–4905. https://doi.org/10.1016/j.cma.2008.07.013

[96.] Warszawski, A., Soares, D., & Mansur, W. J. (2008). A FEM–BEM coupling procedure to model the propagation of interacting acoustic–acoustic/acoustic–elastic waves through axisymmetric media. Computer Methods in Applied Mechanics and Engineering, 197(45–48), 3828–3835. https://doi.org/10.1016/j.cma.2008.03.005

[97.] Daneshjou, K., Nouri, A., & Talebitooti, R. (2008). Analytical model of sound transmission through laminated composite cylindrical shells considering transverse shear deformation. Applied Mathematics and Mechanics, 29(9), 1165–1177. https://doi.org/10.1007/s10483-008-0906-x

[98.] He, Z. C., Liu, G. R., Zhong, Z. H., Zhang, G. Y., & Cheng, A. G. (2011). A coupled ES-FEM/BEM method for fluid–structure interaction problems. Engineering Analysis with Boundary Elements, 35(1), 140–147. https://doi.org/10.1016/j.enganabound.2010.05.003

[99.] Jiang, C. H., & Kam, T. Y. (2013). Vibration analysis of elastically restrained laminated composite sound radiation plates via a finite element approach. Procedia Engineering, 67, 545–558. https://doi.org/10.1016/j.proeng.2013.12.055

[100.] Sahu, A., Niyogi, A. G., Rose, M., & Bhattacharya, P. (2014). A fully coupled finite element-boundary element vibroacoustic analysis for laminated composite structures with enclosed acoustic cavities. The Journal of the Acoustical Society of America, 135(4_Supplement), 2419. https://doi.org/10.1121/1.4878031

[101.] Das, S., Chandra, S., & Niyogi, A. G. (2016). Vibroacoustic analysis inside cross-ply laminated composite cavity. *Procedia Engineering, 144*, 1389–1396. https://doi.org/10.1016/j.proeng.2016.05.169

[102.] Li, P., Yan, Y., & Lin, H. (2016). Numerical simulation and experimental researches on the vibration–acoustic coupled property of an aircraft model under strong reverberation noise. *Journal of Vibration and Control, 23*(17), 2757–2766. https://doi.org/10.1177/1077546315621417

[103.] Zhang, H., Shi, D., Zha, S., & Wang, Q. (2018). A simple first-order shear deformation theory for vibroacoustic analysis of the laminated rectangular fluid-structure coupling system. *Composite Structures, 201*, 647–663. https://doi.org/10.1016/j.compstruct.2018.06.093

[104.] Zhang, H., Zhu, R., Shi, D., Wang, Q., & Yu, H. (2019). Study on vibroacoustic property of composite laminated rotary plate-cavity system based on a simplified plate theory and experimental method. *International Journal of Mechanical Sciences*, 105264. https://doi.org/10.1016/j.ijmecsci.2019.105264

[105.] Kim, H., Kim, S., Kim, B., Ma, P., & Seo, Y. (2020). Sound transmission loss of multi-layered infinite micro-perforated plates. The Journal of the Acoustical Society of America, 147(1), 508–515. https://doi.org/10.1121/10.0000600

[106.] Zhong, R., Hu, S., Liu, X., Qin, B., Wang, Q., & Shuai, C. (2022). Vibroacoustic analysis of a circumferentially coupled composite laminated annular plate backed by double cylindrical acoustic cavities. Ocean Engineering, 257, 111584. https://doi.org/10.1016/j.oceaneng.2022.111584

[107.] Zhang, H., & Chen, T. (2022). Vibroacoustic characteristics analysis of the rotary composite plate and conical–cylindrical double cavities coupled system. *Journal of Intelligent Manufacturing and Special Equipment, 3*(1), 67–96. https://doi.org/10.1108/jimse-01-2022-0002

[108.] AllahTavakoli, Y., Ichchou, M., Marquis-Favre, C., & Hamzaoui, N. (2023). On a hybrid updating method for modelling vibroacoustic behaviours of composite panels. *Journal of Sound and Vibration, 565*, 117902. https://doi.org/10.1016/j.jsv.2023.117902

[109.] Chen, Q., Fei, Q., & Zheng, R. (2023). Investigation of statistical energy analysis coupling loss factors of vibroacoustic systems under thermal environment. *Journal of Vibration and Control*. https://doi.org/10.1177/10775463231203768

[110.] Zhang, K., Pan, J., Lin, T. R., Guo, H., & Zhang, B. (2023). Vibroacoustic response of ribbed-panel-cavity systems due to an internal sound source excitation. *Journal of Vibration and Control, 30*(5–6), 1063–1079. https://doi.org/10.1177/10775463231156062

[111.] Wang, H., Guo, H., Wang, Y., Du, Y., & Cai, W. (2023). Study on vibroacoustic performance of composite laminates under transient impact excitation. *Journal of Physics Conference Series, 2458*(1), 012006. https://doi.org/10.1088/1742-6596/2458/1/012006

[112.] Huang, Y., Hu, J., Wang, J., Sun, J., You, Y., Huang, Q., & Xu, E. (2023). Sound quality performance of orthogonal antisymmetric composite laminates embedded with SMA wires. *Materials, 16*(9), 3570. https://doi.org/10.3390/ma16093570

[113.] El Kharras, B., Garoum, M., & Bybi, A. (2023). Vibroacoustic analysis of multi-layered micro-perforated plates coupled to an acoustic enclosure. *Building Acoustics, 30*(3), 265–292. https://doi.org/10.1177/1351010X231169827

[114.] Tarkashvand, A., Montasheri, M., & Daneshjou, K. (2024). Analysis of vibroacoustic behaviour of partially coupled fluid-structure laminated composite cylinders using two coordinate systems. *Ocean Engineering*. https://doi.org/10.1016/j.oceaneng.2023.116525

[115.] Zhang, H., Ding, Y., He, L., Shuai, C., & Jiang, C. (2024). The vibroacoustic characteristics analysis of the coupled system between composite laminated rotationally stiffened plate and acoustic cavities. *Applied Sciences, 14*, 1002. https://doi.org/10.3390/app14031002

[116.] Lachat, J. C., & Watson, J. O. (1976). Effective numerical treatment of boundary integral equations: A formulation for three-dimensional elastostatics. *International Journal for Numerical Methods in Engineering, 10*(5), 991–1005. https://doi.org/10.1002/nme.1620100503

[117.] Rizzo, F. J., & Shippy, D. J. (1977). An advanced boundary integral equation method for three-dimensional thermoelasticity. *International Journal for Numerical Methods in Engineering, 11*(11), 1753–1768. https://doi.org/10.1002/nme.1620111109

[118.] Cheng, C. Y. R., Seybert, A. F., & Wu, T. W. (1991). A multi-domain boundary element solution for silencer and muffler performance prediction. *Journal of Sound and Vibration, 151*(1), 119–129. https://doi.org/10.1016/0022-460x(91)90655-4

[119.] Wu, T. W., & Dandapani, A. (1994). A boundary element solution for sound transmission through thin panels. *Journal of Sound and Vibration, 171*(2), 145–157. https://doi.org/10.1006/jsvi.1994.1110

[120.] Layton, J. B., Ganguly, S., Balakrishna, C., & Kane, J. H. (1997). A symmetric Galerkin multi-zone boundary element formulation. *International Journal for Numerical Methods in Engineering, 40*(16), 2913–2931. https://doi.org/10.1002/(sici)1097-0207(19970830)40:16<2913::aid-nme197>3.0.co;2-8

[121.] Gaul, L., Wagner, M., & Wenzel, W. (1999). Teaching boundary element methods in acoustics. *Journal of the Acoustical Society of America, 105*(2_Supplement), 1123. https://doi.org/10.1121/1.425242

[122.] Ju, H.-D., & Lee, S.-B. (2001). Multi-domain structural-acoustic coupling analysis using the finite element and boundary element techniques. *KSME International Journal, 15*(5), 555–561. https://doi.org/10.1007/bf03184371

[123.] Wu, T. W., Cheng, C. Y. R., & Zhang, P. (2002). A direct mixed-body boundary element method for packed silencers. *The Journal of the Acoustical Society of America, 111*(6), 2566–2572. https://doi.org/10.1121/1.1476920

[124.] Jeong, J.-H., Ih, J.-G., & Lee, B.-C. (2003). A guideline for using the multi-domain BEM for analysing the interior acoustic field. *Journal of Computational Acoustics, 11*(3), 403–424. https://doi.org/10.1142/s0218396x03002000

[125.] Zeng, Y. Q., Liu, Q. H., & Zhao, G. (2004). Multi-domain Pseudospectral Time-Domain (PSTD) method for acoustic waves in lossy media. *Journal of Computational Acoustics, 12*(3), 277–299. https://doi.org/10.1142/s0218396x04002081

[126.] Jeong, J.-H., Ih, J.-G., & Lee, B.-C. (2005). Acoustic design sensitivity analysis for interior spaces using the multi-domain BEM. *Journal of Computational Acoustics, 13*(1), 127–144. https://doi.org/10.1142/s0218396x0500258x

[127.] Hyeon-Don, J., & Shi-Bok, L. (2005). Transmission loss estimation of three-dimensional silencers with perforated internal structures using multi-domain BEM. *Journal of Mechanical Science and Technology, 19*(8), 1568–1575. https://doi.org/10.1007/bf03023934

[128.] Ju, H.-D., Lee, S.-B., & Park, Y.-B. (2007). Transmission loss estimation of splitter silencer using multi-domain BEM. *Journal of Mechanical Science and Technology, 21*(12), 2073–2081. https://doi.org/10.1007/bf03177466

[129.] Wu, T. (2008). Multi-domain boundary element method in acoustics. In S. Marburg & B. Nolte (Eds.), *Computational Acoustics of Noise Propagation in Fluids - Finite and Boundary Element Methods* (pp. 345–368). Springer. https://doi.org/10.1007/978-3-540-77448-8_14

[130.] Cheng, H., Chen, J., Zhang, Y., Bi, C., & Gao, Y. (2009). A multi-domain boundary element formulation for acoustic frequency sensitivity analysis. *Engineering Analysis with Boundary Elements, 33*(6), 815–821. https://doi.org/10.1016/j.enganabound.2008.12

[131.] Soares, D. (2011). Coupled numerical methods to analyze interacting acoustic-dynamic models by multi-domain decomposition techniques. *Mathematical Problems in Engineering, 2011*, 1–28. https://doi.org/10.1155/2011/245170

[132.] Larbi, W., Deü, J.-F., & Ohayon, R. (2015). Vibroacoustic analysis of laminated double-wall: Finite element formulation and reduced-order model. *Multiphysics Modelling and Simulation for Systems Design and Monitoring*, 349–358. https://doi.org/10.1007/978-3-319-14532-7_36

[133.] Zhang, Z., Yu, H., Duan, N., & Hua, H. (2020). A multi-domain spectral method for analysis of interior vibroacoustic systems with segmented boundaries. *Shock and Vibration, 2020*, 1–18. https://doi.org/10.1155/2020/6910174

[134.] Wang, G., Kong, D., Li, W., Ni, J., & Shi, X. (2022). Acoustic modelling and eigenanalysis of the coupled cavities with panels. *Mechanical Systems and Signal Processing, 165*, 108307. https://doi.org/10.1016/j.ymssp.2021.108307

[135.] Preuss, S., Gurbuz, C., Jelich, C., Baydoun, S. K., & Marburg, S. (2022). Recent advances in acoustic boundary element methods. *Journal of Theoretical and Computational Acoustics, 30*(3). https://doi.org/10.1142/s2591728522400023

[136.] Chai, P., Zhang, J., Xiao, R., et al. (2023). A multi-domain BEM based on the dual interpolation boundary face method for 3D potential problems. *Acta Mechanica, 234*, 451–469. https://doi.org/10.1007/s00707-022-03414-0

[137.] Tang, Y., Zhou, Q., Lü, X., Ji, G., & Tan, L. (2024). A numerical method for scattering from multi-domain structures based on near-field artificial boundary. *Journal of Vibration Engineering & Technologies, 12*(4), 7021–7033. https://doi.org/10.1007/s42417-024-01296-1

[138.] Chen, L.H., & Schwikert, D.G. (1963). Sound radiation from an arbitrary body. *Journal of the Acoustical Society of America, 35*(10), 1626–1632.

[139.] Chertock, G. (1964). Sound radiation from vibrating surfaces. *Journal of the Acoustical Society of America, 36*(7), 1305–1313.

[140.] Williams, W., et al. (1964). Acoustic radiation from a finite cylinder. *Journal of the Acoustical Society of America, 36*(12), 2316–2322.

[141.] Copley, L.G. (1967). Integral equation method for radiation from vibrating bodies. *Journal of the Acoustical Society of America, 41*(4), 807–816.

[142.] Schenck, H. A. (1968). Improved integral formulation for acoustic radiation problems. *The Journal of the Acoustical Society of America, 44*(1), 41–58. https://doi.org/10.1121/1.1911085

[143.] Burton, A. J., & Miller, G. F. (1971). The application of integral equation methods to the numerical solution of some exterior boundary-value problems. *Proceedings of the Royal Society A: Mathematical, Physical and Engineering Sciences, 323*(1553), 201–210. https://doi.org/10.1098/rspa.1971.0048

[144.] Engblom, J. J., & Nelson, R. D. (1975). Consistent formulation of sound radiation from arbitrary structure. *Journal of Applied Mechanics, 42*, 295–300. https://doi.org/10.1115/1.3423570

[145.] Bell, W. A., Meyer, W. L., & Zinn, B. T. (1977). Predicting the acoustics of arbitrarily shaped bodies using an integral approach. *AIAA Journal, 15*(6), 813–820. https://doi.org/10.2514/3.60712

[146.] Stepanishen, P. R. (1977). The radiation impedance of a rectangular piston. *Journal of Sound and Vibration, 55*(2), 275–288. https://doi.org/10.1016/0022-460X(77)90599-5

[147.] Meyer, W. L., Bell, W. A., Zinn, B. T., & Stallybrass, M. P. (1978). Boundary integral solutions of three-dimensional acoustic radiation problems. *Journal of Sound and Vibration, 59*(2), 245–262. https://doi.org/10.1016/0022-460X(78)90504-7

[148.] Watson, J. O. (1979). Advanced implementation of the boundary element method for two- and three-dimensional elastostatics. *Developments in Boundary Element Methods, 1*, 31–63.

[149.] Koopman, G. H., & Benner, H. (1982). Method for computing the sound power of machines based on the Helmholtz integral. *Journal of the Acoustical Society of America, 71*(1), 78–89.

[150.] Seybert, A. F., et al. (1983). Application of the BIE method to sound radiation problems using an isoparametric element. *ASME Paper No. 82-WA/NCA-1*.

[151.] Levine, H. (1983). On the radiation impedance of a rectangular piston. *Journal of Sound and Vibration, 89*(4), 447–455. https://doi.org/10.1016/0022-460X(83)90346-2

[152.] Amini, S. (1982). Boundary integral methods for the solution of Helmholtz equation in the exterior domain. *MOD Rep 1*, Department of Mathematics, Statistics and Computing, Plymouth Polytechnic, U.K.

[153.] Amini, S. (1983). Highly accurate numerical methods for boundary integral formulations of the Helmholtz equations in the exterior domain. *MOD Rep 2*, Department of Mathematics, Statistics and Computing, Plymouth Polytechnic, U.K.

[154.] Piaszczyk, C. M., & Klosner, J. M. (1984). Acoustic radiation from vibrating surfaces at characteristic frequencies. *The Journal of the Acoustical Society of America, 75*(2), 363–375. https://doi.org/10.1121/1.390480

[155.] Brod, K. (1984). On the uniqueness of solution for all wavenumbers in acoustic radiation. *The Journal of the Acoustical Society of America, 76*(4), 1238–1243. https://doi.org/10.1121/1.391418

[156.] Imai, M., Suzuki, S., Sugiura, N., & Sato, H. (1985). Radiation efficiency of engine structures by holographic interferometry and boundary element calculation. *SAE 861411*.

[157.] Seybert, A. F., & Holt, J. A. (1985). A technique for the prediction of the noise field from an arbitrary vibrating machine. *Noise Con*, 51–56.

[158.] Seybert, A. F., Soenarko, B., Rizzo, F. J., & Shippy, D. J. (1985). An advanced computational method for radiation and scattering of acoustic waves in three dimensions. *Journal of the Acoustical Society of America, 77*(2), 362–368.

[159.] Amini, S., & Wilton, D. T. (1986). An investigation of boundary element methods for the exterior acoustic problem. *Computer Methods in Applied Mechanics and Engineering, 54*, 49–65.

[160.] Seybert, A. F., & Cheng, C. Y. R. (1987). Application of the boundary element method to acoustic cavity response and muffler analysis. *Journal of Vib., Acoust., Stress, and Reliab., 109*(1), 15–21. https://doi.org/10.1115/1.3269388

[161.] Seybert, A. F., & Rengarajan, T. K. (1987). The use of CHIEF to obtain unique solutions for acoustic radiation using boundary integral equations. *Journal of the Acoustical Society of America, 81*, 1299–1306.

[162.] Amini, S. (1987). An iterative method for the boundary element solution of the exterior acoustic problem. *Journal of Computational and Applied Mathematics, 20*, 109–117.

[163.] Croker, M. D. (1987). Summary report of experimental work on the Ricardo crankcase simulation rigs, Part 1. *Ricardo Report 87/716*.

[164.] Cunefare, K. A., Koopman, G., & Brod, K. (1989). A boundary element method for acoustic radiation valid for all wavenumbers. *Journal of the Acoustical Society of America, 85*(1), 39–48.

[165.] Kirkup, S. M. (1989). Solution of exterior acoustic problems by the boundary element method. *Ph.D. Thesis*, Department of Mathematical Sciences, Brighton Polytechnic, Brighton, UK.

[166.] Seybert, A. F., Cheng, C. Y. R., & Wu, T. W. (1990). The solution of coupled interior/exterior acoustic problems using the boundary element method. *Journal of the Acoustical Society of America, 88*(3), 1612–1618.

[167.] Stanton, T. K. (1990). Sound scattering by spherical and elongated shelled bodies. *Journal of the Acoustical Society of America, 88*(3), 1619–1633.

[168.] Juhl, P. M. (1993). *The boundary element method for sound field calculations*. Technical University of Denmark, Copenhagen, Denmark.

[169.] Stewart, J. R., & Hughes, T. J. R. (1996). Adaptive finite element methods for the Helmholtz equation in exterior domains. In *Large-scale structures in acoustics and electromagnetics: Proceedings of a symposium* (pp. 122–142). National Academy Press.

[170.] Stewart, J. R., & Hughes, T. J. R. (1997). H-Adaptive finite element computation of time-harmonic exterior acoustics problems in two dimensions. *Computer Methods in Applied Mechanics and Engineering, 146*(1-2), 65–89.

[171.] Zaman, S. I. (2000). A comprehensive review of boundary integral formulations of acoustic scattering problems. Sci. Technol. Spec. Rev., 281–310.

[172.] Lee, Y. Y. (2002). Structural-acoustic coupling effect on the nonlinear natural frequency of a rectangular box with one flexible plate. Applied Acoustics, 63(11), 1157–1175. https://doi.org/10.1016/s0003-682x(02)00033-6

[173.] Schuhmacher, A., Hald, J., Rasmussen, K. B., & Hansen, P. C. (2003). Sound source reconstruction using inverse boundary element calculations. Acoustical Society of America Journal, 113(1), 114–127. https://doi.org/10.1121/1.1529668

[174.] Visser, R. (2004). A boundary element approach to acoustic radiation and source identification (Ph.D. Thesis). University of Twente, Enschede, The Netherlands.

[175.] Marburg, S., & Amini, S. (2005). Cat's eye radiation with boundary elements: Comparative study on the treatment of irregular frequencies. Journal of Computational Acoustics, 13, 21–45.

[176.] Wright, L., Robinson, S. P., Humphrey, V. F., Harris, P., & Hayman, G. (2005). The application of boundary element methods to near-field acoustic measurements on cylindrical surfaces at NPL. National Physical Laboratory: London, UK.

[177.] Guha Niyogi, A. (2006). Structural acoustic problems with absorbent layers within laminated composite enclosures. Journal of Vibration and Acoustics, 128(6), 705. https://doi.org/10.1115/1.2345671

[178.] Denli, H., & Sun, J. Q. (2007). Structural-acoustic optimization of composite sandwich structures: A review. The Shock and Vibration Digest, 39, 189–200. https://doi.org/10.1177/0583102406074086

[179.] Wu, T. (2008). Multi-domain boundary element method in acoustics. In Computational Acoustics of Noise Propagation in Fluids - Finite and Boundary Element Methods (pp. 367–386). https://doi.org/10.1007/978-3-540-77448-8_14

[180.] Marburg, S., & Nolte, B. (2008). Computational Acoustics of Noise Propagation in Fluids - Finite and Boundary Element Methods. https://doi.org/10.1007/978-3-540-77448-8

[181.] Marburg, S., & Wu, T. W. (2008). Treating the phenomenon of irregular frequencies. In S. Marburg & B. Nolte (Eds.), Computational Acoustics of Noise Propagation in Fluids - Finite and Boundary Element Methods (pp. 411–434). Springer.

[182.] Biermann, J., von Estorff, O., Petersen, S., & Wenterodt, C. (2009). Higher order finite and infinite elements for the solution of Helmholtz problems. Computer Methods in Applied Mechanics and Engineering, 198(13–14), 1171–1188. https://doi.org/10.1016/j.cma.2008.11.009

[183.] Wright, L., Robinson, S. P., & Humphrey, V. F. (2009). Prediction of acoustic radiation from axisymmetric surfaces with arbitrary boundary conditions using the boundary element method on a distributed computing system. Journal of the Acoustical Society of America, 125, 1374–1383.

[184.] Venkatesham, B., Tiwari, M., & Munjal, M. L. (2008). Analytical prediction of the breakout noise from a rectangular cavity with one compliant wall. The Journal of the Acoustical Society of America, 124(5), 2952–2962. https://doi.org/10.1121/1.2977671

[185.] Venkatesham, B., Tiwari, M., & Munjal, M. L. (2010). Analytical prediction of break-out noise from a reactive rectangular plenum with four flexible walls. The Journal of the Acoustical Society of America, 128(4), 1789–1799. https://doi.org/10.1121/1.3463801

[186.] Yang, M., Ai, Y., & Xiang, S. (2010). Coupling of FEM and exterior/interior acoustic field with BEM and numerical simulation of vibroacoustic response of elastic target. 2010 International Conference on Measuring Technology and Mechatronics Automation. https://doi.org/10.1109/ICMTMA.2010.534

[187.] Kueppers, T., Biermann, J.-W., & Steffens, J. (2011). Structurized sound design process of electric vehicle interior sound. Journal of the Acoustical Society of America. https://doi.org/10.1121/1.3655178

[188.] Butkus, D., & Januševičius, T. (2011). Acoustic investigations of the exterior and interior wall of a log house. Journal of Environmental Engineering and Landscape Management, 19(2), 140–147. https://doi.org/10.3846/16486897.2011.580919

[189.] Zhou, S. W., & Zhang, S. Q. (2012). Structural-acoustic analysis of automobile passenger compartment. Applied Mechanics and Materials, 236-237, 175–179. https://doi.org/10.4028/www.scientific.net/amm.236-237.175

[190.] Qian, Z.-H., & Yamanaka, H. (2012). An efficient approach for simulating seismoacoustic scattering due to an irregular fluid-solid interface in multilayered media. Geophysical Journal International, 189(1), 524–540. https://doi.org/10.1111/j.1365-246x.2011.05352.x

[191.] D'Alessandro, V., Petrone, G., Franco, F., & De Rosa, S. (2013). A review of the vibroacoustics of sandwich panels: Models and experiments. Journal of Sandwich Structures & Materials, 15(5), 541–582. https://doi.org/10.1177/1099636213490588

[192.] Zhou, Q., Wang, D., & Zhu, Y. (2014). An approximate analytical method of the nonlinear vibroacoustic coupling system. Shock and Vibration, 2014, 1–10. https://doi.org/10.1155/2014/315416

[193.] Ramesh, S. S., Lim, K.-M., & Khoo, B. C. (2015). Comparison of constant and discontinuous quadratic boundary elements for exterior axisymmetric acoustic-wave propagation problems. Journal of Computational Acoustics, 23(4), 1540003. https://doi.org/10.1142/s0218396x15400032

[194.] Raviprolu, P., Jade, N., & Balide, V. (2016). Sound radiation characteristics of a rectangular duct with flexible walls. Advances in Acoustics and Vibration, 2016, Article ID 6053704, 15 pages. https://doi.org/10.1155/2016/6053704

[195.] Jin, G., Shi, S., & Liu, Z. (2016). Acoustic modelling of a three-dimensional rectangular opened enclosure coupled with a semi-infinite exterior field at the baffled opening. The Journal of the Acoustical Society of America, 140, Article 4966626. https://doi.org/10.1121/1.4966626

[196.] Ouedraogo, B., Maréchal, R., Ville, J., & Perrey-Debain, E. (2016). Broadband noise reduction by circular multi-cavity mufflers operating in multimodal propagation conditions. Applied Acoustics, 114, 84–94. https://doi.org/10.1016/j.apacoust.2016.02.001

[197.] Das, S., Chandra, S., & Niyogi, A. G. (2016). Vibroacoustic analysis inside cross ply laminated composite cavity. Procedia Engineering, 144, 1389–1396. https://doi.org/10.1016/j.proeng.2016.05.169

[198.] Galgalikar, R., & Thompson, L. L. (2016). Design optimization of honeycomb core sandwich panels for maximum sound transmission loss. Journal of Vibration and Acoustics, 138(5), 051005. https://doi.org/10.1115/1.4033459

[199.] Shen, C., & Hou, L. (2017). Comparison of various algorithms for improving acoustic attenuation performance and flow characteristic of reactive mufflers. Applied Acoustics, 116, 291–296. https://doi.org/10.1016/j.apacoust.2016.09.034

[200.] Sedaghatjoo, Z., Dehghan, M., & Hosseinzadeh, H. (2017). On uniqueness of numerical solution of boundary integral equations with 3-times monotone radial kernels. Journal of Computational and Applied Mathematics, 311, 664–681. https://doi.org/10.1016/j.cam.2016.07.032

[201.] Marburg, S. (2017). Conventional boundary element techniques: Recent developments and opportunities. In Proceedings of Inter-Noise 2017, Hong Kong, China, 27–30 August, 2673–2688.

[202.] Du, J., Liu, Y., & Liu, L. (2018). Acoustic analysis of enclosed sound space as well as its coupling with flexible boundary structure. In Computational and Experimental Studies of Acoustic Waves. https://doi.org/10.5772/intechopen.69967

[203.] Fahy, F., & Walker, J. (2018). Advanced applications in acoustics, noise and vibration. CRC Press. https://doi.org/10.1201/9781315273396

[204.] Marburg, S. (2018). Boundary element method for time-harmonic acoustic problems. In M. Kaltenbacher (Ed.), Computational Acoustics (Vol. 579, pp. 59–123). Springer. https://doi.org/10.1007/978-3-319-59038-7_3

[205.] Shi, S., Su, Z., Jin, G., & Liu, Z. (2018). Vibroacoustic modelling and analysis of a coupled acoustic system comprising a partially opened cavity coupled with a flexible plate. Mechanical Systems and Signal Processing, 98, 324–343. https://doi.org/10.1016/j.ymssp.2017.04.045

[206.] Li, J., Chen, W., Qin, Q., & Fu, Z. (2018). A modified dual-level fast multipole boundary element method for large-scale three-dimensional potential problems. Computer Physics Communications, 232, 36–47. https://doi.org/10.1016/j.cpc.2018.06.024

[207.] Singh, S., & Mohanty, A. R. (2018). HVAC noise control using natural materials to improve vehicle interior sound quality. Applied Acoustics, 140, 100–109. https://doi.org/10.1016/j.apacoust.2018.05.01

[208.] Zhong, L., Li, Q., Wang, Y., & Yang, Z. (2019). Aerodynamic noise prediction of passenger vehicle with hybrid detached eddy simulation/acoustic perturbation equation method. Proceedings of the Institution of Mechanical Engineers, Part D: Journal of Automobile Engineering, 233(10), 2390–2404. https://doi.org/10.1177/0954407018782856

[209.] Shi, D., Ren, W., Zhang, H., Liu, G., & Wang, Q. (2019). Vibroacoustic coupling characteristics of orthotropic L-shaped plate–cavity coupling system. Journal of Low Frequency Noise, Vibration and Active Control, 38(4), 146134841986063. https://doi.org/10.1177/1461348419860630

[210.] Kirkup, S. M. (2019). The boundary element method in acoustics: A survey. Applied Sciences, 9(8), 1642. https://doi.org/10.3390/app9081642

[211.] Mahmoud, S. A. N. (2019). Acoustics from interior designer perspective. In Acoustics of Materials. https://doi.org/10.5772/intechopen.84167

[212.] Han, M. J., Lee, C. H., & Park, T. W. (2020). Vibroacoustic response in vehicle interior and exterior using multibody dynamic systems due to cleat impacts. International Journal of Automotive Technology, 21(3), 591–602. https://doi.org/10.1007/s12239-020-0056-1

[213.] Zhao, W., Chen, L., Chen, H., & Marburg, S. (2020). An effective approach for topological design to the acoustic–structure interaction systems with infinite acoustic domain. Structural and Multidisciplinary Optimization, 62, 1253–1273. https://doi.org/10.1007/s00158-020-02550-2

[214.] Wang, X., Wang, D., & Liu, B. (2020). Efficient acoustic topology optimization using vibroacoustic coupled Craig–Bampton mode synthesis. Acoustics Australia, 48, 163–172. https://doi.org/10.1007/s40857-020-00194-2

[215.] Qian, K., Hou, Z., Liang, J., Liu, R., & Sun, D. (2021). Interior sound quality prediction of pure electric vehicles based on transfer path synthesis. Applied Sciences, 11(10), 4385. https://doi.org/10.3390/app11104385

[216.] Li, M., Zhou, W., Liu, J., Zhang, X., Pan, F., Yang, H., Li, M., & Luo, D. (2021). Vehicle interior noise prediction based on Elman neural network. Applied Sciences, 11(17), 8029. https://doi.org/10.3390/app11178029

[217.] Qian, K., Hou, Z., Liang, J., Liu, R., & Sun, D. (2021). Interior sound quality prediction of pure electric vehicles based on transfer path synthesis. Applied Sciences, 11(10), 4385. https://doi.org/10.3390/app11104385

[218.] Tang, Y., Zhou, Q., Wang, X., & Xie, Z. (2022). A computational method for acoustic interaction with large complicated underwater structures based on the physical mechanism of structural acoustics. Advances in Materials Science and Engineering, 2022, Article ID 3631241. https://doi.org/10.1155/2022/3631241

[219.] Münder, M., & Carbon, C.-C. (2022). A literature review [2000–2022] on vehicle acoustics: Investigations on perceptual parameters of interior soundscapes in electrified vehicles. Frontiers in Mechanical Engineering, 8, 974464. https://doi.org/10.3389/fmech.2022.974464

[220.] Fakhraei, J., Villamarín, R. A., Pàmies, T., Liravi, H., & Garbí, J. R. (2023). Modified 2.5D singular boundary methods to deal with spurious eigensolutions in exterior acoustic problems. Journal of Sound and Vibration, 550, 117597. https://doi.org/10.1016/j.jsv.2023.117597

[221.] Gonçalves, K. d. A., Santurio, D. S., Soares, D., Costa, P. A., & Godinho, L. (2023). An optimization strategy to position CHIEF points in boundary-element acoustic problems. Applied Sciences, 13(6), 4001. https://doi.org/10.3390/app13064001